THE FLOW OF AQUEOUS HUMOR IN MICROPOROUS MATERIALS

by

C. Ross Ethier

B.Sc.(Eng.), Queen's University, Kingston (1980)

M.Math, University of Waterloo, Waterloo (1982)

S.M., Massachusetts Institute of Technology, (1983)

SUBMITTED TO THE DEPARTMENT OF MECHANICAL ENGINEERING
IN PARTIAL FULFILLMENT FOR THE REQUIREMENTS
FOR THE DEGREE OF

DOCTOR OF PHILOSOPHY

at the

MASSACHUSETTS INSTITUTE OF TECHNOLOGY
September, 1986

Signature of Author_____
Department of Mechanical Engineering
September 12, 1986

Certified by_____
Professor Roger D. Kamm
Thesis Supervisor

Accepted by_____
Professor Ain A. Sonin, Chairman
Department Committee on Graduate Students

THE FLOW OF AQUEOUS HUMOR IN MICROPOROUS MATERIALS

by

C. Ross Ethier

Submitted to the Department of Mechanical Engineering
on September 12, 1986, in partial fulfillment
of the requirements for the degree of
Doctor of Philosophy

Abstract

The aqueous humor is a clear, colorless, blood-derived fluid which fills the anterior segment of the eye. Its flow through the JCM, a tissue permeated by tortuous interconnected pores (diameters ~ 0.1 to 1.0 μ), is thought to play an important role in regulating intraocular pressure in normal and glaucomatous eyes. It is therefore of interest to study the flow of aqueous through submicron size pores.

We have conducted a number of experiments in which aqueous has been perfused through inert microporous materials (Nuclepore and Millipore filters), and have shown that calf, monkey, and rabbit aqueous are all capable of blocking 0.2 μ diameter pores. Furthermore, this behavior is specific to aqueous, as neither calf plasma nor serum exhibit such blockage. The blocking process has been shown to involve two macromolecular components: albumin (and possibly other blood-derived proteins) and a substance which is unique to aqueous and which has been tentatively identified by 2-D gel electrophoresis to have MW 20-30 kdal and pI 6-7. Filter blockage has been shown to involve the hydrophobic, and to a lesser extent, ionic, binding of these components to the membrane surface.

We have also modelled the trans-filter transport of substances which are able to react with (adsorb to) the filter material, and the effect such substances have on filter resistance. Analytical expressions for membrane resistance when adsorbed substances reside within the pore or on the filter face have been derived, as has a description of adsorbed mass within the pore (as a function of position and time) for the case of a dilute solution with Langmuir adsorption kinetics. Theoretical predictions have been compared with experimental data and been shown to be in reasonable agreement.

Thesis Supervisor: Dr. Roger Kamm

Title: Professor of Mechanical Engineering

Acknowledgements

I would like to extend my sincere thanks and appreciation to my supervisor, Roger Kamm, for his continuing help, support, and advice during the course of a tough project. In addition, I am grateful for the suggestions offered by my committee members, Professor Bill Deen, Dr. Thom Richardson and Professor A. Shapiro. In addition, I am particularly indebted to the following individuals: Tony Pavao, for superb 2-D gel work, Mark Johnson, for ongoing criticisms and for having assisted with or performed several experiments reported herein, Paul McGrath for meticulously perfusing late into the night, Thom Freddo for his usual excellent morphology work, and Levon Karaguzian for his practical suggestions and ongoing support. It was a pleasure to work with the members of the Howe lab at the Mass. Eye and Ear Infirmary and the fluids lab at MIT. Finally, I thank my family and friends for their support, and my wonderful wife Karen for all she has done for me.

The financial support of the Alberta Heritage Scholarship Committee, the Natural Sciences and Engineering Research Council of Canada, and the Whitaker Health Sciences Fund, as well as the National Eye Institute (RO1 EY05503), is gratefully acknowledged.

Table of Contents

CHAPTER ONE: INTRODUCTION

The aqueous humor is a clear, colorless, blood-derived fluid which flows within the eye in order to nourish the lens and cornea. The flow of aqueous also serves to maintain a small positive pressure within the eye, the so-called intraocular pressure (IOP). In the normal human eye the aqueous inflow rate and the resistance to its outflow are such as to produce an IOP of approximately 15 mm Hg. However, in the glaucomatous eye the IOP increases to 25 mm Hg or greater, which, if left uncontrolled, causes eventual optic nerve damage and blindness. In most cases the increased IOP seen in glaucoma patients is due to a greater than normal resistance to the outflow of aqueous humor. Thus, an important goal of the study of glaucoma is to determine the major site(s) of aqueous outflow resistance and to determine how this resistance is generated in the normal and glaucomatous eye.

This task is complicated by the fact that the path by which aqueous flows from the eye consists of a complex network of tissues which are not amenable to simple experimental manipulation. However, many researchers believe that the main site of aqueous outflow resistance is the juxtacanalicular meshwork (JCM), a 10 to 25 μm wide tissue composed primarily of extracellular matrix (collagen, elastin, glycosaminoglycans and proteoglycans), and resident cells. Since the JCM is permeated by highly tortuous microscopic channels, previous investigators have treated it as a microporous material and have applied standard porous media theory to JCM electron micrographs in an attempt to theoretically calculate its resistance (Ethier et al., 1986). Interestingly, JCM resistance calculated in this manner is approximately 100 times smaller than observed

values, suggesting that an important resistance-influencing agent (or agents) does not appear on electron micrographs. A number of facts suggest that this agent is a glycosaminoglycan or proteoglycan gel filling the JCM's tortuous flow channels. Thus, from an engineering viewpoint the JCM can be regarded as a complex, gel-filled, microporous material through which the aqueous flows in a passive, non-interacting fashion.

The motivation for the present study was the observation that several types of 0.2 μ pore diameter filters will progressively block up when perfused with calf aqueous humor (Johnson et al., 1986). This result was surprising because most molecular species have characteristic dimensions which are much smaller than 0.2 μ. Because aqueous is essentially isotonic and thus has a Debye length of only 8-10 A, it also seemed unlikely that electrokinetic effects could account for this behavior. This suggested that aqueous contains one or more macromolecules which can alter the resistance of certain types of microporous materials by interacting with them. It thus seemed worthwhile to investigate this phenomenon in order to determine if aqueous-JCM interactions could play a role in modulating or causing aqueous outflow resistance. Proof of such interactions would be of substantial interest to the ophthalmological community. We therefore undertook a study of the interactions of aqueous with microporous membranes via a series of experiments in which the properties of the aqueous humor or of the membrane (or both) were altered and the effect on filter blockage observed. From these studies a number of general characteristics of the blocking materials in aqueous and the nature of their interactions with specific filter types were determined.

Although these experiments were carried out in the context of an ophthalmological problem, the filtration of

macromolecule-containing solutions is by itself a problem of some interest in the engineering sciences. Hence, in addition to the above experimental studies, more traditional engineering experiments were undertaken in which the flowrate and aqueous concentration were varied and the amount of blocking material passing through and remaining on the membrane was assayed. These experiments were augmented by modelling studies which considered the hydrodynamic properties and the trans-filter transport of molecular species which are able to bind to (react with) the filter itself. In this way an attempt was made to generate information of interest to both the ophthalmological and engineering communities.

The goals of this work may therefore be summarized as:

(i) to study the flow of aqueous humor through artificial membranes in an attempt to identify the aqueous component(s) causing filter blockage, as well as to identify the blocking mechanism,
(ii) to apply the information so obtained to the JCM so as to determine if a similar blockage process could be operating *in vivo*, and
(iii) to study the general problem of filtation of protein solutions.

The layout of the thesis is as follows: in Chapter Two background information on the eye and protein/membrane interactions is presented. Chapter Three describes the experimental methods, while Chapter Four summarizes the experimental results. In Chapter Five an attempt is made to model the blocking process and hence explain some aspects of the experimental data. Chapter Six discusses and interprets the results, while in Chapter Seven the conclusions of the study are summarized.

CHAPTER TWO: BACKGROUND

2.1 The Characteristics of Aqueous Humor

The aqueous humor flows within the anterior and posterior chambers of the eye and has the primary function of providing essential nourishment for the avascular lens and cornea (Figure 2.1). Its site of production is the ciliary processes, the highly folded surface of the ciliary body, and its composition is similar to that of a dilute plasma solution (with certain exceptions-- see below), which may be ascribed to the fact that aqueous is derived from blood flowing within the ciliary body and the root of the iris. The fact that aqueous has a different composition than does blood implies the existence of a blood-aqueous barrier which is only partially permeable to plasma proteins. Morphologically, this barrier is composed of the tight (non-fenestrated) caplilliary endothelium within the iridial stroma and the non-pigmented epithelium of the ciliary processes.

The composition of the aqueous humor has been examined by a number of authors. Of particular interest to us are measured protein levels, several of which are summarized in Table 2.1. Generally, total aqueous protein concentrations are 100- to 500-fold less than serum levels. Many of the reported values have been measured by the Lowry-Folin assay, and are therefore probably slightly high due to reaction with oligopeptides and free amino acids (Dernouchamps, 1982). There is also some question as to how closely the composition of aspirated aqueous corresponds to that *in situ*, the concern being that the trauma of corneal puncture and aspiration may disrupt the

Figure 2.1 The gross anatomy of the eye

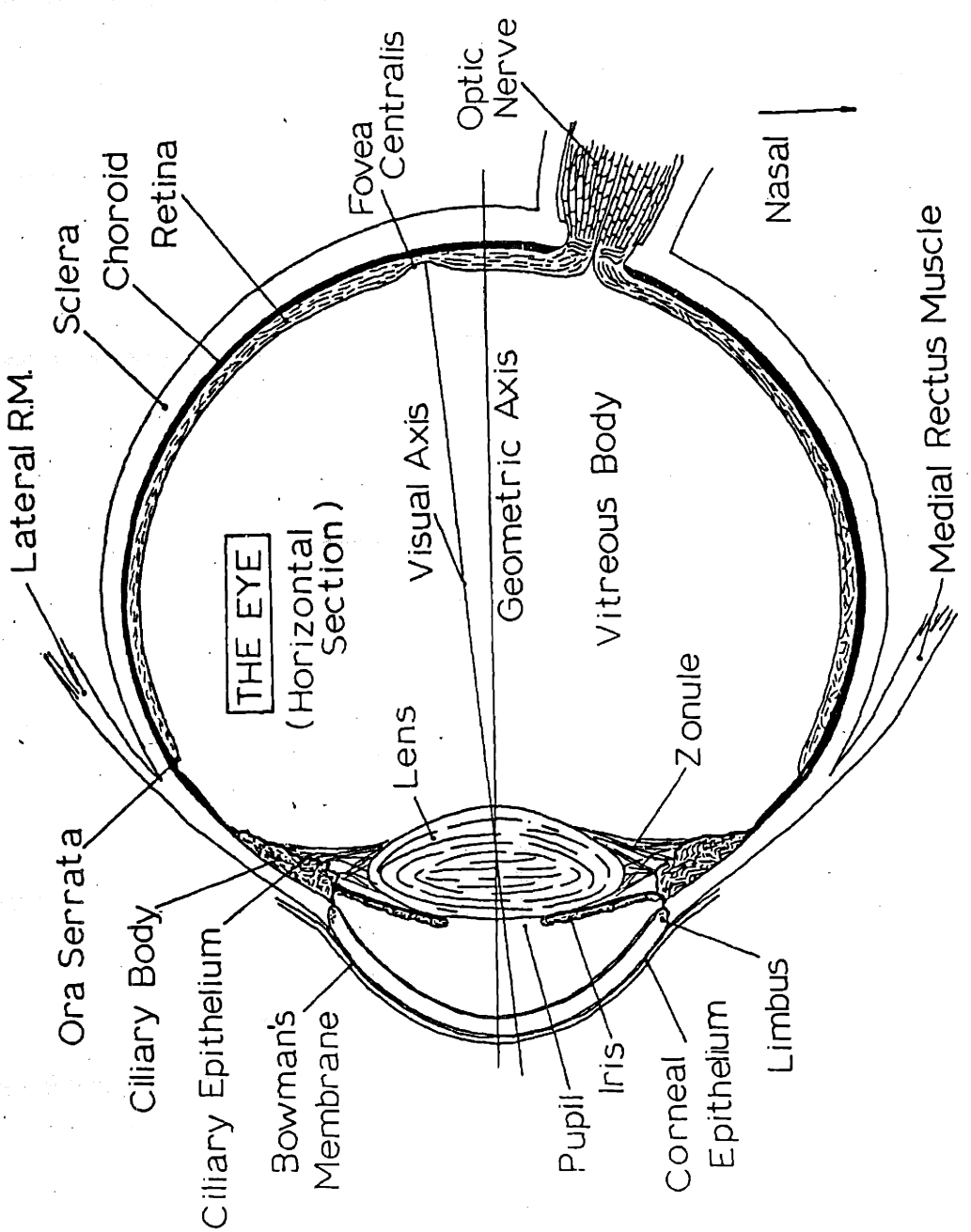

blood-aqueous barrier. In this connection Kraus and Raunino (1969) have shown that protein levels in aqueous aspirated from ostensibly normal humans increased with the amount collected, the protein concentration in the final 20 μl of a 250 μl sample being approximately double that of the first 20 μl. Neupert and Lawrence (1970) have shown that rabbit aqueous humor is highly enriched in protein (40 mg/ml versus the normal 0.6 mg/ml) if IOP falls below 12.5 mm Hg during the aspiration process. In addition, the albumin/globulin ratio of even slightly enriched aqueous was similar to that for serum, the conclusion being that the blood-aqueous barrier disruption occurs at an IOP of less than 12.5 mm Hg, if not before. These results are consistent with the known fragility of the rabbit blood-aqueous barrier. Finally, it is noted that aqueous protein levels increase after death (Grabner et al., 1978). For example, the mean concentrations of albumin and immunoglobulin G are 2.5 to 5 times greater in post mortem aqueous than in aqueous collected *in vivo* (Zirm and Schmut, 1976). In summary, only aqueous collected *in vivo* from non-traumatized eyes (i.e. eyes having an intact blood-aqueous barrier) can strictly said to be physiologic..

The concentration of selected proteins in aqueous has also been estimated. Due to their high serum levels, albumin and the globulins are the two most prevalent aqueous proteins. Grabner at al. (1978) measured 247 μg/ml of albumin and 27 μg/ml of γ-globulin in aqueous taken from cataract patients. In rabbits, albumin and the globulins accounted for the following fractions of total aqueous protein content: albumin 68%, α-globulin 9%, β-globulin 12% and γ-globulin 11%. Dernouchamps (1982) has found that transferrin concentration in the aqueous is higher than would be expected if aqueous was a simple ultrafiltrate of plasma. This was ascribed to a local production of transferrin, its presence perhaps being desirable due to its

bacteriostatic effect. Lam et al. (1983) were unable to detect fibrinogen in normal rabbit aqueous (sensitivity limit was 10 μg/ml), while fibronectin levels in bovine aqueous were measured as 2.5 μg/ml (Reid et al., 1982).

In addition, a number of authors have examined the non-protein components of aqueous. Gaasterland et al. (1979) measured amino acid and ionic content of pooled rhesus monkey aqueous. They found that: (i) aqueous osmolality equalled that of serum; (ii) ascorbate levels were approximately 70-fold higher in aqueous than in serum, and (iii) the concentration of charged free amino acids was lower in aqueous than in serum. Trope and Rumley (1985) detected norepinephrine in cataractous aqueous, while Laurent (1981) measured 1-4 μg/ml of hyaluronate in aqueous. Sandberg and Closs (1979) found very low but measurable levels of lens crystallins in normal human aqueous (α-crystallin: up to 5 ng/ml, γ-crystallin: up to 50 ng/ml).

As well as measuring concentrations of various materials in the aqueous, several authors have attempted to characterize this fluid by gel electrophoresis (SDS-PAGE) and gel exclusion chromatography (Saari et al., 1983). Litin and Herschler's (1984) one dimensionsal SDS-PAGE results showed some differences between human aqueous and serum, the most evident being a relative excess of high molecular weight proteins in the aqueous. These results led the authors to conclude that aqueous was not a simple ultrafiltrate of plasma, perhaps because certain proteins are produced and/or concentrated in the ciliary body and thus appear in aqueous with higher than expected concentrations.

In summary, the aqueous humor can be considered to be a complex mixture derived primarily as an ultrafiltrate of serum, with modifications due to leakage from tissues

within the eye (e.g. the lens) and local production of other materials (e.g. ascorbate).

Species	Total Protein (μg/ml)	Reference
Cow	582	[1]
	650	[2]
Human	112 - 230	[3]
	98 - 500	[4]
Rabbit	259	[4]
	630	[5]
Rhesus Monkey	333	[6]

Table 2.1 Previously reported aqueous humor protein levels from various species. Aqueous collected *in vivo*, protein levels measured by Lowry-Folin method, except for [4] (TCA precipitation) and [5] (Biuret method). Reference codes: [1] Hazel et al. (1985); [2] Reid et al. (1982); [3] Krause and Raunino (1969); [4] Dernouchamps (1982); [5] Neupert and Lawrence (1970); [6] Gaasterland et al. (1979).

2.2 The Aqueous Outflow System

One condition necessary for the maintenance of proper visual acuity is that the imaging and focussing components of the eye maintain a fixed geometry with respect to each other. Since the globe of the mammalian eye is inherently "floppy", rigidity is ensured by maintaining the interior of the eye at a positive pressure with respect to its surroundings. This positive IOP is generated as the aqueous humor drains from the eye through a series of resistive tissues. Thus, the flow of aqueous, in addition to providing nourishment for important intraocular tissues, serves to "inflate" the eye.

Figure 2.2 The anterior angle of the primate eye. Legend: I: iris stroma, CB: ciliary body, C: cornea, SC: Schlemm's canal, TM: trabecular meshwork. The arrow denotes the flow of aqueous humor. From Hogan et al. (1981).

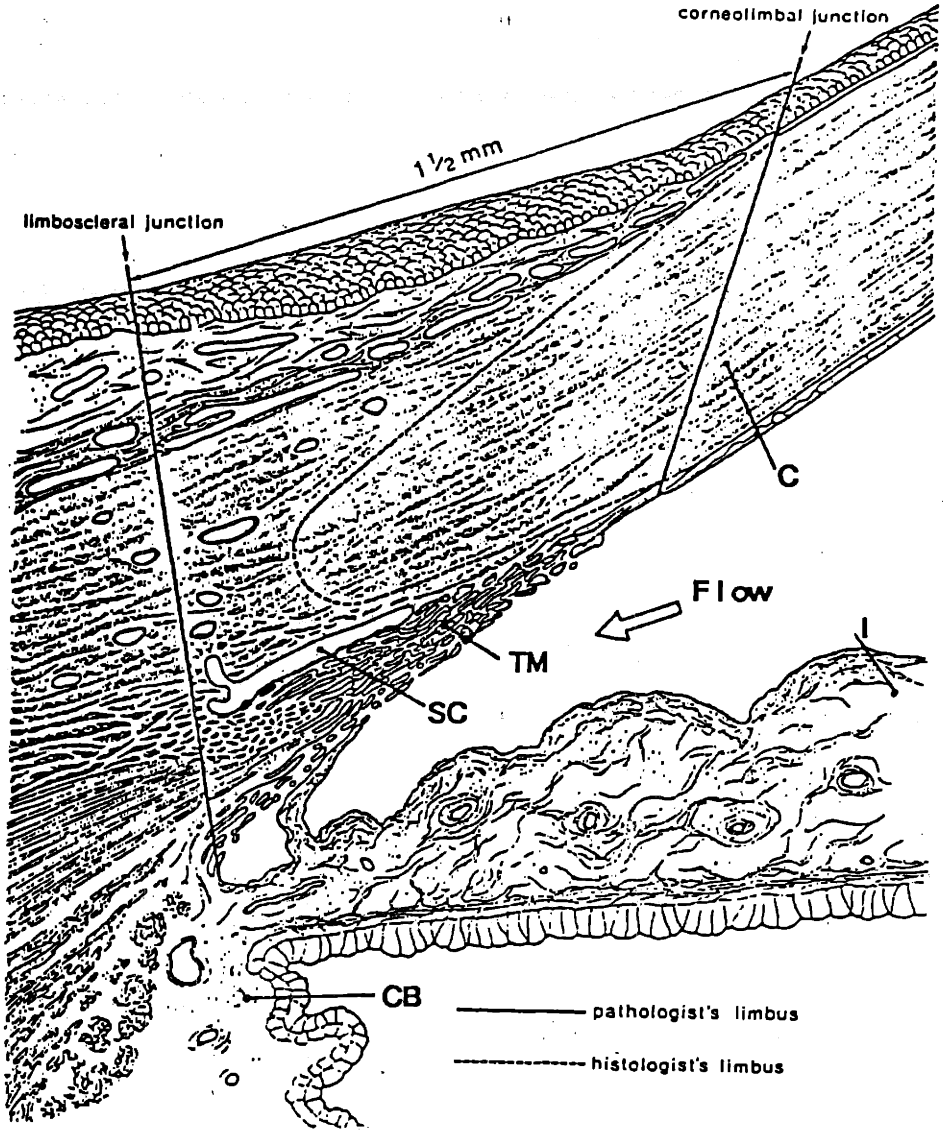

IOP is determined by three factors: the rate of aqueous production, Q, the resistance to aqueous outflow, R, and the "downstream" pressure seen by the aqueous as it leaves the eye (episcleral venous pressure). Under normal circumstances the first and last of these factors are fairly constant, so that IOP is primarily controlled by aqueous outflow resistance. It is therefore important to understand the source(s) of this resistance, which in turn leads to a study of the tissues making up the aqueous outflow system.

With reference to Figure 2.2, the major components of the so-called conventional aqueous outflow pathway (AOP) in primates may be identified as: the trabecular meshwork (TM), the canal of Schlemm and its endothelial-like lining, and the aqueous veins (collector channels). This pathway in the calf is slightly different, the TM being situated somewhat more posteriorly and Schlemm's canal being replaced by an aqueous plexus. Aqueous humor leaving the anterior chamber flows in turn through each of the above tissues before draining into the episcleral venous system, so that total aqueous outflow resistance is simply the sum of the resistances associated with each of the above components.

Attempts to estimate the relative resistance of each component by microsurgical manipulations have indicated that in the normal human eye (at normal IOP) approximately 50% of the total resistance is located in the trabecular meshwork and/or Schlemm's canal (Rosenquist et al., 1985). Theoretical analyses (Moses, 1979; Johnson and Kamm, 1983) indicate that the resistance of Schlemm's canal at normal IOP is small, and hence attention has been focussed upon the trabecular meshwork and the endothelial-like lining (inner wall) of Schlemm's canal.

Components of the Aqueous Outflow Pathway

Structurally, primate TM is composed of endothelial- and fibroblast-like cells and extracellular matrix material, and is permeated by a series of apparently open channels. It may be subdivided into three morphologically distinct regions: the uveal meshwork, the corneo-scleral meshwork (CSM) and the juxtacanalicular meshwork (JCM). Architecturally, the TM varies from a relatively open sheet-like network (the CSM) to a denser and less organized assemblage of extracellular matrix material (the JCM). The JCM, by virtue of its high density, has been felt by some investigators (Ethier et al., 1986) to be the best candidate as the primary site of outflow resistance, and there has been some very indirect experimental evidence supporting this hypothesis (Bill et al., 1980; Svedbergh, 1974). Ultrastructurally, this 10 to 15 μ thick region is composed of collagen, some elastin, and a significant amount of fibrillar material (presumably largely glycosaminoglycans, or GAGs), in addition the the resident cells and a network of "open" channels (Lutjen-Drecoll, 1973; Lindenmayer, 1983). Corrosion casting studies (Ujiie and Bill, 1984) have suggested that the JCM is quite heterogeneous, there being preferred flow pathways at several positions circumferentially about the eye, although this result may be due to a surface tension artifact associated with the casting material.

A morphometric analysis of the JCM in primates indicates that the fraction of open spaces (tissue porosity) increases with increasing fixation IOP, ranging from 17% (immersion fixation, i.e. IOP = zero) to 59% (IOP=15 mm Hg). Further analysis indicates that the apparently open channels in immersion-fixed human eyes have an effective hydraulic radius of approximately 0.4 μ (specific surface = 1.13 μ^{-1}),

and that surprisingly, the resistance of this network of channels is approximately 100 times lower than expected (Ethier et al., 1986). It has therefore been postulated that the apparently open spaces within the JCM are in fact filled with a resistive gel, a supposition which appears to be consistent with existing data on the concentration of gel-forming material within the JCM (Ethier et al., 1986).

Once the aqueous has percolated through the JCM it must traverse the inner wall of Schlemm's canal to gain entry into the canal lumen. This process is felt to either be passive (no metabolic energy required) or be of very low resistance, since most metabolic poisons (Barany, 1953) and cold (van Buskirk and Grant, 1974) have little or no effect on outflow resistance. The concept of passive transport is consistent with observations of pressure dependent "giant vacuoles" which distend into the lumen of Schlemm's canal from the inner wall endothelium. In a careful analysis of these vacuoles and the pore structures (openings) which they occasionally contain, Bill and Svedbergh (1972) have concluded that the inner wall of Schlemm's canal accounts for only about 10% of total outflow resistance. The possibility of intercellular flow through the inner wall has been considered by Raviola and Raviola (1981), the conclusion being that the magnitude of such flow was insignificant. Thus, it is most commonly held that aqueous traverses the inner wall of Schlemm's canal by flowing through vacuole-associated pores and that such pores represent a small fraction of aqueous outflow resistance. However, it should be noted that this process is very poorly understood and that the above scenario is not the only possible one.

The Gel-filled JCM Model and the Washout Effect

If the pores within the JCM are in fact filled with a resistive gel it is important to ascertain how and where this gel is produced, if and how quickly it turns over, etc. Two possible production mechanisms are: (i) the gel is produced by the local cell population, or (ii) the gel elements are produced elsewhere and are then convected into the JCM by the aqueous. A second fundamental question concerns the manner by which the gel is held in place within the JCM: is it structurally bound to solid elements (e.g. cell membranes), or does it simply "pile up" within the JCM? If the latter scenario is true one would have to postulate that the inner wall of Schlemm's canal or the JCM itself acts like a partially rejecting membrane which retains the gel-forming material while allowing free passage of fluid. Since the mechanism of fluid transport across the inner wall is not well understood, this scenario should not be excluded from the realm of possibility.

In this connection it is of interest to mention the "washout" effect, the term given to the progressive decrease in outflow resistance which occurs when eyes are artificially perfused. Although several hypotheses have been proposed to explain this phenomenon, its basic cause remains unknown. It is age-independent and species-specific: it appears to be absent in human eyes, to proceed at the remarkably similar rate of 0.4 to 0.5% of initial facility per minute in both bovine and monkey eyes (Basset-Chu and Erickson-Lamy, 1986), and to occur at a reduced rate in rabbit eyes (0.2% per minute) (Ruben et al., 1985). Because the rate of washout is less in cattle eyes preperfused with the GAG-degrading enzyme hyaluronidase, washout has been postulated to involve a washing-out of GAGs and/or proteoglycans from within the trabecular meshwork

(for review see Ruben at al., 1985). However, Knepper et al. (1984) were unable to measure any decrease in total meshwork GAG levels after prolonged perfusion and asssociated washout of rabbit eyes, suggesting that washout in the rabbit eye occurs by a different mechanism. This is in accordance with the findings of Ruben et al. (1985), who were able to stabilize outflow facility in the rabbit eye by addition of ϵ-aminocaproic acid (EACA) to the perfusion solution. EACA inhibits plasminogen activation and/or plasmin activity and is also a general serine protease inhibitor. Perhaps then the washout phenomenon in the rabbit eye is due to fibrinolytic and/or proteolytic activity and subsequent wash-out of digested fragments. Thus, it is not inconceivable that washout in rabbits may proceed by a different mechanism than in calves.

Assuming that the gel-filled meshwork model holds, there are two attractive mechanistic descriptions of washout, each one corresponding to a scenario about how the resistance-causing gel within the meshwork is established. The first of these, which is most consistant with the idea of a locally synthesized gel, proposes that the absence of some critical component(s) within artificial perfusates impairs the production of, or causes the removal of, the resistance-causing gel. The second hypothesis postulates that some component normally present in aqueous actually forms or maintains the gel, the assumption being that the gel is normally in a steady state with the convective supply of distally produced blocking materials being balanced by a local degredation or removal.

If the second hypothesis is correct, it should be possible to eliminate washout either by perfusing eyes with aqueous humor or a close analogue. In this regard Gaasterland et al. (1978, 1979) have claimed that washout in rhesus monkey eyes can be eliminated by perfusion with

aqueous humor or a mock aqueous containing many of the same components as aqueous. This latter claim has been disputed by Erickson and Kaufman (1981), who showed that Gaasterland's mock aqueous produced the same rate of washout as Barany's perfusate, a buffered saline solution containing several essential ions and glucose. The second scenario would also imply that the meshwork is capable of trapping resistive molecules. In this regard, Epstein et al. (1978a) demonstrated a decrease in facility when enucleated human eyes were perfused with serum, suggesting a plugging of the outflow channels. A similar effect has been noted due to perfusion with lens homogenates and high molecular weight soluble lens proteins (Epstein et al., 1978b). Thus, it appears that the meshwork has the ability to trap incoming resistive materials, although it is not clear that such a mechanism need operate in the normal eye.

Another consequence of this second hypothesis is that an excess of resistive material will build up in the JCM if normal degredation or removal functions are impaired. If removal is effected by resident cells, as seems likely, this could occur either due to a decrease in cell number or in cell activity. It is therefore of interest that Alvarado et al. (1981) have observed a decrease in meshwork cellularity in glaucomatous eyes, while several authors (e.g. Knepper et al., 1978) have noted that steroid administration (and hence presumably cell slowdown) leads to elevated IOP, even though GAG levels are essentially unchanged or reduced.

2.3 Filtration of Protein Solutions

Experimental Results

The filtration of protein solutions is a process of considerable practical importance in, for example, protein fractionation and/or concentration and solvent purification, and thus has been extensively studied. Experimental studies have typically employed ultrafiltration (UF) membranes designed to exclude materials having molecular weights in the tens of thousands, and thus a typical efective pore diameter for a UF membrane is on the order of 30 to 100 A (Michaels, Nelson and Porter, 1971). The membranes employed in the present study do not fall within the UF category since their effective pore diameters (~2000 A) are at least an order of magnitude greater than those for UF membranes. Hence, the filtration phenomenon examined in this work differs in this fundamental aspect from previously reported studies of protein UF. A second distinction between previous work and the current study involves the manner in which the membrane is perfused. In this work constant flow perfusion has been used, while previous experiments have been conducted at constant pressure.

The efficacy with which a particular membrane rejects a given solute is characterized by the rejection coefficient, R_m, defined as

$$R_m = 1 - \frac{c_f}{c_w} \qquad (2.3.1)$$

where c_f is the concentration of the solute in the filtrate and c_w is the solute concentration immediately adjacent to

the upstream face of the filter. Most generally, R_m depends upon filter pore geometry, solute geometry, flow conditions, and solute-pore energetic interactions, and varies between zero (non-rejecting) and one (perfectly rejecting membrane). Solute rejection can be due to simple steric exclusion, or may involve more complex interactions such as electrical effects.

A good filter has an R_m value close to one, implying that rejected solute must accumulate upstream of the filter to form a so-called polarized layer. This rejected solute acts to decrease the solvent flux, leading to the membrane fouling which is characteristic of protein (and other solute) ultrafiltration. There have classically been two mechanisms whereby rejected species can act to decrease effective membrane permeability: gel-layer formation and increased upstream osmotic pressure. In the first of these the local solute concentration at the membrane face becomes high enough for a gel layer to form on the upstream face and offer additional flow resistance (Trettin and Doshi, 1980), while in the second the excess solute upstream of the filter produces an increased osmotic pressure opposing the driving pressure gradient (Vilker et al., 1981). A model combining both mechanisms has been presented by Reihanian et al. (1983).

Several authors have investigated the importance of protein adsorption onto the filter surface. Cheryan and Merin (1980) present transmission electron micrographs of UF membranes used in filtering cottage cheese whey which show a well-defined adsorbed layer of thickness 0.1 to 0.5 μ on the upstream membrane face. Matthiasson (1983), Fane et al. (1983b) and Ingham et al. (1980) have measured adsorbed protein levels on UF membranes and correleted adsorbed amount with membrane resistance. Adsorbed levels varied from ~1 $\mu g/cm^2$ (Matthiasson, 1983) to ~175 $\mu g/cm^2$ (Ingham et

al., 1980), and increased membrane resistance was consistent with the formation of an adsorbed layer on the upstream face. Fane et al. (1983b) also demonstrated that filter washing with distilled water reduced membrane resistance, presumably by removing loosely-associated protein.

The membranes used in the above-mentioned studies had exclusion limits sufficiently low as to ensure almost complete solute rejection, and thus it seems reasonable to expect that protein adsorption would occur on the upstream membrane face. When one instead considers protein filtration through partially rejecting membranes (pore diameter $\geq$ protein characteristic dimension) it seems possible that protein adsorption onto both the pore walls and the membrane surface could occur. This is supported by the work of Fane et al. (1983a), who noted that partially permeable membranes blocked up more quickly and to a greater extent than did impermeable ones. These authors attributed such effects to protein adsorption within the pore and subsequent pore plugging. This is consistent with reports by Munch et al. (1979), Schultz et al. (1979) and Yavorsky (1981) indicating that monolayer adsorption onto pore walls occurs when track-etched membranes are exposed to albumin and γ-globulin solutions. Yavorsy has also noted that the effective layer thickness for albumin adsorbed onto mica track-etched membranes irreversiby increased during perfusion experiments when wall shear stresses exceeded 50 Pa, which was attributed to shear-induced denaturation of the adsorbed albumin.

Theory

The general problem of solute transport through rejecting membranes has been elegantly treated by Kedem and Katchalsky (1958) and further refined by Spiegler and Kedem

(1966). By using irreversible thermodynamics to relate solute and solvent fluxes to their driving forces, the following expressions for the volume flux of solvent, J_v, and molar flux of solute, J_s, were derived

$$J_v = L_p(\Delta p - \sigma\Delta\pi) \qquad (2.3.2)$$

$$J_s = \omega\Delta\pi + (1-\sigma)J_v c \qquad (2.3.3)$$

Here Δp and $\Delta\pi$ are the transmembrane differences in pressure and osmotic pressure, while L_p, ω and σ are proportionality constants which characterize the membrane/solute/solvent combination. Specifically, L_p is the membrane hydraulic permeability (solvent permeability), ω is the solute permeability and σ is the Staverman refelection coefficient ($1 \geq \sigma \geq 0$). The rejection coefficent R_m is a function of both the reflection coefficient σ and the axial pore Peclet number $Pe = (1-\sigma)J_v L/D_{pore}$,

$$R_m = \frac{\sigma(1 - e^{-Pe})}{1 - \sigma e^{-Pe}} \qquad (2.3.4)$$

In the above definition of Peclet number L is the pore length and D_{pore} is the solute diffusion coefficient within the pore (hindered diffusion coefficient). It is seen that at high flow rates ($Pe \gg 1$) R_m approaches σ, while for low flow rates R_m approaches zero (for $\sigma \neq 1$).

Because all filtration characteristics for a given membrane/solute/solvent combination are in principle specified by L_p, ω and σ, it is desirable to relate them to observable properties such as pore and solute geometries.

For example, if one assumes that the membrane is traversed by n cylindrical pores per unit area (radius = R_o) then

$$L_p = \frac{n\pi R_o^4}{8\mu L} \qquad (2.3.5)$$

where μ is solvent viscosity. Unfortunately, estimation of σ and ω is considerably more difficult. The situation of steric exclusion of hard spheres within cylindrical pores has been treated with some success by Anderson and Quinn (1974), while calculations of σ for rigid non-spherical solutes in circular and rectangular shaped pores has been undertaken by Anderson (1981). Situations in which finite solute concentration and/or electrical effects are important have also been considered (e.g. Mitchell and Deen, 1984).

For the transport of rigid solutes of various shapes through cylindrical pores, Anderson (1981) has shown that σ can be closely approximated by

$$\sigma = (1 - \Phi)^2 \qquad (2.3.6)$$

where Φ is equilibrium bulk-pore partitioning coefficient, i.e. the ratio of bulk to in-pore concentration (based on total pore volume). This formula assumes that pore-bulk equilibrium exists, i.e. that no seiving occurs at the pore mouth, which will be the case when the Peclet number based on pore radius $Pe_a = Ua/D$ is much less than one (Munch et al., 1979). For the particular case of steric exclusion of spherical solutes of radius a from cylindrical pores of radius R_o, $\Phi = (1 - a/R_o)^2$, while Φ values for other geometries may be obtained from Anderson's 1981 paper. In the case of high Peclet number (convection dominated) flow

the solute and solvent fluxes will be primarily governed by L_p and σ ($=R_m$ for $Pe \gg 1$), and thus the system is described by equations (2.3.2) through (2.3.6).

2.4 Protein Adsorption onto Artificial Surfaces

It has long been recognized that artificial surfaces in contact with blood or other protein-containing solutions will adsorb proteins from bulk solution. The layer of adsorbed protein which forms is believed to mediate interactions between cells and the artificial substrate, and hence its characteristics are an important determinant of the biocompatibilty and/or thrombogenicity of implanted artificial materials (Horbett, 1982). This has made the problem of protein/substrate interaction an important bioengineering topic in its own right.

A review of the literature indicates that protein/substrate interactions are highly complex and that adsorption behavior depends strongly on protein type. These characteristics are primarily due to the heterogeneous and complex three-dimensional structure of proteins, which allows both positively- and negatively-charged regions and/or hydrophilic and hydrophobic regions to coexist on the surface of a single macromolecule. This fact, as well as the relatively "rigid" structure of proteins, explains why statistical thermodynamic theories describing the adsorption of random coiling macromolecules (e.g. Motomura and Matuura, 1969) are not applicable to proteins.

Isotherms

The uniqueness of the adsorption characteristics for each protein/substrate pair complicates the drawing of general conclusions about adsorption isotherms, although common features do emerge. Considering first the adsorption from single protein solutions, it is found that at equilibrium the mass of protein adsorbed per unit area, Γ, is an increasing function of the bulk protein concentration, c, and that at high values of c the adsorbed amount almost always tends towards some plateau concentration, Γ_∞. Although there is considerable variation, Γ_∞ typically ranges from 0.1 to 1 $\mu g/cm^2$ and is attained at bulk solution concentrations between 50 and 1000 $\mu g/ml$. Typical values for Γ_∞ for albumin, fibrinogen and fibronectin are displayed in Table 2.2.

As concerns the precise shape of the isotherm, several investigators have claimed Langmuir adsorption

$$\frac{\Gamma}{\Gamma_\infty} = \frac{c}{k_2/k_1 + c} \qquad (2.4.1)$$

which is characterized by a linear increase in Γ for low bulk concentrations and an asymptotic approach to Γ_∞ at high concentrations (see Figure 2.3). The ratio k_2/k_1 is a characteristic concentration (at which $\Gamma = 0.5\Gamma_\infty$), while k_1 and k_2 may be identified as kinetic adsorption and desorption rate constants (see equation (2.4.2)). Experimental studies showing Langmuir-like behavior include those of Lee and Kim (1974) concerning the adsorption of albumin, γ-globulin and prothrombin to silastic rubber, flourinated ethylene/propylene and urethane/urea copolymer, and those of Chan and Brash (1981) for fibrinogen adsorption

Figure 2.3 The Langmuir isotherm. The adsorbed amount asymptotes to $\Gamma/\Gamma_\infty = 1$ and is one half of maximal at $c=k_2/k_1$.

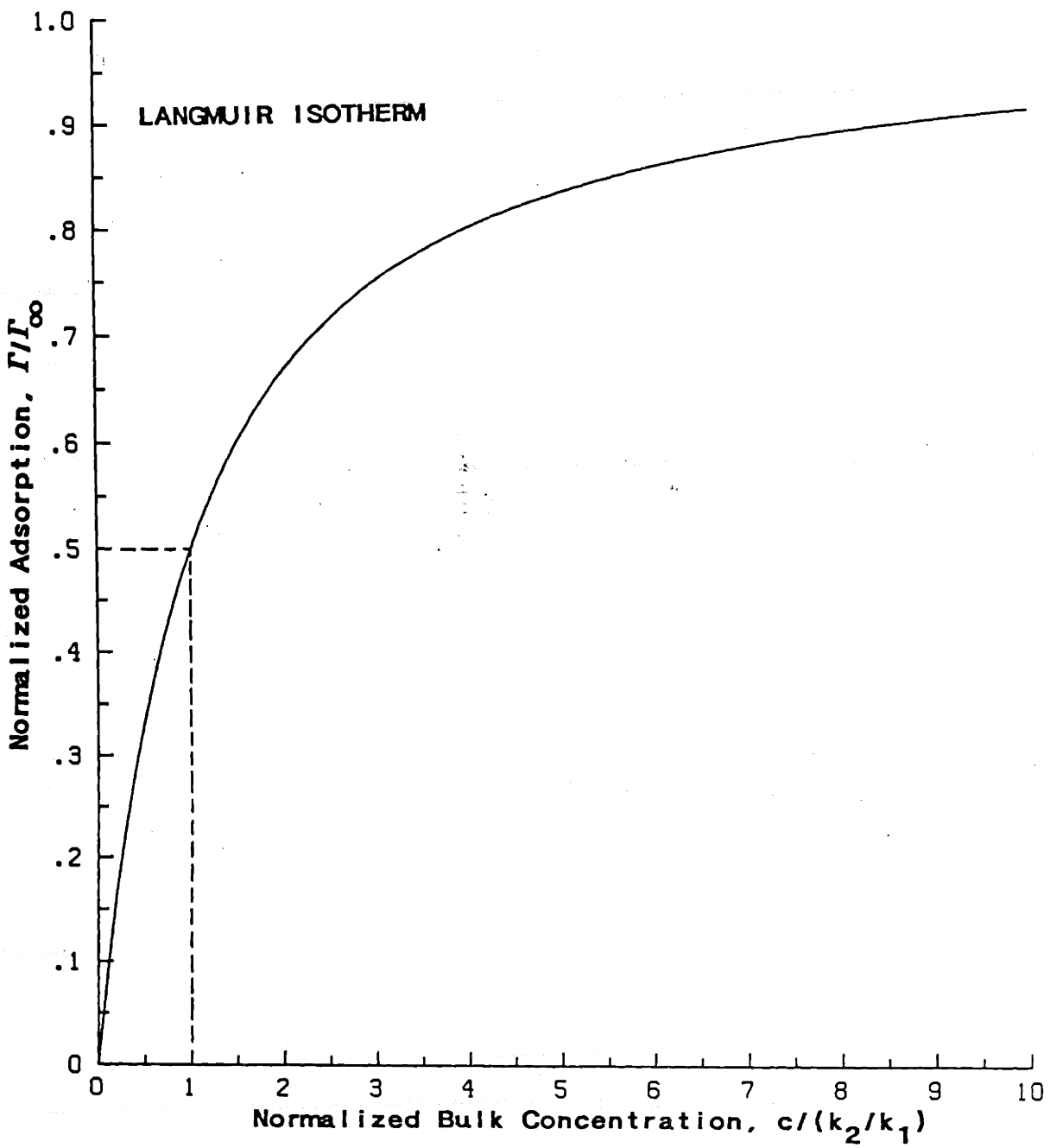

Brynda et al. (1984) for albumin adsorption onto polyethylene appear to be distinctly non-Langmuirian, while Lok et al. (1983) have shown that albumin adsorption onto poly(dimethylsiloxane) has both Langmuirian and non-Langmuirian characteristics. Furthermore, Lyklema (1984) has noted that Langmuir-like protein adsorption may be fortuitous, since several of the ususal Langmuir premises are not satisfied. In particular, surfaces are often heterogeneous, the protein is usually altered upon adsorption and lateral interactions are important. (In this connection, Marmur and Cooper (1982) have presented an alternate model which leads to Langmuir-like isotherms.) In summary, considerable variation in isotherm type exists from study to study, but at least for certain protein/substrate combinations the Langmuir isotherm seems to be appropriate.

Other factors complicating isotherm description are the effects of fluid shear stress at the interface and the "aging" of the protein layer. For example, Chan and Brash (1981) have showed that equilibrium adsorption of fibrinogen onto glass is independent of wall shear rate γ up to γ-2100 s^{-1}, while Lee and Kim (1974) demonstrated a strong dependance of Γ on shear for albumin adsorption onto silastic rubber. The "aging" of adsorbed protein appears to be a fairly ubiquitous phenomenon in which adsorbed protein (initially perhaps bound at only one site), slowly changes its conformation so as to be able to bind to the substrate at multiple sites (Lyklema, 1984). As this process occurs desorption should become less likely, and studies generally show that desorption of established protein films from hydrophobic surfaces proceeds very slowly, if at all (e.g. Lok et al., 1983; Soderquist and Walton, 1980). Soderquist and Walton have postulated that initial protein uptake is reversible, but that as protein resides on the surface it becomes less likely to desorb. This scenario is contradictory to the usual equilibrium concept in which

adsorption and desorption balance at each point on the isotherm, and implies that the shape of the isotherm will depend to some extent on the history of protein exposure to the surface, as has occasionally been experimentally observed (e.g. Jonsson et al., 1982). A second observation which emphasizes the complex nature of the equilibrium adsorption process is that although desorption of established protein films into pure buffer occurs very slowly, this exchange is much more rapid into protein-containing buffer (Brash and Samak, 1978). In the latter case the rate of turnover is found to be dependent on shear rate, while the extent of turnover is dependent both upon shear rate and bulk protein concentration, suggesting that desorption may be facilitated by protein-surface collisions.

Adsorption from protein mixtures is even more complex. For example, adsorption from mixtures of albumin and fibrinogen shows an initial enrichment of albumin on the surface, followed by a gradual replacement by fibrinogen (Gendreau et al., 1982). Brash and ten Hove (1984) have shown that more fibrinogen is adsorbed from plasma diluted 100-fold than there is from pure plasma, i.e. that the adsorption isotherm exhibits a clear maximum, an effect which was ascribed to competition for fibrinogen binding sites by an unknown protein (Horbett, 1984; Brash and ten Hove, 1984).

Protein/Surface	$\Gamma_\infty(\mu g/cm^2)$	Plateau c ($\mu g/ml$)	Method	Ref.
albumin/PDMSO	0.14	100	TIRF	[1]
albumin/various	0.1 - 0.32	1000	RL	[2]
albumin/various	0.55 - 4.5	30 - 90	RL	[3]
albumin/poly-ethylene	0.35	4000	RL	[4]
fibrinogen/various	0.03 - 1.12	1000	RL	[2]
fibrinogen/various	0.23 - 0.77	1000	SD	[5]
fibrinogen/various	0.2 - 0.6	8000 - 19000	SD	[6]
fibrinogen/glass	0.75	200	RL	[7]
fibronectin/hydro-phobic silica	0.27	20-30	EL	[8]
fibronectin/hydro-phobic silica	0.19	NR	TIRF	[9]

Table 2.2 Published values for maximal (plateau) adsorbed amounts, Γ_∞, and corresponding bulk concentrations, c, for albumin, fibrinogen and fibronectin on various surfaces. TIRF- total internal reflection flourescence, PDMSO- poly(dimethylsiloxane), RL - radiolabelling, SD - solution depletion, EL - elipsometry, NR - not reported. Reference codes: [1] Lok et al. (1983), [2] Brash and Uniyal (1979), [3] Lee and Kim (1974), [4] Brash and Samak (1978), [5] Brynda et al. (1981), [6] Soderquist and Walton (1980), [7] Brash and Davidson (1976), [8] Jonsson et al. (1982), [9] Iwamoto et al. (1985).

Kinetics

As has been shown by Lok at el. (1983), adsorption is often fast enough to be rate limited by diffusional transport to the adsorbing surface. Hence, in the absence of data to the contrary, experimentally observed kinetic rates should be regarded as lower bounds.

Due to the complexity of the adsorption/desorption process, kinetic data are usually presented as $d\Gamma/dt$ values at the beginning of an adsorption or desorption experiment. For our purposes it will be convenient to reduce data for $d\Gamma/dt$ to estimates for rate constants, which in turn requires a model description of the adsorption/desorption kinetics. Perhaps the simplest such model is that describing Langmuir adsorption (Adamson, 1960)

$$\frac{d\Gamma}{dt} = k_1 c\Gamma_\infty(1- \frac{\Gamma}{\Gamma_\infty}) -k_2\Gamma \qquad (2.4.2)$$

where k_1 (k_2) is the adsorption (desorption) rate constant introduced earlier. The first and second terms in equation (2.4.2) represent adsorption and desorption, respectively, equation (2.4.1) being obtained when they are equated.

Equation (2.4.2) may be regarded as a simple first attempt to characterize kinetic behavior in terms of rate constants k_1 and k_2. From (2.4.2) we identify

$$k_2 = - \frac{1}{\Gamma} \frac{d\Gamma}{dt} \quad \text{(desorption exp't., } c=0\text{)}$$

$$k_1\Gamma_\infty = \frac{1}{c} \frac{d\Gamma}{dt} \quad \text{(adsorption exp't., } \Gamma=0\text{)}$$

and values for k_2 and $\Gamma_\infty k_1$ calculated in this manner from published reports are displayed in Tables 2.3 and 2.4. It can be seen that there is considerable variation among the presented data, especially for desorption. This may represent real variation, experimental artifact (transport-limited behavior), measurement limitations or the inadequacy of (2.4.2). Nonetheless, the data does serve to approximately indicate expected orders of magnitude for kinetic constants.

Adsorbed Layer Structure

Adsorbed amounts are usually consistent with monolayer formation (Lyklema, 1984), although for some protein/surface pairs multilayer formation does seem to be a possibility (Burghardt and Axelrod, 1981). Paynter et al. (1984) have noted that protein coverage may be non-uniform, i.e. that the adsorbed layer may be interrupted by "holes", although this contradicts the scanning electron microscopic studies of Rudee and Price (1985) for fibrinogen and albumin adsorption onto polycarbonate. Jonsson at el. (1982) have suggested that adsorbed fibrinogen unfolds at low surface concentrations (but not at high), a result sililar to that reported for γ-globulin adsorption by Horbett (1982). Denaturation seems to be more likely to occur if the surface is strongly hydrophobic and the protein is less stable (Walton and Koltisko, 1982).

To summarize, because of the complexity of the adsorption process, it is difficult to predict specific details about how quickly and to what extent aqueous proteins will adsorb onto test filters. Comparison of previously reported adsorption characteristics with those observed in the present study will be primarily qualitative in nature.

Protein/Surface	$k_1 \Gamma_\infty$ (cm/s)	Method	Ref.
albumin/hydrophilic quartz	2.2×10^{-5}	TIRF	[1]
γ-globulin/hydrophilic quartz	6.0×10^{-5}	TIRF	[1]
albumin, γ-globulin, prothrombin/various	0.7×10^{-5} to 5×10^{-5}	radio-labelling	[2]
albumin/glass, siliconized glass and polystyrene	2.6 to 6.4×10^{-5}	radio-labelling	[3]
albumin/PDMSO	$> 1.7 \times 10^{-4}$	TIRF	[4]
fibrinogen/PDMSO	$> 6.7 \times 10^{-5}$	TIRF	[4]

Table 2.3 Published values for measured protein adsorption rates onto various surfaces. See text for calculation method. TIRF= total internal reflection flourescence, PDMSO=poly(dimethylsiloxane). Reference codes: [1] van Wagenen et al. (1982); [2] Lee and Kim (1974); [3] van Dulm and Norde (1983); [4] Lok et al. (1983).

Protein/Surface	k_2 (s^{-1})	Method	Ref.
albumin/hydrophilic quartz	0.4	TIRF with buffer flow	[1]
γ-globulin/hydrophilic quartz	3.7×10^{-3}	" " "	[1]
albumin/polyethylene	$5 - 11 \times 10^{-6}$	double labelling	[2]
albumin/hydrophilic quartz	5×10^{-3}	TIRF/photobleaching	[3]

Table 2.4 Published values for measured protein desorption rates from various surfaces. See text for calculation method. TIRF= total internal reflection flourescence. Reference codes: [1] van Wagenen et al. (1982); [2] Brash and Samak (1978); [3] Burghardt and Axelrod (1981).

2.5 Membrane Characterization

Pore Geometry of Track-Etched (Nuclepore) Membranes

This study has employed track-etched polycarbonate and polyester membranes manufactured by Nuclepore Corp. (Pleasanton, CA). Track-etched membranes are characterized by their highly uniform, regular and straight-through pore geometry, a consequence of their two-step manufacturing process, in which a thin film of polymer substrate is exposed to a collimated beam of ionizing radiation and then bathed in an etching solution. As was first demonstrated by Price and Walker (1962), the etching preferentially occurs along the damage tracks produced by the radiation, resulting initially in very fine, straight through pores. By altering the exposure time of the polymer sheet to the etching solution, the degree of etching, and hence also the pore diameter, can be controlled. Thus, in principle it is possible to obtain a homogeneous population of right cylindrical pores with axes normal to the polymer sheet.

The actual pore geometry of Nuclepore polycarbonate membranes has been experimentally studied. Using scanning electron microscopy of sectioned membranes, Liabastre and Orr (1978) confirmed the right circular cylindrical pore geometry claimed by the manufacturer, while scanning electron micrographs of the filter surface indicated only a small degree of pore overlap for 0.2 μ nominal pore diameter membranes. Micrographs also revealed that not all pores have axes normal to the filter surface, presumably due to imperfect collimation of the ionizing radiation. Deen at al. (1981) have estimated that this pore "tilting" causes

the mean pore length to exceed the filter thickness by 6.8 %, and measured pore lengths L (Deen at al., 1981; Deen and Smith, 1982) are in good agreement with values calculated from the formula

$$L = 1.068 \text{ (nominal membrane thickness)} \qquad (2.5.1)$$

Unfortunately, the remaining geometric parameters which characterize a membrane, namely the mean pore radius $\overline{R}_o$ and the pore density n usually deviate somewhat from the manufacturer's nominal values. Experimental studies suggest that actual and nominal pore densities are in slightly better agreement than are actual and nominal pore diameters, and that larger pore diameter membranes more closely conform to nominal specifications. (Table 2.5).

Mean Pore Diameter (μ)		Number Density (cm^{-2})	
Nominal	**Measured**	**Nominal**	**Measured**
0.030	0.058 0.043	6×10^8	4.3×10^9 8.73×10^8 [1]
0.1	0.135	3×10^8	3.3×10^8 [2]
0.2	0.24	3×10^8	4×10^8
0.4	0.39	1×10^8	1.2×10^8
0.6	0.63	3×10^7	2.8×10^7
1.0	0.84 1.15	2×10^7	2.3×10^7 1.9×10^7 [2]

Table 2.5 Previously published values for measured and nominal characteristics of Nuclepore polycarbonate membranes. Measured values from Liabastre and Orr (1978), except: [1] mean of 4 values from Deen and Smith (1982), [2] Deen et al. (1981).

The pore size distribution on a single filter has been measured by Liabastre and Orr (1978) and Spurney and Lodge (1968), and their data indicate a fairly tight distribution about the mean. For example, as a first approximation the data of Liabastre and Orr for nominal 0.2 μ diameter membranes can be fit to a normal distribution with mean radius $\bar{R}_o = 0.121\ \mu$ and standard deviation $\sigma_R = 0.013\ \mu$. Assuming that the relationship $\sigma_R \sim 0.1\bar{R}_o$ is typical, one can estimate the difference between the number mean pore radius and the mean pore radius measured in a perfusion experiment, $\bar{R}_{flow}$. Assuming Poiseuille's law for flow through N parallel pores of length L and radii $\{R_i\}_{i=1\ldots N}$ holds, the quantity $\bar{R}_{flow}$ is given by (for N large)

$$(\bar{R}_{flow})^4 = \frac{8\mu QL}{N\pi\,\Delta p} = \frac{1}{N}\sum R_i^4 = \int_0^\infty R^4\, p(R)\, dR \qquad (2.5.2)$$

where Q is the total flow through the filter, Δp is the driving pressure drop and p(R) is the pore size distribution function. If the pore radii are assumed to be normally distributed with mean $\bar{R}_o$ and standard deviation σ_R, equation (2.5.2) produces

$$\bar{R}_{flow} = \bar{R}_o \left[1 + 6\left[\frac{\sigma_R}{\bar{R}_o}\right]^2 + 3\left[\frac{\sigma_R}{\bar{R}_o}\right]^4\right]^{1/4} \qquad (2.5.3)$$

Thus, if $\sigma_R \sim 0.1\bar{R}_o$ then $\bar{R}_{flow}$ and $\bar{R}_o$ will differ by less than 2%, and we may consider $\bar{R}_o$ to be equal to $\bar{R}_{flow}$. We

will therefore simply identify membranes by a single pore radius, R_o ($=\bar{R}_o$).

In the present study we have characterized membranes by measuring their hydrodynamic resistance, a quantity which will in general depend on N, R_o and L. In order to fix two of these three unknowns we will assume that N and L are given by their nominal values (in conjunction with equation (2.5.1)), and will regard R_o as a measured parameter. The justification for this approach is twofold: (i) membrane thickness and pore density appear to deviate somewhat less from nominal specifications than does pore radius; and (ii) because of the fourth power dependence of hydrodynamic resistance on R_o, results will be much more sensitive to errors in this parameter than they would to errors in N or L.

There will in general be pore entrance pressure losses in addition to the usual Poiseuille pressure drop. If we approximate the flow into a pore mouth as flow from an infinite half-plane through a circular aperture of radius R_o the associated pressure drop is given by Sampson's relationship (Happel and Brenner, 1973)

$$\Delta p_{entry} = \frac{3q\mu}{R_o^3} \tag{2.5.4}$$

where q is the volumetric flow through the pore. Comparing this with the Poiseuille pressure drop Δp_{pore} associated with flow down a pore of length L one obtains

$$\frac{\Delta p_{entry}}{\Delta p_{pore}} = \frac{3\pi}{8}\frac{R_o}{L} \tag{2.5.5}$$

which for the pore sizes of interest is much less than one. Similarly, for $R_o \ll L$, a parabolic velocity profile will

quickly develop within the pore, and thus we need not concern ourselves with entrance effects.

The pore geometry of polyester track-etched filters has been studied less extensively than that of polycarbonate membranes. However, in this study we will not require detailed information about polyester filter pore geometry, and hence we will accept the manufacturer's nominal pore geometry as being approximately correct.

Surface Chemistry of Track-Etched Membranes

The substrate material used to manufacture polycarbonate membranes is a polymeric derivative of bisphenol-A, which results in a hydrophobic (non-wetting) filter. A wettable filter is produced by bathing the etched poycarbonate substrate in a bath of poly(vinylpyrollidone) (PVP) and alcohol and then allowing the alcohol to evaporate off. This results in an adsorbed (rather than covalently bonded) layer of PVP on the polycarbonate surface which can be desorbed by appropriate agents. If the PVP bathing step is skipped one obtains a surfactant-free (PVP-free) non-wetting membrane which has the same pore geometry as a regular (wettable) polycarbonate membrane.

Several studies (Deen and Smith, 1982; Bisio et al., 1980; Meares and Page, 1972) have observed that the pore walls of polycarbonate filters carry a negative charge, the magnitude of which increases with increasing salt concentration. In 0.1 M NaCl Meares and Page (1972) calculated surface charge densities of between -5.2 and -8.1 mC/m^2, the exact value depending on the pore size of the filter.

Pore Geometry of Tortuous Path (Millipore) Membranes

This study has also employed tortuous path membranes of the Durapore type, manufactured by Millipore Corp. (Bedford, MA), which are composed of a randomly oriented polymer matrix, leading to a highly irregular pore structure. Because of this irregular geometry it is impossible to give a precise value of pore diameter for such membranes. In practice, filters are characterized by an effective pore diameter derived from a surface tension experiment (bubble point test) in which the break-through pressure required to force air through a wetted filter is measured. Since air will break through the largest pores first, one may expect that pore dimensions obtained in this manner will be an upper bound for the actual pore size distribution.

In addition to differences in pore geometry, Millipore (Durapore) and Nuclepore filters differ in porosity and thickness. For example, Nuclepore 0.2 μ polycarbonate filters have a thickness of 10 μ and a porosity of ~15 %, while 0.22 μ Durapore membranes are ~100 μ thick and have a porosity of ~80 %. Thus, the total pore volume in a 0.22 μ Durapore membrane is approximately 50 times larger than that in a 0.2 μ polycarbonate filter.

Surface Chemistry of Tortuous Path Membranes

Durapore membranes are manufactured from the non-wetting material polyvinylidine diflouride (PVDF), and are then coated with a surfactant (wetting agent) to produce a wettable membrane. In contrast to Nuclepore filters, the wetting agent is grafted (covalently bonded) directly to the

filter material, and thus should remain on the filters except under extreme conditions. Both wettable (GVWP type) and non-wettable (GVHP type) filters are available from the manufacturer.

CHAPTER THREE: MATERIALS AND METHODS

This chapter describes experimental protocols utilized in the course of this work.

3.1 Cleaning Procedures

Since small particulate matter can occlude sub-micron size filter pores and hence lead to erroneous test results, it was necessary to scrupulously clean all glassware, syringes, pipettes, etc. before each filter perfusion experiment. This was accomplished by filtering a large volume (approximately 5 litres) of distilled deionized water through a 0.08 μm Nuclepore polycarbonate membrane using a filter flask. Each piece of equipment which came in contact with either the test fluids or the filters was first washed at least three times with this filtered water (henceforth, FH_2O). Washed equipment and containers of test fluid were protected from airborne dust by covering with Parafilm M (American Can Co., Greenwich, Conn.).

3.2 Collection and Preparation of Calf Aqueous Humor

Calf eyes were obtained from a commercial slaughterhouse (Joseph T. Trelegan and Co., Cambridge, MA). The calves (Gurnsey and Holstein breeds) were raised at New England area farms and were generally 2 to 8 days of age at death. They were killed by exsanguination after being stunned and inverted. The eyes were enucleated at the slaughterhouse (usually by the same person on each day) and were transported in an insulated container filled with a mixture of frozen and liquid isotonic saline. Eyes typically arrived within 3 to 4 hours of death and were used

as soon as possible upon arrival (ususally within one hour). In several experiments aqueous was withdrawn from eyes at the slaughterhouse immediately after death.

The aqueous humor was withdrawn from the anterior chambers of up to 30 calf eyes and pooled. Eyes were rejected if they were noticeably bloody in the limbal region, had large nicks in the cornea or sclera, had lens material or other opaque substances in the anterior chamber or displayed other anterior chamber abnormalities, as determined by simple visual observation.

A 3 ml Monoject Syringe (polypropyelene barrel: Sherwood Medical, St. Louis, MO) with attached 23 gauge needle (stainless steel with aluminum hub) was filled with approximately 1 ml of FH_2O, which was then used to wash the cornea. Aqueous was withdrawn by inserting the needle through the mid-peripheral cornea at approximately a 45 degree angle with the plane of the iris. The needle opening was positioned over the pupil with the bevel at 90 degrees to the cornea and the aqueous was slowly aspirated from the anterior chamber. Gentle aspiration continued until the anterior chamber had collapsed, a typical collected volume per eye being 200 to 500 μl, depending on the size of the eye. The needle was slowly removed from the eye and the aqueous was pooled in a Pyrex beaker. The first 3 to 5 drops of aqueous (last drops collected) were discarded so as to exclude material which might have entered the syringe during the last stages of aqueous withdrawal, when the anterior chamber was nearing complete collapse. The same syringe was then filled with ~1 ml of FH_2O and the above process was repeated. Partially filling the syringe with FH_2O in this manner served the dual purposes of rinsing the cornea and cleaning the syringe between collections. The pooled aqueous was kept at room temperature during the collection process (~25 minutes) and subsequently

refrigerated at 4 C.

The pooled aqueous humor was then pipetted into ultracentrifuge tubes (Ultra-clear, type 344091; Beckman Instruments Inc., Palo Alto, CA) and ultracentrifuged in a Beckman type 50 fixed angle rotor for 1 hour at 4 C with a peak centrifugal force of 100,000 to 110,000 g, with the exception of several runs which were carried out under the same conditions in a Beckman swinging bucket rotor (type SW28) with Ultra-clear type 344061 tubes. After ultracentrifugation the upper 75-80% of the supernatant was gently pipetted off and transferred to a Venoject vacuum blood collection tube (silicone coated borosilicate glass: Trumo Medical Corp., Elkton, MD). This tube was packed in ice and transported to MIT for testing. The entire process typically took 4 hours.

In several tests fresh aqueous was collected immediately after death, the same general procedure being used with the following slight variations. Aqueous was collected from eyes *in situ*, and a separate syringe was used for each eye. On several occasions eyes were then enucleated and dissected to check for suprachoroidal hemorrhage, and if evidence of hemorrhage was found the collected aqueous was discarded. Aqueous was then pooled and transported on ice to be centrifuged and processed as usual.

In several tests a sample of pooled calf aqueous was drawn into a 3 ml Monoject syringe, frozen and stored at -20 C for four weeks. It was then thawed, prepared and tested in the usual manner.

Fibronectin and fibrinogen were selectively precipiated from calf aqueous by addition of 9% chilled absolute ethanol according to the protocol of Cohn et al. (1946).

Citrated aqueous was prepared by adding 7 volumes of aqueous to 1 volume of filtered 3.8% sodium citrate, prepared in filtered Ca- and Mg-free phosphate buffered saline, pH 7.3. In addition to the usual washing with FH_2O, all glassware, etc. used in this experiment was washed with filtered 3.8% sodium citrate prior to use.

Calf aqueous humor was separated into high and low molecular weight-containing fractions by using a washed Centricon-10 centrifugal micro-concentrator (Amicon Corp., Danvers, MA). This centrifugally driven ultrafiltration cell contains a membrane with nominal molecular weight cutoff of 10,000 daltons. Separation was effected by centrifugation at 5000 g for 1 hour at 10 C. The retentate (containing high molecular weight material) and filtrate (containing low molecular weight material) were diluted with filtered Dulbecco's phosphate buffered saline (DPBS -- see Section 3.4) so that their volumes equalled the original aqueous volume, and were then ultracentrifuged and processed in the usual manner.

3.3 Collection and Processing of Aqueous from Other Species

Monkey aqueous humor (courtesy of Dr. Douglas Gaasterland) was obtained from live rhesus monkeys (*Macaca mulatta*) anesthetized with sodium phenobarbitol. The collection procedure was similar to that for calf eyes, except that the collection syringe was not washed or emptied between each collection, the aqueous being allowed to accumulate in the syringe. The collection was carried out *in situ* with a 23 gauge needle, and the cornea was not washed with FH_2O before collection. Approximately 150 to 200 μl of aqueous was collected from each eye.

Several samples of monkey aqueous humor were ultracentrifuged in the ususal manner, while a second batch was tested without ultracentrifugation. This second batch was further subdivided and either tested directly or after being prefiltered through a 1.0 μm Nuclepore polycarbonate filter. In all cases the fluid was tested 5 to 6 hours after collection.

Human aqueous humor was collected during the course of extracapsular cataract extraction surgery or glaucoma filtration surgery (courtesy of Dr. Robert Bellows). The procedure was described to patients who then gave verbal consent or signed informed consent forms. Conjunctival bleeding was prevented by cauterization. A small half-thickness limbal incision was made in the cornea with a Wheeler knife and the surrounding area was irrigated, care being taken to avoid contamination of the collection site. A 30 gauge needle was inserted into the anterior chamber through the incision and aqueous was withdrawn. Due to sterility requirements the collection syringes were not prewashed, but an attempt was made to control for this (see section 3.4). A separate syringe was used for each sample, and collected volume ranged from 15 to 150 μl. Protein concentration for each sample was assayed by aliquotting 20 μl and using the Bio-Rad micro-assay (see Section 3.11). The human aqueous was either processed in the same manner as calf aqueous after being diluted approximately 5-fold with filtered DPBS . After centrifugation and transport to MIT, samples were further diluted with filtered DPBS (if needed) to obtain a testable volume of fluid.

Rabbit aqueous humor (courtesy of Dr. Thomas Freddo) was collected from 14 male and female New Zealand albino rabbits (body weight: ~2.5 kg), each of which had received an injection in the left eye of 1 μg *E. coli* O55:B55 endotoxin (Sigma Chemical Co., Saint Louis, MO) in

10 μl sterile saline vehicle. This endotoxin was administered approximately 24 hours prior to aqueous collection by entering the eye through the pars plana with a 30 gauge needle and injecting into the anterior central vitreous under direct observation through the pupil. The contralateral eyes (OD) were left untouched and were treated as control eyes. Immediately (2 to 5 minutes) before aqueous collection each rabbit was sacrificed by an intravenous overdose of pentobarbitol. The cornea was washed with FH_2O (as described for collection of calf aqueous) and the eye was gently rotated *in situ* to allow convenient corneal puncture near the limbus with a 23 gauge needle attached to a 1 ml prewashed tuberculin syringe. Once the tip of the needle was positioned over the distal pupillary margin the needle was rotated until the bevel was at 90 degrees to the cornea and gentle aspiration was begun. Aspiration ceased when the anterior chamber had collapsed. The syringe was then refilled with FH_2O and the procedure was repeated. A separate syringe was used for the injected and control eyes, and the collected aqueous was pooled in two batches (injected and control). Approximately 150 μl of aqueous was collected from each control eye, while ~80 μl was collected from injected eyes, the lower yield from experimental eyes being due to fibrin clogging the needle and hypotony. After collection the aqueous was centrifuged and tested in the usual manner. A 50 μl sample of each batch of aqueous was frozen for later use in 2-D gel electrophoresis.

All animals were used in accordance with the ARVO Resolution on the Use of Animals in Research.

3.4 Solution Preparation

Unless otherwise noted all solutions were made up in Gibco Dulbecco's phosphate buffered saline (DPBS) (Life Science Technologies Inc., Chagrin Falls, OH). This isotonic saline solution has a pH of 7.2 and contains: $CaCl_2$ (0.1 g/l), KCl (0.2 g/l), KH_2PO_4 (0.2 g/l), $MgCl_2 \cdot 6H_2O$ (0.1 g/l), NaCl (8 g/l) and $Na_2HPO_4 \cdot 7H_2O$ (2.16 g/l). Filtered DPBS was prepared in the same manner as FH_2O.

Papain (P4762, Sigma), pronase (Calbiochem, La Jolla, CA) and protease (from *Streptomyces griseus*, P0652 Sigma) were prepared as 1 mg/ml solutions. Bovine serum albumin (A0281, essentially fatty acid free), bovine γ-globulin (G5009, Bovine Cohn fraction II, 99% γ), bovine fibrinogen (F4753, Type IV, 99% clottable), bovine plasma fibronectin (F4789) and ascorbate oxidase (A2769, 250 units/mg) were obtained from Sigma as lyophilized powders and used as received. Fibrinogen was dissolved by adding DPBS to lyophilized powder followed by gentle stirring. Typically not all fibrinogen went into solution, but was present as flocculant removable by ultracentrifugation. Triton-X 100 (T6878, Sigma), lauryl sulfate (SDS; L4509, Sigma), CHAPS (C3023, Sigma), ferritin (10 mg/ml; F7879, Sigma) and spermine (S4513, Sigma) were obtained commercially. Hyaluronic acid solutions were prepared by dissolving human umbilical cord hyaluronic acid (H1751, Grade I, Sigma) in filtered DPBS overnight in the refrigerator. Hyaluronidase used was Wydase (150 USP/ml, Wyeth Lab, Philadelphia, PA). 0.46 μ latex microspheres were purcahsed from Dow Chemical (Indianapolis, IN).

Bovine lens γ-crystallins were obtained by ion-exchange chromatography of pooled lens homogenates (courtesy of Dr. John Thompson, MIT). They were stored in a 1.2 mg/ml

aqueous solution and preserved by addition of 0.02% sodium azide and 0.2 mM DTT.

Prepared solutions which were to be added to aqueous or perfused through filters were typically made up in filtered DPBS and then either ultracentrifuged (100,000 g for 1 hour) or were prefiltered through a 0.08 μm Nuclepore polycarbonate membrane prior to use. Two exceptions were the ferritin and microsphere solutions, which were simply made up in filtered DPBS, since centrifugation or fltration removed most of the ferritin or spheres from solution.

Calf serum was obtained by centrifuging whole calf blood to remove the red cells and allowing the fibrin to clot out of the plasma at room temperature in a glass tube. Once no further fibrin formation was observed for a half hour period the serum was either diluted 10:1 or 100:1 with filtered DPBS and ultracentriguged in the usual manner.

Calf plasma was obtained by collecting 7 volumes of whole calf blood in one volume of 3.8% sodium citrate, followed by immediate dilution 30:1 with the filtered Ca- and Mg-free buffered saline. The red cells were removed by centrifugation and the citrated plasma was ultracentrifuged in the ususal manner.

In order to test for possible accidental introduction of unwanted particulate matter into test solutions a control solution was prepared for each experiment. The steps taken in the preparation of this solution mimicked as closely as possible the preparation of the test fluid (e.g. calf aqueous). Hence, for calf aqueous experiments, control saline was prepared from filtered DPBS by repeatedly "mock handling" the saline in a cleaned syringe, pipetting it into an ultracentrifuge tube, ultracentrifuging it with the aqueous and transporting it on ice in a Venoject blood

collection tube. In one experiment the syringe containing filtered DPBS was introduced into the anterior chamber (no aspiration) in an effort to control for possible collection of corneal debris.

A similar procedure was followed for the control saline in the monkey and rabbit aqueous experiments, with no corneal penetration. In the human aqueous experiments filtered DPBS was aspirated into syringes identical to those used for aqueous collection and was then subjected to exactly the same steps as the aqueous.

3.5 Preparation of Membranes

Polycarbonate, surfactant-free polycarbonate (see Section 2.5) and polyester track-etched membranes of various pore diameters were obtained from Nuclepore Corporation. It was found that filters gave a more repeatable baseline resistance if they were pretreated before use. For regular (surfactant-treated) polycarbonate filters this involved placing several membranes in ~20 ml of FH_2O and subjecting this mixture to ultrasound treatment for 4 minutes. Typically, filters would curl slightly during this process, although this posed little problem in membrane handling. The protocol for PVP-free polycarbonate membranes involved forcing ~0.5 ml of clean methanol through the filter, followed by ~1.5 ml of FH_2O. The membranes were then subjected to ultrasound as described above. Polyester membranes were subjected to ultrasound in FH_2O for 15 minutes. It is postulated that the ultrasound treatment aids in entry of water into the filter pores, producing a more uniformly wetted membrane.

Tortuous path membranes of the Durapore type were purchased in both hydrophobic (GVHP) and hydrophilic (GVWP)

varieties from Millipore Corp. Hydrophilic membranes were pretreated by bathing them in FH_2O and subjecting them to ultrasound for 5 minutes. Hydrophobic membranes were treated in the same fashion after first being wet with methanol and cleaned with FH_2O as for the PVP-free polycarbonate filters.

3.6 Filter Perfusion System and Protocol

A schematic description of the perfusion system is shown in Figure 3.1. Two different syringe pumps were used in the course of this work: a Houston Microinjector digital stepping pump (Model 1002, Houston Atlas, Houston, TX) and a Harvard syringe pump (Model 944, Harvard Apparatus Co., South Natick, MA). The pump control software allowed the system to be run in either constant pressure or constant flow mode. Pump speed was occasionally checked by measuring the time taken for the syringe barrel to traverse a certain distance or by measuring the pressure drop across a known resistance. Flow rates measured in this manner were within ±2 % of the set point.

Pressure measurements were made with a MicroSwitch Honeywell piezoelectric pressure transducer (model 130PC, Marshall Industries, Burlington, MA) powered by a 9-volt battery to avoid noise problems. Full scale output corresponded to approximately 250 mm Hg, and sensitivity was approximately ±0.02 mm Hg. Calibration was carried out by measuring the hydrostatic pressure of a water column of known height. The pressure-voltage correlation obtained from fitting a straight line through 4 such readings at different heights typically had a correlation coefficient $\geq$ 0.9999. Thus the transducer output was highly linear over the pressure range of interest.

Figure 3.1 Schematic description of perfusion setup

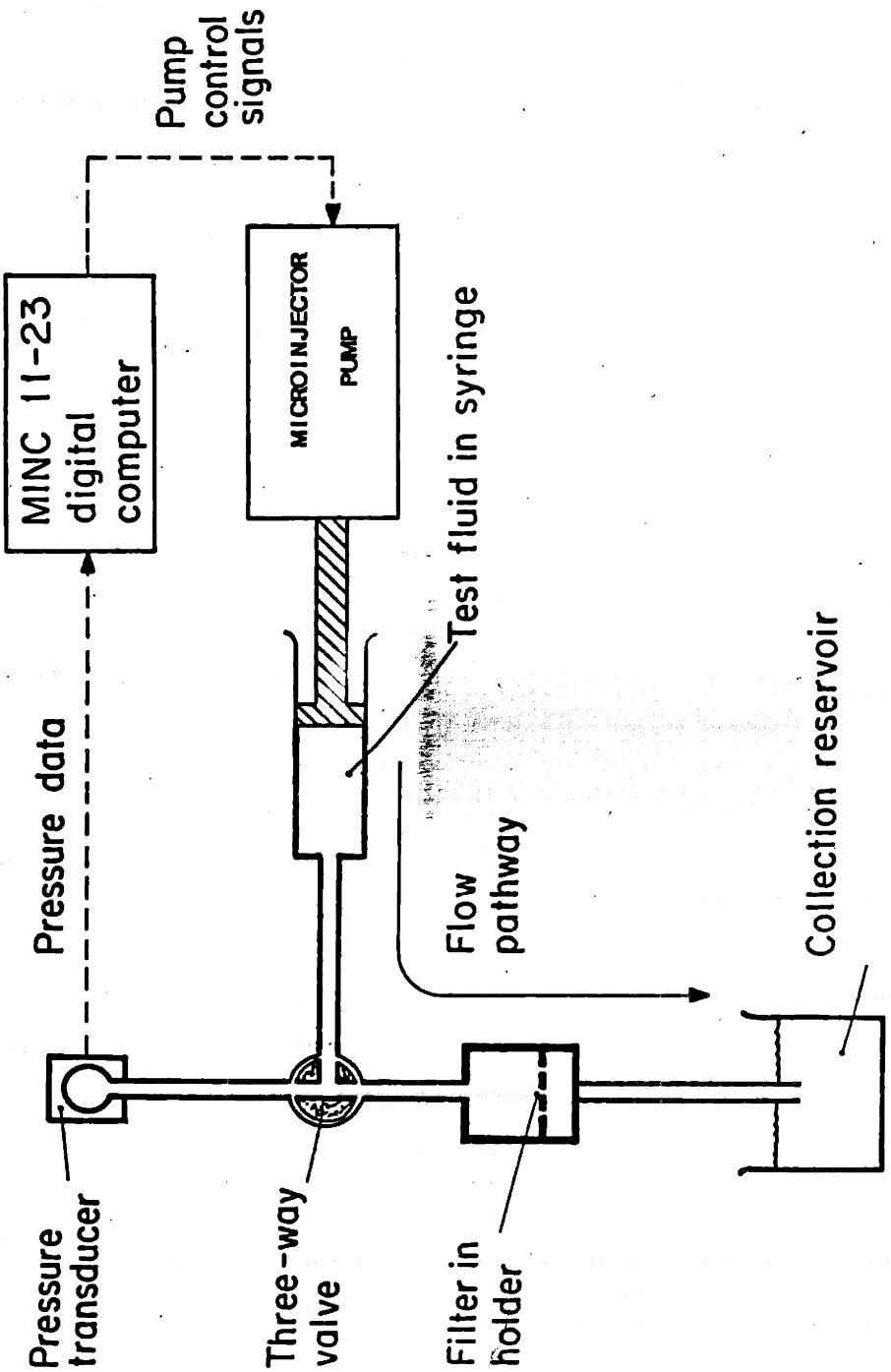

During perfusion experiments a ~400 μl air bubble was introduced into the syringe and attached to the syringe plunger head by displacing the syringe very slightly from horizontal. This added compliance to the system and hence filtered out higher frequency noise. The compliance of the perfusion system (both with and without an air bubble present) was measured by constant flow perfusion with an impermeable disk in the filter holder in place of a filter. Measured values were $C = 0.48$ μl/mm Hg (0.019 μl/mm Hg without air bubble), where compliance C is defined as

$$C = \frac{Q}{dp/dt}$$

for Q=constant. For a filter of resistance R = 0.1 mm Hg/μl/min the system will therefore have a characteristic pressurization time constant of τ=RC=3 sec (0.1 sec without air bubble), which is much shorter than a typical perfusion test. In addition to pressurization transients, the syringe pump required 5 to 10 seconds to reach operating speed, and thus pressure traces typically displayed start-up transients.

Once the pressure transducer had been calibrated and all glassware repeatedly washed with FH_2O, the test fluid was loaded into a glass syringe (Hamilton Syringe Co, Reno, Nevada) and used to fill the system up to and including the upstream half of the filter holder (Swinnex polypropylene holder, silicone gasket, Millipore Corp.). The treated filter was placed in the holder and the downstream side of the holder was attached and backfilled with DPBS. The exposed filter area was 0.71 cm^2. The flow pathway was visually inspected for bubbles which (if present) were purged. The pump drive plate was moved forward so as to just contact the syringe plunger. Usually a very small volume of test fluid (5 to 10 μl) was forced through the

filter as a result of this step.

After the pressure readings stabilized the sensed pressure was assigned the value of zero, so that pressures recorded during the perfusion test represented the pressure drop between the three-way valve and the collection reservoir. The zero pressure set point was stable over the length of a typical perfusion, drifting less than 0.2 mm Hg during 1500 seconds.

Perfusions were conducted at constant flow, so that pressure drops measured were directly proportional to flow resistance. All pefusions were conducted at room temperature. Between perfusion tests the flow pathway was extensively washed with FH_2O to avoid cross-contamination of test fluids.

In several tests a modified filter holder was used which accepted 2 filters separated by a small void space (volume = 380 μl) into which a pressure tap was inserted. By simultaneously measuring the total pressure drop across both filters and the inter-filter pressure it was possible to calculate the trans-filter pressure drop for each filter. The filters were sequentially placed in the holder as for the single filter perfusions, care being taken to ensure that the intermediate void space was filled with only filtered DPBS.

In several tests the fluid in the upstream portion of the filter holder was stirred at various times during the perfusion. This was accomplished by placing three 1 mm diameter stainless steel ball bearings in the filter holder, inverting the holder so that the bearings rested on the upstream filter surface, and attaching the entire holder to a variable speed shaker motor.

Scraping of the upstream surface of pefused filters was accomplished by supporting the filter on the downstream half of the filter holder, grasping the edge with jewelers forceps and repeatedly drawing either a cleaned razor blade or a cleaned Weck-cel surgical spear (E. Weck and Co., Research Triangle Park, NC) over the upstream face.

In some tests filters were perfused with two different solutions (e.g. aqueous followed by Triton-X). In such cases the downstream half of the filter holder (with the filter adhering to it) was removed while the system was washed and refilled with the second perfusate. This minimized filter manipulation.

Filters were washed after aqueous perfusion by one of two methods. In the first the filter was simply dropped in a washed vial containing 800 μl of 0.006% Triton-X and the vial was subjected to ultrasound for 20 minutes. In the second method the filter was placed in a modified holder which had the downstream chamber largely cut away, and 150 μl of 0.035% Triton-X was manually perfused through the filter and collected from the downstream holder by aspiration into a syringe. This fluid was retained and assayed for protein (see Section 3.11). In several instances a second 150 μl volume of Triton-X was perfused and collected from the same filter.

3.7 Enucleated Eye Perfusions

Enucleated calf eyes were obtained and evaluated as described in Section 3.1. Perfusion solutions were made up in DPBS with 5.5 mM glucose added, and prefiltered through a Nuclepore PVP-free 0.2 μ polycarbonate membrane before use. The eye was immersed to the limbus in gauze soaked in

isotonic saline and the cornea was kept moistened with isotonic saline at all times. Perfusions were conducted at room temperature.

Two 23 gauge butterfly needles with attached tubing (Abbott Hospitals Inc., North Chicago, IL) were inserted into the eye through the mid-peripheral cornea. One needle (infusion needle) was carefully positioned with the tip in the posterior chamber, care being taken to avoid the lens and occlusion by the iris, while the second needle was placed directly into the anterior chamber. This needle was only used to exchange fluid within the anterior chamber, and the attached tubing was clamped off during the perfusion.

Perfusions were carried out at constant pressure Δp=15 mm Hg (with respect to the pressure on the surface of the eye at the limbus). The eye was first perfused with a control solution of DPBS (see above) for one hour so as to obtain a half hour of baseline facility data after the initial half hour filling and stabilization period. The perfusion syringe was then filled with the test solution, to which fluorescein (CooperVision, San German, Puerto Rico) had been added, and the anterior chamber was exchanged by infusing fluid into the posterior chamber while simultaneously withdrawing from the anterior chamber. During this procedure IOP was monitored and care was taken to avoid under- or overpressurizing the eye. Once the anterior chamber appeared to be fully filled with fluorescein the withdrawal line was again clamped off and the perfusion was restarted at 15 mm Hg.

Eyes were fixed at pressure (15 mm Hg) by infusion through the anterior chamber (via the inlet and outlet needles) of 2.5% glutaraldahyde, 2.5% paraformaldahyde and 0.016 M $CaCl_2$ in 0.08 M cacodylate buffer, pH 7.3, for one hour, followed by hemisection and immersion fixation of the

anterior portion of the eye. Eyes were then washed in half strength cacodylate buffer overnight at 4 C. Samples were prepared for light microscopy by cutting the anterior segment of the eye into radially-oriented wedges from which series of 1 mm wide, radially-oriented slices were cut, so that each slice contained all the anterior angle structures. The slices were postfixed in 1% OsO_4 and 1.5% potassium ferrocyanide in distilled water, dehydrated in a graded series of ethanols and embedded in an Epon-Araldite mixture. One micron sections were cut, stained with toluidine blue and examined with a Leitz Orthoplan photomicroscope.

3.8 Gel Filtration Chromatography

Gel exclusion chromatography was performed on both a fast protein liquid chromatography (FPLC) system and a high pressure liquid chromatography (HPLC) system. The FPLC setup (Pharmacia, Piscataway, NJ) employed a P500 pump and Superose-12 column material. This cross-linked agarose based medium has an exclusion limit of 2×10^6 daltons and an optimal separation range of 1000 to 3×10^5 daltons, and is known to be slighly hydrophobic (Superose-12 instruction manual, Pharmacia). The elution buffer contained 0.04 M phosphate, 0.02 % sodium azide, pH 7.4, and was thoroughly degassed and filtered prior to use. In several runs 0.1 M NaCl was added to the elution buffer, while in one run 10% filtered and degassed glycerol was added. Before each series of runs the column was equilibrated with two column volumes of buffer. Injected sample volume ranged from 350 to 500 μl, and eluate flow rate was either 0.5 or 1.0 ml/min. Particulate matter was removed from the samples either by prefiltration through a 0.45 μm Millipore Durapore membrane (Millex filter unit) or by centrifugation at 10,000g for 10 minutes. Detection was at 280 nm with a

Pharmacia single path UV-1 monitor.

The HPLC system (Model SP8000, Spectra Physics, Santa Clara, CA) used a GF-250 Zorbax silica gel column (DuPont Bioresearch Systems, Wilmington, DE). This material is a zirconia-stabilized silica gel characterized by its hydrophilic nature, has an exclusion limit of 4×10^5 daltons and an optimal separation range of 10,000 to 2.5×10^5 daltons. The buffer contained 0.1 M KH_2PO_4 and 0.02% sodium azide, pH 7.0. Injected sample volumes were either 50 or 100 μl, and flow rate was 1.0 ml/min. Particulate matter was removed from samples by centrifugation at 15000 g for 30 minutes. Detection was at 230 nm with a Spectra Physics model 770 Spectrophotometric detector.

3.9 Protein Assay Techniques

Solution protein levels were determined by either the method of Bradford (1976) (Bio-Rad asssay), the Lowry-Folin method, or, on some occasions, both. For all assays a 6-point standard curve was prepared fresh daily by appropriate dilution of a protein standard. Sample concentrations fell within the limits of the standard curves, and all samples and standards were prepared together. Standard curves were usually linear over their entire range.

Assays of Aqueous

The Bradford assay method is based on the colorometric change which occurs when Coomassie Brilliant Blue

G-250 dye binds to proteins, and is supplied in kit form by Bio-Rad (Richmond, CA). The assay can be run in two distinct modes: as a standard assay suitable for measuring solutions with protein levels betwen 200 and 1400 μg/ml, and as a microassay for measuring less than 20 μg protein. Unless otherwise stated, "Bio-Rad assay" will refer to the standard technique. Standard assay protocol followed the procedure recommended by Bio-Rad (Protein Assay Instruction Manual), with a bovine plasma γ-globulin standard (Bio-Rad standard I). Duplicate assay samples were prepared except on infrequent occasions when sample volume was insufficient; reported concentrations are the mean of the two samples.

If the tested sample contained a substance which partially interferes with the assay (e.g. ethanol or dilute detergents) dual standard curves were prepared: one as described above and a second in which the concentration of the interfering substances was equal to that in the test sample. In such cases assayed protein levels were read from the second standard curve.

An attempt was made to estimate the error inherent in this assay by measuring the spread in assayed protein levels obtained from 10 identically prepared solutions. The standard error among these samples was 26 μg/ml about a mean value of 692 μg/ml, the latter being a typical value for calf aqueous protein concentration. Hence we expect protein levels assayed by the standard Bio-Rad procedure to be accurate within approximately $\pm$5 %.

The microassay also followed Bio-Rad's recommended protocol, including daily preparation of a 6-point standard curve from a standard γ-globulin solution. Sample volumes were usually too small to allow for duplicate assays. Because those agents which interfere with the standard Bio-Rad assay do so more strongly with the microassay,

particular care was taken to make up dual standard curves, as described above.

The Lowry-Folin assay was carried out according to the protocol detailed by Cooper (1977). This assay is based on: (i)the formation of a protein-copper complex between the Biuret reagent and compounds with 2 or more peptide bonds, and (ii) the reduction of Folin-Ciocalteu reagent by tyrosine and tryptophan residues (Alexander et al., 1986). Standards were prepared from a standard bovine plasma albumin solution (Bio-Rad, Standard II).

Assays of Filter Eluate

Perfused filters were washed with detergents as described in Section 3.8 and the eluates assayed by the Bio-Rad micro method. Since detergents interfere strongly with this method it was necessary to carefully prepare double standard curves, as described above. In addition, in some experiments a third standard curve was prepared by making up protein solutions in Triton-X and subjecting them to exactly the same steps as were used to elute protein from the filters, i.e. ultrasound for 20 minutes or perfusing 150 μl through a filter and collecting the fluid (see Section 3.8).

The volume of filter eluate obtained by the ultrasound technique was measured and corrected to 800 μl by addition of 0.006% Triton-X or removal of fluid. Assayed protein values were later corrected if the measured volume exceeded 800 μl, although this factor was usually small (3%). In a similar fashion the volume of the filter eluate collected in the perfusion teechnique was measured and corrected to 150 μl (addition of 0.035% Triton-X or removal of fluid). The sample was then diluted to 800 μl with

distilled H_2O. A similar procedure was followed for the standards which had been forced through a filter, as described above. Assayed protein levels were corrected if original volumes exceeded 150 μl, this correction once again being small.

3.10 Gel Electrophoresis

Two-dimensional gel electrophoresis of various samples was conducted by A.F. Pavao of the Howe lab, Massachusetts Eye and Ear Infirmary. Aqueous and serum were obtained as previously described, except that glassware, etc. was not washed in FH_2O. Material adhering to filters was obtained by elution with Triton-X after a rinsing step designed to remove loosley-associated molecules. Specifically, 0.2 μ polycarbonate PVP-free Nuclepore membranes were manually perfused with ~1.5 to 3 ml of centrifuged calf aqueous, were reperfused with ~1 ml DPBS and were then placed in ~1 ml of 1% Triton-X and subjected to ultrasound for ~1/2 hour. The filters were discarded and the eluate was prepared for gel electrophoresis as described below.

Two-dimensional electrophoresis was carried out according to a modified O'Farrell technique (1975). All samples were treated with concentrated sample lysis/denaturing buffer to obtain a final concentration of 0.0625 M Tris, 0.2% SDS, 2.5% (DTT) and 10% glycerol, pH 6.8. The sample was heated at 95 C for 10 minutes and then frozen at -20 C or -80 C for storage. After thawing at room temperature, and immediately prior to sample loading for the isoelectric focussing run, the following were added to give the indicated final concentrations: urea (9M), CHAPS or Triton-X 100 (2%), and Pharmalyte 3-10 (4%) (Pharmacia).

Isoelectric focussing rod gels were 12 to 14 cm in length and either 2.7 mm in diameter (rabbit aqueous samples) or 1 mm in diameter (other samples), and were cast from 5% acrylamide, 3% Bis-acrylamide (Sigma), with 9M urea, 1% Triton-X 100 and 4% Pharmalyte 3-10 added. The gels were not prefocussed but were loaded directly with 20 to 40 μg of protein according to the method of Marshall et al. (1984). The catholyte was 0.1 M NaOH (pH 12.3 ±0.1), the anolyte was 0.05 M H_2SO_4 (pH 1.4 ±0.1), and the samples were focussed at 500 V for 10,000 volt-hours at room temperature. Rod gels were then frozen at -80 C in 0.0625 M Tris-HCl (pH 6.8), 1% SDS, 1% DTT, 10% glycerol and 0.002% bromophenol blue for storage.

Separation in the second dimension by SDS-PAGE using the discontinuous system was done on precast 14 cm by 16 cm by 1 mm slab gels having acrylamide gradients of either 2.5 to 27% to 10 to 20% (Isolab Inc., Akron, OH). The 1 mm diameter rod gels were placed directly onto the slab gels, while the 2.7 mm rod gels were separated from the slab gels by an agarose stacking gel. The electrophoresis buffer contained 25 mM Tris, 192 mM glycine, 0.1% SDS, pH 8.3, and gels were run at 30 mA for 4 to 5 hours. Gels were silver stained with Rapid-Ag-Stain according to the manufacturer's suggested protocol (ICN Radiochemicals, Irvine, CA).

3.11 Filter Morphology

Overnight immersion fixation and washing of filters for scanning electron microscopy was carried out using the solutions described in Section 3.7 for processing perfused calf eyes. Samples were dehydrated by addition of graded ethanols, critical point dried, gold palladium sputter coated for two minutes and viewed in a JEOL scanning

electron microscope.

Transmission electron microscopy of filters was performed by Dr. Thomas Freddo of Boston University School of Medicine. Perfused and control filters were fixed by overnight immersion in 4% paraformaldehyde and 5% gluteraldehyde in 0.2 M phosphate buffer, pH 7.4, and were then washed in buffer. Samples were postfixed with 1.0 % OsO_4 and 1.5% potassium ferrocyanide in distilled water. Filters were dehydrated in a graded series of glycol methacrylate to 95%. The glycol resin was slowly exchanged with an Epon-Araldite mixture and the filters were embedded in Epon-Araldite. One micron sections were cut and stained with toluidine blue for light microscopic examination. Thin sections were mounted on uncoated copper grids, stained with uranyl acetate and lead citrate and examined with a Phillips-300 transmission electron microscope.

CHAPTER FOUR: EXPERIMENTAL RESULTS

This chapter describes the experimental results obtained during the course of this work. Because of the large number of experiments undertaken, an attempt has been made to organize the chapter by theme, and to defer in-depth interpretation to Chapter Six. For convenience, experimental results have been summarized in tabular form in Section 4.13.

4.1 Baseline (Saline) Filter Perfusions

By carefullly following the cleaning procedures described in Section 2.1 stable and repeatable saline baseline perfusions on 0.2 μ polycarbonate Nuclepore filters were obtained. During the course of a 1500 second perfusion (total perfused volume = 1 ml) baseline filter resistance typically rose five to ten percent. Five different batches (manufacturer's lots) of polycarbonate 0.2 μ filters were used during the course of this study, and it was found that there was some inter-batch variation in membrane resistance (Table 4.1). On the other hand, filters drawn from the same lot generally gave fairly consistent baseline resistance values, with the exception of Lot C, which showed an unaccountably high variation.

Baseline perfusions on polyester track-etched membranes showed a much greater degree of intra-lot variablity (Table 4.1). In addition, it was often difficult to achieve a stable saline baseline, and hence perfusions on polyester membranes will be primarily used for qualitative comparisons. The measured resistance and calculated pore

radii of the membranes used in this study are presented in Table 4.1.

FILTER TYPE		Baseline Resistance R_{bl} (mm Hg/μl/min)	Pore radius, R_o (μ)
0.2 μ Nuclepore PC	lot A (33)	0.053 ± .005	0.128 ± .003
	lot B (13)	0.059 ± .010	0.125 ± .005
	lot C (8)	0.096 ± .015	0.110 ± .004
	lot D (21)	0.053 ± .008	0.128 ± .005
	lot E (14)	0.050 ± .010	0.130 ± .007
0.4 μ Nuclepore PC (2)		0.011	0.25
0.6 μ Nuclepore PC (1)		0.0081	0.36
0.2 μ Nuclepore PE (17)		0.082 ± .043	0.115 ± .015
0.2 μ Nuclepore PVP-free	lot F (4)	0.048 ± .008	0.131 ± .006
	lot G (4)	0.061 ± .006	0.124 ± .003
0.22 μ Millipore GVWP (1)		0.062	---
0.22 μ Millipore GVHP (1)		0.073	---

Table 4.1 Measured baseline resistances R_{bl} and calculated pore radii of tested membranes. Values are mean ± standard deviation (where shown), bracketed numbers refer to number of membranes tested. Pore radii have been calculated from measured resistances, nominal pore densities (Table 2.5) and equations (2.5.1) and (2.5.2). All Nuclepore membranes shown have nominal thicknesses of 10 μ. Abbreviations: PC - polycarbonate, PE - polyester.

The total pressure drop measured during a perfusion is due to the resistance of the perfused filter and losses within the connecting tubing. Experimental data for filter perfusions will be presented in terms of a normalized filter resistance, R, defined by

$$R = \frac{\Delta p - QR_{sys}}{QR_{bl}} \qquad (4.1.1)$$

where Q is the perfusion flowrate, Δp is the measured pressure drop for the entire system, R_{bl} is the appropriate filter baseline (saline) resistance (Table 4.1), and R_{sys} is the system resistance. The normalized resistance given by (4.1.1) is simply the total filter resistance normalized with respect to that membrane's resistance to saline.

4.2 Calf Aqueous Collection and Protein Levels

In order to address concerns about possible contamination of aqueous samples by corneal fragments which may have entered the needle lumen during corneal puncture, syringes filled with control saline were introduced into the anterior chamber, as described in Section 3.4. Control saline processed in this way did not significantly block 0.2 μ polycarbonate filters, i.e. it showed the small degree of blockage routinely seen for control saline solutions, and thus we conclude that corneal debris capable of filter blockage was not present in collected aqueous samples.

A second possible source of aqueous humor contamination is accidental aspiration of lens material. To investigate this possibility, as well as to obtain an estimate of the variablility in aqueous humor protein levels from eye to eye, individual (unpooled) aqueous samples were collected from 26 eyes after which the eyes were closely examined using a fiber optic lamp. The distribution of aqueous protein levels from individual eyes, as assayed by the Bio-

Figure 4.1 Histograms of aqueous humor protein concentration from individual calf eyes. Each histogram represents one batch of eyes. Double hatched samples in (a) indicate eyes that were observed to have lens capsule damage. All assays by Bio-Rad method on uncentrifuged aqueous.

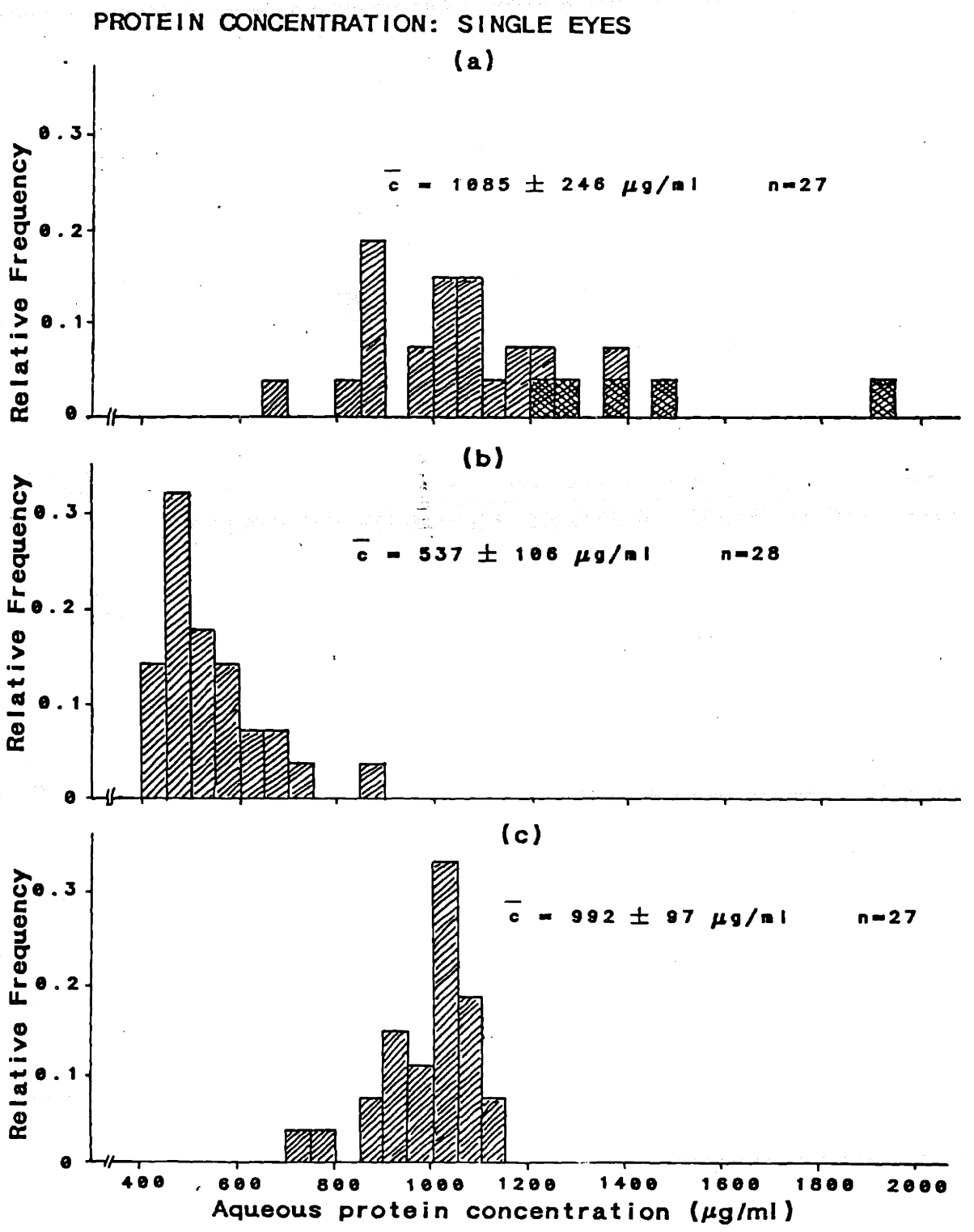

Rad method, showed substantial inter-eye variability and unusually high mean protein concentration (Figure 4.1(a)). Under visual examination, three eyes showed definite signs of lens capsule damage, while two other eyes showed signs of slight lens capsule abrasion. The aqueous from these eyes also had high protein content (1240-1930 μg/ml), suggesting that in these eyes lens proteins were being aspirated along with the aqueous. If aqueous samples from the five eyes showing lens damage were *a prosteriori* excluded from the data set, the mean protein concentration and standard deviation were reduced, from 1085 $\pm$ 246 (all eyes) to 1015 $\pm$ 153 (lens damage eyes excluded). Thus, possible indicators of lens damage during aqueous collection are high protein concentrations and high inter-eye protein level variabilty.

Because of these findings the aqueous collection procedure was modified so as to: (i) withdraw the aqueous humor much more slowly and gently, and (ii) discard the aqueous collected at the end of the aspiration procedure (Section 3.2). Individual aqueous humor samples collected with this improved technique were once again assayed for protein on two separate occasions (Figure 4.1(b) and (c)). It is seen that protein levels in aqueous collected with the improved technique show significantly less variability, although in one instance (panel (c)) the mean protein levels were relatively high. In addition, eyes inspected after aqueous collection with the improved technique showed no signs of lens damage. Thus, it is concluded that the improved collection technique avoided lens damage and concomitant aspiration of lens material. The modification in collection technique occured early in the course of this work, and the change in collection procedure did not seem to alter the blocking behavior of calf aqueous on test filters.

For the protein measurements of July 12, 1985 (Figure 4.1 (b)) half of the eyes were delivered in the usual manner, while the remaining half were delivered without ice. These two groups of eyes were further subdivided by having two investigators withdraw the aqueous humor, so that each investigator collected aqueous from half of the "cold" eyes and half of the "warm" eyes. No significant difference ($p>0.2$, 2 sided t-test) was seen between aqueous humor protein levels from "warm" eyes *versus* "cold" eyes (561 ± 119 μg/ml *versus* 512 ± 88 μg/ml) or between protein levels collected by investigator 1 versus investigator 2 ($p>0.2$, 2 sided t-test).

In addition to the above three occasions in which the protein content of individual aqueous humor samples was measured, protein concentration in the pooled aqueous humor was routinely measured by the Bio-Rad method prior to ultracentrifugation. The distribution of protein levels is shown in Figure 4.2, while Figure 4.3 shows this same data plotted as a function of collection date (time of year). The mean protein level (average of all batches) was 820 ± 274 μg/ml (n=50). Figure 4.3 suggests that the protein level of calf aqueous humor collected during the summer months (May through August) is slightly higher than that in aqueous collected at other times during the year. Subdividing the data presented in Figure 4.3 into three groups according to collection date (group 1: January 1-April 30, group 2: May 1-August 31, group 3: September 1-December 31) confirms this impression. Mean concentrations and standard deviations for the three groups are: 686 ± 243 μg/ml (group 1), 894 ± 223 μg/ml (group 2) and 883 ± 329 μg/ml (group 3), and a statistical analysis indicates a marginally significant ($p<0.06$, 2-sided t-test) difference between the mean for group 2 and that of groups 1 and 3 combined. The difference between the mean protein

Figure 4.2 Histogram of protein levels from pooled batches of calf aqueous humor. All assays by Bio-Rad method on uncentrifuged aqueous.

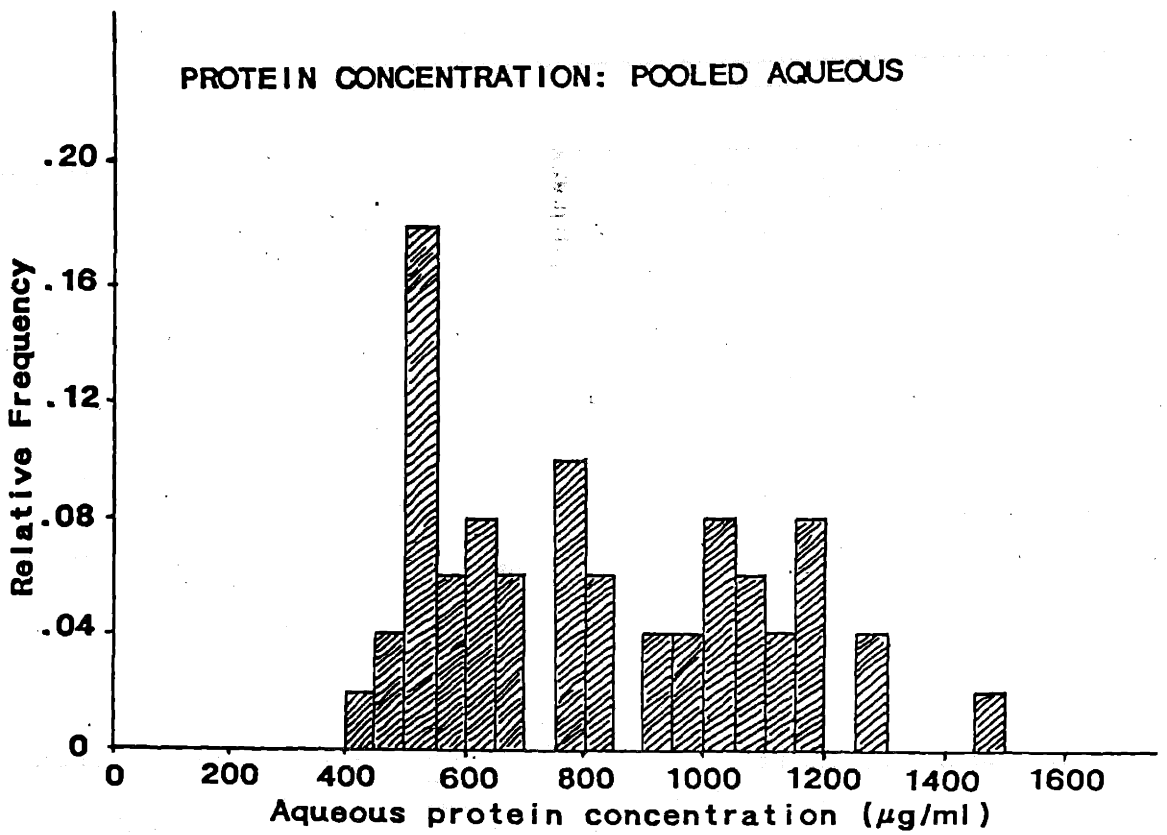

Figure 4.3 Plot of calf aqueous humor protein level (pooled batches) as a function of time of year. All assays by Bio-Rad method on uncentrifuged aqueous.

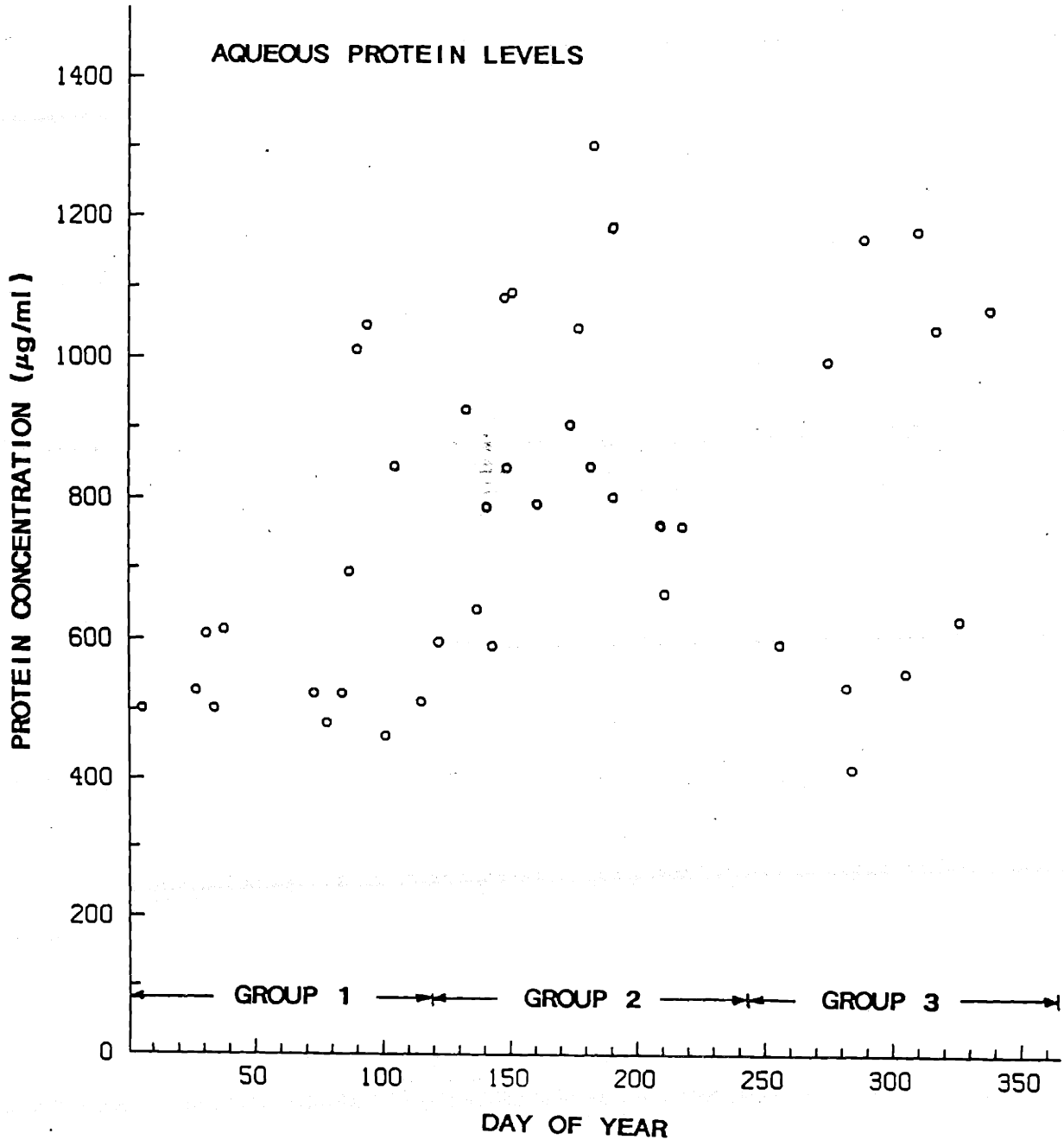

concentrations of groups 1 and 2 is particularly significant ($p<0.01$, 2-sided t-test), and thus we conclude that the protein content of calf aqueous humor is higher during the summer months (May 1- Aug. 31), especially when compared to fluid collected during the period Jan. 1- April 30.

Most previous measurements of aqueous humor protein levels have employed the Lowry-Folin or modified Lowry-Folin techniques (Table 2.1), while this study has primarily used the Bio-Rad (Bradford) assay. However, in ten batches of aqueous protein levels were measured by both the Lowry-Folin and Bio-Rad techniques, using bovine serum albumin and gamma-globulin standards, respectively. Interestingly, the values produced by the two techniques were in close agreement and could be well fit by the linear relationship ($r=0.991$)

$$c_{\text{Bio-Rad}} = 1.17\, c_{\text{Lowry}} - 93\ \mu g/ml \qquad (4.2.1)$$

where the concentrations are expressed in $\mu g/ml$. The Lowry-Folin and Bio-Rad assays are based on different reactions, each of which depends to a large extent on the particular structure of the protein substrate, and will generally not yield identical readings from identical solutions even when calibrated against the same standard. Hence, the agreement expressed in equation (4.2.1) is somewhat fortuitous, but it does suggest that protein levels measured in this work may be directly compared with previously published results.

In two experiments the aqueous humor was separated into low (<10 kdal) and high (>10 kdal) molecular weight-containing fractions with a Centricon-10 miniconcentrator. The protein levels in both the high and low molecular

weight-fractions as well as in unfractionated aqueous humor were assayed by both the Bio-Rad and Lowry-Folin methods. The assayed values are shown in Table 4.2, and indicate that the Bio-Rad assay did not detect small (<10 kdal) molecules, while the Lowry-Folin assay did. This is consistent with the known tendancy of the Folin reagent to react with small oligopeptides and certain free amino acids. A second and more significant observation is that even though the two aqueous humor batches had substantially different overall protein levels, the concentration of low molecular weight material (measured by Lowry-Folin) was similar, suggesting that differences in aqueous humor protien levels are due to species of molecular weight greater than 10 kdaltons.

	Assay Technique	Protein Levels (μg/ml) Aqueous	HMW	LMW
Nov. 6, 1985	Lowry-Folin	902	647	218
	Bio-Rad	1040	961	0
Nov. 22, 1985	Lowry-Folin	498	342	233
	Bio-Rad	510	541	0

Table 4.2. Measured protein levels in two batches of aqueous humor, and in the low and high moecular weight-containing fractions obtained from those batches. Protein concentration in the low and high molecular weight-containing fractions were normalized by calculating total protein mass and dividing by original aqueous volume. LMW-low molecular weight fraction, HMW-high molecular weight fraction. The protein recovery for November 22 probably exceed 100% due to errors associated with measuring the small volume of the HMW fraction after separation.

The effect of ultracentrifugation on aqueous humor protein levels was also investigated by measuring protein concentration before and after ultracentrifugation on several occasions. The results, plotted in Figure 4.4,

Figure 4.4 Plot of the decrease (due to ultracentifugation) of the protein concentration of pooled calf aqueous humor *versus* the original (uncentrifuged) protein level. All protein levels determined by Bio-Rad asssay. Line is the linear least squares fit: drop = 0.23 (original concentration) - 75 μg/ml (r=0.80).

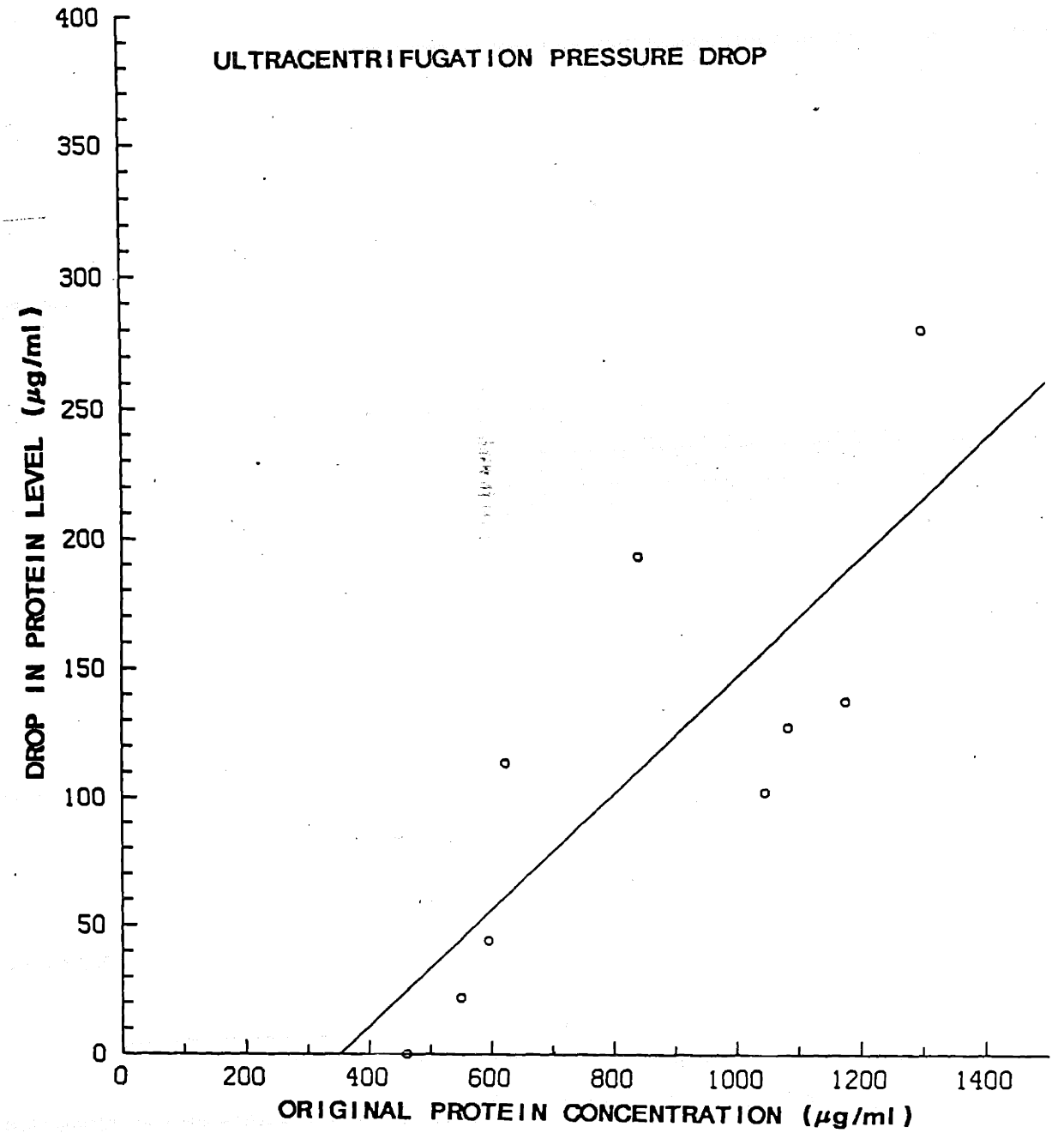

show a correlation between the decrease in aqueous protein content due to ultracentrifugation and the original protein concentration, and thus we conclude that ultracentrifugation slightly affects the protein composition of aqueous. We also note that after ultracentrifugation a tiny grey or black pellet was often seen, presumably due to pigment particles.

On one occasion the protein concentration in aqueous humor obtained within 25 minutes of death from enucleated eyes was measured and found to be 902 μg/ml. This aqueous humor was collected between May 1-August 31 (group 2), and its protein level was not significantly different from the mean concentration of this group.

4.3 Behavior of Calf Aqueous Humor on Polycarbonate Filters

Figure 4.5 displays several representative plots of normalized filter resistance versus (dimensional) time for calf aqueous passing through 0.2 μ polycarbonate Nuclepore filters (each curve corresponds to a separate aqueous humor batch). Substantial inter-batch variablity is seen: some curves appear to rise smoothly to a steady state, (curves 1) while others show no tendency towards levelling off, (curves 2), and on occasions (~10 % of the time) resistance actually reaches a maximum and then declines slightly (curves 3). The data presented in Figure 4.5 and in subsequent figures has been slightly smoothed, and a representative smoothed and unsmoothed trace may be compared in Figure 4.5 (a). Tests which show no tendency to level off were terminated when the total measured pressure drop exceeded 75 mm Hg (system limitations), and thus we have no information as to when or if these curves would level off.

Figure 4.5 Selected representative traces of normalized filter resistance as a function of time for calf aqueous humor perfusions through 0.2 μ polycarbonate filters (Q=40 μl/min). (a) Curves which appear to rise smoothly to a steady state (type 1). *: denotes curve with non-smoothed original data superimposed, **: denotes curve which has best exponential fit (equation (4.3.1)) superimposed. (b) Curves which show no evidence of reaching a steady state (type 2), and curves which exhibit a maximum in resistance (type 3).

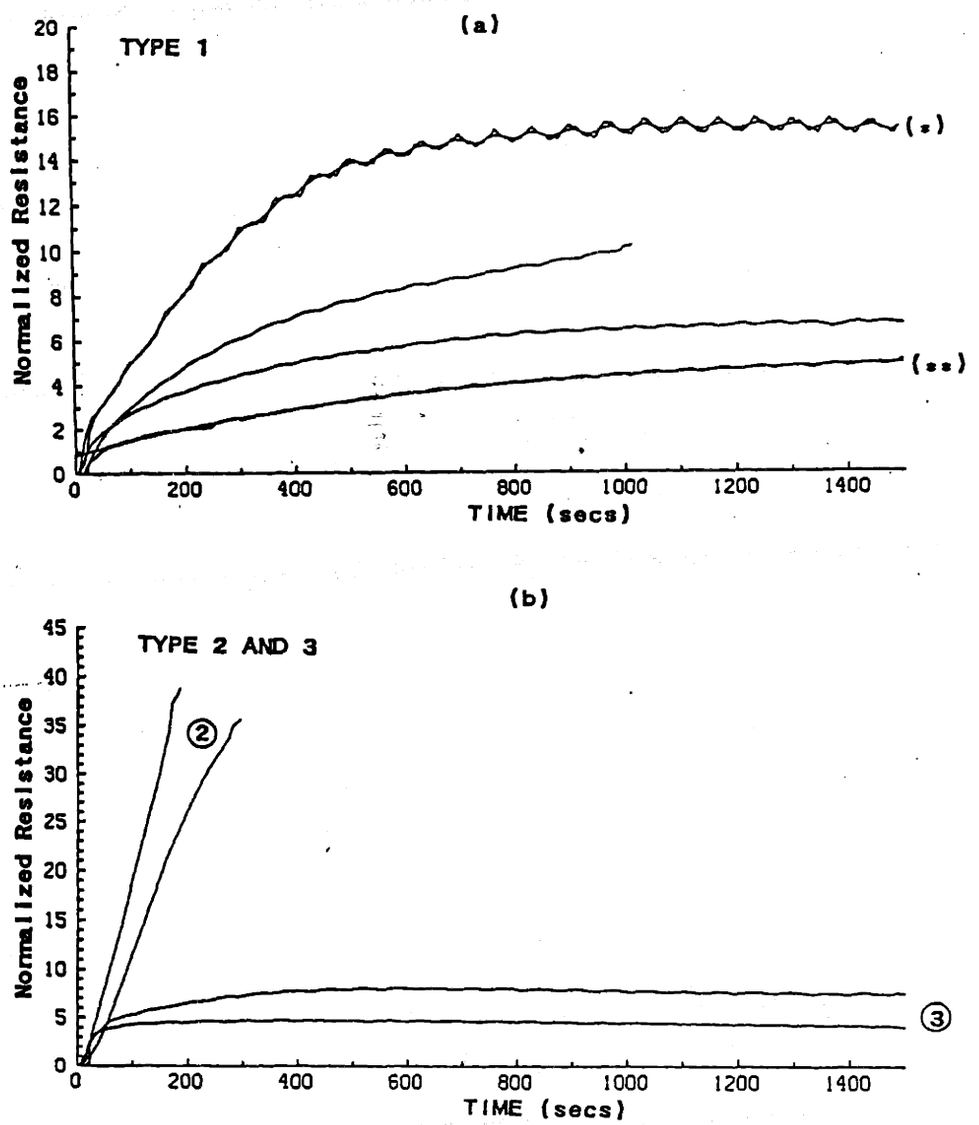

Although the resistance traces of Figure 4.5 show variability, they share several important qualitative features. Most significantly, in all cases calf aqueous humor blocked 0.2 μ polycarbonate filters and thus behaved differently from saline. This has been confirmed in over 100 perfusions, all of which have shown a readily discernable difference between the behavior of calf aqueous and saline. With the exception of the minority of curves which exhibit a maximum, the blocking is seen to be progessive, i.e. resistance appears to increase monotonically until steady state is reached, if ever. The filter blockage appears to proceed in two stages: a fast initial blockage ($t < 50$ seconds) and a slower rise in resistance ($t > 50$ seconds). Since the start-up time constant for the perfusion system is on the order of ten seconds (Section 3.6), the time course of the rapid initial resistance rise is difficult to resolve, and it may be that the filter's resistance is somewhat elevated from the beginning of the test. This could be due to blocking which occured during pump drive-plate positioning and system equilibration prior to perfusion (Section 3.6).

On several occasions long-term perfusions (>2000 secs) of calf aqueous on 0.2 μ polycarbonate filters were carried out. The results are shown in Figure 4.6, and indicate that in at least two cases out of four the approach to steady state seen between 0 and 1500 seconds is illusory, since the filter resistance appears to increase once again after 2500 seconds. In interpreting the curves in Figure 4.6 the possible effects of particulate contamination over such long perfusion times should be taken into account. Thus, over a 6000 second test (total perfused volume = 4 ml), the saline baseline resistance increases appreciably, and it is likely that the slow linear rise (seen after ~3000 seconds) of at least one trace in Figure 4.6 can be explained by this phenomenon.

Figure 4.6 Normalized resistance traces from long term calf aqueous pefusions through 0.2 μ polycarbonate membranes (Q = 40 μl/min). Dotted line: saline baseline perfusion under the same conditions.

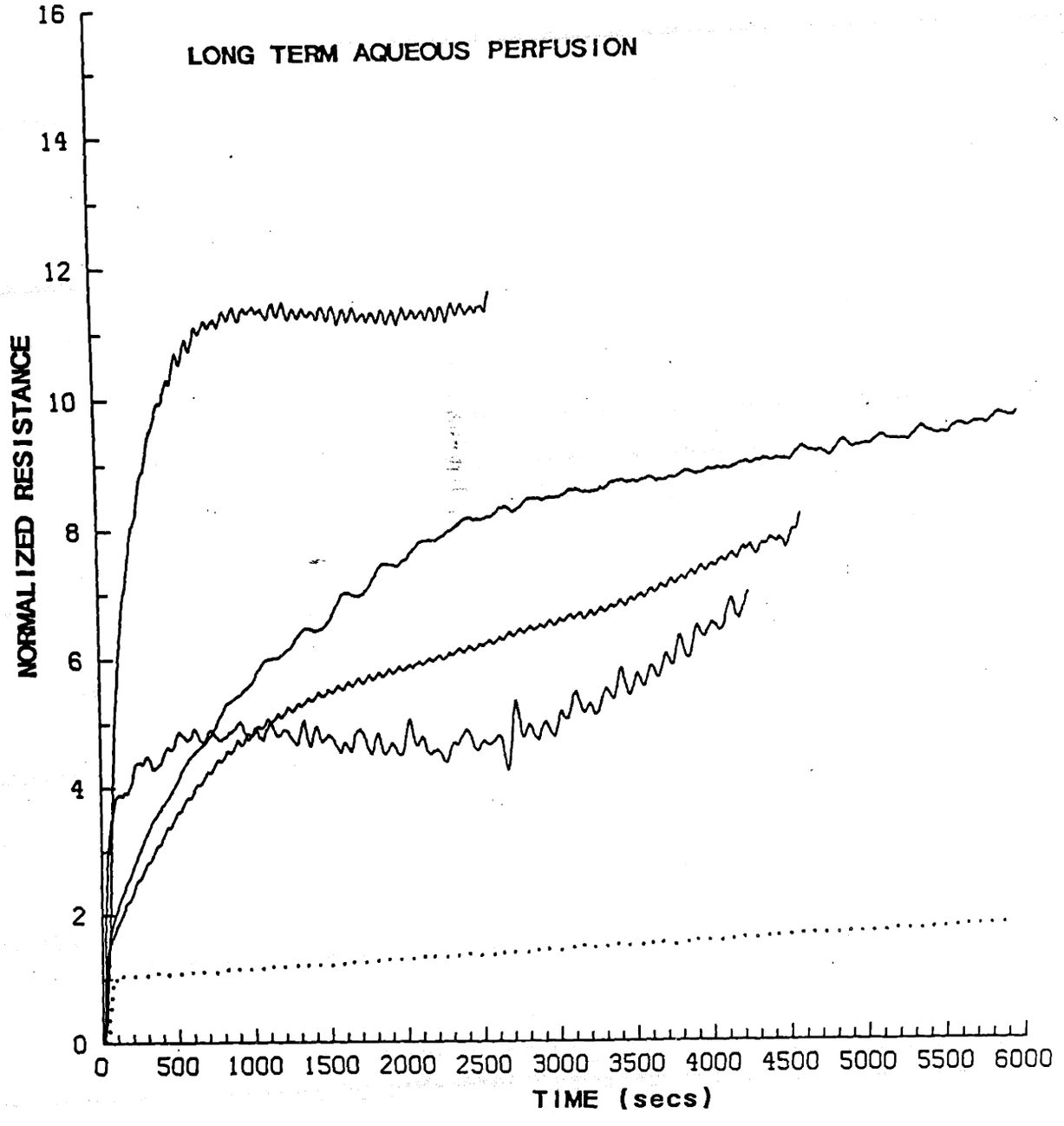

In one instance calf aqueous was not ultracentrifuged, but simply prefiltered through a 1.0 μ polycarbonate membrane to remove large particulate matter. When compared to ultracentrifuged aqueous from the same batch it showed a greatly (at least ten times) increased level of blocking, and thus we conclude that ultracentrifugation decreases the blocking capacity of aqueous (data not shown).

The "Aging" Effect

In addition to the variability seen between different batches of aqueous humor, a lesser but noticeable variability between aqueous runs taken from the same pooled source was found. This difference was correlated with the order in which the tests were performed, those conducted later in a given series usually having a lower resistance than those conducted near the beginning the that series (Figure 4.7). One less-than-perfect but convenient indicator of the decrease in aqueous blocking potential with time is the ratio

$$\frac{R_{500} \text{ for first test}}{R_{500} \text{ for second test}}$$

where R_{500} is the normalized resistance at 500 seconds and the two tests are taken from the same aqueous batch. This ratio had a mean value and standard deviation of 1.25 ± 0.40 (results from 18 separate batches), the mean being significantly ($p=0.008$, one-sided t-test) greater than one.

Figure 4.7 The 'aging' effect of calf aqueous humor. Representative traces of two runs drawn from the same batch of aqueous. "early": early during test series, "late": three hours later in same test series.

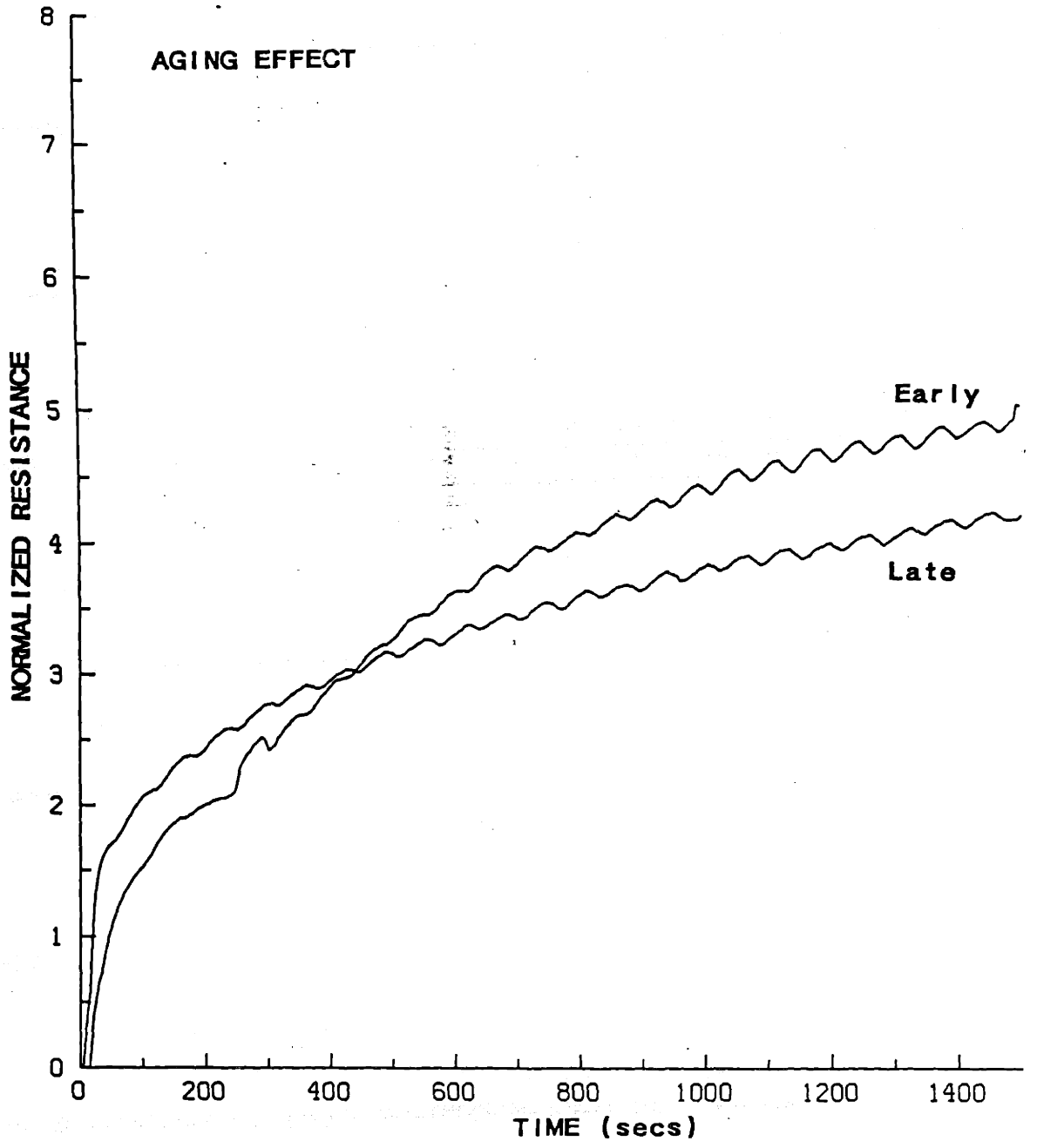

Thus, we conclude that over the one to two hours which typically elapsed between the first and second tests, calf aqueous lost ~20% of its blocking capacity. The extent of this decrease was weakly correlated (r=0.27) with protein level. In addition, the rate of decrease seemed to level off with time, the second and third tests showing somewhat less difference than the first and second.

In the course of a normal series of tests the aqueous humor was stored at 4 C. To determine if this "aging" phenomenon was related to storage conditions, two aliquots of pooled aqueous humor were withdrawn at the beginning of one test series. One ("cold") was stored in the refrigerator as usual, while the second ("warm") was stored at room temperature. After approximately four hours they were perfused and compared to aqueous which had been tested earlier. Both the warm and cold aqueous humor showed the same degree of aging, implying that this phenomenon was not due to storage temperature. One likely explanation of this phenomenon is that the blocking components in calf aqueous (which will be seen to act by binding to the filters), also bind to the container surfaces during storage, so that their concentration in aqueous decreases with time.

When fresh aqueous humor was collected immediately after death from eyes *in situ*, it was also found to block 0.2 μ polycarbonate filters, although at a slightly reduced rate. Thus, we conclude that the blocking capacity of calf aqueous is not due to changes in aqueous composition which occur between 15 minutes *post mortem* and the usual collection time.

Resistance-Protein Correlation

There was a discernible correlation between aqueous humor protein levels and blocking capacity, as shown in Figure 4.8. In this figure aqueous humor protein level is plotted versus normalized filter resistance at 500 seconds for the first aqueous test from each aqueous batch, where once again R_{500} is taken as a less-than-perfect but convenient indicator of filter blockage. On this graph tests which were terminated before 500 seconds due to extensive filter blockage (pressure limitations) are arbitrarily given a normalized resistance of 40. Protein levels were correlated with blocking capacity (Figure 4.8), with linear least-squares fitting giving the expression

$$R_{500} = 0.027 \text{ (protein conc.)} - 6.09 \qquad (4.3.1)$$

(protein concentration in μg/ml) [r=0.494, n=63]. Figure 4.8 also indicates that the vast majority of aqueous tests fall within a relatively consistent group (delimited by dashed lines, Figure 4.8), while a second group of tests exhibit an unusually high blocking capacity. The reason for this bimodal behavior is not known. A least squares fit to the data points within the first group yields

$$R_{500} = 0.0091 \text{ (protein conc.)} + 1.38 \qquad (4.3.2)$$

[r=0.633, n=52], once again confirming the protein-resistivity correlation. Note however that this correlation has an r value appreciably different than one, indicating a substantial degree of variability.

Figure 4.8 Plot of calf aqueous humor protein levels *versus* normalized pefusion resistance at 500 seconds. Solid circles: aborted runs assigned a normalized resistance of 40 (see text). Solid line represents linear least squares fit to points within dashed line boundaries. All tests on 0.2 μ polycarbonate membranes at 40 μl/min.

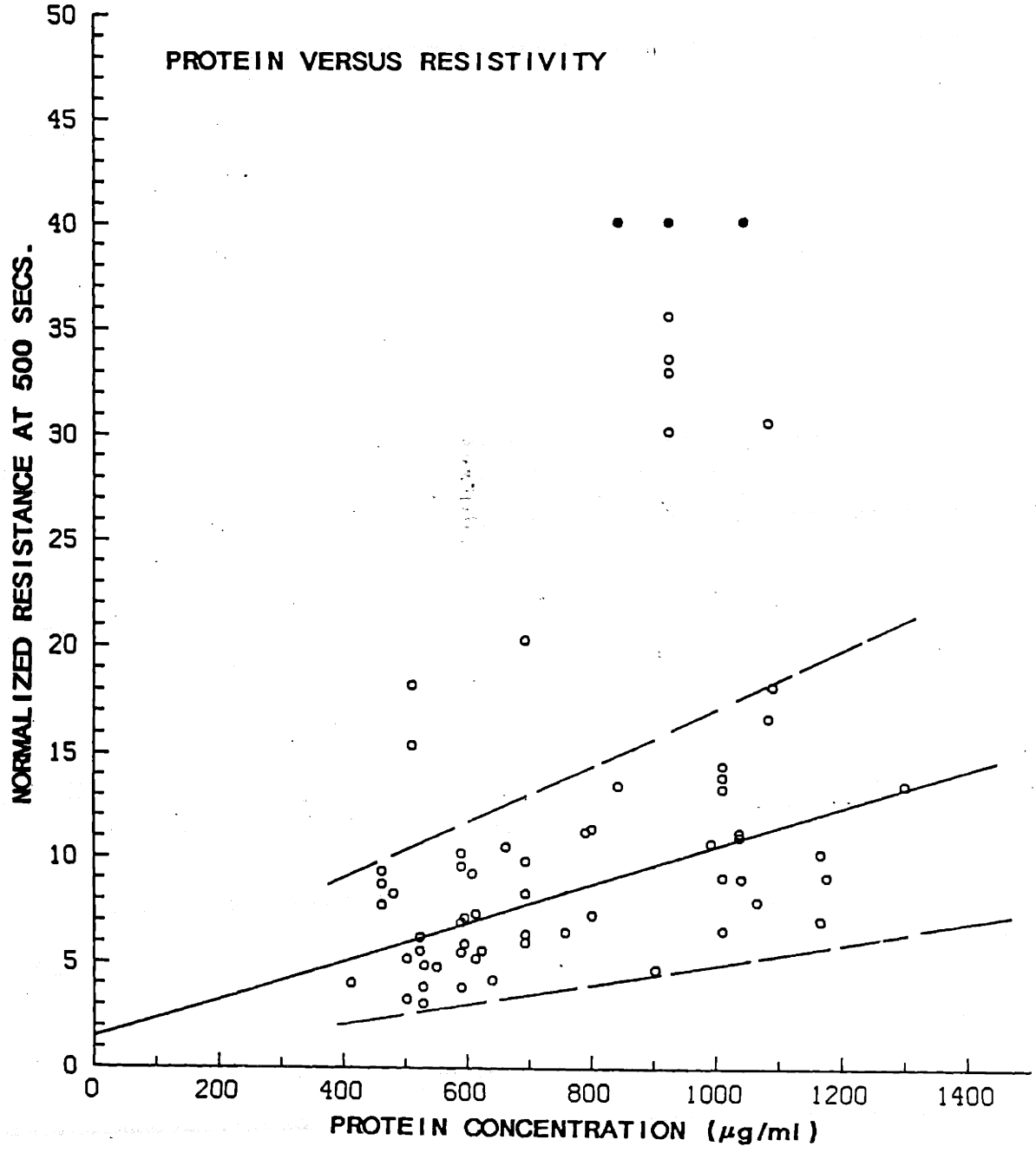

Since aqueous protein content changes seasonally, it is of interest to determine if aqueous blocking capacity varies in a similar fashion. Subdividing the R_{500} data of Figure 4.8 into the 3 groups employed in Section 5.2 and computing means and standard deviations gives: 11.82 ± 11.0 (group 1), 14.33 ± 12.41 (group 2) and 9.98 ± 11.27 (group 3). The mean resistivity in the summer months (group 2) is seen to be higher than that during the rest of the year, but because of the large standard deviations this difference is not significant ($p>0.3$, 2-sided t-test). Hence, we are unable to conclude that aqueous collected during the summer months is more resistive than that collected during the rest of the year.

It is useful to characterize resistance measurements by a characteristic time and a final (steady state) resistance. Those curves which show no tendency towards steady-state behavior are assumed to be initial transients for very highly resistive perfusions. One approximate way of estimating these parameters is to fit each (unsmoothed) data curve to the simple exponential

$$\frac{R}{R_\infty} = 1 - \left[\frac{R_\infty - R_0}{R_\infty}\right] e^{-t/\tau} \qquad (4.3.3)$$

using a non-linear least squares algorithm to obtain the three parameters R_0 (normalized initial resistance), R_∞ (normalized steady-state resistance), and τ. A much better fit was obtained if the first 50 seconds (10 points) of experimental data were discarded, presumably because initial transients were overlooked. In Figure 4.5 (a) the best exponential fit is superimposed on its generating data for one trace, the match being quite close. This particular fit had an r value of 0.995, which was judged to be the cutoff

point for acceptable fitting, and only fitted results from curves with $r \geq 0.995$ (first ten points discarded) will be presented.

When the fitted parameters R_∞, R_o and τ were compared with measured protein levels there was found to be a moderate positive correlation between R_∞ and protein levels (r=0.32)

$$R_\infty = 0.29 \text{ (protein conc.)} - 128, \qquad (4.3.4)$$

no corelation between protein concentration and τ (r=0.000) and a slight negative correlation between protein level and R_o (r=-0.29). Interestingly, resistivity and τ were correlated, with

$$\tau = 24.7\ R_{500} + 510 \qquad (4.3.5)$$

(r=0.35). Because correlations with fitted data are somewhat worse than those given by equations (4.3.1) and (4.3.2), there seems to be little advantage to be gained from fitting the data by (4.3.3).

Effects of Flowrate and Dilution

In several series of tests calf aqueous was perfused through 0.2 μ filters at different flowrates. Traces of normalized filter resistance as a function of total perfused volume for two different aqueous batches are shown in Figure 4.9, and it is seen that resistance scales well with total flow through the filter. Note however that the range of flowrates represented in Figure 4.9 is relatively small (less than one order of magnitude).

Figure 4.9 Normalized resistance of 0.2 μ filters as a function of total flow of calf aqueous humor perfused at 40 μl/min (solid lines) and 9 μl/min (dotted lines). (a) Perfusion on polycarbonate filters, (b) perfusion on PVP-free filters. Dotted lines in panel (b) represent an interrupted perfusion and restart on the same filter.

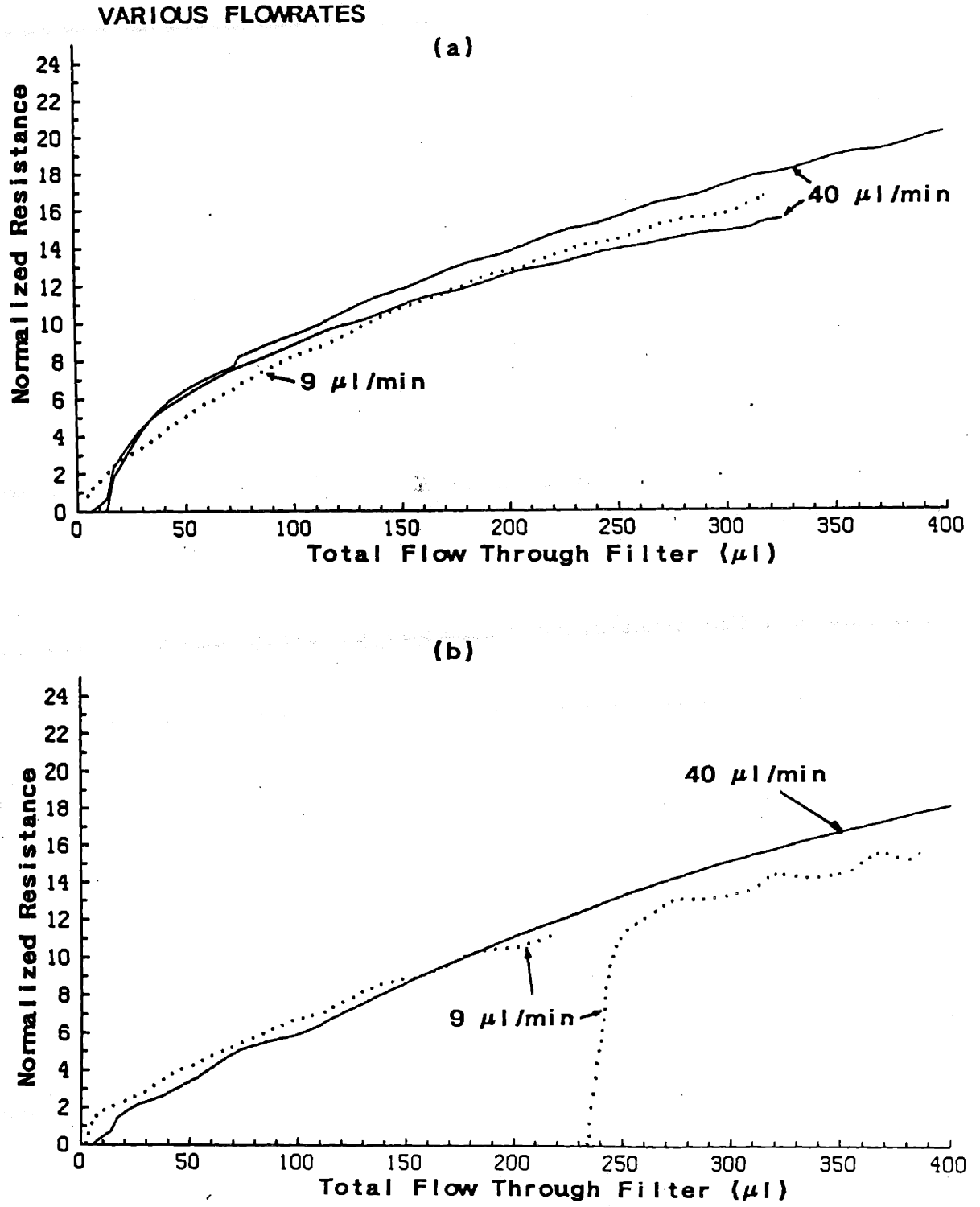

The behavior of calf aqueous humor which had been diluted by varying amounts was also studied. The effect of dilution was somewhat variable, and in some cases blockage scaled reasonably well with the volume of aqueous perfused through the filter, i.e. with the total perfused volume multiplied by the aqueous fraction in sample (Figure 4.10 (a)), while in other cases it did not (Figure 4.10 (b)). When perfused volume scaling did exist, some departure was seen at higher dilutions (10% curve in Figure 4.10 (a)). These results are further discussed in Chapters Five and Six.

4.4 Effects of Modifying Calf Aqueous Humor Composition

In an effort to identify the component(s) of calf aqueous humor responsible for filter blockage, a series of experiments were carried out in which selected aqueous constituents were removed, added or modified, and the effect on blockage observed.

Proteases

It was found that addition of broad spectrum proteases to calf aqueous humor eliminated its blocking capacity. In one series of experiments 0.5 ml papain was added to 1.5 ml calf aqueous and compared to aqueous which had filtered DPBS (rather than papain) added to it. When perfused through 0.2 μ polycarbonate filters, treated aqueous humor behaved like saline, suggesting that proteins (or protein moieties) are involved in the blocking process (Figure 4.11 (a)).

Figure 4.10 Plot of normalized resistance of 0.2 μ polycarbonate filters as a function of extent of aqueous humor dilution (Q = 40 μl/min). The abscissa is the total perfused aqueous volume, equal to total perfused volume multiplied by the aqueous dilution factor. Numbers on curves are fraction of aqueous in sample (dilution factor), and panels (a) and (b) represent perfusions from two different aqueous batches.

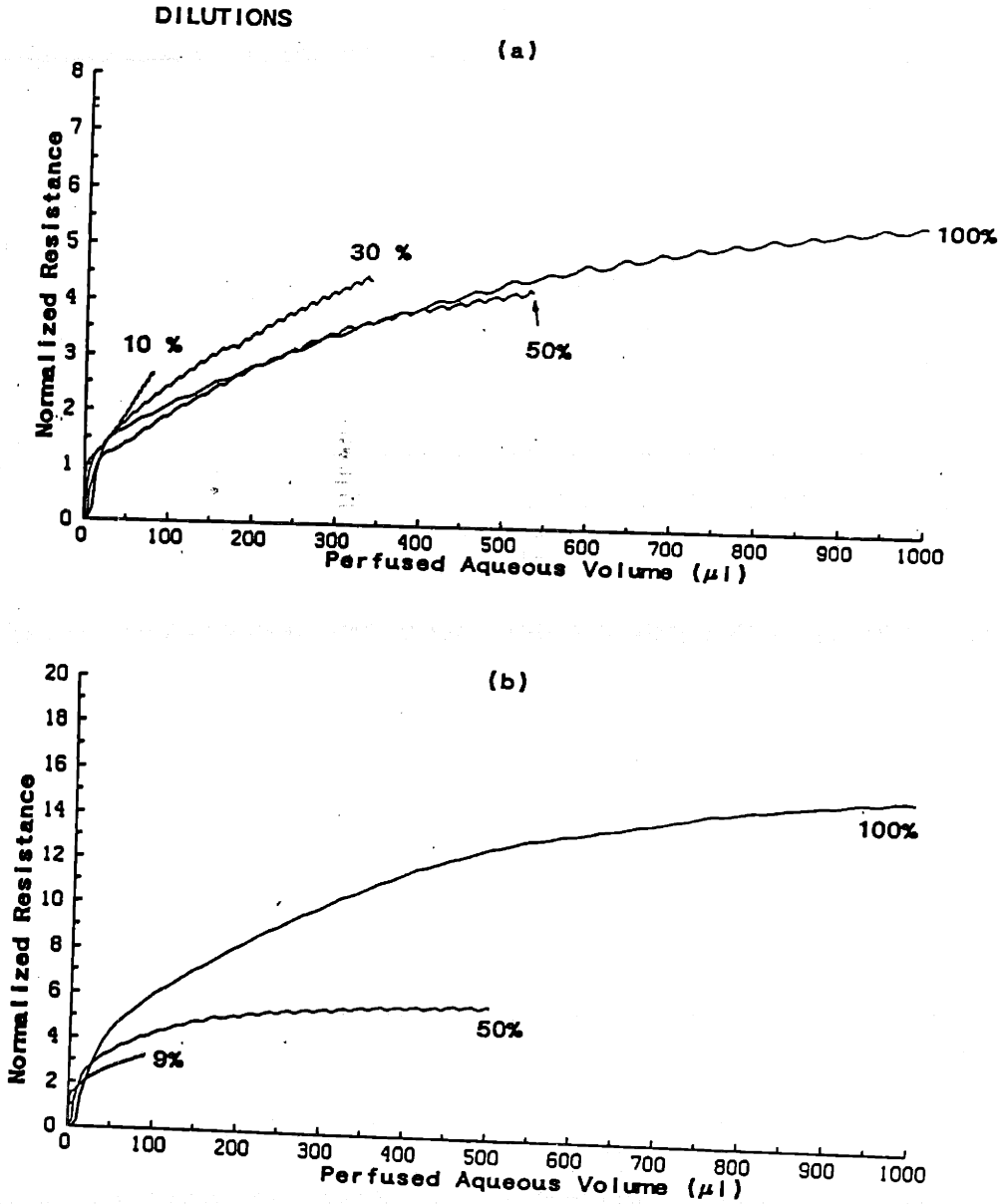

Figure 4.11 The effects of papain and Protease on the filter-blocking potential of calf aqueous humor. Legend: "Control" denotes aqueous diluted with saline (3:1), numbers on curves denote incubation time with appropriate enzyme. (a) Aqueous mixed with papain 3:1, incubation at 40 C, tests on 0.2 μ polycarbonate filters. (b) Aqueous mixed with Protease (3:1), incubation at 38 C, tests on 0.2 μ PVP-free filters. All tests at 40 μl/min.

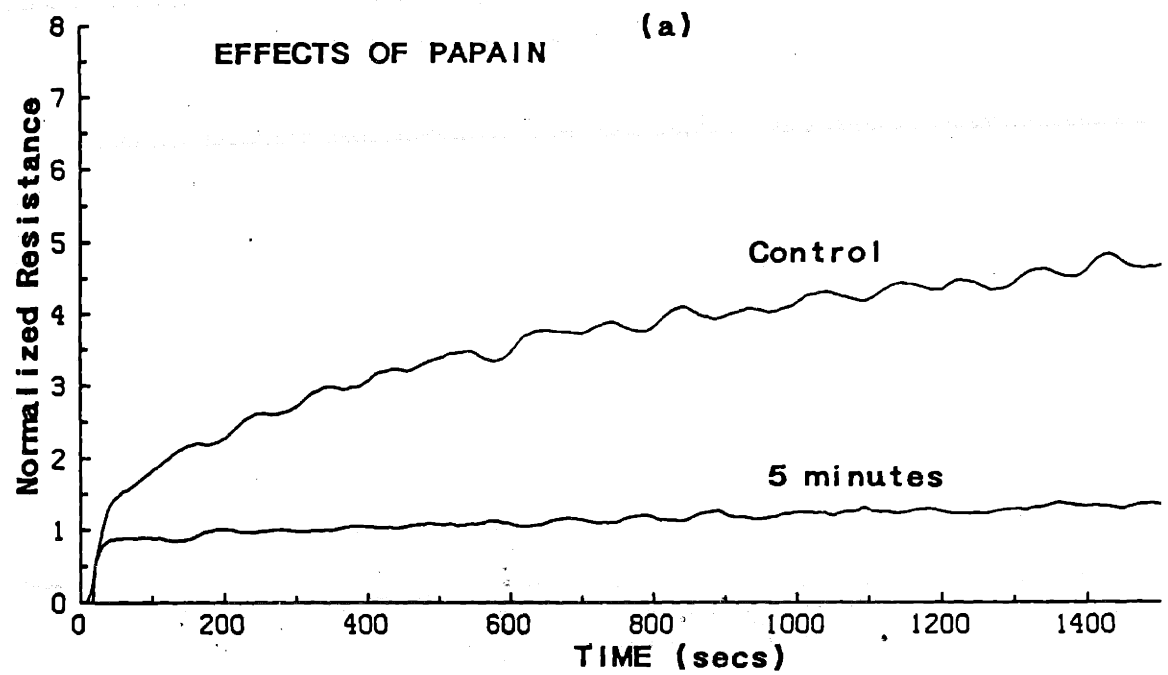

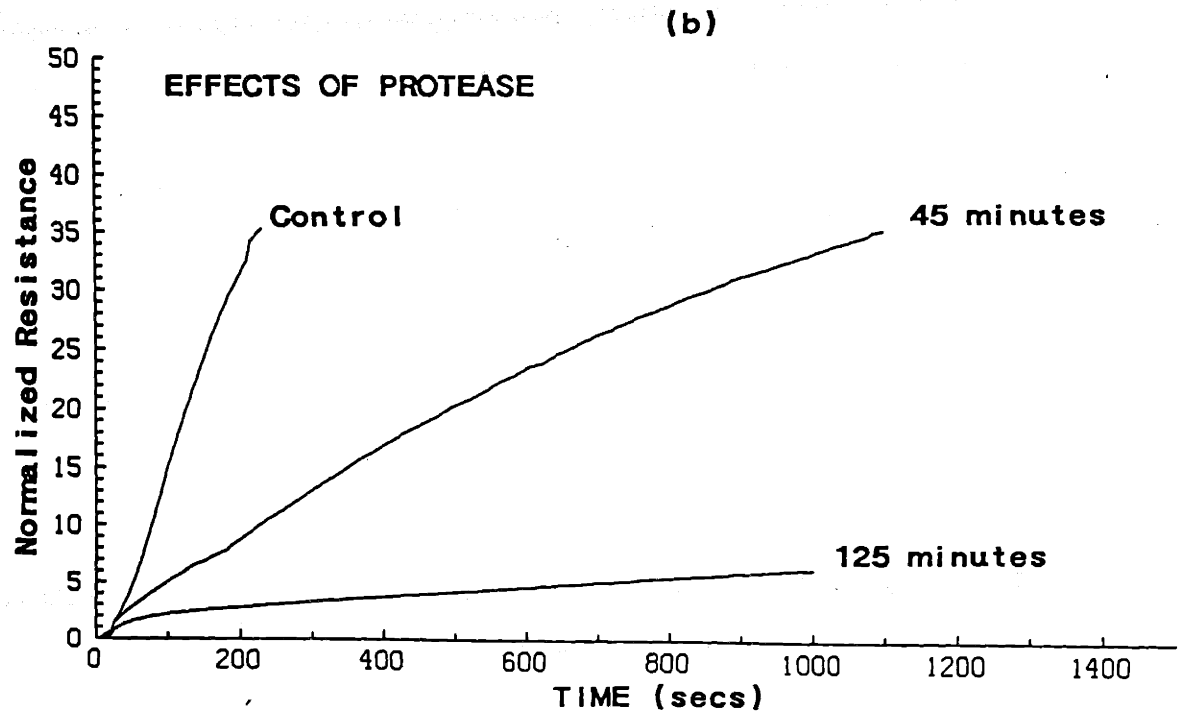

To eliminate the possibility that papain was indirectly removing the blocking effect by acting upon the PVP surfactant within the filters, a second series of tests on 0.2 μ PVP-free filters was conducted, in which 0.5 ml Protease was incubated with 1.5 ml aqueous humor for various times. Figure 4.11 (b) shows that although protease eliminated the blocking effect on 0.2 μ PVP-free membranes, it required a much longer incubation time to accomplish this. (It is presumed that incubation for longer than 125 minutes would completely eliminate the blocking capability of aqueous.) One possible explanation is that blocking material is adsorbed to the PVP-free filters at multiple sites and thus requires extensive digestion to be removed from the filter. Nonetheless, we conclude that proteases are not affecting aqueous blockage by acting upon the PVP surfactant.

In a second set of experiments a 0.2 μ polycarbonate filter was first perfused (blocked) with aqueous, after which it was post-perfused with a 1 mg/ml Pronase solution. As shown in Figure 4.12 Pronase post-perfusion quickly (after 1000 seconds) eliminated the initial resistance due to aqueous humor, further confirming that the blocking component(s) is a protein or protein-containing compound.

Hyaluronidase

A similar set of experiments was carried out to determine if GAGs were involved in the blocking process. Hyaluronidase addition was shown to completely eliminate the blocking capability of 400 μg/ml solutions of hyaluronic acid, while having a marginal (but observable) effect on aqueous humor blocking (Figure 4.13). In addition, the

Figure 4.12 The effects of Pronase postperfusion on blocked 0.2 μ polycarbonate filters (Q=40 μl/min). Solid lines: original aqueous blockage followed by Pronase postperfusion (1 mg/ml). Dotted line: baseline perfusion with pure Pronase solution on a second filter.

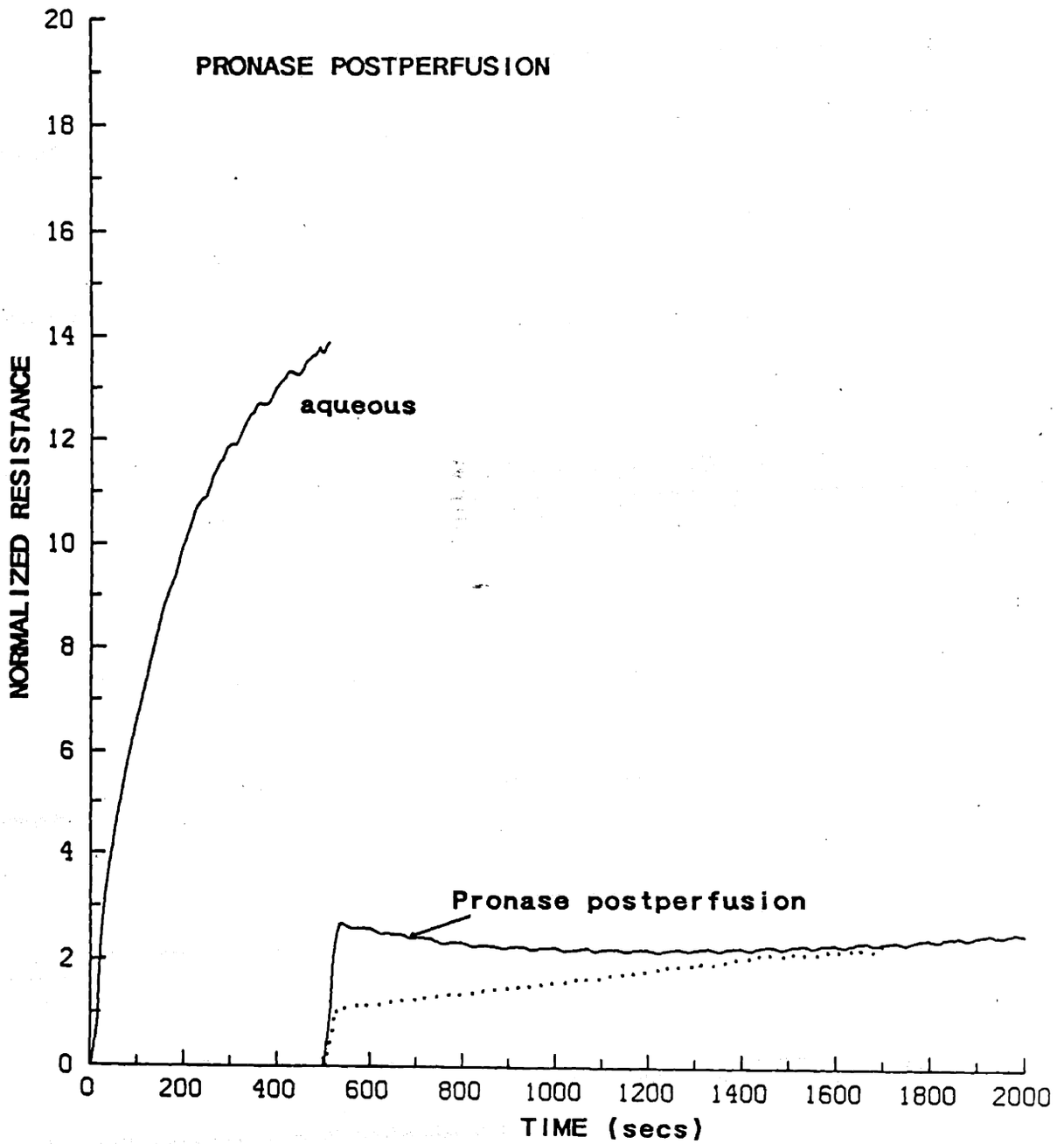

Figure 4.13 The effects of hyaluronidase upon the blocking potential of hyaluronic acid and calf aqueous humor. Solid lines: Control solution of hyaluronic acid or aqueous diluted with saline (3:1). Dotted lines : mixtures of hyaluronic acid or aqueous with hyaluronidase (3:1). All incubations at room temperature for 5-10 minutes, except for curve (*) (panel (d)), where incubation time was 100 minutes. (a) Hyaluronic acid, 400 μg/ml, (b)-(d) three separate batches of calf aqueous. All perfusions on 0.2 μ polycarbonate membranes at 40 μl/min.

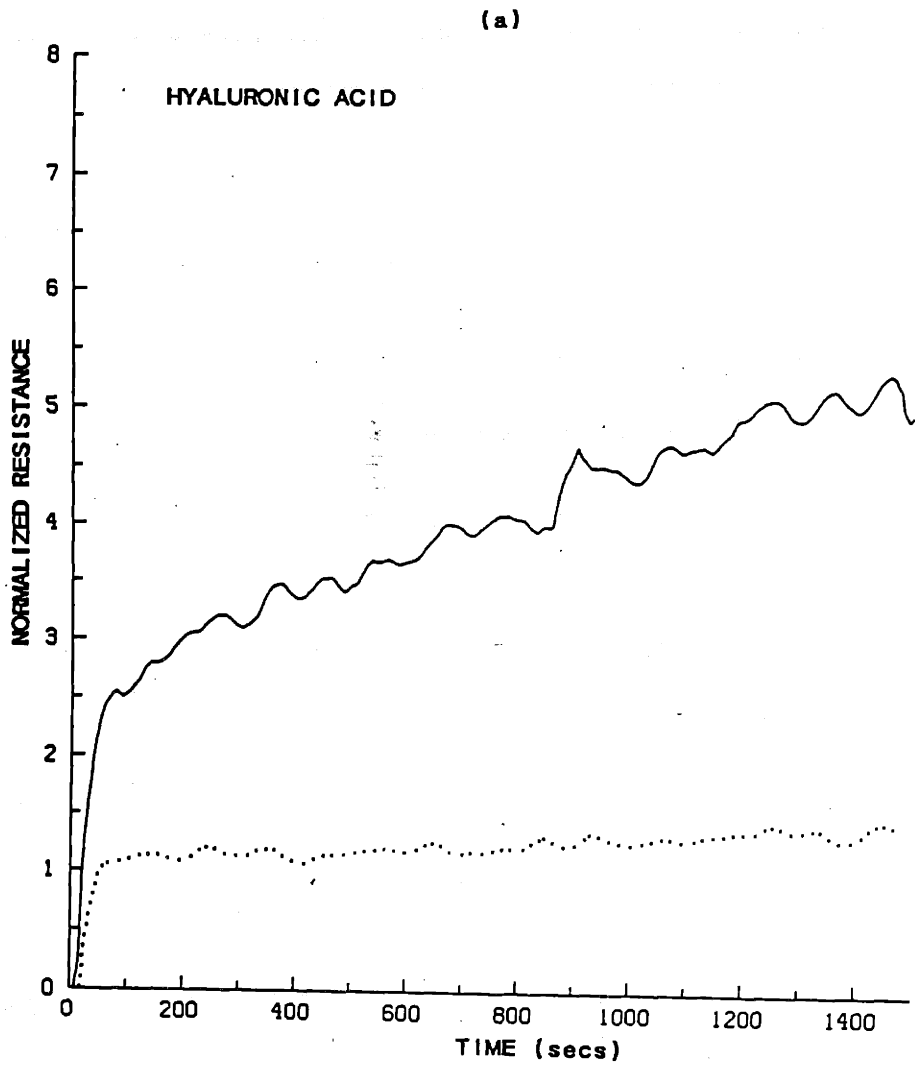

Figure 4.13 (continued).

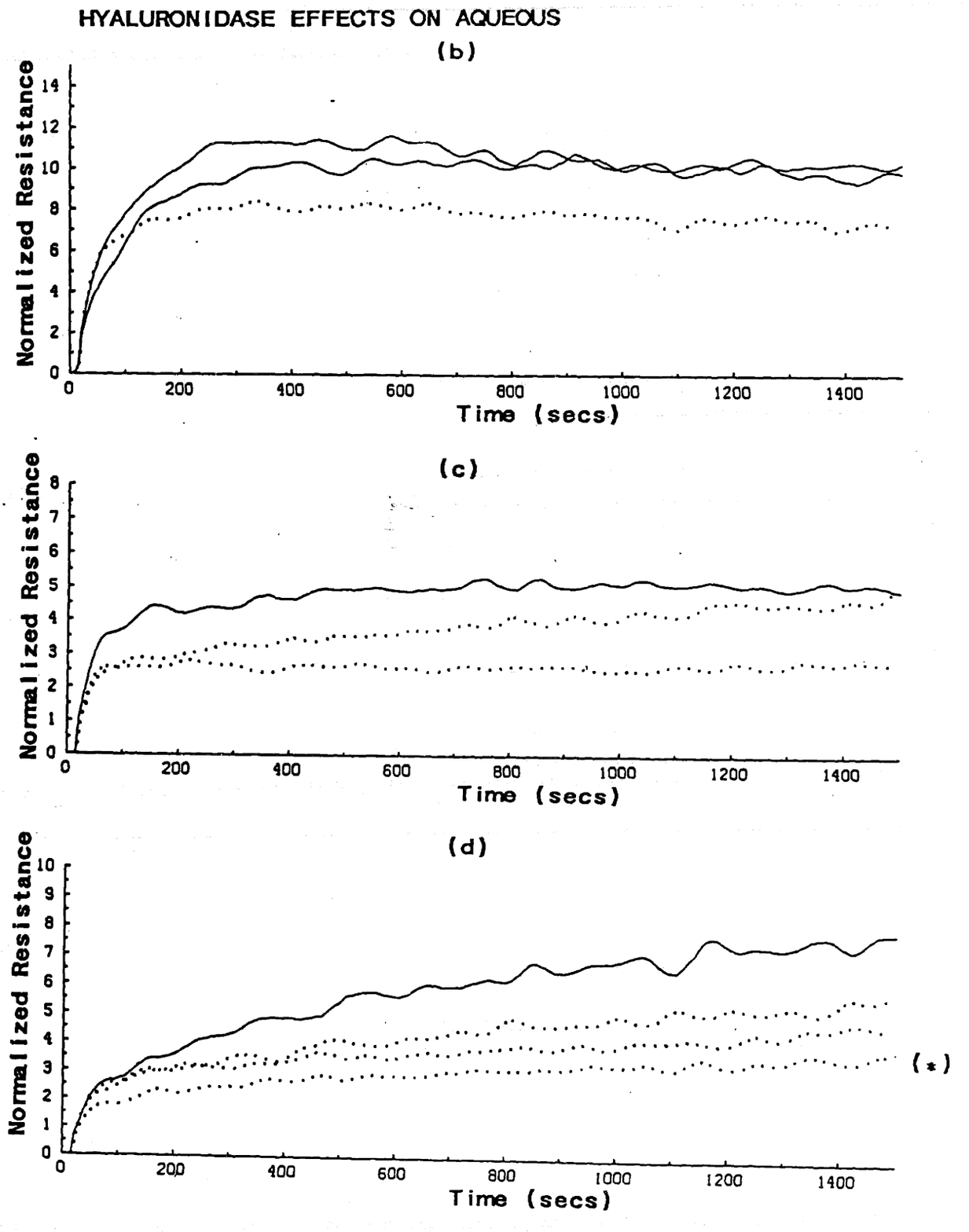

concentration of hyaluronic acid needed to obstruct 0.2 μ polycarbonate filters at the same rate as aqueous humor was 50-100 times higher than estimates for calf aqueous levels. Thus, it appears that GAGs play at most a secondary role in the filter-obstruction process.

Albumin and γ-Crystallin Spiking

A series of experiments were then conducted to determine which aqueous humor protein(s) were responsible for the blocking effect. One possible candidate is albumin, due to its relatively high concentration in the aqueous humor. When calf aqueous (initial protein concentration = 1166 μg/ml) was "spiked" by the 1:1 addition of a 3.5 mg/ml solution of bovine serum albumin, the resulting solution was seen to block the filters to a greater extent than pure aqueous humor and aqueous humor diluted 1:1 with DPBS (Figure 4.14 (a)). Paradoxically, albumin alone (at the same concentration) did not block 0.2 μ polycarbonate filters. A similar experiment in which aqueous (original protein concentration: 765 μg/ml) was spiked 1:3 with lens γ-crystallins (original concentration: 1200 μg/ml) showed that the aqueous/lens protein mixture blocked 0.2 μ filters to a greater extent than did a 1:3 aqueous:DPBS mixture (Figure 4.14 (b)), while lens proteins alone did not block 0.2 μ polycarbonate filters. When aqueous was spiked with a dilute solution of γ-crystallins (100 μg/ml) there was no increase in blocking capacity, while spiking aqueous with an albumin/γ-globulin mixture (3.5 and 1.0 mg/ml, respectively) gave results similar to the albumin spiking experiment. Finally, when lens proteins were mixed with this latter protein solution, the resulting fluid did not block 0.2 μ polycarbonate filters.

Figure 4.14 The effects of spiking calf aqueous humor with albumin or lens proteins. (a) Addition of albumin (3.5 mg/ml) to calf aqueous (total protein-1166 μg/ml). (b) Addition of lens γ-crystallins (1200 μg/ml) to calf aqueous (total protein-765 μg/ml). All perfusions at 40 μl/min on 0.2 μ polycarbonate membranes.

(a)

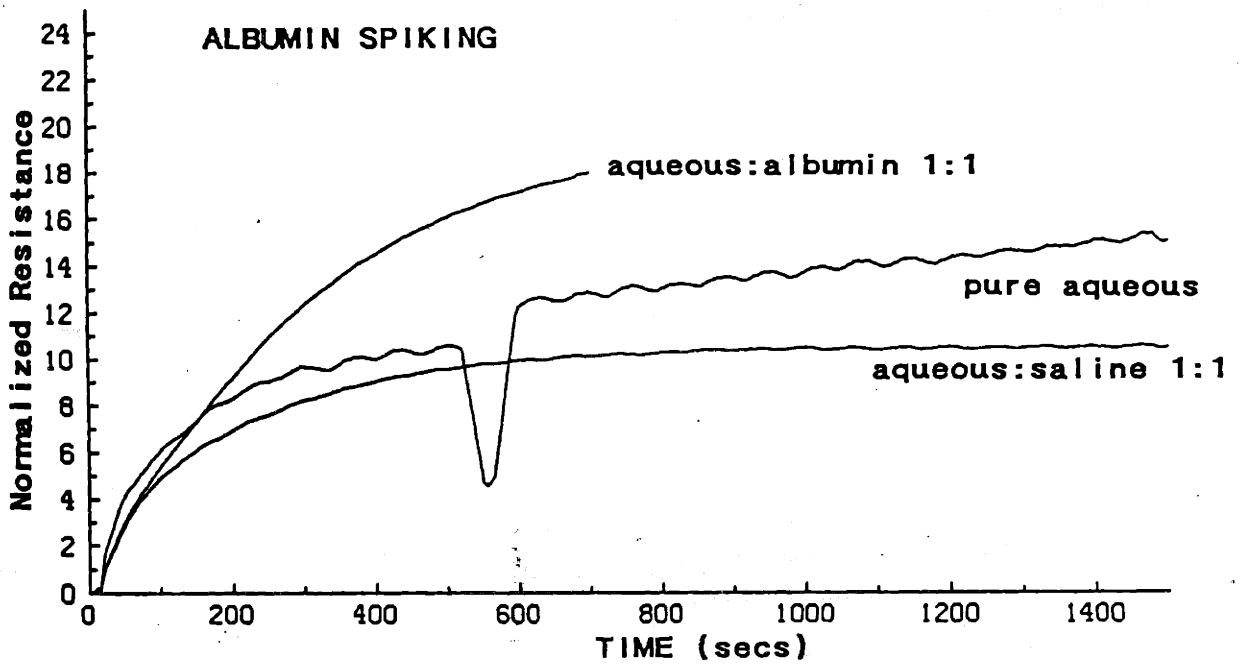

(b)

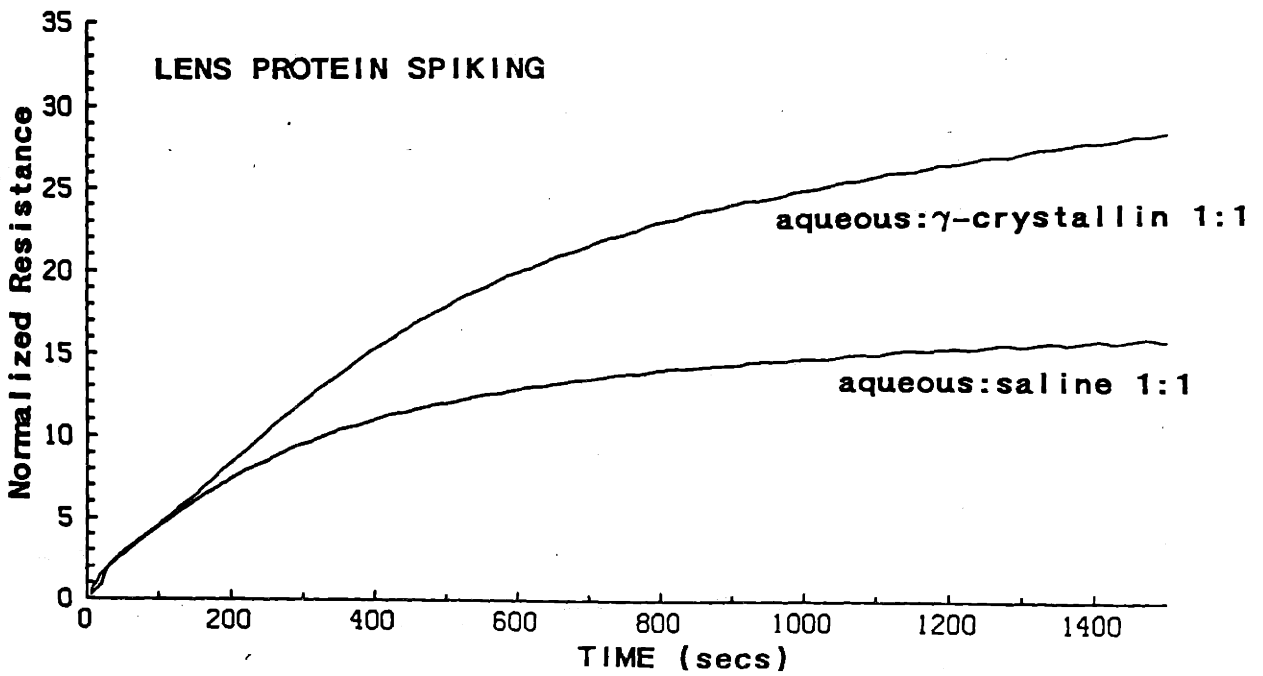

To summarize, the addition of albumin and lens γ-crystallins in high concentrations enhances the blocking capacity of aqueous, yet these substances individually and in combination do not block 0.2 μ filters. Furthermore, the additional blocking capacity conferred by spiking is less than proportional to the increase in total protein content. For example, estimating the albumin concentration in the aqueous humor used in the albumin spiking experiment to be 700 μg/ml, 1:1 addition of albumin at 3.5 mg/ml should correspond to a tripling of albumin concentration, while the increase in blocking is clearly less than triple. We have interpreted these results to mean that the blocking process requires two classes of components, which for discussion purposes we denote as "A" and "B". Since an albumin/γ-crystallin mixture does not block, both of these proteins belong to the same blocking class, say A. Furthermore, since blocking increases relatively weakly with spiking protein concentration, it seems plausible that the blocking process is essentially limited by the amount of substance B present. These ideas will be further discussed in Chapter Six.

Fibrinogen

In order to test fibrinogen as a blocking candidate, a spiking experiment was conducted in which fibrinogen (500 μg/ml) was added 1:1 to calf aqueous (protein: 661 μg/ml). Although the fibrinogen content of calf aqueous humor is not known, a generous estimate would be 50 μg/ml. Thus, although addition of fibrinogen at 500 μg/ml should produce a 5-fold increase in fibrinogen (including dilution effects), it had little effect on blocking (see Figure 4.15 (a)). It is interesting to note that addition of fibrinogen did seem to modify the nature of the blocking process.

Figure 4.15 The role of fibrinogen in filter blockage. (a) Addition of fibrinogen (500 μg/ml) to calf aqueous (total protein-661 μg/ml). (b) The effects of selective fibrinogen and fibronectin precipitation by ethanol addition on calf aqueous blocking capacity. Perfusions at 40 μl/min on 0.2 μ polycarbonate filters.

(a)

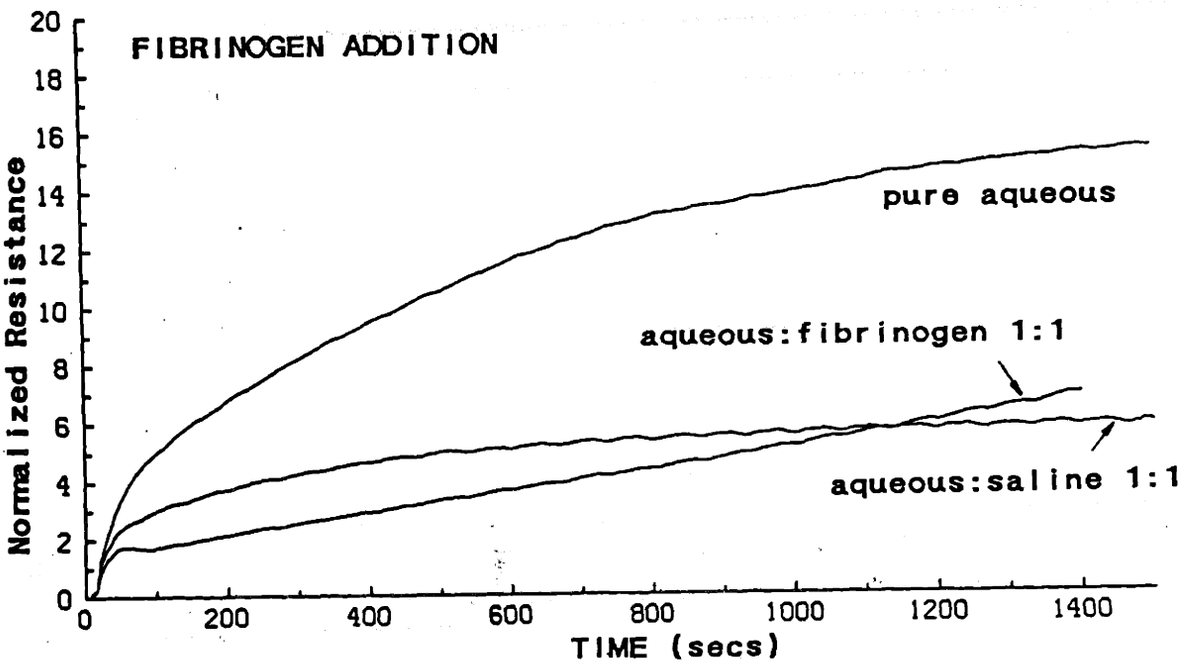

(b)

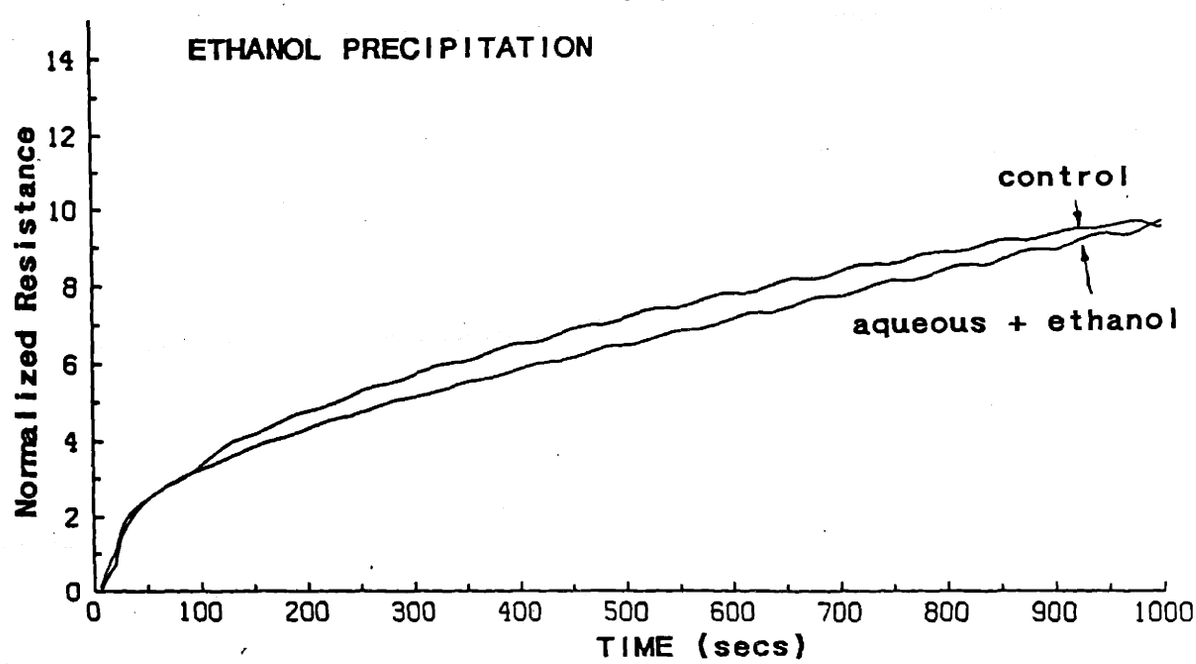

To further investigate the possible role of fibrinogen in the blocking process, a series of experiments were carried out in which fibrinogen and fibronectin (Cohn Fraction I) were selectively precipitated from the aqueous humor by addition of 9% ethanol. The protein content of ultracentrifuged aqueous humor treated in this manner decreased 21-44 μg/ml (compared with ultracentrifuged, untreated aqueous humor, with correction for dilution), and all fibrinogen in a 250 μg/ml test solution was successfully removed by this method. However, the aqueous treated in this manner blocked 0.2 μ polycarbonate filters to the same extent as did untreated fluid (Figure 4.15 (b)), further suggesting that neither fibrinogen nor fibronectin are responsible for the blocking process.

A final series of experiments were carried out in which calf aqueous humor was added to sodium citrate immediately upon collection. This citrated aqueous humor was found to retain its blocking capacity on both 0.2 μ regular and PVP-free polycarbonate membranes. Thus we conclude that neither fibrinogen nor fibronectin are directly responsible for filter blockage.

Freezing

In several experiments calf aqueous humor was frozen for various lengths of time, then thawed and compared to untreated aqueous humor. Although calf aqueous humor frozen for one hour showed a decrease in total protein content (901 μg/ml *versus* 957 μg/ml, both solutions ultracentrifuged), the frozen and untreated fluids behaved identically when perfused through 0.2 μ polycarbonate filters. Calf aqueous humor frozen for 21 days also showed

a slight drop in protein content (790 μg/ml to 772 μg/ml, both solutions ultracentrifuged), and blocked 0.2 μ filters to the same extent (or slightly more) than untreated aqueous humor tested on the day of collection. Hence, we conclude that freezing has no effect on the blocking capacity of calf aqueous.

Detergent Perfusion and Miscellaneous Protocols

The addition of detergents (1% and 0.1% Triton-X 100 and 1% SDS) to aqueous humor was found to eliminate all blocking capability on 0.2 μ polycarbonate filters (Figure 4.16). These results will be further discussed in Section 6.3.

In one experiment the pH of calf aqueous humor was raised from 7.6 to 9.0 by addition of 0.1N NaOH. This sample was found to block slightly less than untreated aqueous (Figure 4.17 (a)), but the extent of decrease was relatively small, and thus we conclude that blocking is not highly sensitive to pH.

Addition of 0.7 mg (175 units) of the enzyme ascorbate oxidase to 3 ml of calf aqueous humor was found to slightly increase the blocking capacity of calf aqueous (Figure 4.17 (b)). Addition of ascorbate oxidase to pure ascorbate solutions was spectrophotometrically found to eliminate the majority of ascorbate present, and thus we conclude that ascorbate is not a necessary component in the blocking process. This does not rule out the possibility of dihydroascorbate (the oxided form of ascorbate) playing a role.

Figure 4.16 The effects of detergent and spermine addition on the blocking potential of calf aqueous humor. Curve 1: calf aqueous humor:saline control mixture (2:1), curve 2: calf aqueous humor:0.2 mg/ml spermine mixture, curve 3: calf aqueous humor:1% Triton-X 100 mixture (2:1), curve 4: calf aqueous humor:0.1% SDS mixture (2:1). All perfusions at 40 μl/min on 0.2 μ polycarbonate memebranes.

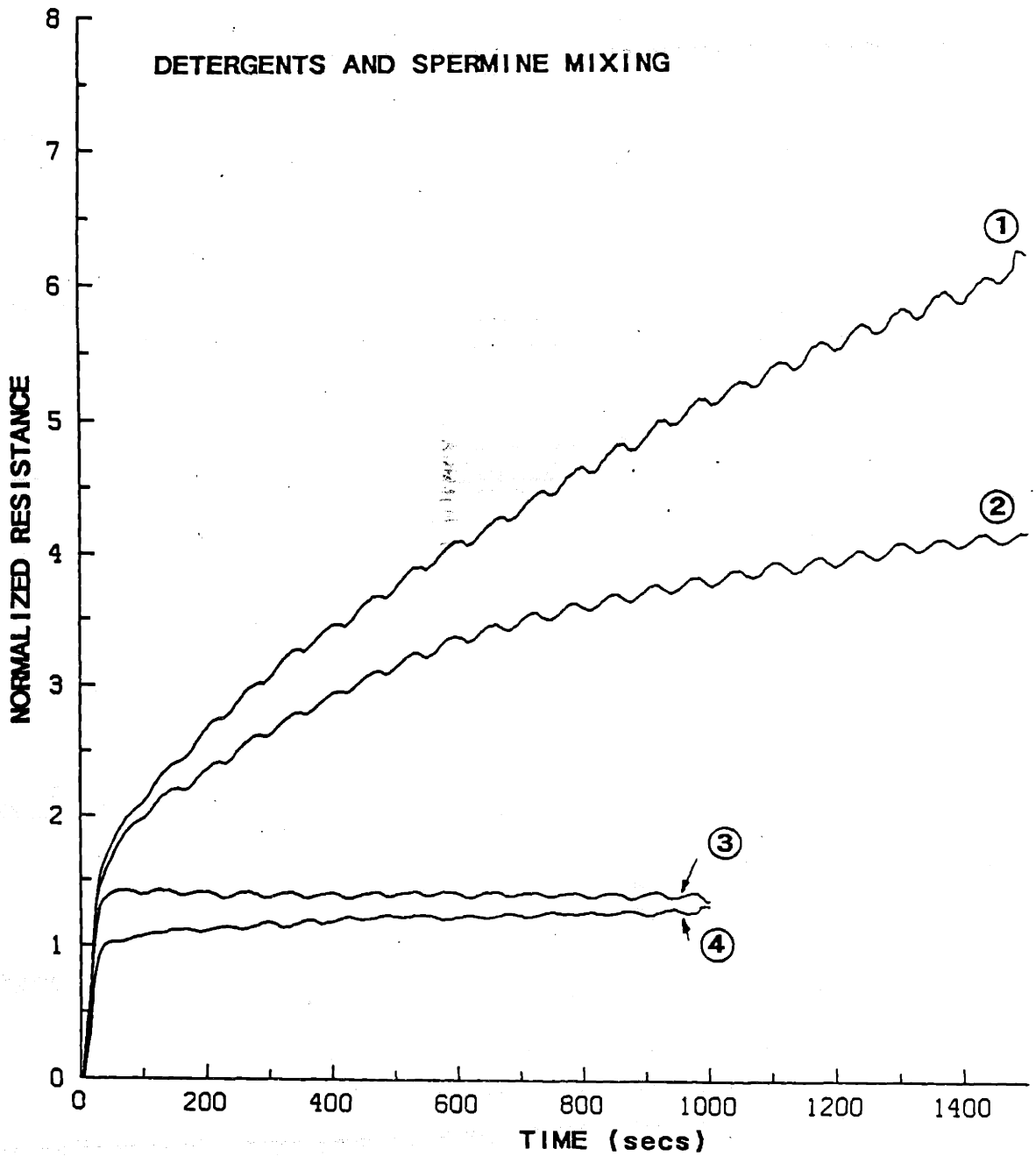

Figure 4.17 The effects of pH and ascorbate concentration on the blocking potential of calf aqueous humor. (a) The blocking behavior of basic calf aqueous humor on 0.2 μ polycarbonate filters. (b) The effects of ascorbate oxidase addition on the blocking potential of calf aqueous humor on 0.2 μ PVP-free membranes. Curve 1: aqueous:ascorbate oxidase mixture (60 units/ml aqueous, incubation at room temperature for 45 minutes).

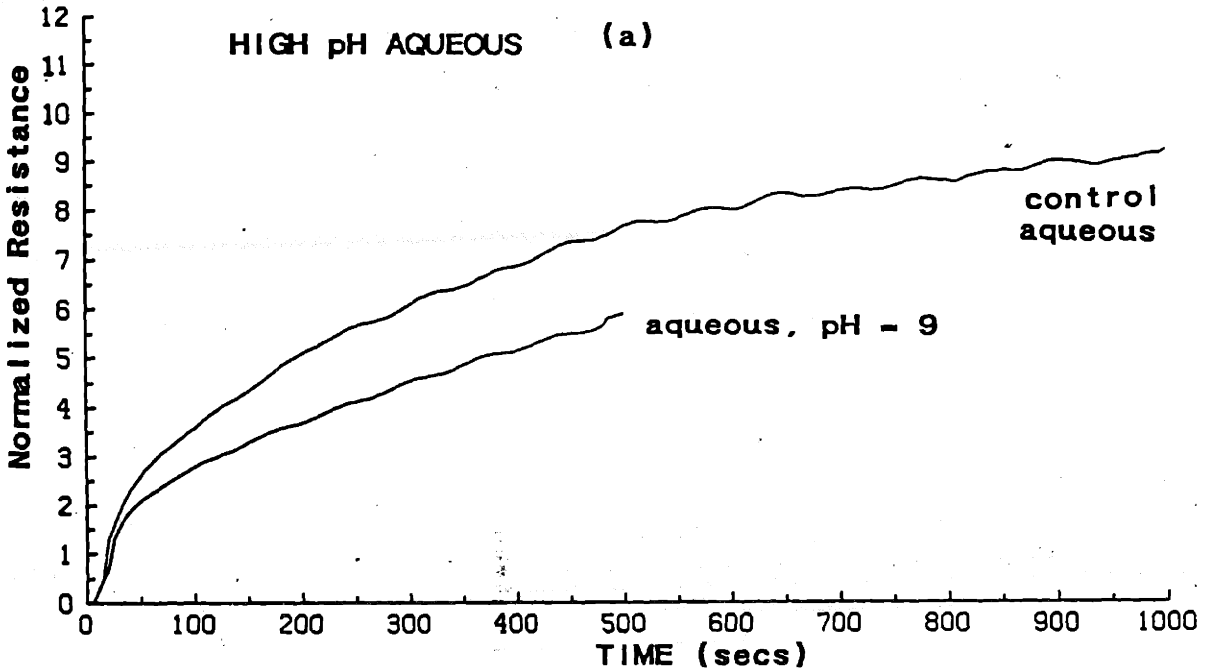

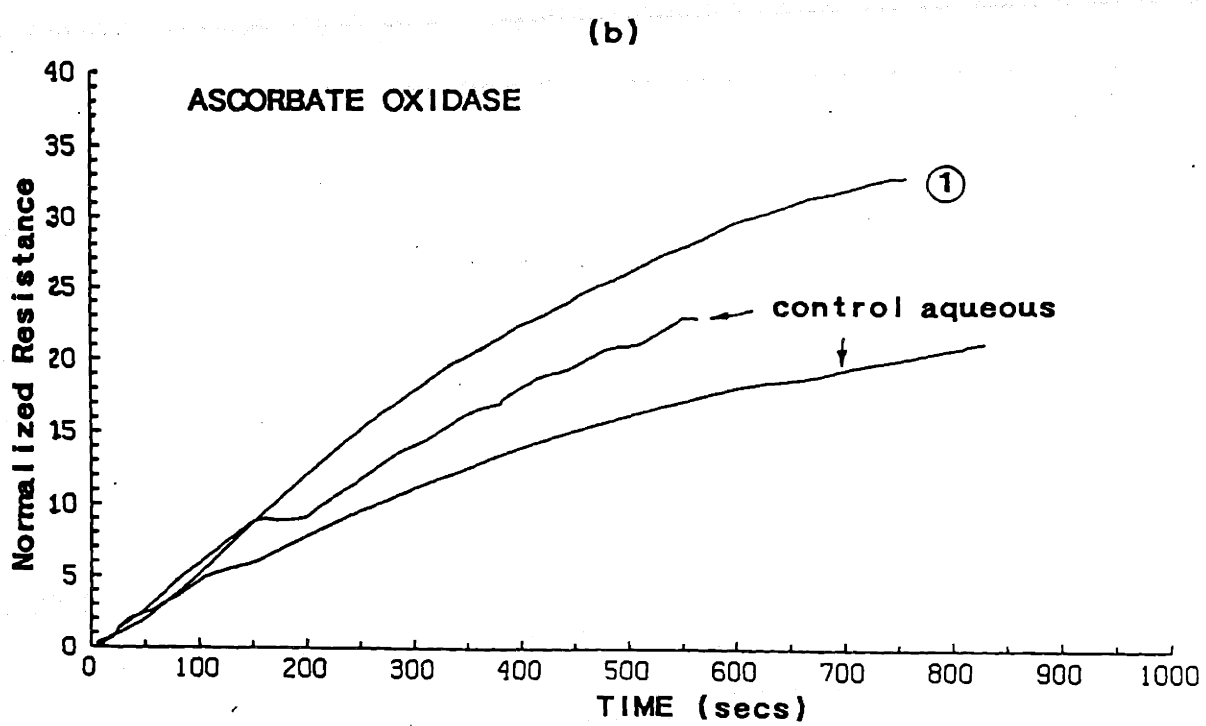

Addition of a 0.2 mg/ml solution of the polycationic polyamine spermine to calf aqueous humor was found to reduce the blocking capacity of aqueous humor on 0.2 μ polycarbonate filters, when compared to aqueous humor diluted to the same extent with DPBS (Figure 4.16). This result will be further discussed in Section 6.3.

4.5 Effects of Filter Surface Chemistry and Pore Geometry

Filter Surface Chemistry

The rate and extent of calf aqueous humor blockage was found to depend very strongly upon filter substrate material, and hence presumably on filter surface chemistry. In particular, calf aqueous humor blocked to a much greater extent on 0.2 μ polycarbonate PVP-free membranes than it did on regular polycarbonate membranes, suggesting that membrane hydrophobicity is an important determinant of blocking behavior. This conclusion is supported by tests on Millipore GVWP (hydrophilic) and GVHP (hydrophobic) membranes (pore diameter 0.22 μ) showing little or no blocking of GVWP membranes and readily discernible blocking on GVHP membranes. Finally, aqueous humor was found to aggressively block 0.2 μ polyester membranes. These results are summerized in Figure 4.18, where representative curves (not all taken from the same aqueous humor batch) are displayed for each membrane type.

In addition to perfusing calf aqueous humor through filters of different materials, the effects of filter surface chemistry were investigated by exposing membranes to

Figure 4.18 Representative plots of calf aqueous humor blockage on four different membrane types. All perfusions at 40 μl/min.

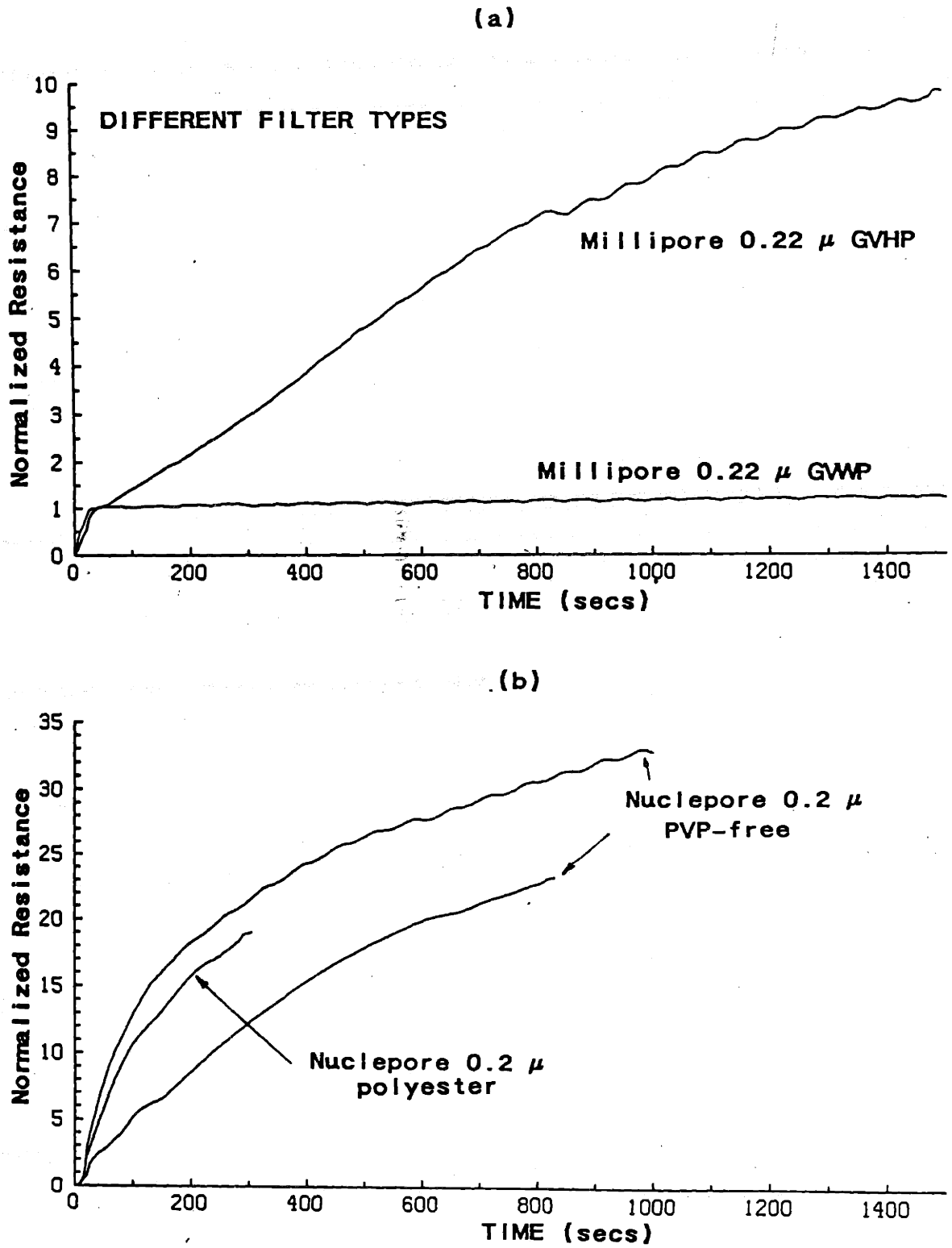

various surface-altering agents before perfusion. For example, preperfusing 0.2 μ polycarbonate filters with 1.0 and 0.1 % Triton-X 100 prior to aqueous perfusion significantly enhances blockage (Figure 4.19). A second agent which has been found to be effective in modifying the blockage behavior of 0.2 μ polycarbonate filters is spermine. Figure 4.19 shows that spermine preperfusion causes a significant decrease in blocking, while preperfusion with a mixture of spermine and Triton-X causes an intermediate effect. The dimunition of blocking capacity of 0.2 μ polycarbonate filters due to spermine preperfusion was variable, but in all cases it was significant. On the other hand, spermine preperfusion of 0.2 μ polyester membranes had no discernible effect on blockage.

A series of experiments was conducted in which filters were exposed to quiescent (non-flowing) calf aqueous humor for various lengths of time before being perfused. The protocol consisted of "presoaking" the membrane in 0.5-3.0 ml of aqueous humor for 5-40 mintues, then immediately perfusing the membrane with either fresh aqueous humor or saline. Figure 4.20 shows the results of five such tests on 0.2 μ polycarbonate membranes, and it is seen that presoaking produces a large decrease in the filter blockage. In addition, presoaking appeared to slightly elevate membrane baseline resistance, as determined by saline perfusion. In one test (not shown) where the membrane was presoaked in only 200 μl of aqueous humor the extent of the decrease was not as great (although still significant).

Similar tests on 0.2 μ polyester and PVP-free filters gave variable results which differed from those for 0.2 μ polycarbonate membranes (Figure 4.20 (b)). It is hypothesized that these results are due to the fact that polyester and PVP-free membranes are highly effective

Figure 4.19 The effects of filter pretreatment on the blocking behavior of 0.2 μ polycarbonate membranes. Curve 1: filter preperfusion with 0.5 ml 1% Triton-X, curve 2: preperfusion with 0.2 ml 0.2 mg/ml spermine and 1% Triton-X mixture (1:1), curve 3: untreated filter, curve 4: preperfusion with 1 ml 0.2 mg/ml spermine solution. All preperfusions and aqueous tests at 40 μl/min.

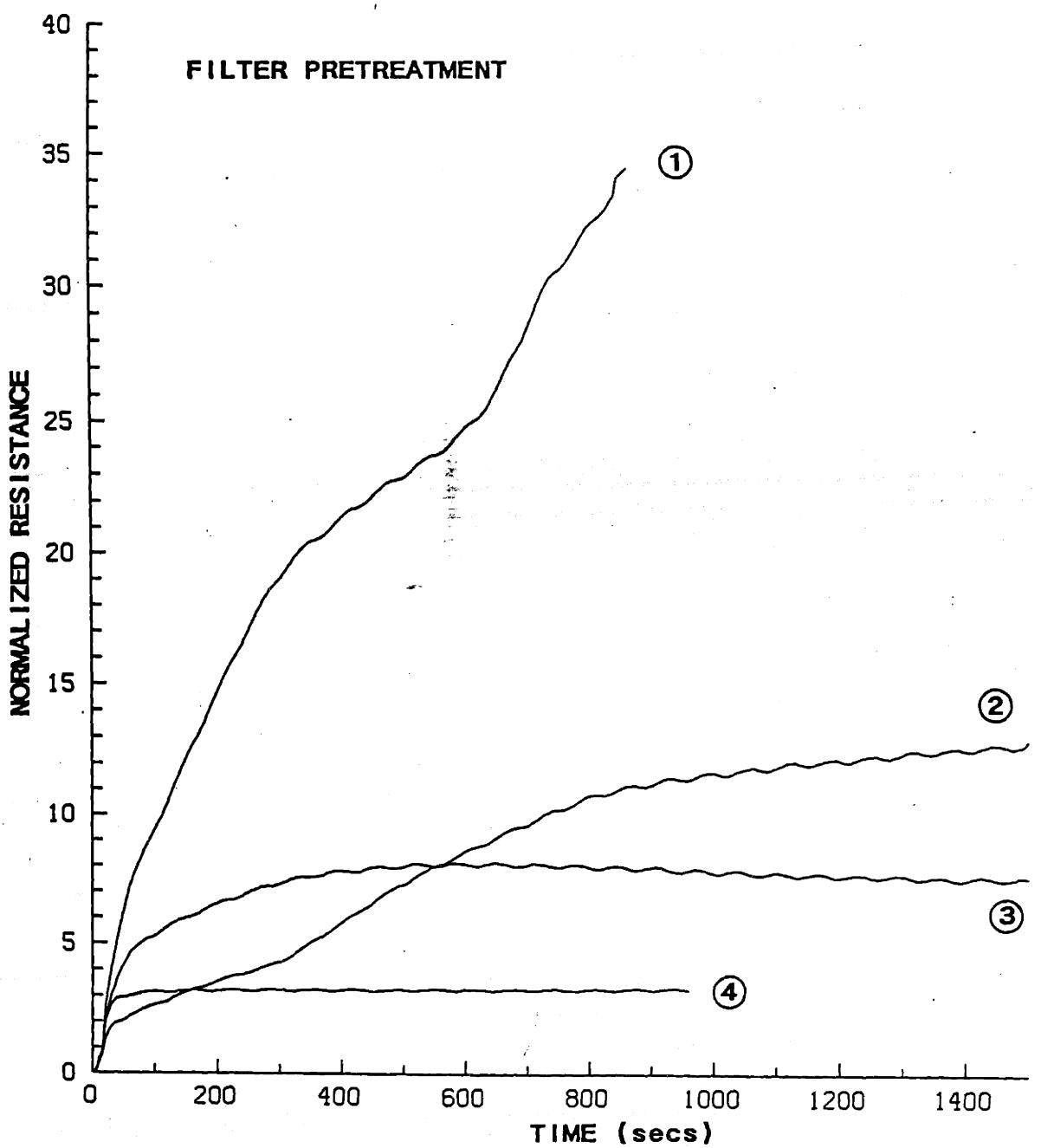

Figure 4.20 The effects of presoaking filters in calf aqueous humor. Curves 1: calf aqueous pefusion on untreated membranes, curves 2: calf aqueous perfusion on presoaked filters. (a) Presoaking of 0.2 μ polycarbonate membranes. Three separate aqueous perfusions are shown. Dotted lines: saline perfusion on presoaked filters. (b) and (c) presoaking of 0.2 μ polyester and PVP-free membranes, respectively. All perfusions at 40 μl/min.

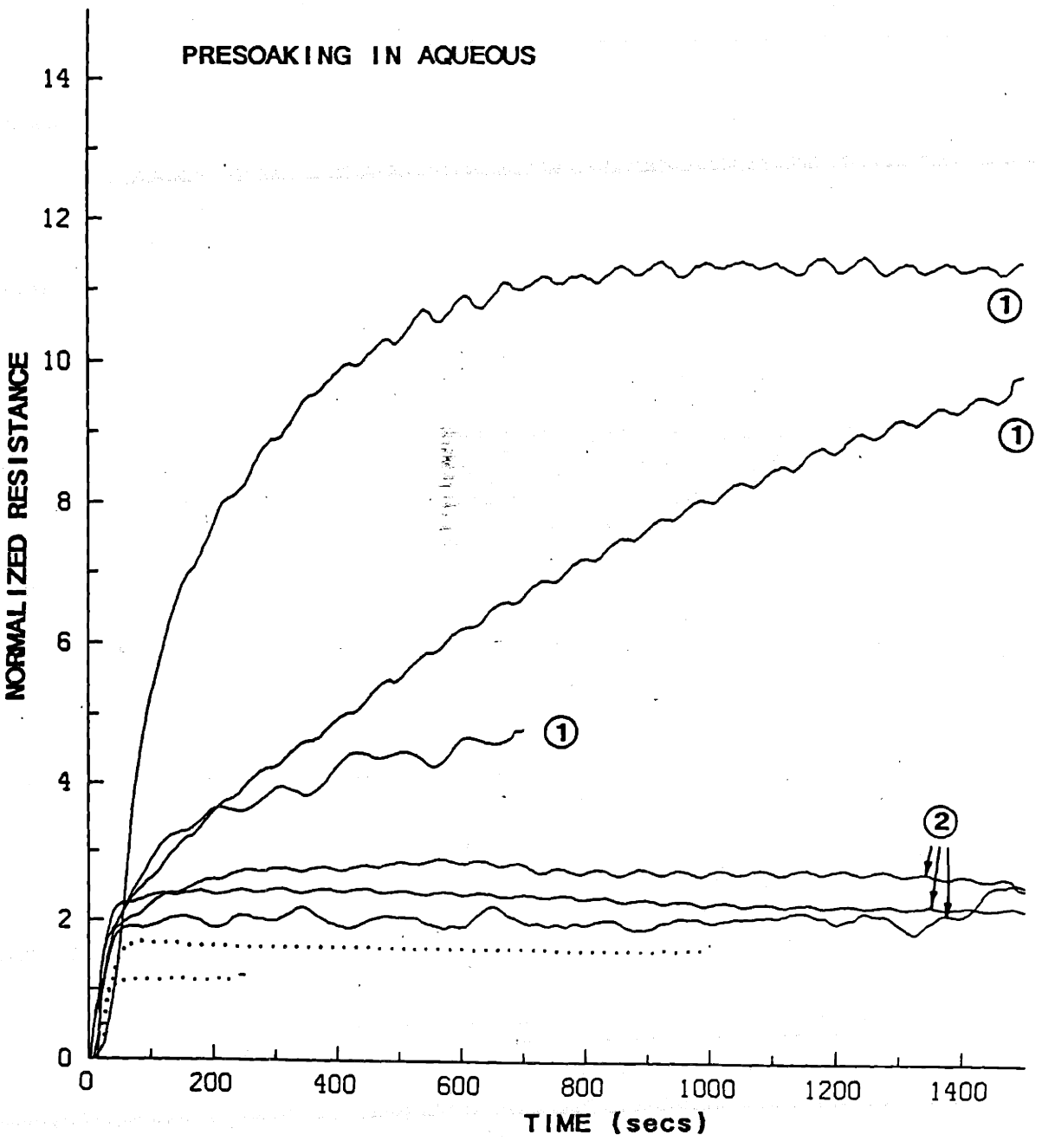

Figure 4.20 (continued).

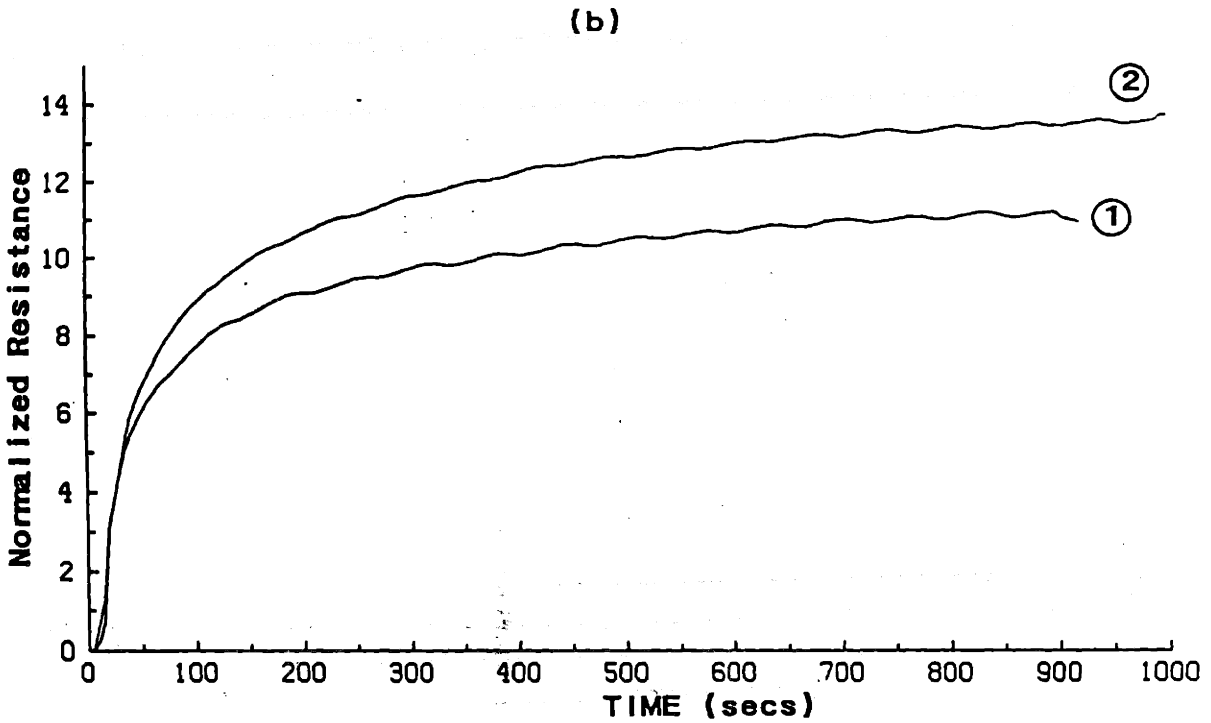

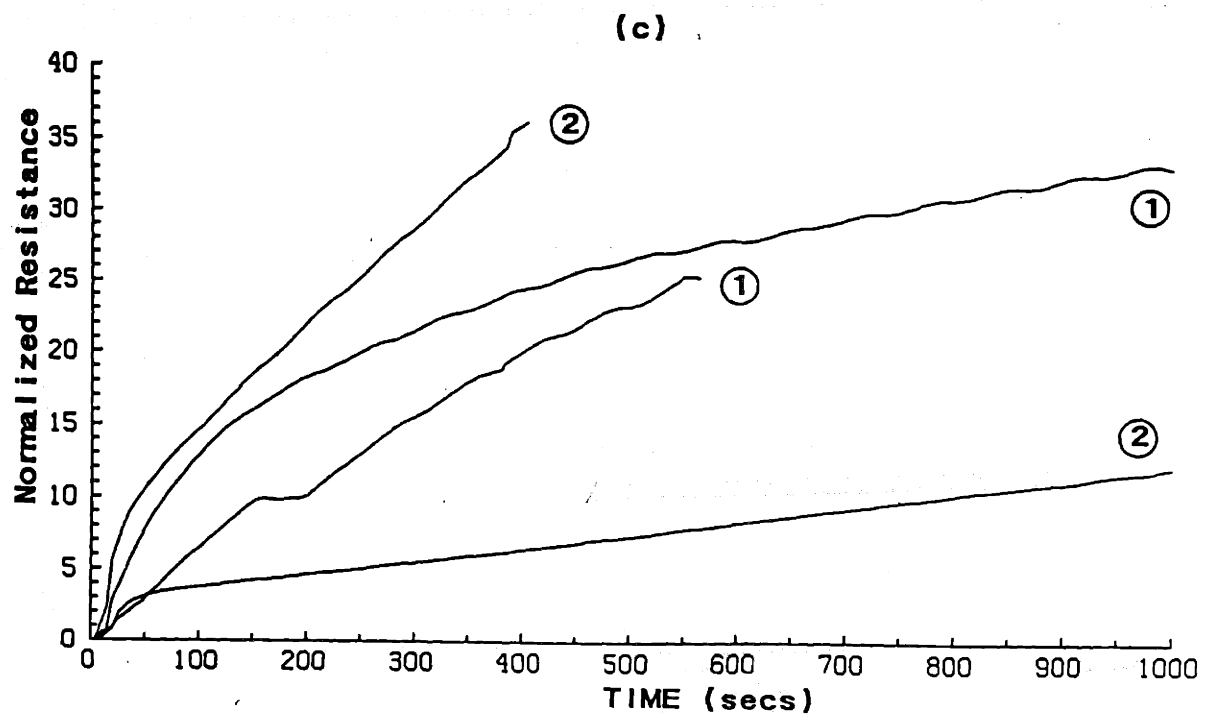

blockers, so that aqueous presoaking of these filters produces a proportionally smaller effect than on polycarbonate membranes.

Pore Geometry

A second filter characteristic upon which the blocking process was found to depend strongly is pore geometry, and in particular, pore diameter. Figure 4.21 shows the results of one series of experiments in which the same batch of diluted calf aqueous humor was perfused through polycarbonate filters having nominal pore diameters of 0.2, 0.4 and 0.6 μ. Evidently, the extent of blocking is much less for the larger pore diameter membranes. A second interesting observation is that the characteristic blocking time decreases sharply with membrane pore diameter. In Figure 4.22 the strong dependence of steady-state resistance on measured pore radius (Table 4.1) is displayed (see also Table 5.2). These results cannot be explained by differences in wall shear rate, γ, since the same behavior was observed in a series of experiments in which flow rate was adjusted to give similar values of γ for 0.2 and 0.4 μ filters. This puzzling phenomenon will be further explored in Sections 5.4 and 6.3.

Tests on Millipore tortuous path membranes have also indicated that the blocking process depends on pore shape. For example, comparing the curves for hydrophobic PVP-free 0.2 μ polycarbonate membranes to those for hydrophobic GVHP membranes (Figure 4.18) indicates that the blocking proceeds much more slowly and to a lesser extent on the GVHP than on the PVP-free membranes. This may be due to the much greater internal pore volume and high degree of pore interconnectivity in the Millipore filters (Section 6.3).

Figure 4.21 Blockage of 0.2, 0.4 and 0.6 μ polycarbonate membranes by perfusions from the same batch of aqueous. (a) Perfusions on 0.2 μ filters at 40 μl/min, (b) perfusions on 0.4 and 0.6 μ filters at 103 μl/min.

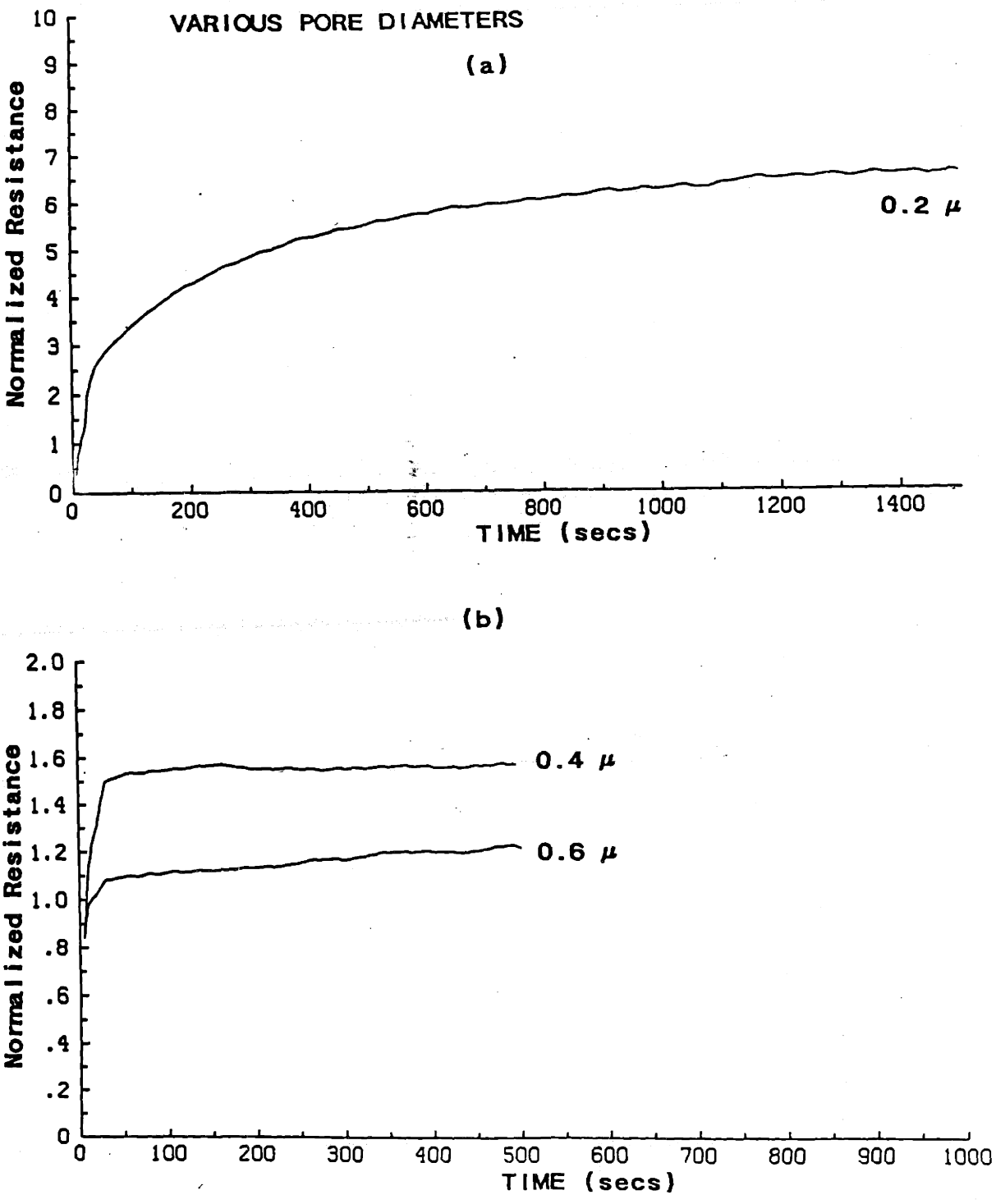

Figure 4.22 Plot of the normalized steady-state resistance as a function of the filter pore radius for 0.2, 0.4 and 0.6 μ nominal pore diameter membranes. Each symbol represents perfusions from one batch of aqueous.

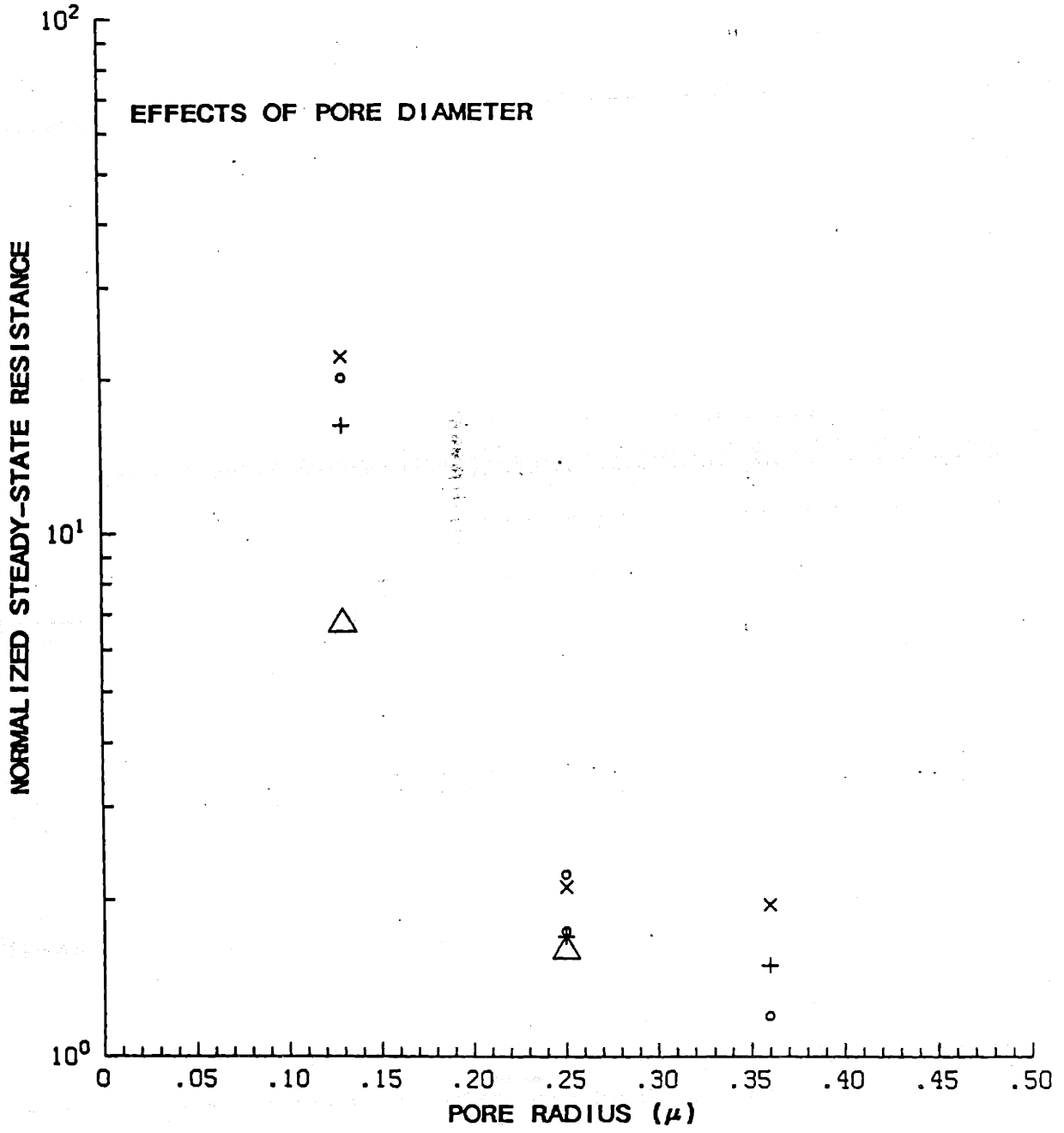

4.6 Other Effects Related to Calf Aqueous Humor Perfusion

Mock Aqueous

In an attempt to identify the blocking component(s) of aqueous humor, solutions of "mock aqueous humor" containing several important calf aqueous constituents were perfused through filters. A mixture of albumin (350 μg/ml), γ-globulin (100 μg/ml), fibrinogen (25 μg/ml) and thrombin (2.5×10^{-3} NIH units/ml) was found to block 0.2 μ polycarbonate filters to a very small extent (Figure 4.23), while these components perfused individually at the indicated concentrations produced no discernible blockage (data not shown). A second protein mixture containing albumin (350 μg/ml), γ-globulin (100 μg/ml), fibrinogen (27.4 μg/ml) and fibronectin (10 μg/ml) was also found to show no progressive blocking on 0.2 μ polycarbonate filters. As reported in Section 4.5, lens γ-crystallins (300 μg/ml), both alone and in combination with albumin and γ-globulin (700 and 200 μg/ml, respectively) do not block 0.2 μ polycarbonate filters, while addition of dilute hyaluronic acid (11 μg/ml) to the above γ-crystallin/albumin/γ-globulin mixture also produced no observable filter blockage. Perfusion of fibrinogen solutions at relatively high concentrations (500 μg/ml) through 0.2 μ polycarbonate filters produced a small but observable amount of blocking (Figure 4.23), and a similar perfusion with a 50 μg/ml solution produced a proportionally smaller effect. In summary, we have been unable to synthesize an "aqueous-like" solution which obstructs 0.2 μ polycarbonate membranes to the same extent as calf aqueous humor.

These results suggest that filter blockage is dependent upon some material which is specific to aqueous,

Figure 4.23 The behavior of various "mock aqueous" solutions on 0.2 μ polycarbonate filters. Curve 1: mixture of albumin, γ-globulin, fibrinogen and thrombin (350 μg/ml, 100 μg/ml, 25 μg/ml and .0025 NIH units/ml, respectively). Curve 2: mixture of albumin, γ-globulin, fibrinogen and fibronectin (350, 100, 27 and 10 μg/ml, respectively). Curve 3: pure fibrinogen solution (500 μg/ml). All perfusions at 40 μl/min.

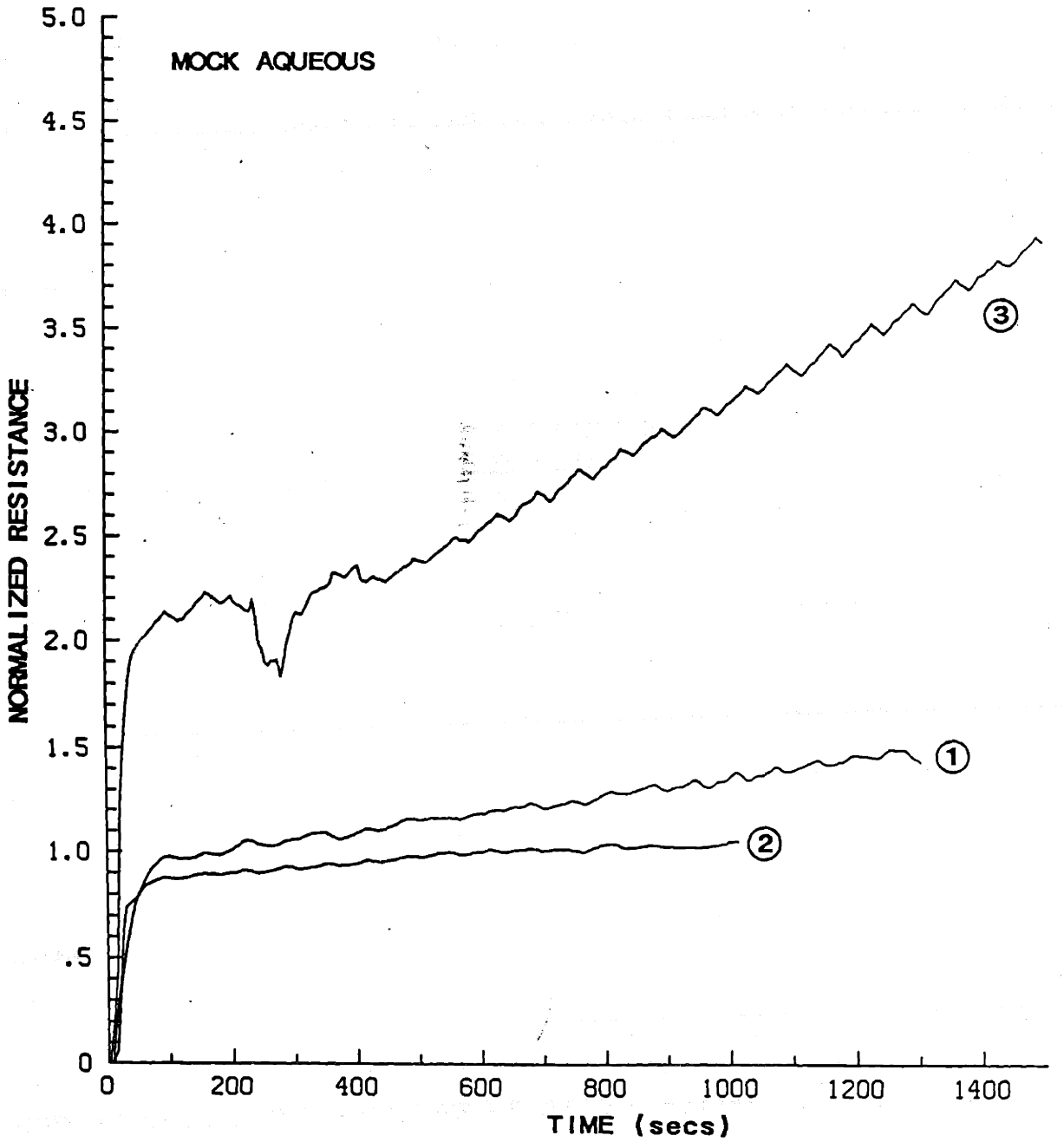

rather than being a general protein obstruction. To further test this hypothesis, bovine plasma and serum which had been diluted to aqueous humor protein levels were perfused through Nuclepore filters. Freshly collected calf serum which had been diluted 100-fold with DPBS was found to exhibit only minimal blocking on 0.2 μ polycarbonate membranes (Figure 4.24). Furthermore, calf serum diluted 10-fold and 100-fold (100-fold dilution protein: 974 μg/ml) showed no discernible blocking on 0.2 μ PVP-free polycarbonate filters, and citrated calf plasma diluted 88:1 (protein: 898 μg/ml) showed only a minimal amount of blocking on 0.2 μ polycarbonate membranes. Finally, citrated diluted calf plasma (protein: 934 μg/ml) which was recalcified immediately before perfusion showed very little blocking on 0.2 μ polycarbonate filters (Figure 4.24). Thus, we conclude that fresh calf plasma and serum, when diluted to aqueous humor levels, do not possess the filter-obstructing capacity of calf aqueous, further confirming the uniqueness of the blocking phenomenon to aqueous.

In one test commercial bovine serum (Gibco Labs) which had been frozen and rethawed was tested on 0.2 μ polycarbonate membranes. When diluted 50-fold this fluid showed a significant blocking capacity, even after prefiltration through a 0.08 μ polycarbonate filter. The difference betweeen this fluid and the freshly collected serum is not known, and this point will be further discussed in Section 6.2.

High and Low Molecular Weight Fractionation

In order to obtain a bound for the molecular weight (MW) of the blocking material in calf aqueous humor, a series of tests in which Centricon-10 miniconcentrators were

Figure 4.24 The behavior of calf plasma and serum on 0.2 μ filters. Curve 1: Calf serum diluted 100-fold perfused through polycarbonate filter. Curve 2: calf serum diluted 10-fold perfused through PVP-free filter. Curve 3: citrated plasma dilted 88-fold on polycarbonate filters. Curve 4: recalcified plasma diluted 85-fold on polycarbonate filter. All perfusions at 40 μl/min.

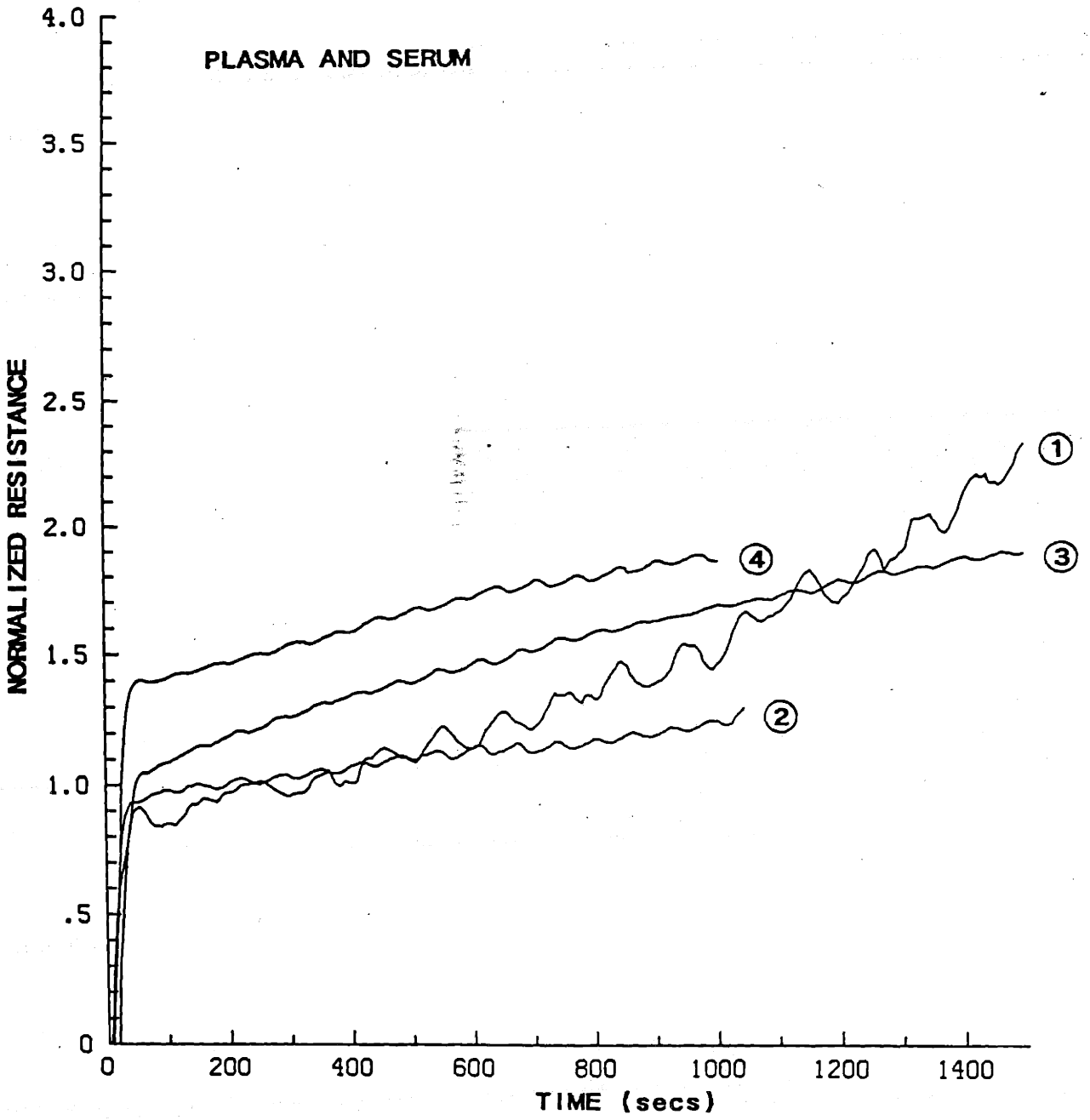

used to divide aqueous into high and low molecular weight containing fractions (HMW and LMW fractions) was conducted. As can be seen from Table 4.2, protein recovery after separation was quite high (~95% for November 6, 1985). Gel exclusion chromatography of the unfractionated aqueous and HMW and LMW components confirmed that protein recovery was high and that fractionation was effective in separating low and high MW components (results not shown).

When perfused through 0.2 μ polycarbonate Nuclepore filters the LMW fraction (MW<10 kdaltons) exhibited no blocking behavior, while the HMW fraction blocked significantly. Interestingly, it was consistently found that the HMW fraction blocked to a greater extent than did the unprocessed aqueous humor, even though the protein concentration in the HMW fluid was less then that in the aqueous humor (Figure 4.25). A 1:1 mixture of the HMW and LMW fractions blocked 0.2 μ polycarbonate filters to approximately the same extent as did the unprocessed aqueous humor diluted 1:1 with saline. Thus, we conclude that calf aqueous contains a component(s) of MW less than 10,000 which inhibits the blocking of 0.2 μ polycarbonate filters, while the blocking components have molecular weights greater than 10 kdaltons.

Prefiltration of Aqueous Humor

As aqueous passes through filters and causes progressive blockage, some constituents should be retained on these filters, implying that aqueous collected after filtration should show a diminished blocking capacity. This effect was investigated in a series of experiments in which calf aqueous was preperfused through various filter types, collected, and tested on a second filter. Preperfusion of

Figure 4.25 Perfusion of calf AH and low and high molecular weight containing fractions through 0.2 μ polycarbonate filters. All perfusions at 40 μl/min.

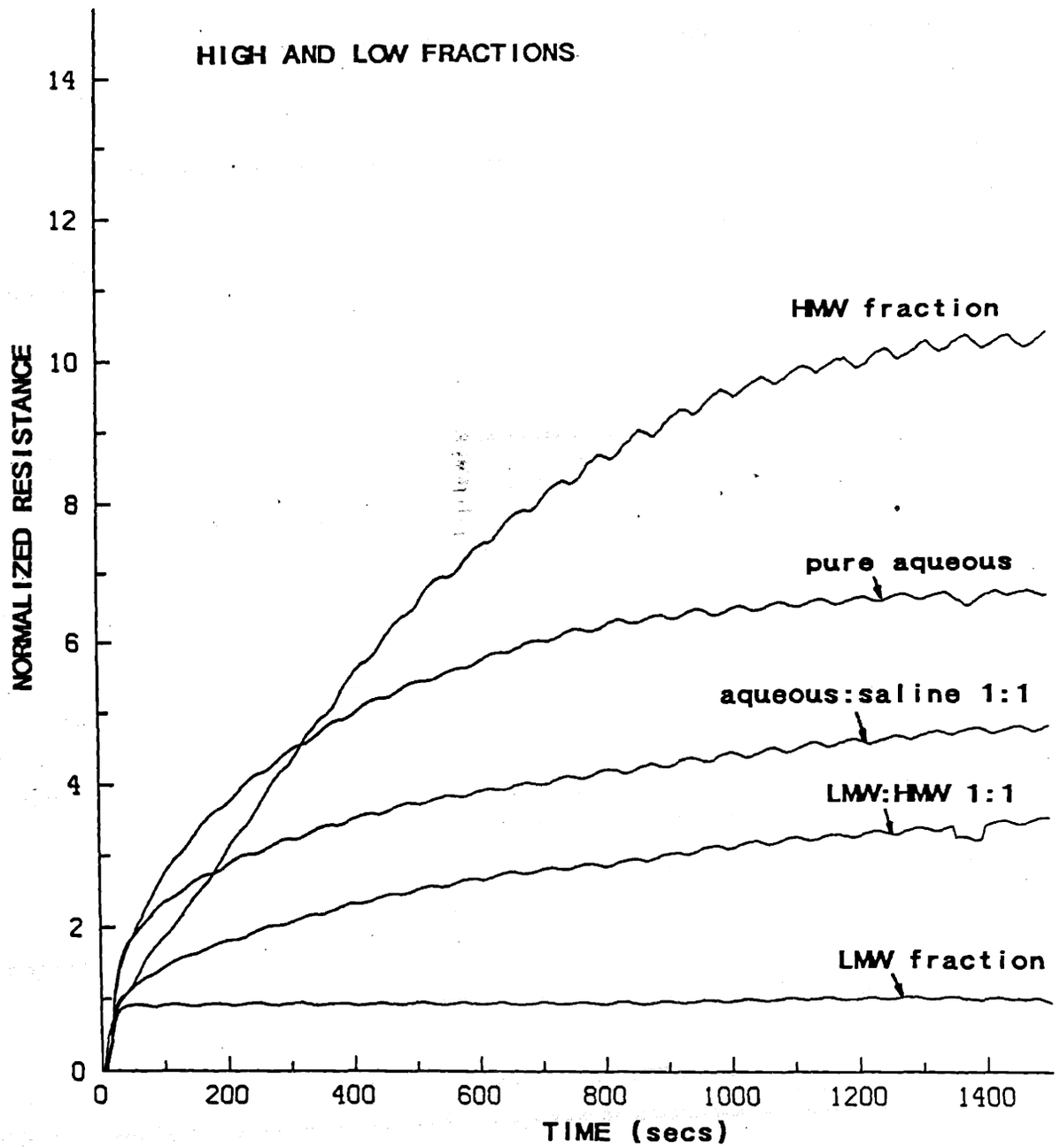

calf aqueous humor through a 0.22 μ GVWP Millipore filter (Q=40 μl/min, total perfused volume=1.1 ml) consistently eliminated most or all of the aqueous blocking capacity as tested on 0.2 μ polycarbonate membranes (Figure 4.26). This result is surprising since the GVWP Millipore membranes themselves showed no signs of blockage (Figure 4.18), and will be discussed in Section 6.3.

Similar preperfusion through 1.0 μ polycarbonate filters (Q=80 μl/min, total perfused volume=1.2 ml), while producing no observable blockage of the 1.0 μ filter, produced only a marginal decrease in the blocking capacity of the perfused fluid as tested on 0.2 μ polycarbonate membranes. (Data not shown.) On the other hand, preperfusion through 0.2 μ polycarbonate filters produced a significant decrease in aqueous blocking capacity, the magnitude of this decrease depending upon the preperfusion conditions. If a large volume of aqueous was preperfused through a single 0.2 μ filter (Q=40 μl/min, total perfused volume=1.1 ml) the aqueous showed a moderate reduction of blocking capacity (Figure 4.27 (a)). However, if the aqueous was preperfused in small batches and pooled, each preperfusion being carried out on a new 0.2 μ polycarbonate filter, the pooled fluid showed a much decreased blocking capacity. Figure 4.27 (b) shows the large decrease obtained by preperfusing approximately 0.2 ml of aqueous humor through six individual 0.2 μ polycarbonate filters and testing the pooled fluid. Hence we conclude that aqueous preperfusion on 0.2 μ polycarbonate filters removes some of the blocking material and that the removal mechanism becomes saturated as greater volumes of aqueous humor are passed through the preperfusion filter.

In the above experiments the concentration of blocking material in aqueous is the mixing cup average over

Figure 4.26 Effects of preperfusion through a 0.22 μ Millipore GVWP membrane on the blocking capacity of calf aqueous. All tests at 40 μl/min on 0.2 μ polycarbonate filters.

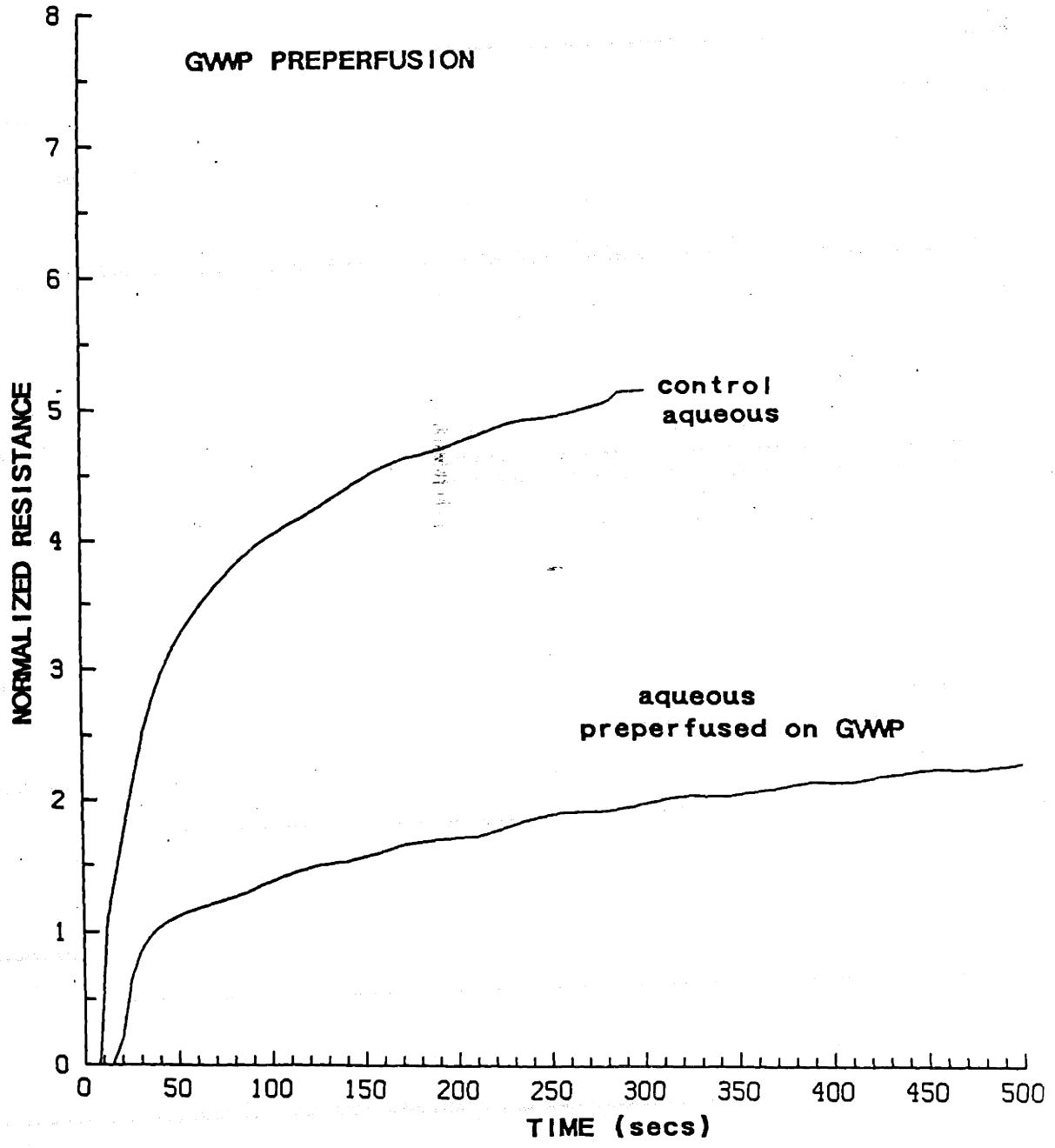

Figure 4.27 The blocking capacity of calf aqueous humor after preperfusion through 0.2 μ polycarbonate filters. (a) Prepefusion through a single filter. (b) preperfusion through a number of filters. All tests on 0.2 μ polycarbonate membranes, all perfusions at 40 μl/min.

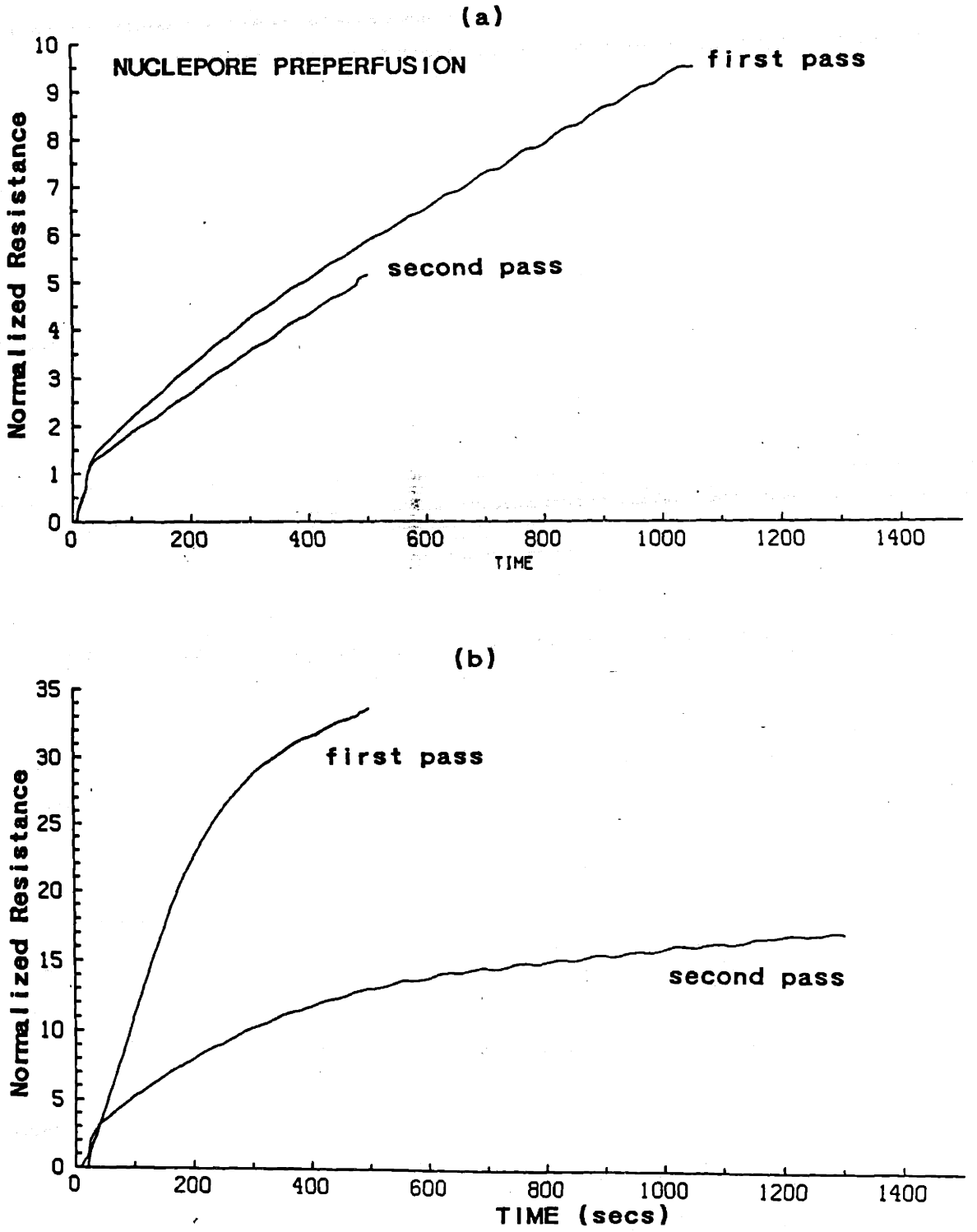

the length of the preperfusion. In order to minimize the effects of this averaging process, perfusions were carried out with the double filter holder apparatus described in Section 3.6. Baseline (saline) perfusions with this system showed that accurate and reliable resistance measurements could be simultaneously made for both filters. In Figure 4.28 the results of a perfusion through two 0.2 μ filters is shown, and it is seen that even after accounting for the time lag needed for aqueous to reach the downstream filter ($\simeq$ 570 seconds) this filter blocks more slowly than does the upstream, indicating that the upstream membrane is removing blocking material from the aqueous. These results will be further analyzed in Section 5.5.

Saline Postperfusion

In an effort to determine how tightly the blocking material is associated with the filter, a series of tests were conducted in which filters were perfused with aqueous and then immediatly (within several minutes) perfused with saline. Filters were handled (with forceps) only once during the interval and had their orientation preserved. Figure 4.29 shows that saline postperfusion on 0.2 μ polycarbonate membranes produced a rapid initial drop in resistance, followed by a slower decrease which usually tended toward a steady state. The results of carrying out this procedure on a number of 0.2 μ polycarbonate filters are shown in Figure 4.30, in which normalized filter resistance at the end of aqueous perfusion is plotted against saline resistance at the beginning of the postperfusion. There is seen to be a good correlation between the two quantities ($R_{saline} = 0.58\ R_{aqueous} + 1.49$, n=26, r=0.955) suggesting that the immediate resistance drop

Figure 4.28 A representative trace of the measured resistances in a double filter perfusion. Perfusion at 40 μl/min through two 0.2 μ polycarbonate filters with aqueous:saline mixture (1:9).

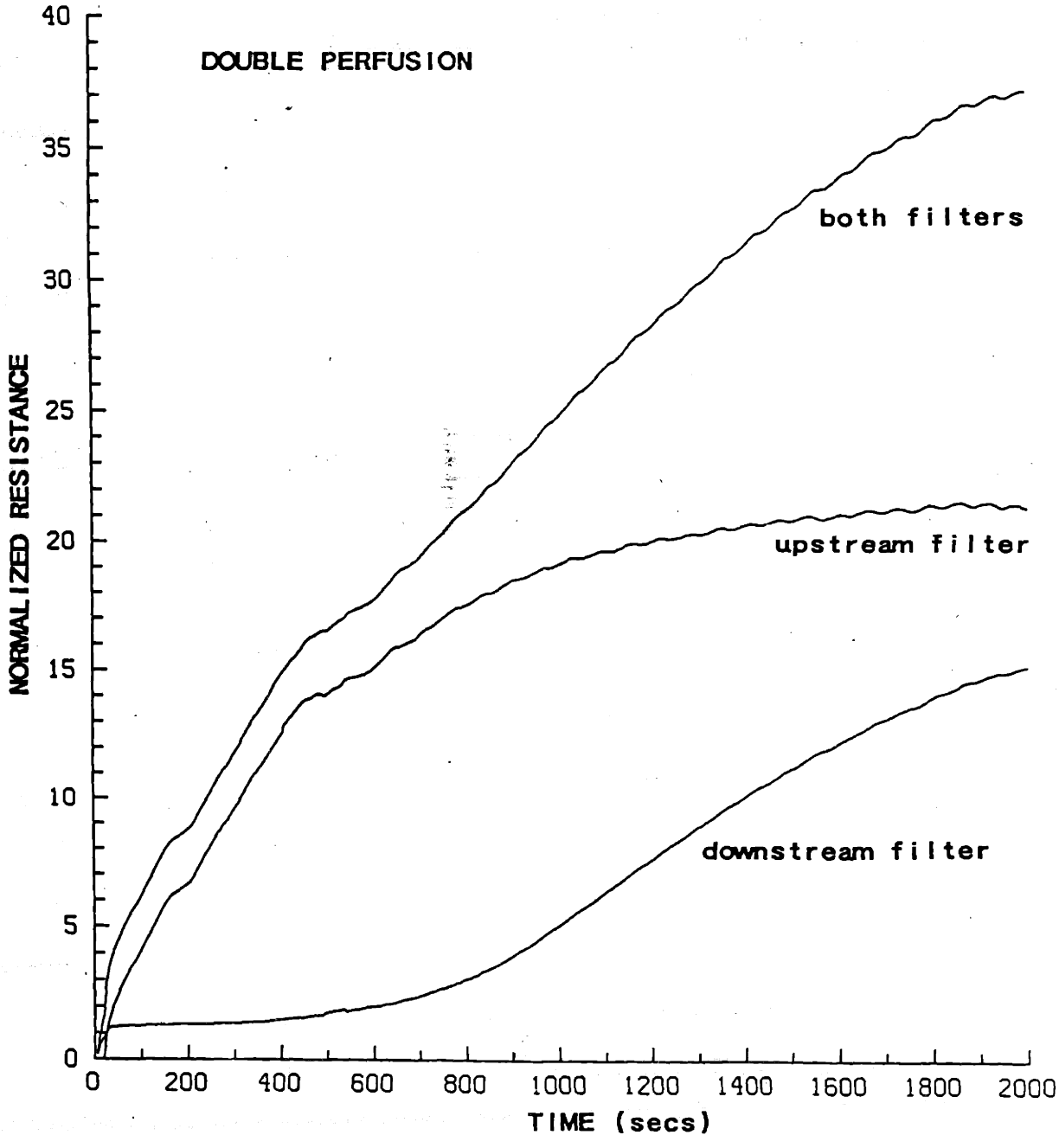

Figure 4.29 The effects of saline postperfusion after calf aqueous blockage on 0.2 μ polycarbonate filters. Perfusions at 40 μl/min.

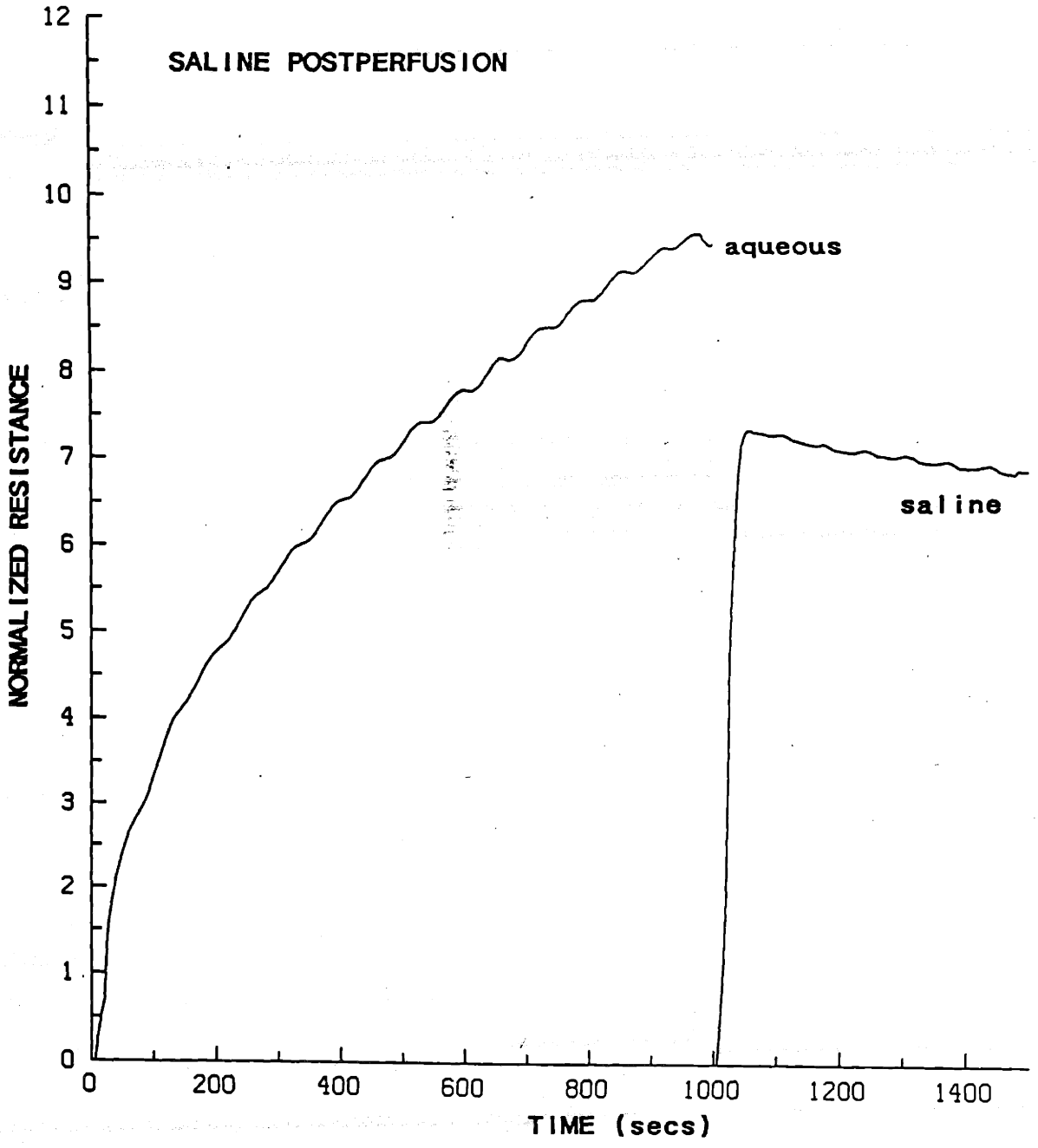

Figure 4.30 Plot of the normalized resistance at the end of aqueous perfusion versus the normalized resistance at the beginning of saline postperfusion. All perfusions at 40 µl/min on 0.2 µ polycarbonate membranes, except as noted below. Special symbols: X: filter orientation reversed for postperfusion, solid square: 1 mM DTT postperfusion (on 0.2 µ PVP-free filter), solid circle: 2M NaCl postperfusion, solid triangle: 2M $CaCl_2$ postperfusion.

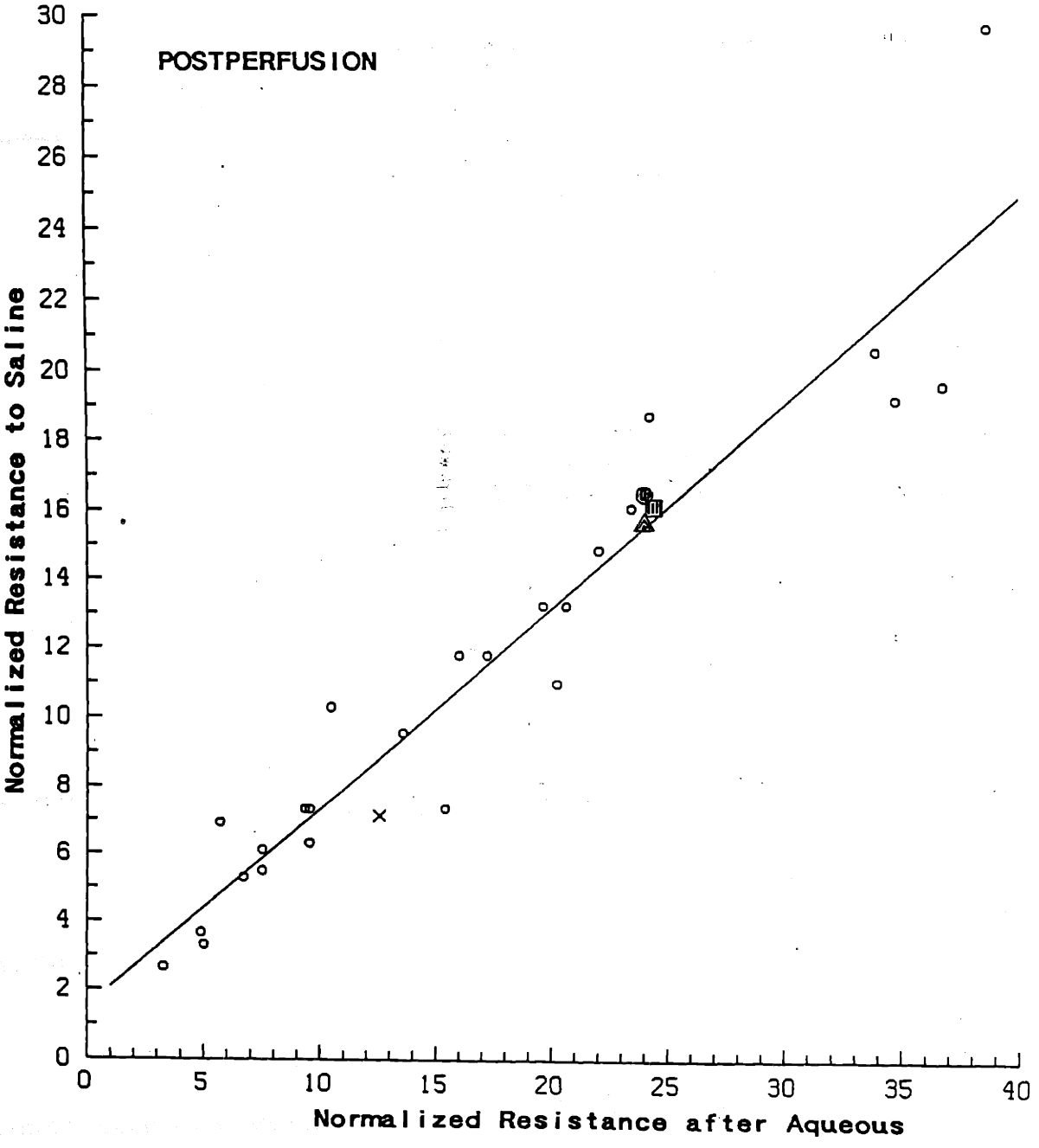

due to postperfusion is not artifactual. These results suggest that there are two types of blocking material/filter interactions, one which is labile and one which is more slowly dissociated. When a single blocked membrane was perfused at varying flowrate (4 to 81 μl/min), the resistance was found to be essentially independant of flowrate. One test in which the filter orientation was reversed for postperfusion gave results similar to those in which the orientation was preserved ("x" in Figure 4.30).

To further investigate this phenomenon, several experiments in which the flow direction was suddenly reversed in mid-test were carried out. Once the flow direction has been changed the filter is being perfused by somewhat diluted aqueous which has been passed through the filter, and thus such a test is somewhat analagous to saline postperfusion. The results of one such test are shown in Figure 4.31, and there is once again seen to be a slow decrease in resistance. Notably absent, however, is the large initial drop seen with saline postperfusion. One possible explanation for this absence is that aqueous residing in the filter during the small time period required to change pump direction continues to block the filter, and that this "extra" blockage (which is not visualized) offsets the rapid initial drop. Alternately, the rapid drop seen with saline postperfusion could be artifactual. A third possibility is that a slow reduction in blockage always occurs once perfusion has ceased (perhaps due to protein "aging") which is not resolved in postperfusion experiments since the filter's resistance is not measured during the interval betweeen aqueous perfusion and saline postperfusion. In summary, although the mechanism responsible for the quick initial resistance drop seen with saline postperfusion is not definitively known, the filter resistance is relatively constant after that initial change,

Figure 4.31 Results of push/pull experiment. Perfusion at ±40 μl/min on 0.2 μ polycarbonate filter.

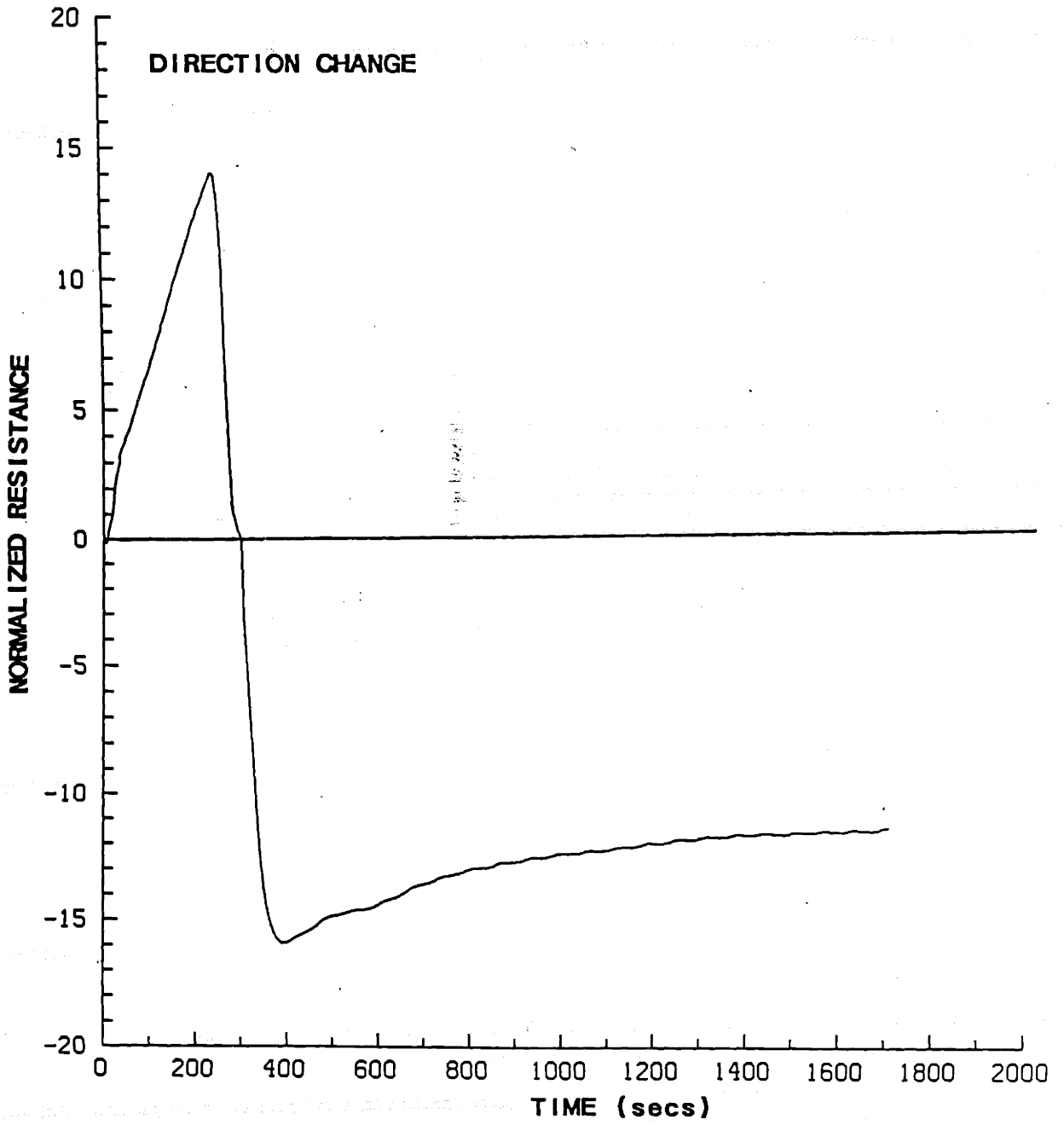

suggesting that the blocking material is fairly tightly bound to the filter.

Detergent Postperfusion

Postperfusion of blocked (aqueous-perfused) membranes with various detergents resulted in a rapid and complete (or nearly complete) elimination of filter blockage. The results of postperfusing a blocked 0.2 μ polycarbonate filter with 1% Triton-X are shown in Figure 4.32 (a), there being an almost immediate elimination of filter blockage. Similar results were obtained with 0.1% Triton-X, while 0.01% Triton-X postperfusion produced a slower and perhaps somewhat incomplete elimination of filter blockage (Figure 4.32 (b)). Results on 0.2 μ PVP-free filters were essentially identical to those on 0.2 μ regular polycarbonate membranes. Similar experiments with 0.1% SDS showed incomplete elimination of blocking, although treatment of blocked filters in 0.1% SDS in ultrsound for 20 minutes returned filter resistance to baseline (Figure 4.33 (a)). Postperfusion with 0.1% DTAB removed only a small fraction of resistance, while 1% DTAB perfusion removed approximately 80% of resistance (data not shown). The effect of 1% and 0.1% CHAPS postperfusion was similar to that of 0.1% and 0.01% Triton-X washing, respectively (data not shown). In summary, detergent postperfusion produces a dose dependent decrease in blockage of 0.2 μ polycarbonate or PVP-free filters, the most effective detergent being Triton-X.

Triton-X postperfusion of blocked 0.22 μ Millipore GVHP filters was also effective in removing blocking, although interestingly the washing step proceeded less quickly than in the case of 0.2 μ PVP-free filters (Figure 4.33 (b)).

Figure 4.32 The effect of posperfusion of blocked 0.2 μ polycarbonate filters with various concentrations of Triton-X. (a) Aqueous pefusion followed by 1% Triton-X, (b) aqueous perfusion followed by 0.01 % and 0.1 % Triton-X. All perfusions at 40 μl/min.

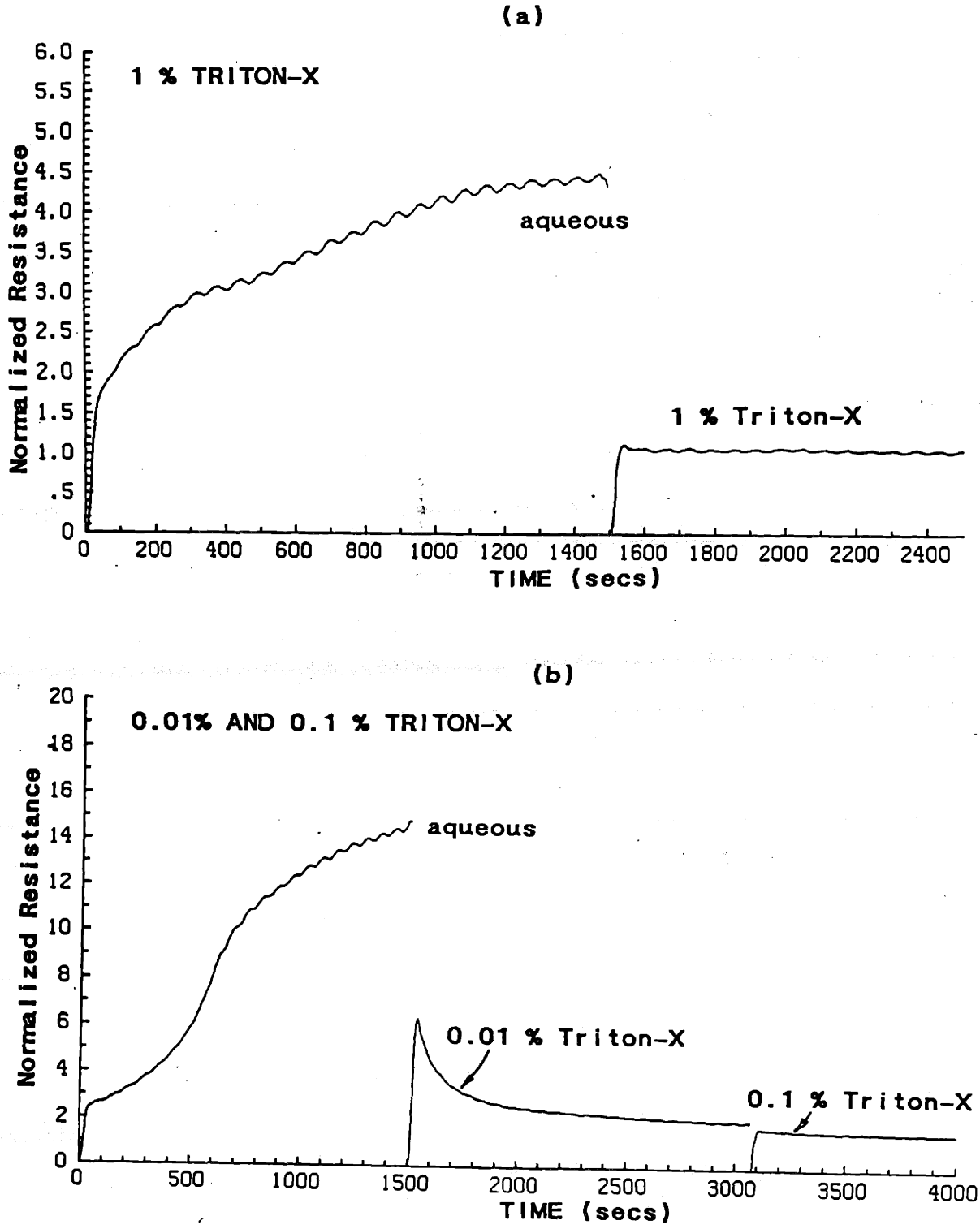

Figure 4.33 Effects of postperfusion of blocked filters with detergent. (a) Calf aqueous blockage, followed by 0.1 % SDS postperfusion and saline perfusion after ultrasound washing on 0.2 μ PVP-free filter. (b) Calf aqueous blockage followed by 0.1 % Triton-X postperfusion on Millipore 0.22 μ GVHP filter. All perfusions at 40 μl/min.

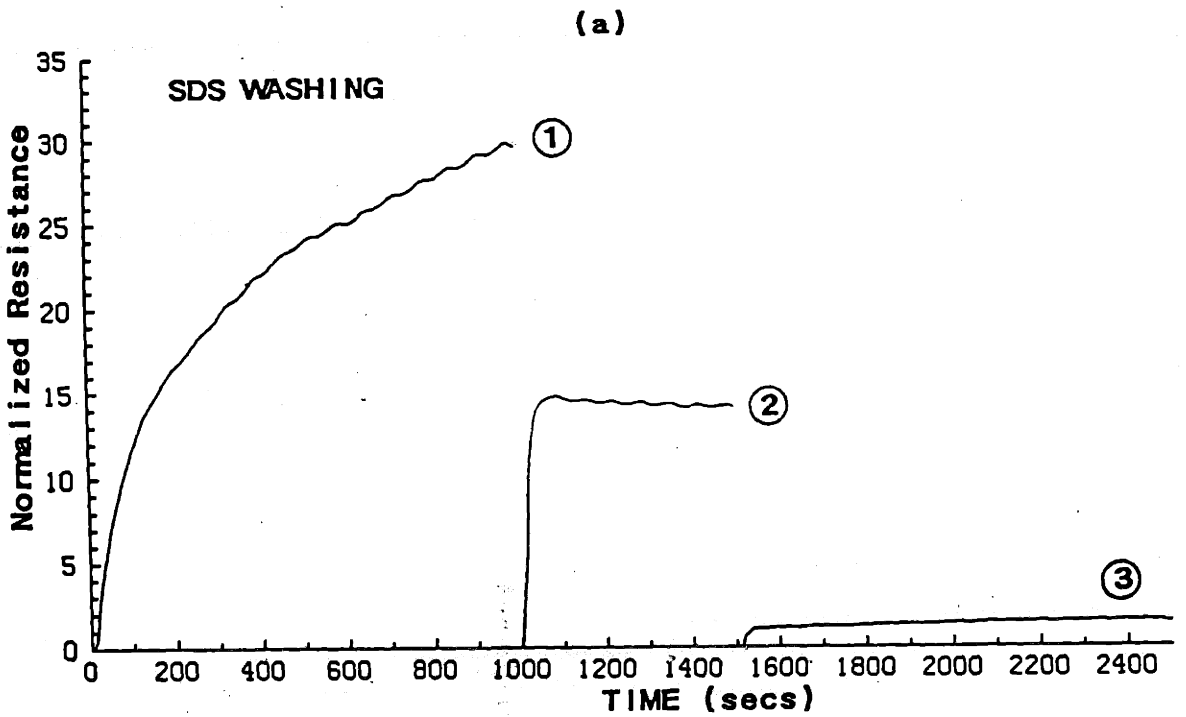

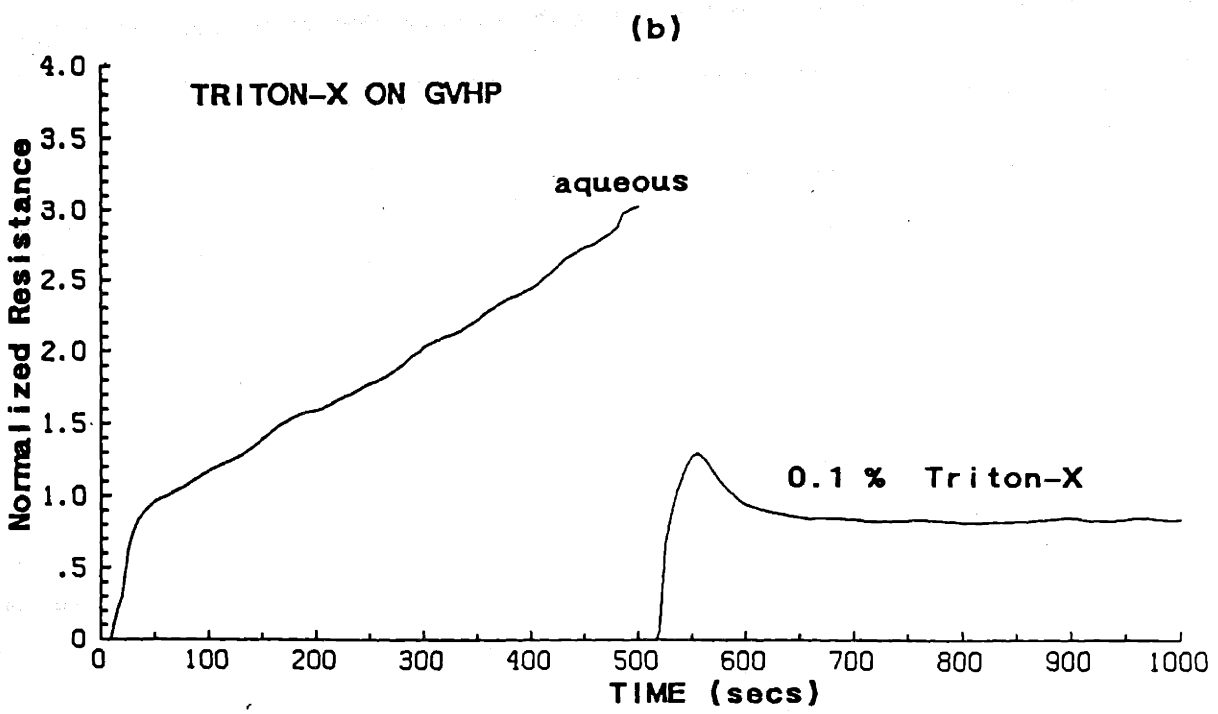

It was also found that Triton-X postperfusion drastically changed the blocking properties of the filter for subsequent aqueous perfusions (Figure 4.34). These results are consistent with those of Section 4.5 showing that the filter pretreatment with Triton-X produces a much more aggressively blocking membrane.

Other Postperfusions

Blocked filters were also postperfused with 1mM DTT and 2M NaCl and $CaCl_2$ (Figure 4.30). These agents appeared to have no effect on filter resistance other than the usual pressure drop seen due to saline postperfusion. Interruption and subsequent restart of aqueous perfusion on a single filter appeared to have only a minimal effect on the blocking process (Figure 4.9 (b)).

Mechanical Effects

In the situation in which membrane pore diameter is comparable to or slightly larger than the blocking material, there are two possible sites for filter blockage: within the pore, and on the upstream face (polarized layer and/or filter cake formation). Filter face blockage should be sensitive to upstream stirring and scraping of the upstream filter face, and thus the effects of such mechanical disruptions were investigated in an attempt to identify the blocking site.

Figure 4.35 (a) shows the effects of upstream stirring on filter blockage by calf aqueous, while Figure 4.35 (b) shows the results of the same test conducted with a 0.46 μ microsphere solution. Stirring was seen to have no

Figure 4.34 Effects of a sequential perfusion of calf aqueous, 0.1 % Triton-X and calf aqueous on the blockage of a 0.2 μ polycarbonate filter (Q = 40 μl/min).

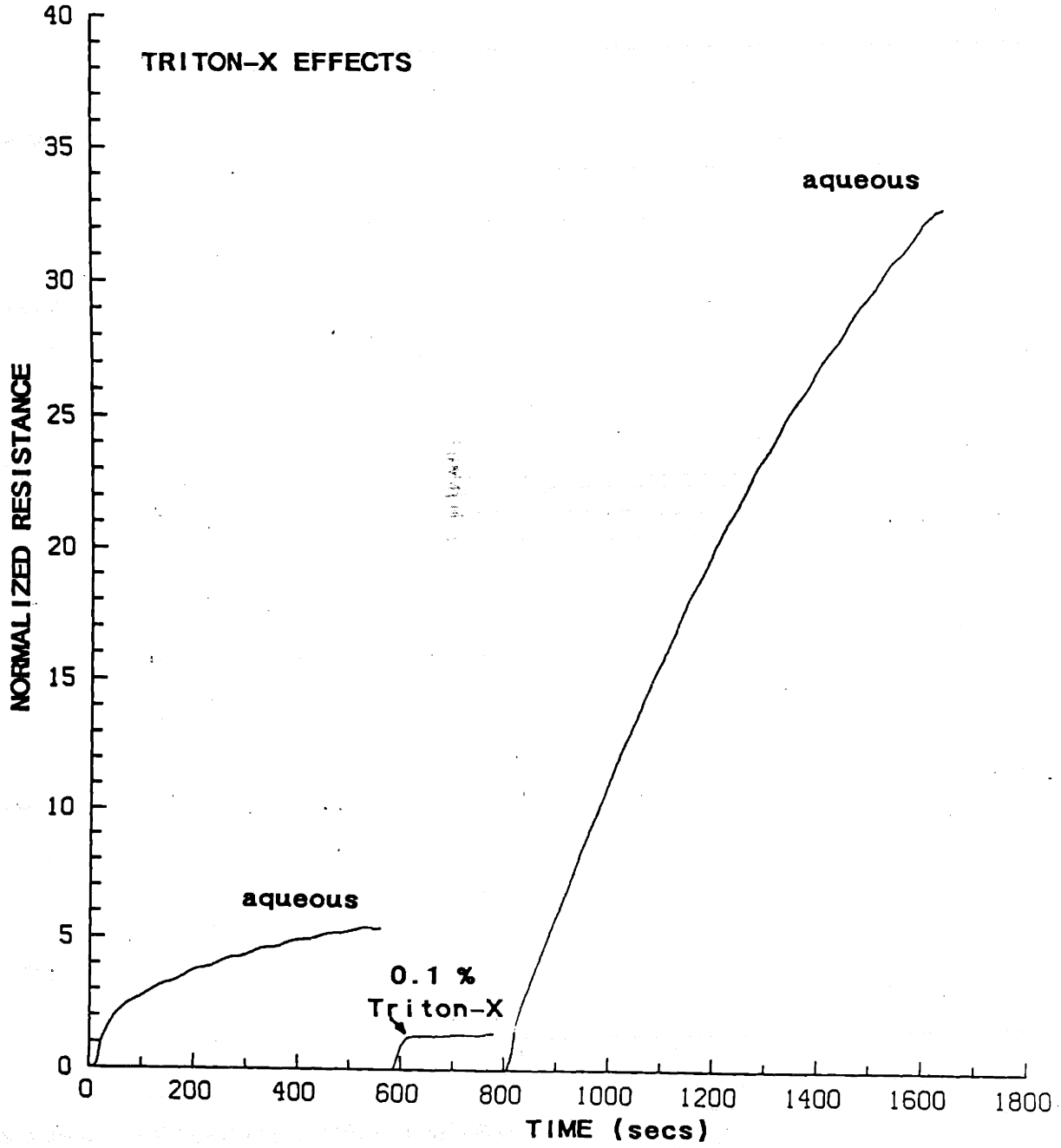

Figure 4.35 The effect of upstream stirring on blockage of 0.2 μ polycarbonate membranes. (a) Perfusion with calf aqueous (solid line) and control saline (dotted line). (b) perfusion with 0.46 μ latex microsphere solution (solid fraction = .005). Perfusions at 40 μl/min, arrow indicates stirring system turned on.

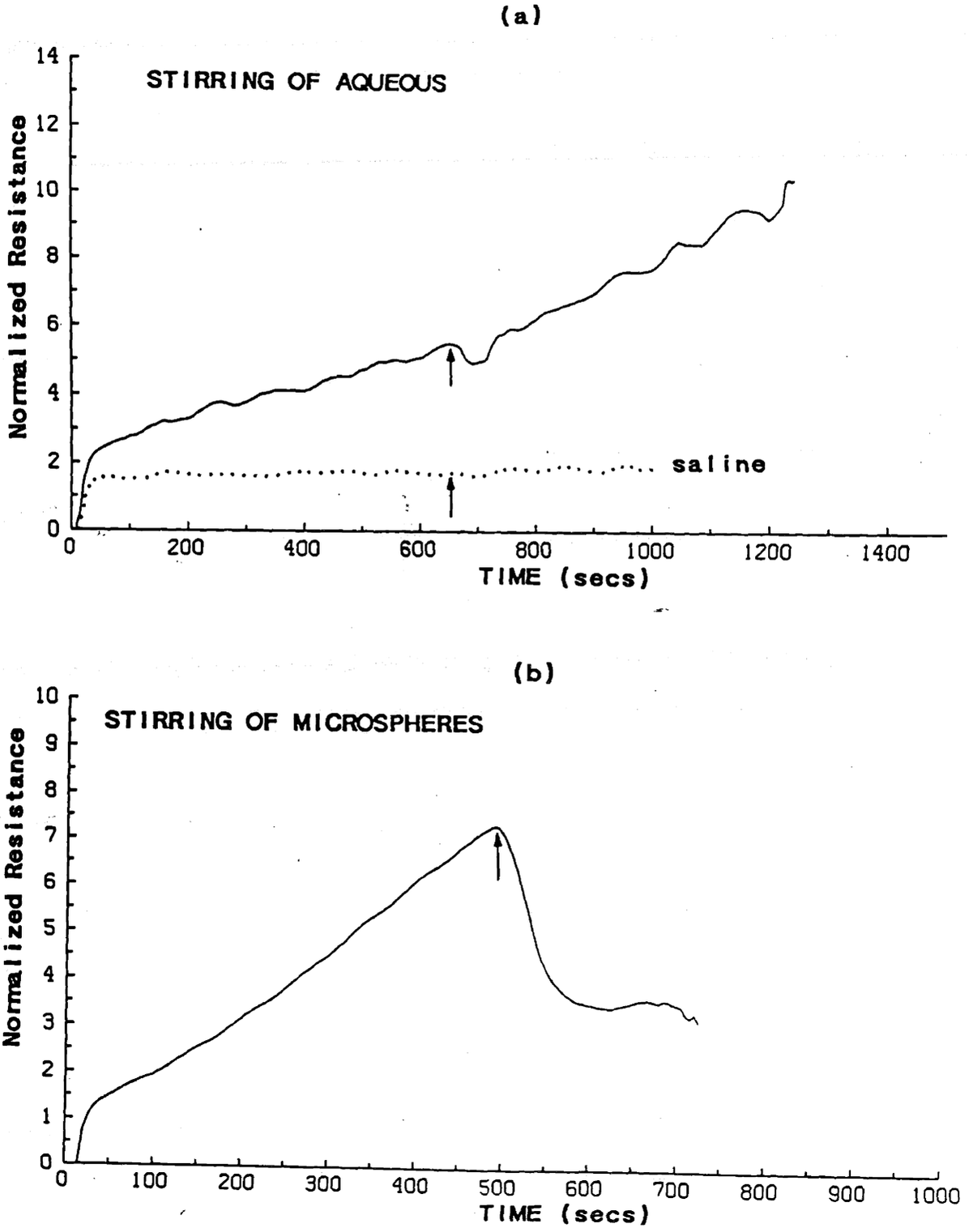

discernible effect on aqueous blockage (confirmed in 3 tests) while having a large effect on microsphere solution blocking rates. Scanning electron microscopy of filters which had been perfused with the microsphere solution (no shaking) showed a thick (~50-100 sphere diameter) layer of microspheres piled up and apparently adhering to the filter face.

Experiments in which blocked filters were scraped on their upstream faces and then postperfused with saline gave highly variable results, ranging from complete elimination of all blocking (one case) to no effect beyond the normal resistance drop due to saline postperfusion (three cases). There were also three intermediate cases in which some decrease in resistance (less than that required to return to baseline) was seen. There appeared to be no correlation between scraping effectiveness and aqueous protein content, extent of prescraping blockage, duration of original aqueous perfusion or intensity of scraping. In short, upstream filter face scraping produced no repeatable and consistent effect.

A second mechanical treatment having a somewhat variable effect was subjection of blocked filters to ultrasound, although the extent of resistance elimination appeared to increase with increasing ultrasound exposure (based on only two tests). Finally, forcing water backwards through a blocked 0.2 μ polycarbonate filter at high flowrate (5 ml/min) did not decrease filter resistance. We have interpreted the above results to mean that: (i) blockage occurs within the pore, or (ii) blockage occurs on the filter face and is due to very tightly bound material (not removable by stirring and scraping).

4.7 Quantitation of Protein Levels on Perfused Filters

A series of experiments was undertaken with the goal of measuring the amount of filter-associated protein and thus correlating this amount with the extent of filter blockage. Blocked filters were washed with detergents according to one of the two protocols described in Section 3.9 and tested to ensure washing was effective, while the filter washing fluid was tested for protein content. Triton-X was selected as the washing detergent because of its proven efficacy (Section 4.6).

Ideally the filter washing should be carried out in high concentrations of Triton, since washing efficiency is greatest at these levels. Unfortunately, most protein microassays are interfered with strongly by high detergent levels, and it was therefore necessary to select a detergent concentration which did not interfere with the protein assay, yet returned filter resistance to baseline. Triton-X concentrations of 0.008% and greater were found to interfere with the Bio-Rad microassay to an unacceptably large degree, and thus filter washing in 0.006% Triton-X (in ultrasound) was initially employed. Although this procedure was effective in eliminating most of the blockage, filter resistance did not consistently return to baseline. However, postperfusion of 0.2 μ polycarbonate filters with 150 μl of 0.035% Triton-X was found to consistently eliminate all blocking, as verified by saline postperfusion (Figure 4.36). Subsequent dilution of the washing solution to 800 μl gave a sufficiently low detergent concentration (0.0066%) to enable the Bio-Rad assay to be carried out.

Standards subjected to either of the two washing procedures were in close agreement with unmanipulated standard curves, indicating that protein samples collected

Figure 4.36 The efficacy of filter washing by 0.035 % Triton-X postperfusion. All perfusions at 40 μl/min on 0.2 μ polycarbonate membranes.

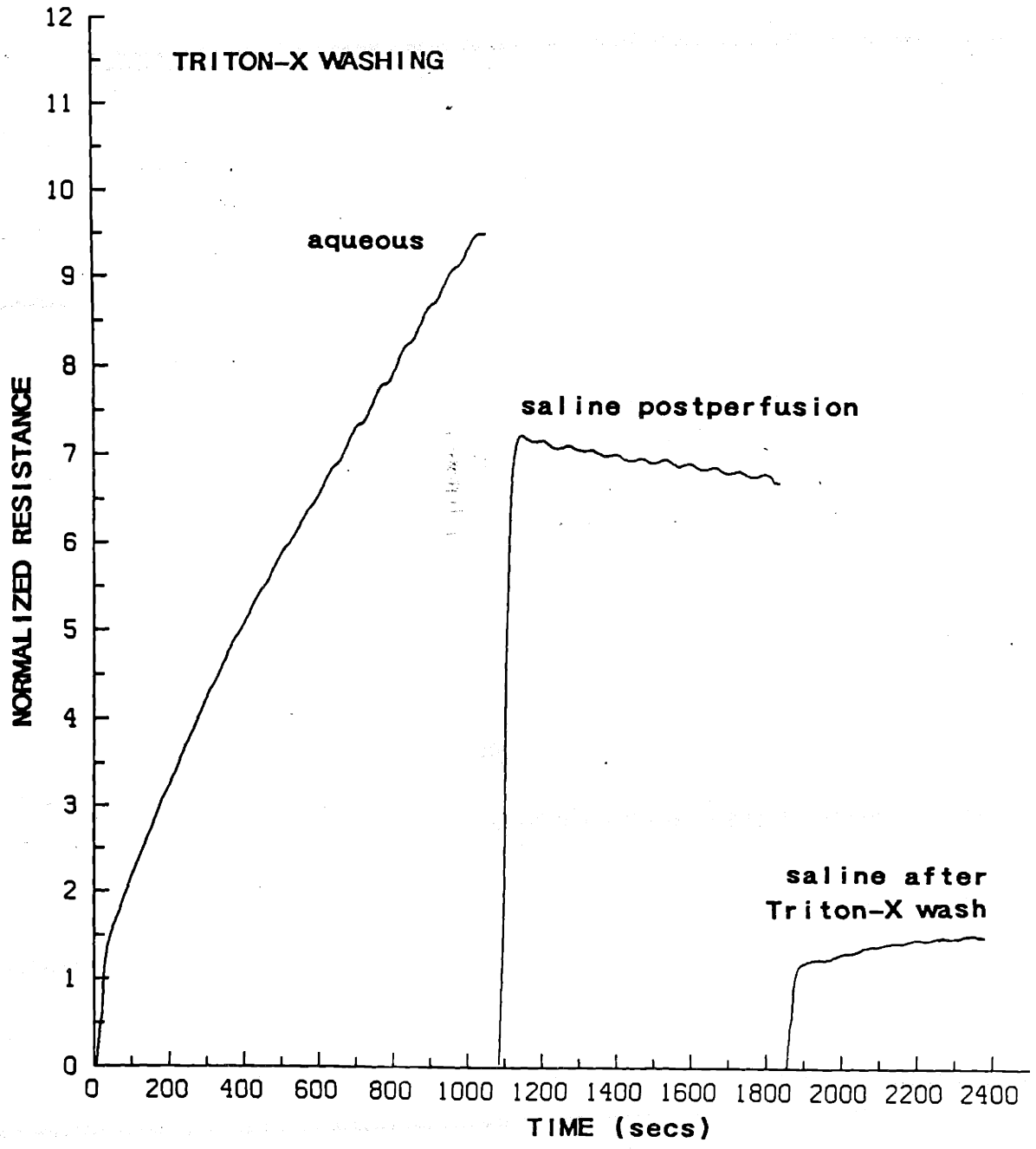

by these washing protocols could be reliably assayed. When samples collected by either of the above protocols were assayed, total protein levels were found to vary between 0 and 1 μg. This was true for filters which had been washed directly after aqueous humor perfusion, after saline postperfusion and after upstream filter face scraping. For the 22 filters assayed there was no correlation between final resistance and protein level, while the assayed levels from blank (unperfused or saline perfused) filters varied over the same range as for perfused filters. We therefore conclude that the sensitivity of the Bio-Rad microassay under these conditions is approximately 1 μg, and that the amount of protein associated with 0.2 μ polycarbonate filters after perfusion with ultracentrifuged calf aqueous humor is less than the sensitivity of the assay, i.e. less than 1 μg.

On one occasion a similar test was conducted with approximately 1 ml uncentrifuged calf aqueous humor perfused through 0.2 μ polycarbonate filters by hand. Protein was washed from the two tested filters by 0.035% Triton-X and assayed amounts were 6.4 and 8.0 μg. This is consistent with standard Bio-Rad assays of pre- and post-filtered non-ultracentrifuged aqueous which suggest a small (10-20 μg/ml) decrease in protein content. We therefore conclude that perfusion with calf aqueous humor which has not been ultracentrifuged deposits significant (approximately 10 μg/ml) amounts of protein on 0.2 polycarbonate filters. In this case deposited protein is presumably relatively large (possibly particulate) material.

Figure 4.37 FPLC chromatographs of calf aqueous humor and serum. (a) Bio-Rad protein standards. V: high molecular weight material appearing in the void fraction, 1: thyroglobulin (MW = 670,000), 2: γ-globulin (158,000), 3: ovalbumin (44,000), 4: myoglobulin (17,000), 5: vitamin B-12 (1350). Calibration bar = 1 ml. (b) Calf aqueous humor. V: as in panel (a), 1: γ-globulin, 2: albumin, 3: ascorbate, 4: tyrosine, 5: tryptophan. Injected volume = 500 μl, vertical gain = 0.5. (c) Calf serum. Injected volume = 50 μl, vertical gain = 2. (d) Calf aqueous with ascorbate oxidized (see text). Injected volume = 500 μl, vertical gain = 0.5. In all tests S denotes start of run.

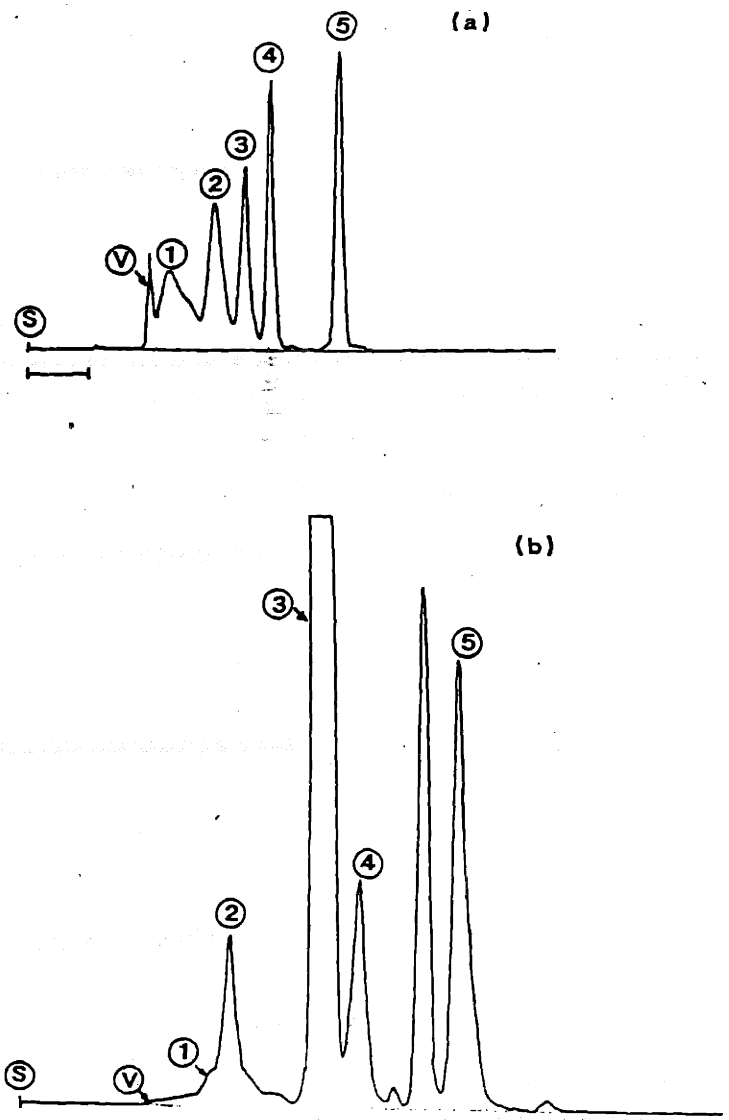

Figure 4.37 (continued).

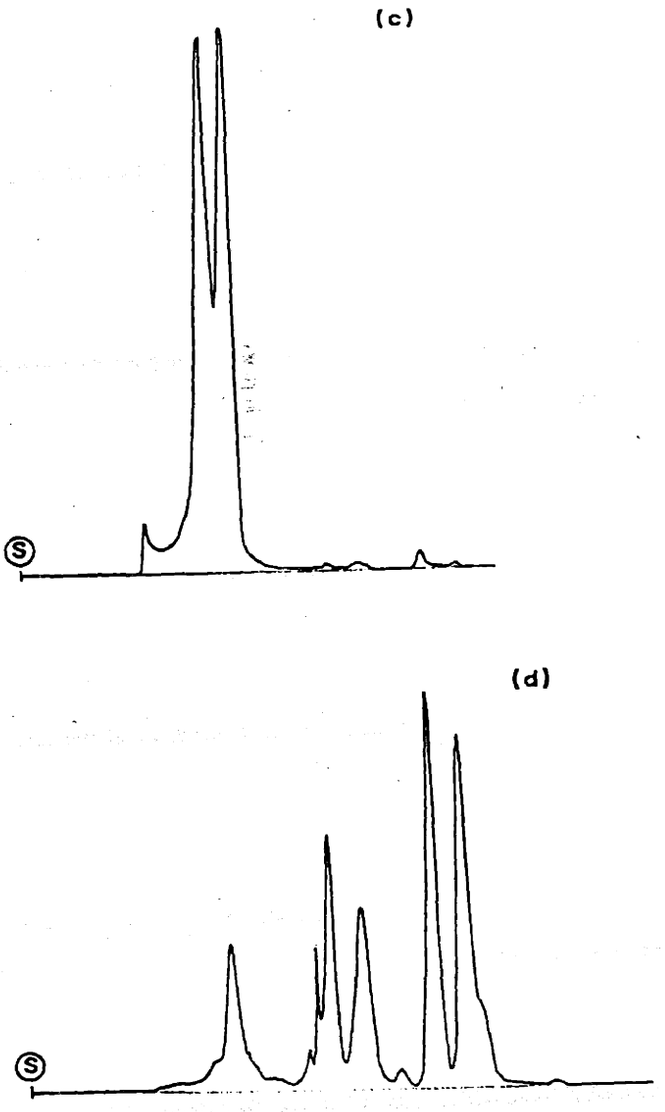

4.8 Gel Filtration Chromatography of Calf Aqueous Humor

Gel exclusion chromatography runs using the FPLC system were found to be consistent and repeatable, with minor variations between runs from the same batch of aqueous and slightly larger differences between batches. A sample aqueous run is shown in Figure 4.37 (a), while Figure 4.37 (b) and (c) present results of runs with calf serum and a globular protein calibration standard (Bio-Rad, gel filtration standard). From Figure 4.37 (c) molecular weight was well correlated (r=-0.999) with elution volume Q by

$$\log_{10} MW = 8.1 - 0.24\ Q \qquad (4.8.1)$$

Based on Figure 4.37 (c) as well as separate runs with ascorbate, tryptophan and tyrosine, most of the calf aqueous humor peaks were identified, as shown in Figure 4.37 (a). Because of the magnitude of the ascorbate peak it seemed possible that there were other smaller peaks in this region which were masked by the ascorbate. Since the oxidized form of ascorbate absorbs only weakly at 280 nm, aqueous humor samples were allowed to sit refrigerated and exposed to light and a small air bubble for 16 hours in an attempt to oxidize any ascorbate present. FPLC traces of such a sample (Figure 4.37 (d)) shows that there are in fact several hidden peaks in the ascorbate region.

It is interesting that tyrosine, tryptophan and an unidentified major peak all appear in the elution profile after ascorbate, since such small molecules are below the column's separation limit and thus should appear simulataneously. A likely explanation for this effect is

that the late-appearing substances were binding to the column material, perhaps due to hydrophobic intractions.

In an attempt to identify a peak (or peaks) removed by perfusion through 0.2 μ polycarbonate membranes, pre- and post-filtered calf aqueous humor was compared by FPLC. Figure 4.38 shows that there are no significant differences between the two batches of calf aqueous, suggesting that the material removed by filtration is either not resolvable on the FPLC system or represents a very small fraction of the total protein content of aqueous humor. Similar experiments in which calf aqueous was filtered through 0.2 μ PVP-free membranes and a Millipore GVWP membrane led to the same result.

One possible explanation of the above phenomenon is that the blocking material is binding to the slightly hydrophobic column gel and never being eluted. However, addition of substances to the elution buffer designed to minimize hydrophobic interactions, such as 0.1 M NaCl (Figure 4.38) and/or 10% gylcerol, gave a similar result. It therefore seems most likely that the amount of protein trapped during filtration represents a small fraction of the total aqueous humor protein levels, consistent with the results of Section 4.7.

In several experiments 0.2 μ filters were perfused with calf aquoeus humor, rinsed with buffer and then washed in 1 ml of 0.1 % SDS in ultrasound for twenty minutes. This filter washing fluid was then run on FPLC and compared to calf aqueous which had undergone ultrasound as well. Figure 4.39 (a) shows that ultrasound has a profound influence on the chromatographic profile, while Figure 4.39 (b) and (c) show that small amounts of material were successfully eluted from the filter. Profiles of the two filter eluates shown

Figure 4.38 FPLC chromatographs of pre- and post-filtered calf aqueous. (a) control aqueous, (b) aqueous after passage through 0.22 μ GVWP filter (perfused volume ~1 ml). In both runs FPLC buffer had 0.1 M NaCl added. S denotes start of run.

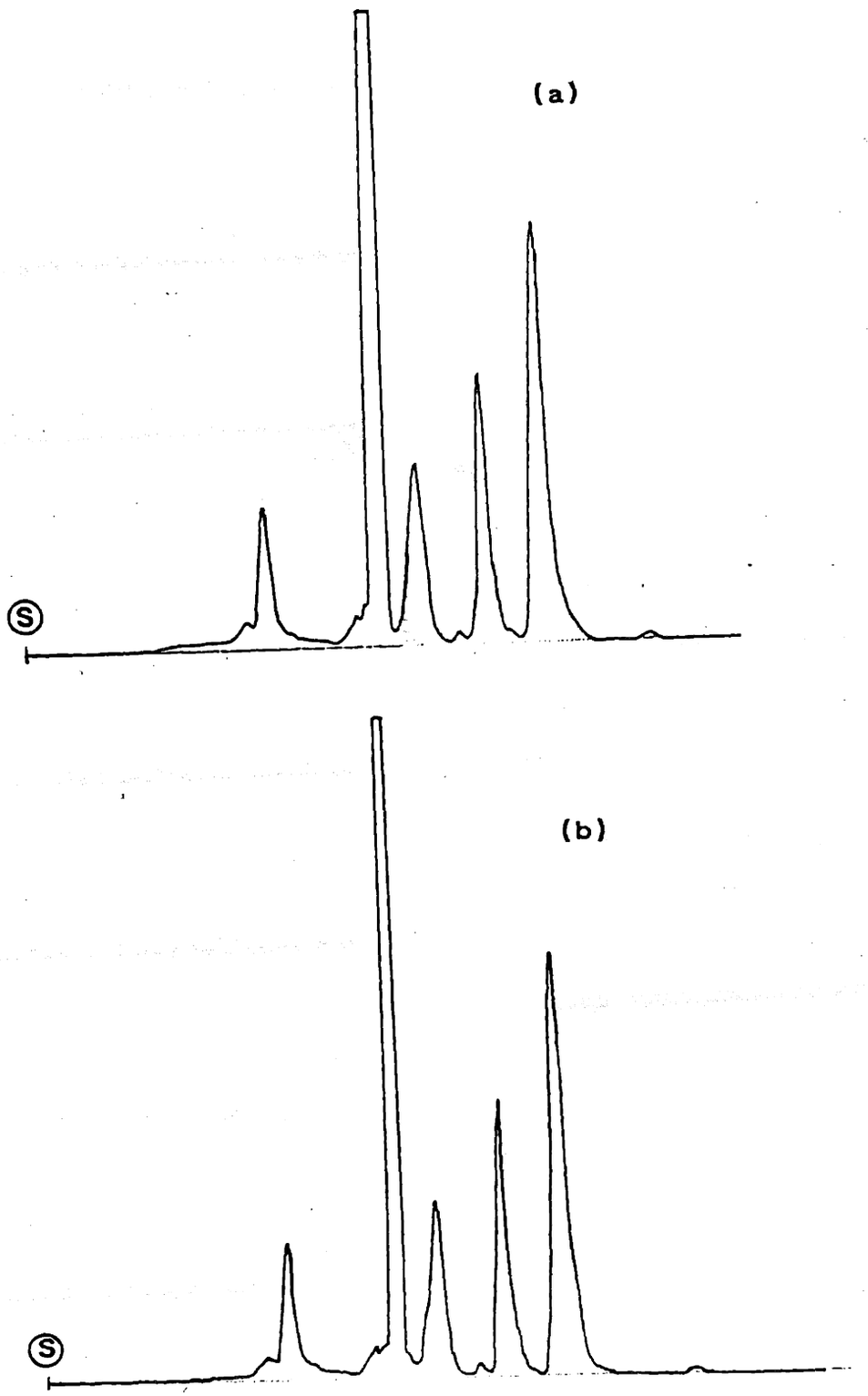

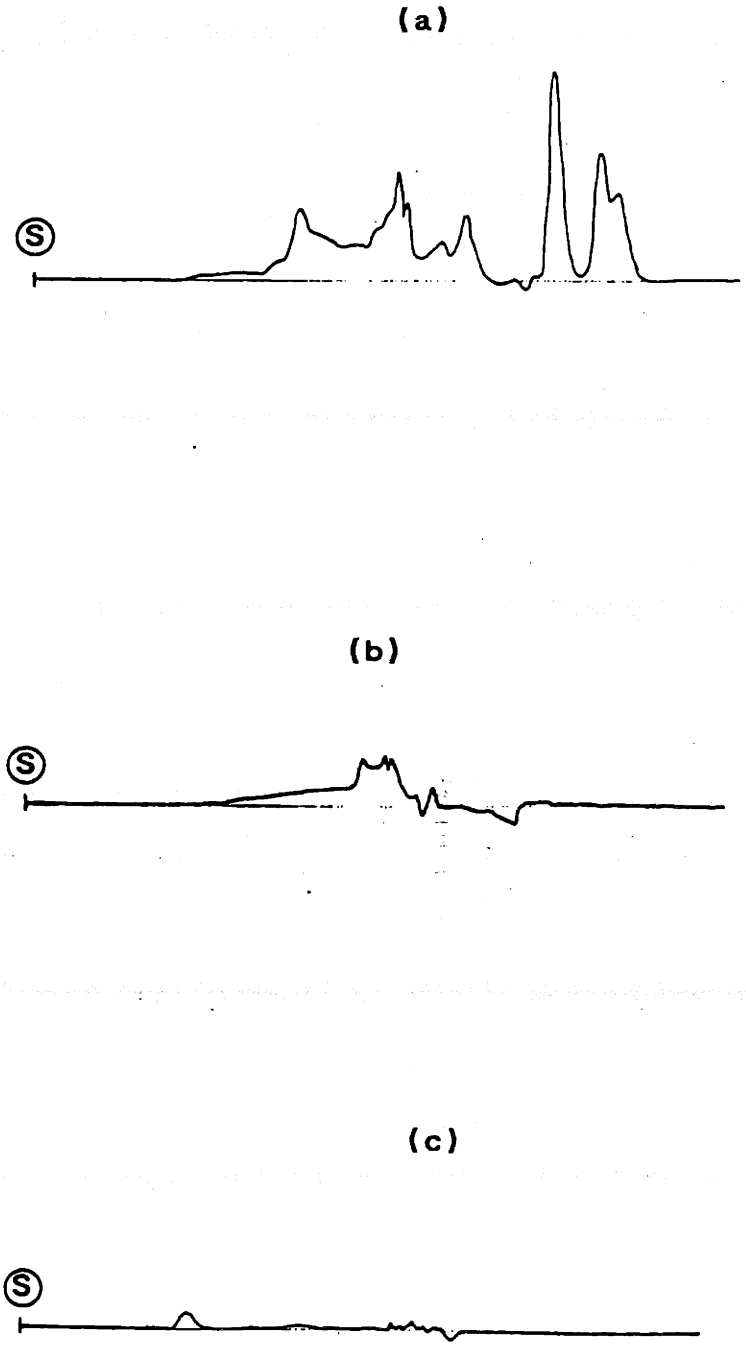

Figure 4.39 FPLC chromatographs of calf aqueous humor and filter blocking material eluted by SDS washing in ultrasound. (a) Calf aqueous humor after 20 minutes of ultrasound. (b) Material washed from 0.2 μ polycarbonate membrane (perfused aqueous volume ~1 ml). (c) Material washed from 0.2 μ PVP-free filter (perfused aqueous volume ~1.5 ml). In run (c) FPLC buffer had 0.1 M NaCl and 10% glycerol added. S denotes start of run.

as well as that of a third test (not shown) are highly variable, perhaps due to differences in buffer or filter type. It is difficult to identify any single peak present in calf aqueous which is enhanced in the filter washing material, except perhaps for peak A of Figure 4.39 (b) (MW = 9000 by (4.8.1)).

As a futher test to ensure that calf aqueous blocking components were not binding to the column material, calf aqueous humor was run on a hydrophilic silica gel HPLC column before and after perfusion through a 0.2 μ PVP-free polycarbonate membrane. Once again, no consistent differences were seen (Figure 4.40).

4.9 Two-Dimemsional Gel Electrophoresis

Gel electrophoresis runs were carried out by A.F. Pavao of the Mass. Eye and Ear Infirmary, except for several preliminary runs carried out by Dr. David Lee (no results shown). Runs of calf aqueous humor and serum on 10-20% gradient gels are shown in Figure 4.41. With reference to the serum protein map reproduced in Figure 4.42, the large spot in the center of the gel matches for albumin, which, as expected, is the most prevalent protein. Runs at lower protein concentrations indicate that this albumin spot obscures several smaller spots. The complexity of the protein pattern makes direct identification of aqueous/serum differences difficult. However, generally speaking, aqueous contains a large number of low molecular weight materials which are absent from serum.

An electrophoretogram of the filter blocking material on 10-20% gradient gels is shown in Figure 4.43. Comparing this figure with Figure 4.41 (a) shows that aqueous and the

Figure 4.40 HPLC chromatographs of pre- and post-filtered calf aqueous humor. (a) Untreated (control) aqueous, (b) aqueous after manual filtration through 0.2 μ PVP-free membrane (filtered volume ~1 ml). The numbers appearing on the chromatogram are the elution times for the peaks, in tenths of minutes.

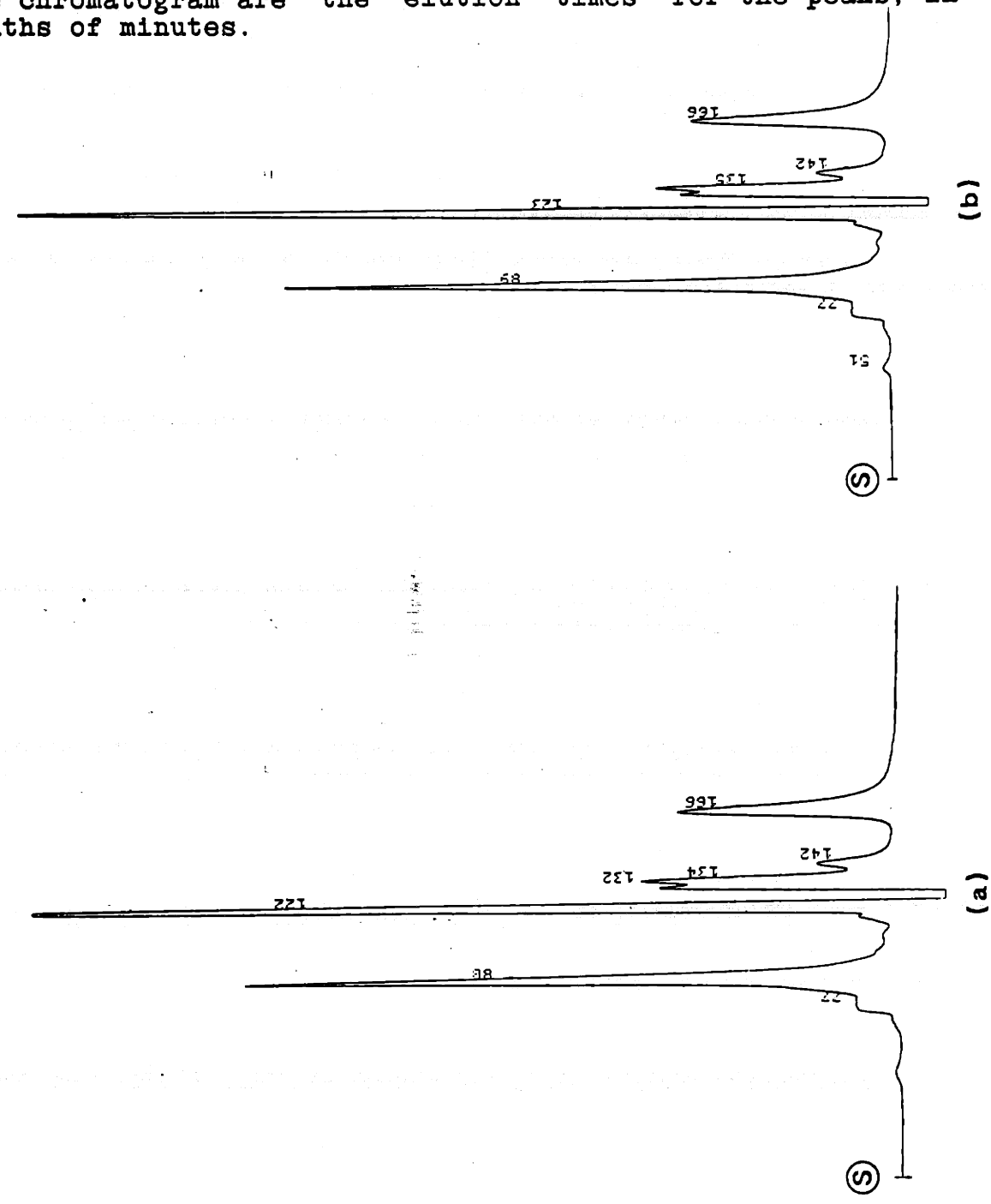

Figure 4.41 Two dimensional SDS-PAGE electrophoretogram of calf aqueous humor (a) and serum (b). In all electrophoretograms the upper scale refers to gel pH, while molecular weight markers are identified by their size (in kdaltons). "S" denotes internal pI standards (MW - 36,000), while the identity of the bracketed proteins "B" is discussed in the text. Loaded protein mass was 40 μg.

Figure 4.41

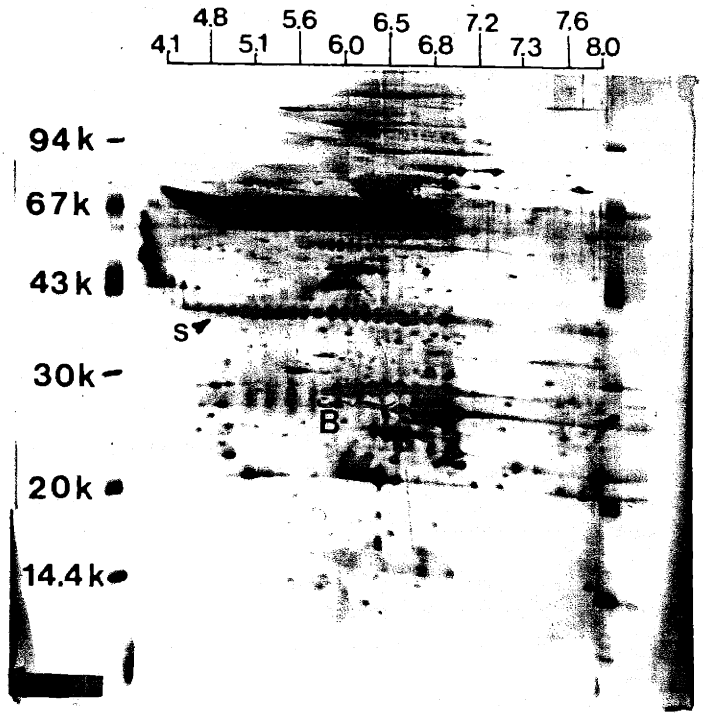

(a)

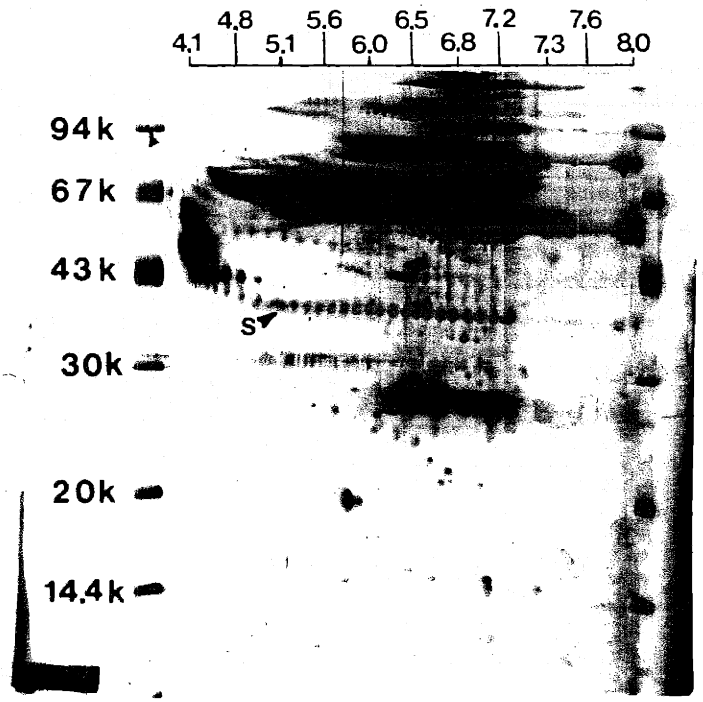

(b)

Figure 4.42 A 2-D SDS-PAGE reference map for serum proteins (from Danfeldt and Harrison, 1984).

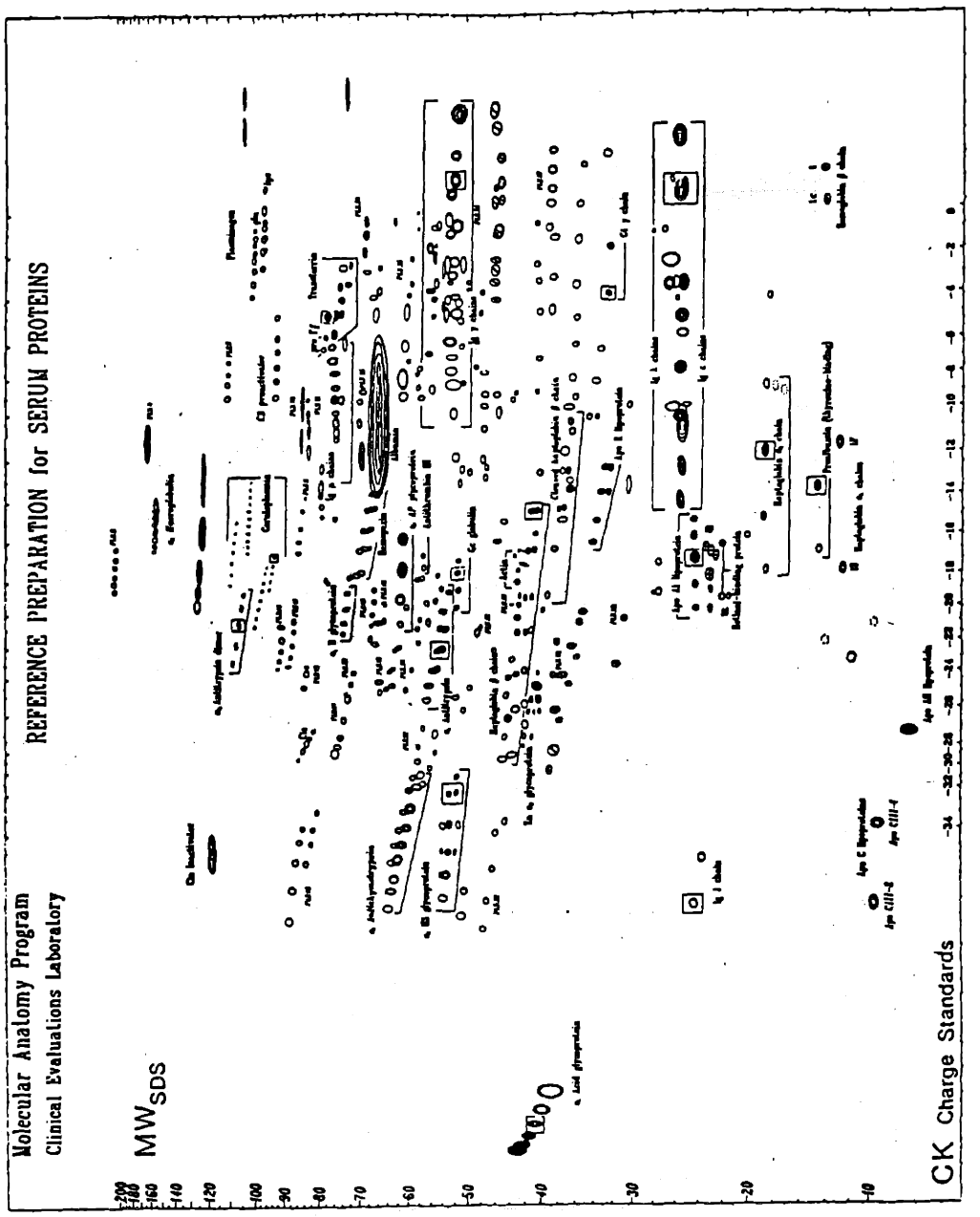

Figure 4.43 Two-dimensional SDS-PAGE runs of filter washing material. Conditions as for Figure 4.41. Loaded protein mass was 6 μg. Symbols as in Figure 4.41.

Figure 4.43

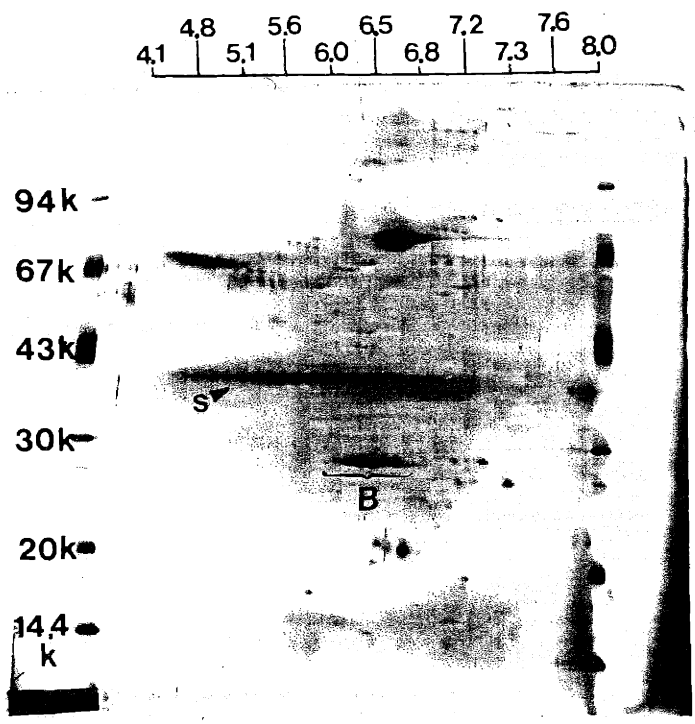

blocking material have different electrophoretic profiles, implying that certain proteins are preferentially adsorbed during the blocking process. A significant quantity of albumin appears to be present in the blocking material, confirming the results of the albumin spiking experiments which suggested that albumin plays a role in blockage. Of particular interest is the sequence of 5 spots of molecular weight ~25 kdaltons and pI values 6-7 which have been identified in Figures 4.41 (a) and 4.43. This material is seen to be present in aqueous, to be absent from serum and to be present in relatively high concentrations in the blocking material, suggesting that it may play an important role in the blocking process. This point will be further discussed in Section 6.2.

4.10 Filter Morphology

Scanning electron microscopy of the surface of saline- and aqueous-perfused 0.2 μ PVP-free filters indicated neither gross diferences in filter appearance, nor the presence of a covering layer. Approximately the same amount of debris was seen on both filters, while the aqueous-perfused filter showed a suggestion of buildup in the neighbourhood of some pore mouths, leading to "halo" formation about these pores. However, the general impression was that the slight differences observed did not seem to account for the extreme filter blockage seen on the aqueous-perfused filter (final resistance greater than 20 times baseline).

Transmission electron microscopy of 0.2 μ polycarbonate filters was carried out by Dr. Thomas Freddo of the Boston University School of Medicine. Sample

micrographs of unperfused and aqueous-perfused 0.2 μ polycarbonate membranes are shown in Figure 4.44. In all filters (including unperfused filters) a thin dense plaque was seen on both filter faces, and most probably was particulate matter which adhered to the filter during fixation and/or processing. Although additional amorphous material was occasionally seen on the filter face and/or within the pores, there were no consistent differences between unperfused, saline-perfused and aqueous-perfused filters that could be correctly identified in a masked fashion. It was therefore concluded that the resistance-causing material was not visualized by this technique.

In an attempt to localize the site of blocking, the flow tracer cationic ferritin was perfused through filters either alone or in combination with calf aqueous or calf serum. A thin layer of ferritin was seen to coat both the pore walls and the filter face, and there did not appear to be any preferential localization of ferritin except in one experiment in which perfusion with an aqueous:ferritin mixture produced a highly blocked membrane and a thick (1-2 μ), dense surface layer. Ferritin perfusion alone produced an increase in filter resistance, while preperfusion with spermine did not prevent ferritin adhesion to the filter surface. In summary, no definitive conclusions about the nature of the calf aqueous blocking mechanism were reached from the above ultrastructural studies.

Figure 4.44 Transmission electron micrographs of 0.2 μ polycarbonate filters. (a) Unperfused filter. (b) Filter perfused with ~1 ml of calf aqueous humor (Q=40 μl/min). Magnification - 9400 x.

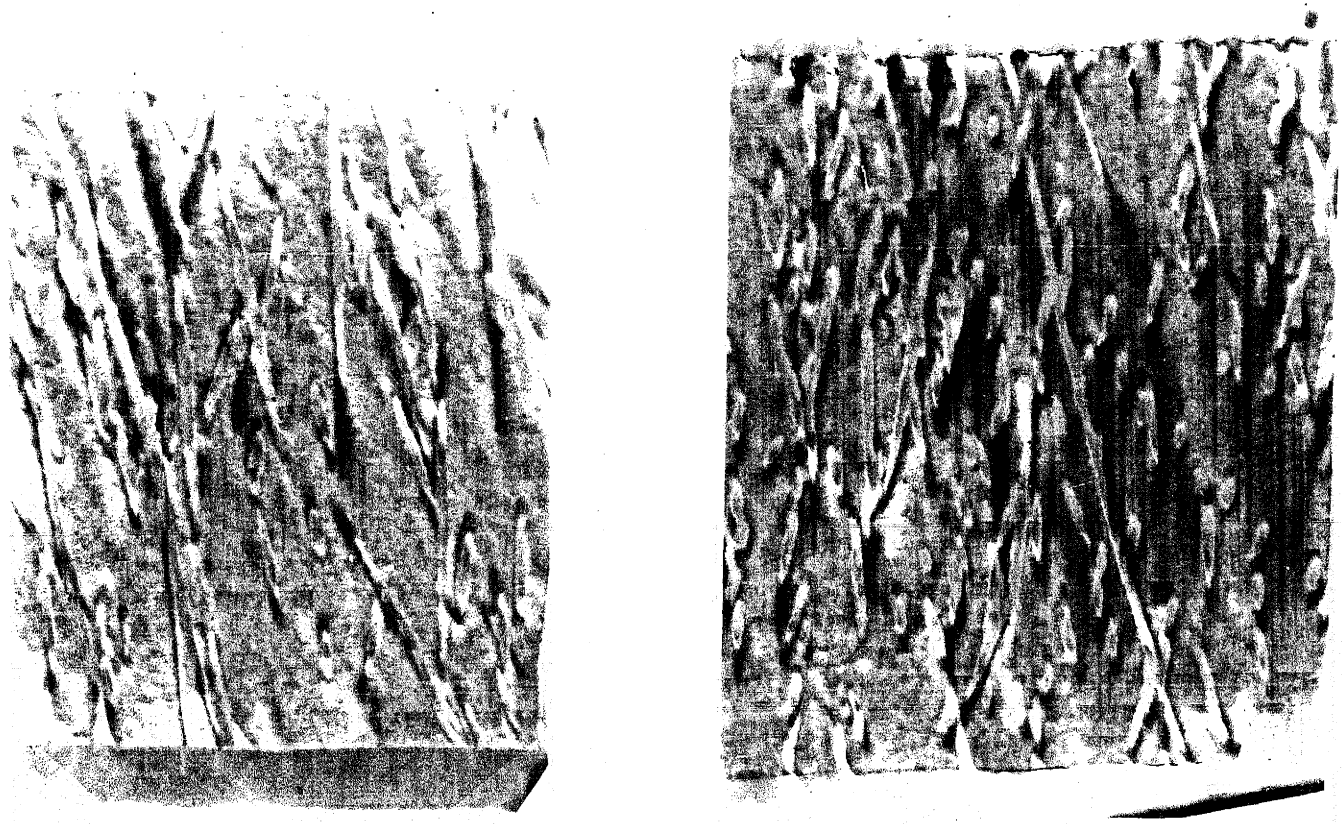

(a) (b)

Figure 4.44

4.11 Behavior of Human, Monkey and Rabbit Aqueous

Human Aqueous

Because of the small volume of fluid collected (50-200 μl) it was neccessary to dilute samples in order to obtain sufficient fluid. When human aqueous samples were diluted (usually approximately six fold) and tested on 0.2 μ polycarbonate or PVP-free filters they showed a slight tendency towards blockage (Figure 4.45). However, the magnitude of the effect was too small to be judged significant, and thus we have yet to demonstrate that human aqueous can block 0.2 μ filters.

Protein levels from individual human aqueous samples were determined by the Bio-Rad microassay, and appeared to fall into two groups, 150-300 μg/ml (three samples) and 450-800 μg/ml (four samples). In one of the latter samples a small reddish pellet was seen after ultracentrifugation and thus it is conjectured that samples with very high protein levels were contaminated with blood.

Monkey aqueous

Figure 4.46 shows the results of passing ultracentrifuged and untreated monkey aqueous humor through 0.2 μ polycarbonate filters. Although the amount of blockage is small (compared to calf aqueous humor), masked investigators were able to correctly identify the saline (control) and aqueous humor samples. Since both ultracentrifuged and non-ultracentrifuged samples behaved in a similar fashion we conclude that the blocking effect is not due simply to particulate fouling. Monkey aqueous

Figure 4.45 Blockage of 0.2 μ PVP-free polycarbonate membranes by perfusion with diluted human aqueous humor on (Q=40 μl/min). Solid lines: Perfusion of saline (0-300 seconds) followed by human aqueous, diluted 6.3-fold. Dotted lines: same protocol with saline substituted for human aqueous. Tests from 0-300 seconds establish membrane baseline resistance.

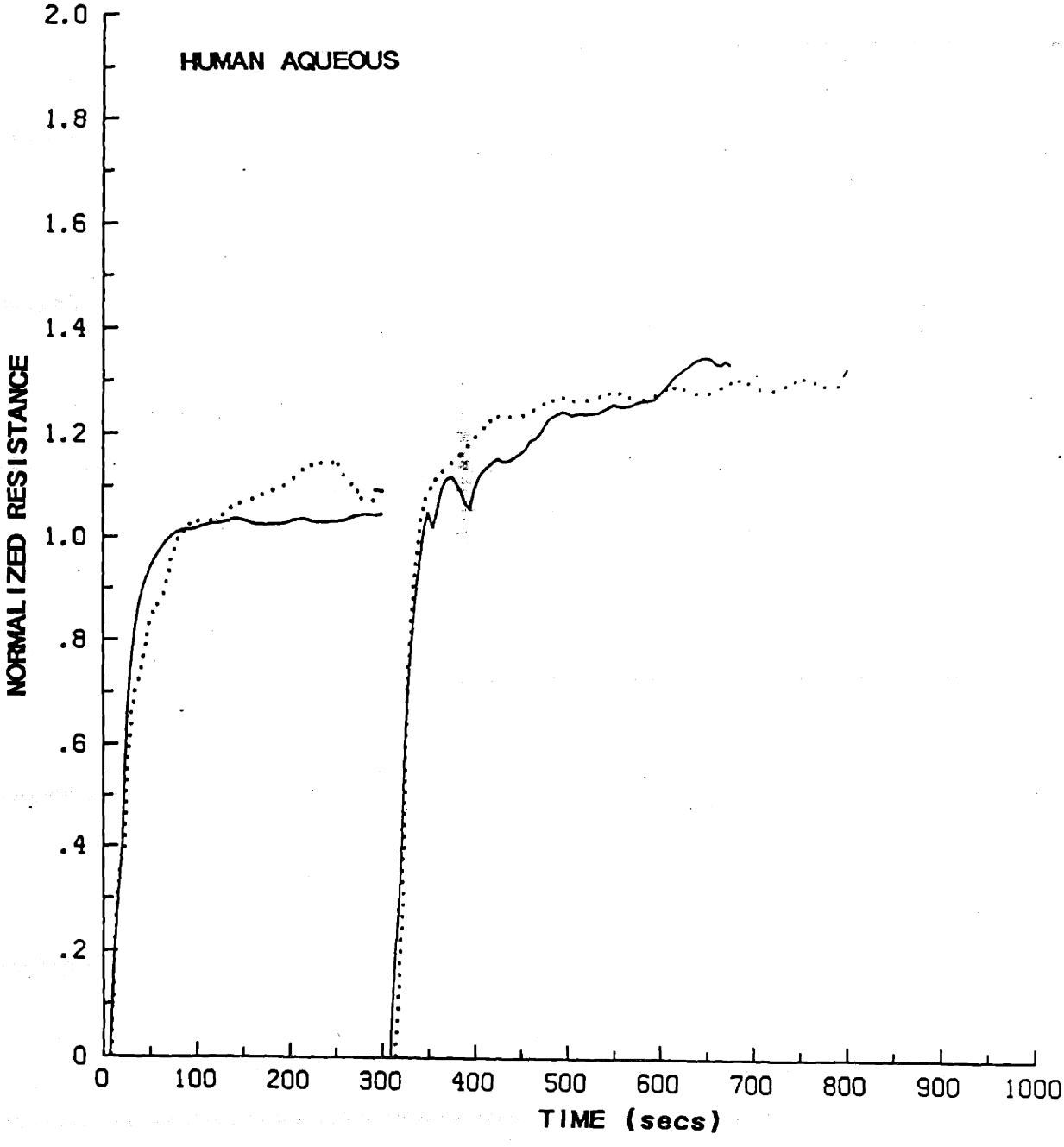

Figure 4.46 Blockage of 0.2 μ polycarbonate membranes by monkey aqueous humor (Q= 40 μl/min). Solid lines: aqueous humor, dotted lines: control saline solution. (a) Ultracentrifuged samples. (b) Samples which were not ultracentrifguged.

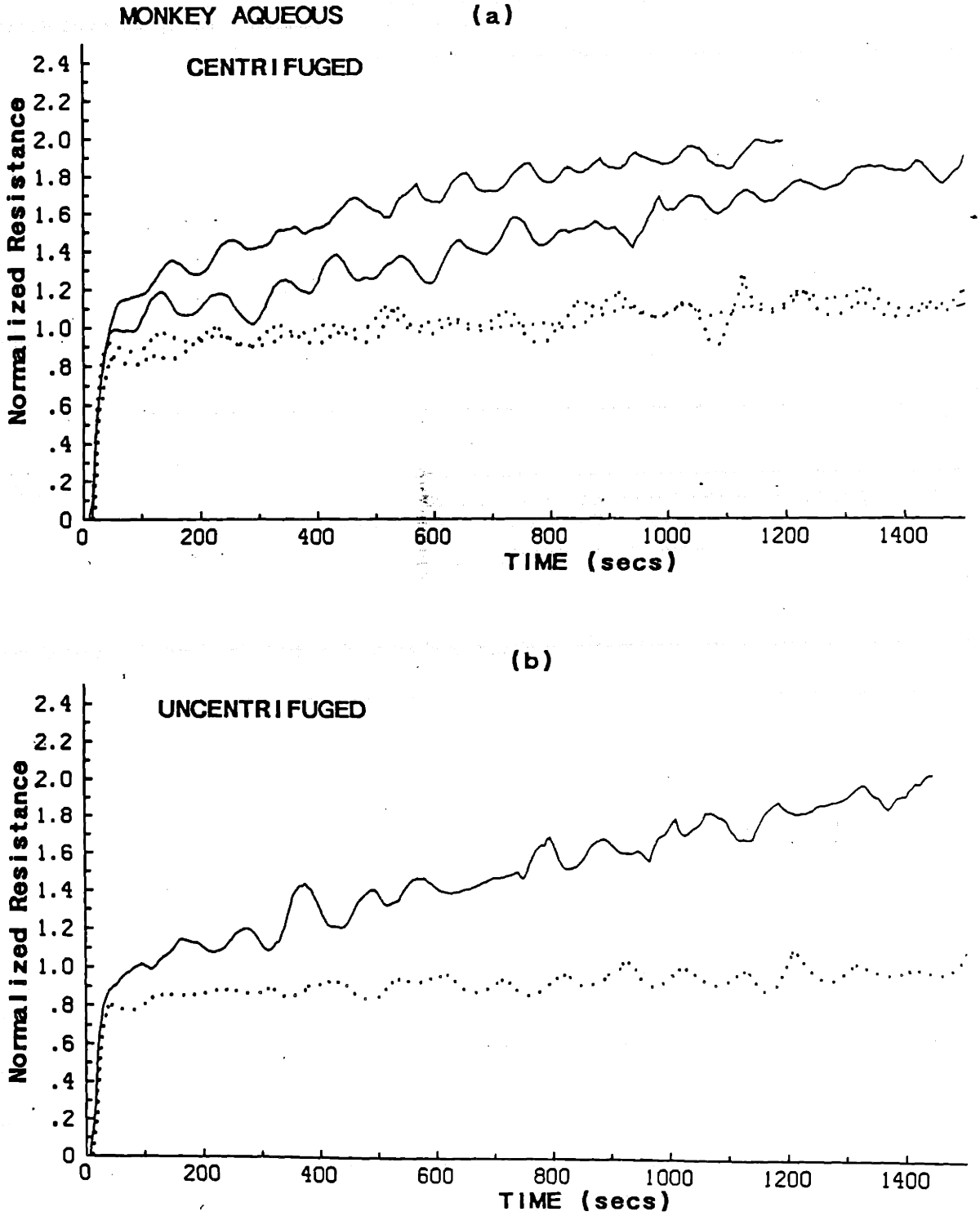

prefiltered through a 1 μ polycarbonate Nuclepore filter behaved similarly to non-prefiltered fluid.

Rabbit Aqueous

Protein levels in pooled rabbit aqueous collected from eyes with induced uveitus ("uveitic aqueous") and from contralateral eyes ("control aqueous") were measured by the Bio-Rad method and found to be approximately 22 mg/ml and 3.4 mg/ml, respectively. The latter figure is unusually high for rabbit aqueous (Table 2.1), and may be due to a contralateral effect from the endotoxin injection, the trauma of death, or the collection procedure. Figure 4.48 shows that both the control and uveitic aqueous blocked 0.2 μ PVP-free filters, the degree of blocking for uveitic aqueous being much greater. The blocking potential of control rabbit aqueous is seen to be less than that of calf aqueous.

It is interesting that although the character of the control aqueous blockage is similar to that seen for calf aqueous, that of the uveitic aqueous is quite different. Comparison of uveitic aqueous diluted approximately to control aqueous protein levels (curve 3) with control aqueous (curve 4) indicates that uveitic and control aqueous differ in more than total protein content. This point is further discussed in Section 6.4.

Although electrophoretograms of uveitic and control aqueous samples (Figure 4.47) show slight differences, the profiles are fairly similar overall. However, the protocol used to carry out electrophoresis of rabbit aqueous was slightly different than that used for calf aqueous gels, and thus the resolution in the gels of Figure 4.47 is inferior

Figure 4.47 Two-dimensional SDS-PAGE electrophoretogram of rabbit aqueous humor on 10-20 % gradient gels. (a) Normal (control) aqueous. (b) Uveitic aqueous. Upper scale refers to gel pH. Loaded protein mass was 25 μg.

Figure 4.47

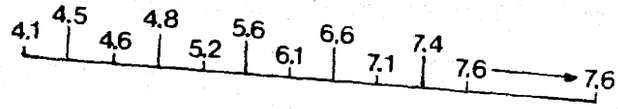

(a)

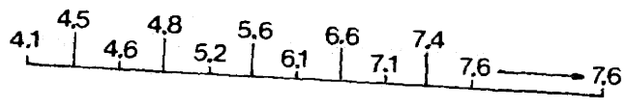

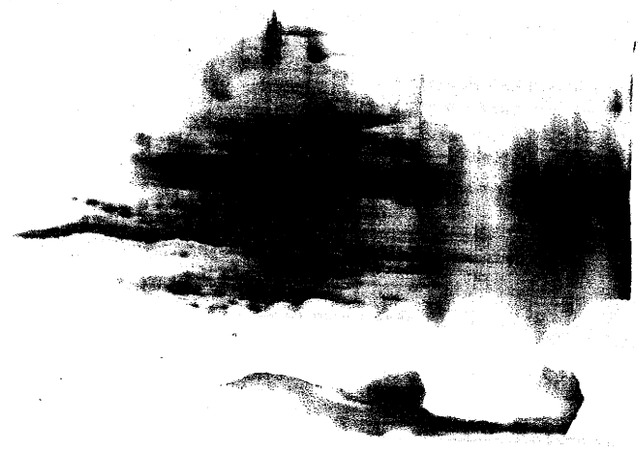

(b)

Figure 4.48 Blockage of 0.2 μ PVP-free filters by normal and uveitic rabbit aqueous (Q=40 μl/min).

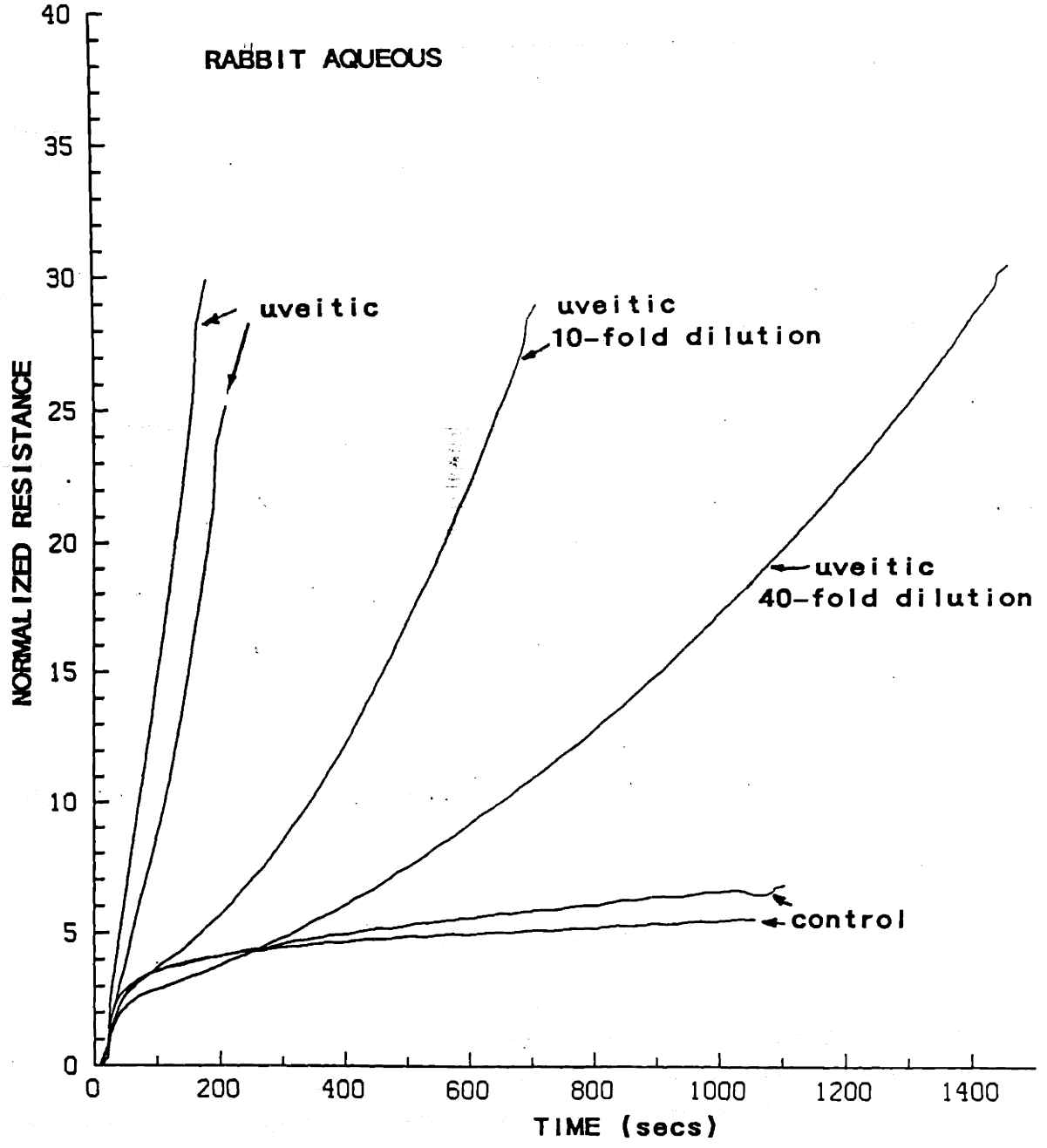

to that seen in Figures 4.41 and 4.43. This has made comparison of electrophoretograms of control and uveitic rabbit aqueous difficult, and hence it seems likely that differences between these two fluids exist which have not been visualized in Figure 4.47.

4.12 Enucleated Eye Perfusions

In an attempt to determine if an obstruction process similar to that which occurs in microporous filters occurs within the small channels of the aqueous outflow network, enucleated calf eyes were perfused with Triton-X. This detergent was selected for two reasons; (i) it is less damaging to protein structure than other detergents (P. John Anderson, Mass. Eye and Ear Infirmary, personal communication), and (ii) it is known to be effective at washing blocking material off perfused filters.

Figure 4.49 shows the results of baseline perfusion with DPBS (glucose added) followed by anterior chamber exchange with 0.2% Triton-X and continued perfusion with 0.2% Triton-X. As the eye fills the pump runs at maximum speed, reaching a steady state once filling and visco-elastic stretching of the globe are complete. Baseline facilities and washout rates were computed from facility data taken after this initial transient.

As shown in Figure 4.49 (b), washout rate appeared to increase in Triton-X perfused eyes. Data from perfusion of 10 eyes with various concentrations of Triton-X are summarized in Table 4.3, from which the mean and standard deviation of the change in washout rate may be calculated for eyes perfused with 0.2 % Triton-X (1.1 $\pm$ 1.2 %, n=5) and

Figure 4.49 Representative results of enucleated calf eye pefusion with 0.2% Triton-X 100. Perfusions were carried out at 15 mm Hg. (a) Plot of inflow as a function of time. (b) Same data plotted in terms of facility with filling transients supressed. Straight lines are used to determine washout rates.

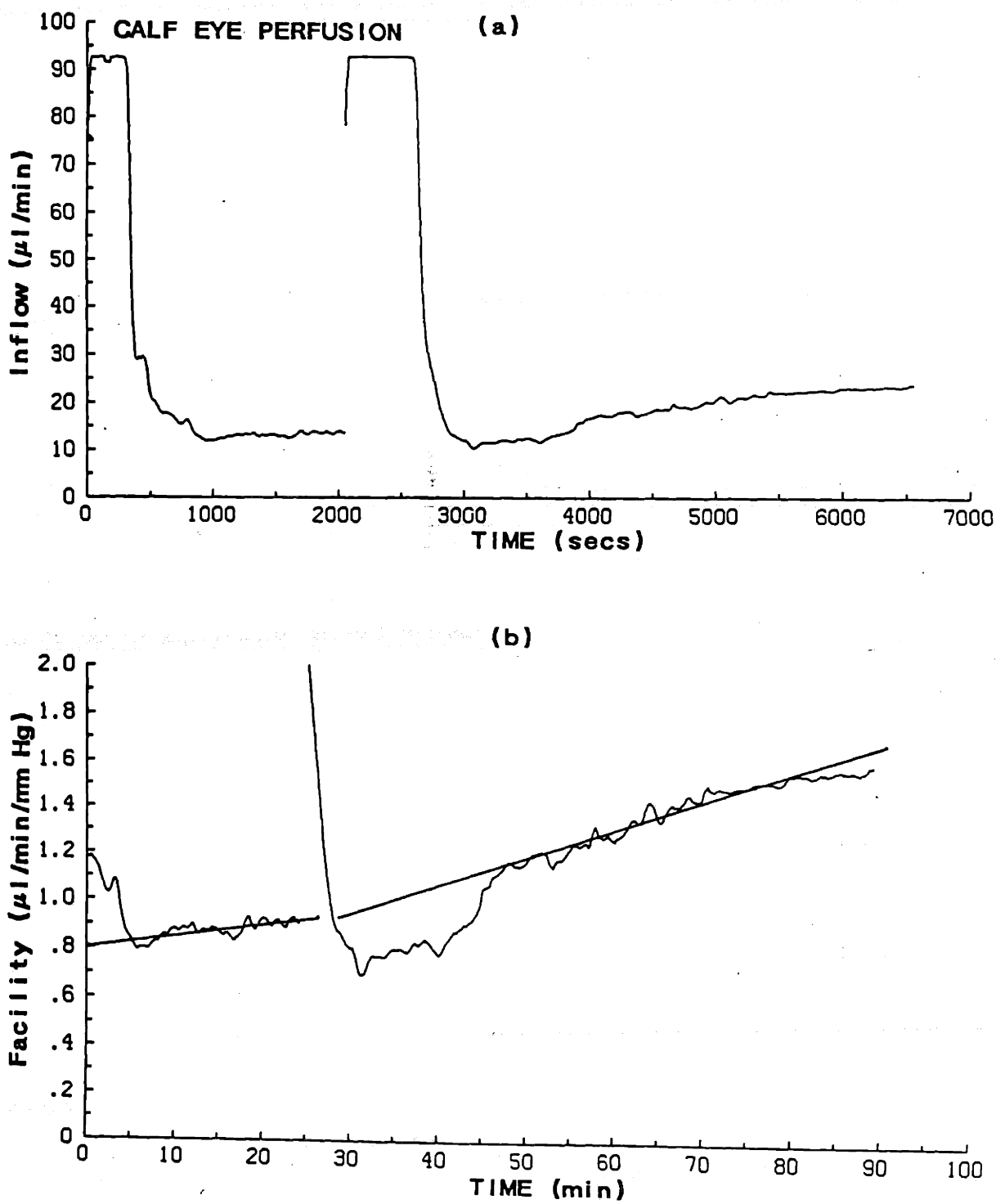

with lower detergent concentrations (0.1 ± 0.6 %, n=5). These data suggest that infusion of 0.2 % Triton-X increases washout rate (when compared to infusion of 0.07 % or lower concentrations of Triton-X), although the high degree of variability makes this conclusion only marginally significant ($p<0.07$, 1-sided t-test).

Triton-X Concentration	Initial Facility	Baseline Washout Rate	Triton-X Washout Rate	Change in Washout Rate
	0.83	0.5 %	1.5 %	1.0 %
	0.81	0.3 %	3.3 %	3.0 %
0.2 %	0.85	0.8 %	1.1 %	0.3 %
	0.65	0.0 %	-0.1 %	-0.1 %
	0.63	0.0 %	1.4 %	1.4 %
0.07%	1.4	0.8 %	-0.1 %	-0.9 %
	0.9	0.8 %	0.8 %	0 %
0.02 %	0.49	-0.3 %	0.5 %	0.8 %
	0.94	1.7 %	1.8 %	0.1 %
0.005 %	0.85	0.5 %	1.0 %	0.5 %

Table 4.3 Results of enucleated eye perfusions with Triton-X 100. Facility has units of μl/min/mm Hg, washout rates are calculated from percent change in facility (referenced to initial facility) divided by perfusion time, and have units of min^{-1}. The change in washout rate is column 2 minus column 1.

A concern regarding the above tests was that Triton-X infusion at high concentrations was simply rupturing cells within the outflow network and thereby influencing washout by a mechanism independent of removal of blocking material. In order to test this hypothesis, various concentrations of Triton-X were added to the medium covering cultured calf trabecular meshwork cells, and the cells were examined at 5 minutes, 1 hour and 24 hours after addition. Addition of

0.002% and 0.02% Triton-X caused no observable changes in cell shape or arrangement as seen by light microscopy. However, addition of 0.2% Triton-X produced an immediate and permanent disruption of all cells, characterized by the disappearance of cell boundaries and the appearance of debris floating in the culture medium. It seems most probable therefore that 0.2% Triton-X extensively disrupted the cell membranes of the cultured cells, leading to almost immediate cell lysis.

Because cultured cells can behave differently than cells *in situ*, the outflow pathways of calf eyes which had been perfused with high (0.2%) and low (0.005%) concentrations of Triton-X were examined by light microscopy. Morphological examination, carried out by Dr. Thomas Freddo of the Boston University School of Medicine, indicated that the meshwork of the eye which had been exposed to 0.005 % Triton-X appeared normal, with no cell swelling, no debris in the open spaces and a vacuolated inner wall. On the other hand, the meshwork which had been exposed to 0.2 % Triton-X showed cell swelling in the superficial meshwork, extensive ($\geq$ 50%) cell lysis in the deeper aspects of the CSM, a less compact JCM and an absence of vacuoles. Interestingly, cells within the JCM of the latter eye did not show evidence of lysis and the ciliary epithelium appeared normal. However, it seems clear that 0.2 % Triton-X caused extensive disruption of the meshwork, and thus the increase in washout rate seen with 0.2 % Triton-X perfusion may have been artifactual, i.e. not related to removal of resistive material within the flow channels of the JCM.

4.13 Summary

For convenience, major experimntal results are summarized in tabular form below. For the effects of detergents, see Table 6.1.

EXPERIMENT	RESULT
Protein assay	- higher protein in summer - drop in protein due to centrifugation
Unmodified calf aqueous perfusion	- filter blockage, variable behavior - "aging" of aqueous - protein-resistivity correlation - blockage scaling with pefused volume - variable effects of dilution
Protease addition	- elimination of blocking
Hyaluronidase addition	-little or no effect
Freezing	- no effect
Spiking or removal of aqueous components	- addition of albumin, γ-globulin and γ- crystallin increases blocking - no effect from fibrinogen addition, citration, removal of fibrinogen and fibronectin - spermine addition decreses blocking
Vary membrane type	- more blocking on hydrophobic filters
Spermine preperfusion	- decrease in blocking
Aqueous presoak	- decreased blocking on 0.2 μ PC
Mock aqueous	- no blocking
Plasma and serum perfusion	- no blocking on PC or PVP-free
Fractionation	- blocking material › 10 kdal

Table 4.4 Summary of major experimental results relating to calf aqueous perfusion on 0.2 μ filters.

CHAPTER FIVE: MODELLING

5.1 Overview

As noted in Chapter One, the transport of macromolecule-containing solutions through small-pore membranes is a problem of considerable interest in the engineering sciences, and indeed the experiments reported in Chapter Four may be regarded as a particular instance of this more general problem. In an attempt to better understand this transport process we have formulated a model which describes: (i) the transport of macromolecules through a filter composed of cylindrical pores, and (ii) the effect that such molecules may have on membrane resistance. Ultimately we wish to compare the predictions of this model to several of the experimental results of Chapter Four.

We therefore consider the transport of a dilute protein solution (more generally, a dilute macromolecule-containing solution) through a filter permeated by a homogeneous population of long ($L/R_o \gg 1$) right circular cylindrical pores. The flow is creeping ($Re \ll 1$) but protein transport is convection dominated ($Pe_L = UL/D \gg 1$). The protein is able to bind to (adsorb onto) the filter material in a saturable fashion, and the bound material is assumed to impede fluid flow, i.e. to block the filter. We consider two possible blocking scenarios: (i) binding occurs primarily to the pore wall, producing a partially or completely protein-filled pore, and, (ii) binding occurs primarily on the filter face, leading to occlusion of the pore mouth.

5.2 The Resistance of a Gel-Filled Pore

To investigate the effects of protein binding to the pore walls (formation of a gel layer) the resistance of a partially or completely gel-filled pore must be calculated. Consider the formation of a layer of thickness Δ and permeability K within a pore of radius R_o, as shown in Figure 5.1. To calculate the velocity distribution within the porous material it is necessary to take account of the presence of the wall and of the fluid flowing within the free inner core.

The problem of fluid in an open region (such as the inner core) flowing over the surface of a porous material has traditionally been treated in one of two ways: either by a "slip" boundary condition at the fluid/porous material interface, or by modifying Darcy's law within the porous material. In the first case the boundary condition takes the form (Beavers and Joseph, 1967)

$$\left.\frac{\partial u}{\partial y}\right|_{y=0^+} = \frac{\alpha}{\sqrt{K}} (u - u_D)$$

where u is the average axial velocity of the free fluid, u_D is the axial velocity within the porous material predicted by Darcy's law, y is the direction normal to the interface and α is a dimensionless constant. Unfortunately, α has been found to depend strongly on small variations in interface geometry (Beavers and Joseph, 1967), and for certain flows can actually become negative depending on where the interface location is taken (Larson and Higdon, 1986).

The second approach has been to use the Debye-Brinkman equation within the porous material (Wiegel, 1980)

Figure 5.1 The geomtery of a partially gel-filled pore, as seen in cross-section. The radius of the gel-free inner core is $R = R_o - \Delta$.

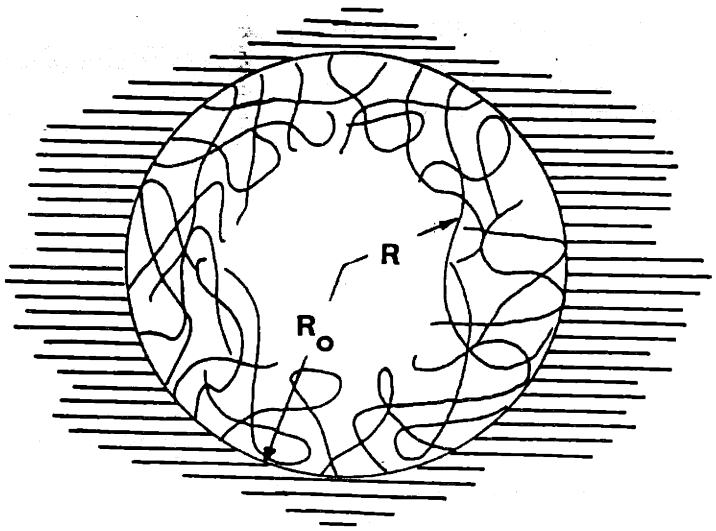

$$\Delta = R_o - R$$

$$\nabla p = \mu \nabla^2 \underline{u} - \frac{\mu}{K_{gel}} \underline{u} \qquad (5.2.1)$$

where the velocity $\underline{u}$ is an averaged (macroscopic) quantity, analagous to the superficial velocity which appears in Darcy's law. The Debye-Brinkman equation is best-suited to describing flow through highly porous media, and may be thought of the superposition of the Stokes equations and Darcy's law which arises when the resistance exerted by the porous material is represented as a distributed body force, $\mu\underline{u}/K_{gel}$. Although the Debye-Brinkman equation is an approximation, it gives results which agree well with the detailed numerical calculations carried out by Larson and Higdon (1986) for shear flow over isotropic idealized porous materials, leading these authors to conclude (at least for this model problem) that use of equation (5.2.1) is preferable to use of the slip boundary condition. We have therefore chosen to use the Debye-Brinkman equation in our modelling studies, despite its inherent shortcomings (see below). This equation has been previously used by Varoqui and Dejardin (1977) to treat the partially gel-filled pore problem, although a closed form solution was not obtained, and by Wiegel (1980) to obtain an analytical solution for flow through a fully gel-filled pore.

When using equation (5.2.1) it is important to specify the length scale of interest, since the equation as it stands involves macroscopic quantities obtained by averaging local variables over many microscopic length scales δ. To ensure the applicability of (5.2.1) we therefore require that the characteristic dimensions over which $\underline{u}$ and p vary are much greater than δ. From the form of the Debye-Brinkman equation it is seen that $\underline{u}$ will vary over distances proportional to $\sqrt{K_{gel}}$ (see also Figure 5.2), so that we require $K_{gel}/\delta^2 \gg 1$. In the present problem δ

is the characteristic internal spacing within the porous material, e.g. the interfibre spacing in the case of a fibrous gel. For the particular case of uniform, highly porous fibrous materials, the predictions of several theoretical models are well approximated by (Ethier, 1986)

$$K_{gel} = 0.319\, a^2\, \phi^{-1.17} \qquad (5.2.2)$$

where a is the fibre radius. For this geometry $\delta \sim a\phi^{-1/2}$, so that the ratio $K_{gel}/\delta^2 \sim \phi^{-0.17}$ varies between 2 and 5 for ϕ between 10^{-2} and 10^{-4}. Thus, the condition $K_{gel}/\delta^2 \gg 1$ is not strictly satisfied, and the velocity profile in the regions of thickness $\sqrt{K_{gel}}$ adjacent to the wall and the free inner core will only be approximately valid. However, in the limits as K_{gel} approaches zero or ∞, either the thickness of this layer is vanishingly small or the porous material has no influence on the flow, and thus in either case the error involved in calculating the total flow through the pore is vanishingly small. It is therefore hoped that in the intermediate region $K_{gel}/R_o^2 \sim 1$ the error associated with equation (5.2.1) will be relatively small.

Under the usual Poiseuille assumptions the governing equations become

$$\frac{1}{r}\frac{d}{dr}\left[r\,\frac{du_2}{dr}\right] = \frac{1}{\mu}\frac{dp}{dx} - \frac{u_2}{K_{gel}} \qquad R_o \geq r \geq R \text{ (gel region)} \qquad (5.2.1a)$$

$$\frac{1}{r}\frac{d}{dr}\left[r\,\frac{du_1}{dr}\right] = \frac{1}{\mu}\frac{dp}{dx} \qquad R \geq r \geq 0 \text{ (inner core)} \qquad (5.2.3)$$

where $R = R_o - \Delta$ and we have set $dp_1/dx = dp_2/dx$. The appropriate boundary conditions are

$$u_2 = 0 \qquad \text{at } r = R_o \qquad \text{(no slip)} \qquad (5.2.4)$$

$$u_1 = u_2 \qquad \text{at } r = R \qquad \text{(velocity matching)} \qquad (5.2.5)$$

$$\frac{du_1}{dr} = \frac{du_2}{dr} \qquad \text{at } r = R \qquad \text{(shear matching)} \qquad (5.2.6)$$

In formulating the matching boundary conditions (5.2.5) and (5.2.6) it is important to recall that u_2, the velocity within the porous material, is a macroscopic, i.e. averaged, quantity. Consideration of velocity matching therefore requires that the core velocity u_1 also be a macroscopic quantity, obtained by averaging the local velocity over the surface of the interface. In our particular problem we have circumferential independence, so that this area averaging simply reduces to an average in the axial direction, given by

$$u_1(x,r) = \frac{1}{2M\delta} \int_{x-M\delta}^{x+M\delta} u_{1,loc}(\xi,r)\, d\xi \qquad (5.2.7)$$

where M is of order 1 to 10. With equation (5.2.7) and a similar expression for $u_2(x,r)$ the velocity matching condition (5.2.5) then folows from <u>local</u> velocity matching at the interface

$$u_{1,loc}(x,r=R) = u_{2,loc}(x,r=R) \qquad (5.2.8)$$

and subsequent averaging. The shear matching condition (5.2.6) can be obtained by considering a force balance on an annular element of thickness δr containing the interface

r=R, and allowing δr to approach zero. In this limit the drag on the porous material within the control volume and thus also the shear stresses within the solid material at the control volume boundary are vanishingly small, since the drag is expressed as a body force. Thus, equilibrium requires that the total fluid shear stresses at the interface arising from flow within the core and within the porous material be equal, which leads to equation (5.2.6) when u_1 and u_2 are regarded as macroscopic quantities.

The general solutions to (5.2.2a) and (5.2.3) are

$$\hat{u}_1 = \frac{K_{gel}}{R_o^2}\left[A_1 - \frac{\hat{r}^2}{4}\right] \qquad (5.2.9)$$

$$\hat{u}_2 = \frac{K_{gel}}{R_o^2}\left(1 + B_1\, I_o(\hat{r}) + B_2\, K_o(\hat{r})\right) \qquad (5.2.10)$$

where the dimensionless radial co-ordinate $\hat{r}$ and the dimensionless velocities $\hat{u}_i$ are given by

$$\hat{u}_i = \frac{u_i}{-\frac{R_o^2}{\mu}\frac{dp}{dx}} \quad ; \quad \hat{r} = \frac{r}{R_o}\frac{R_o}{\sqrt{K_{gel}}} = \frac{r}{\sqrt{K_{gel}}} \qquad (5.2.11)$$

and I_o and K_o are the modified Bessel functions of the first and second kind of order zero. The three constants A_1, B_1 and B_2 are determined from the boundary conditions as

$$B_1 = -\frac{K_1(\hat{R}) + (\hat{R}/2)K_0(\hat{R}_0)}{D(\hat{R}_0,\hat{R})}$$

$$B_2 = -\frac{I_1(\hat{R}) - (\hat{R}/2)I_0(\hat{R}_0)}{D(\hat{R}_0,\hat{R})} \qquad (5.2.12)$$

$$A_1 = 1 + \frac{\hat{R}^2}{4} + B_1 I_0(\hat{R}) + B_2 K_0(\hat{R})$$

where $D(x,y) = I_0(x)K_1(y) + K_0(x)I_1(y)$

In Figure 5.2 representative velocity profiles are plotted for different values of the parameter K_{gel}/R_o^2, which measures the relative magnitude of the drag exerted by the pore wall to that exerted by the gel. For large values of this parameter the profile is essentially parabolic, while for values $<<$ 1 the gel significantly impedes flow. The existence of a transition layer adjacent to the wall and the inner core can be clearly seen for $K_{gel}/R_o^2 << 1$.

By integrating the velocity profile across the pore cross-section to obtain the total volume flow q through a single pore, the net pore permeability K_{net} can be calculated from Darcy's law

$$\frac{q}{A} = -\frac{K_{net}}{\mu}\frac{dp}{dx} \qquad (5.2.13)$$

where the area $A=\pi R_o^2$. This yields the expression

Figure 5.2 Plot of the normalized axial velocity as a function of normalized radial position within a partially gel-filled pore (Δ/R_o = 0.5), as calculated from (5.2.9) and (5.2.10).

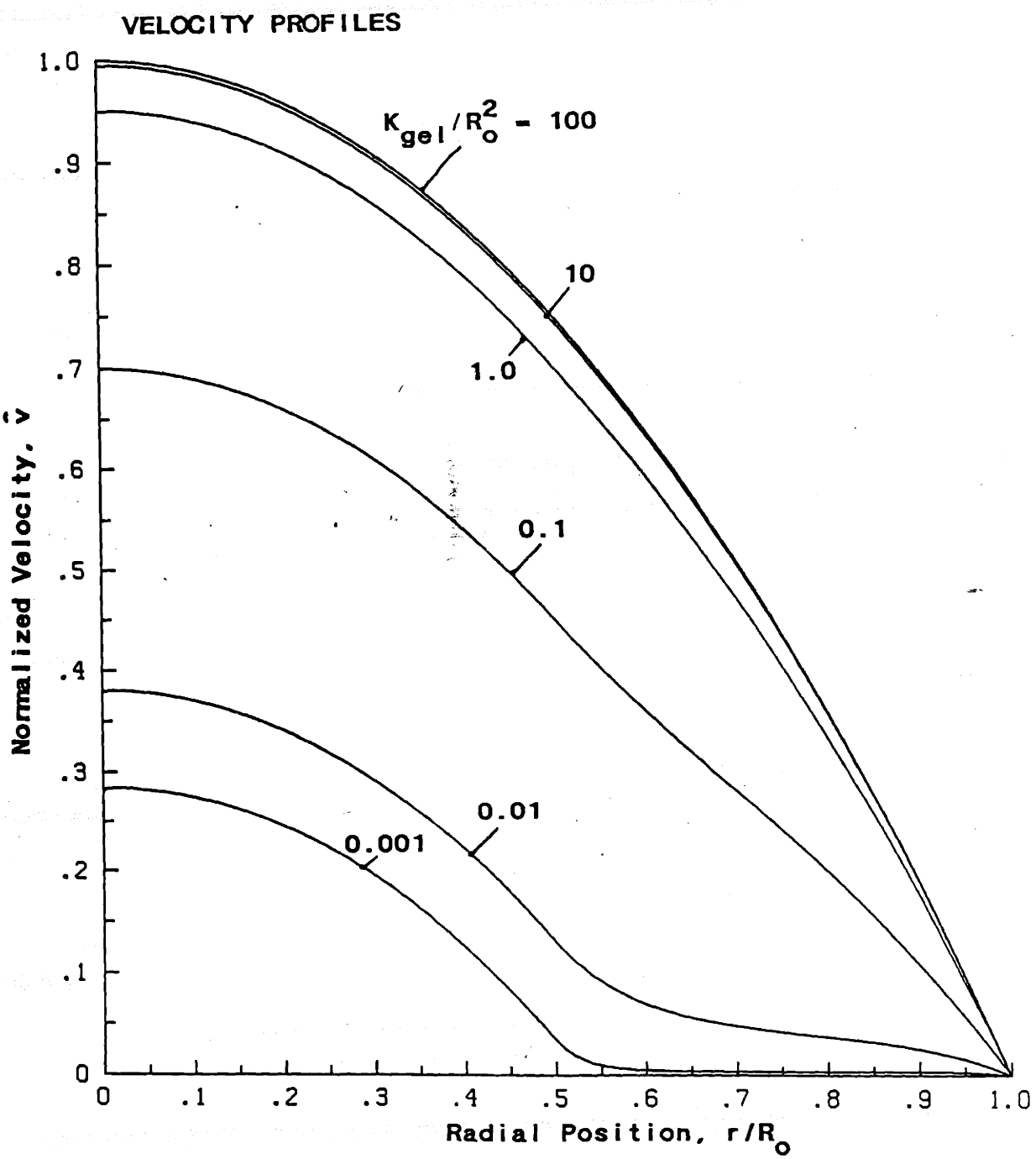

$$\frac{K_{net}}{K_{gel}} = \left[1 + \frac{\hat{R}^2}{8}\right]\left[\frac{\hat{R}}{\hat{R}_o}\right]^2 + 1 + 2C_1 + 2C_2 \qquad (5.2.14)$$

where

$$C_1 = B_1\left[\frac{I_1(\hat{R}_o)}{\hat{R}_o} + \frac{I_o(\hat{R})}{2}\left[\frac{\hat{R}}{\hat{R}_o}\right]^2\right]$$

$$C_2 = B_2\left[\frac{K_o(\hat{R})}{2}\left[\frac{\hat{R}}{\hat{R}_o}\right]^2 - \frac{K_1(\hat{R}_o)}{\hat{R}_o}\right]$$

This expression has the expected limiting behavior, namely: (i) as Δ approaches zero, K_{net} aproaches $R_o^2/8$, (ii) as Δ approaches R_o, K_{net} approaches the solution for a fully gel-filled pore (see below), and as K_{gel} approaches zero, K_{net} approaches $(R^2/8)(R/R_o)^2$.

The related problem of the velocity distribution in a fully gel-filled pore has been solved in a similar fashion by Wiegel (1980). In this case the net permeability may be calculated as

$$\frac{K_{net}}{K_{gel}} = 1 - \frac{2}{\hat{R}_o}\frac{I_1(\hat{R}_o)}{I_o(\hat{R}_o)} \qquad (5.2.15)$$

This has the limiting form $K_{net} \Rightarrow R_o^2/8$ as K_{gel} approaches ∞.

In Figure 5.3 the dimensionless net pore permeability K_{net}/R_o^2 (as given by (5.2.14) and (5.2.15)) is plotted as a function of K_{gel}/R_o^2 for various layer thicknesses Δ/R_o. This enables the permeability of a uniformly coated pore (thickness independent of θ and axial position) to be

Figure 5.3 Plot of the dimensionless net pore permeability K_{net}/R_o^2 as a function of dimensionless gel permeability K_{gel}/R_o^2 for various gel layer thicknesses, Δ, as calculated from (5.2.12).

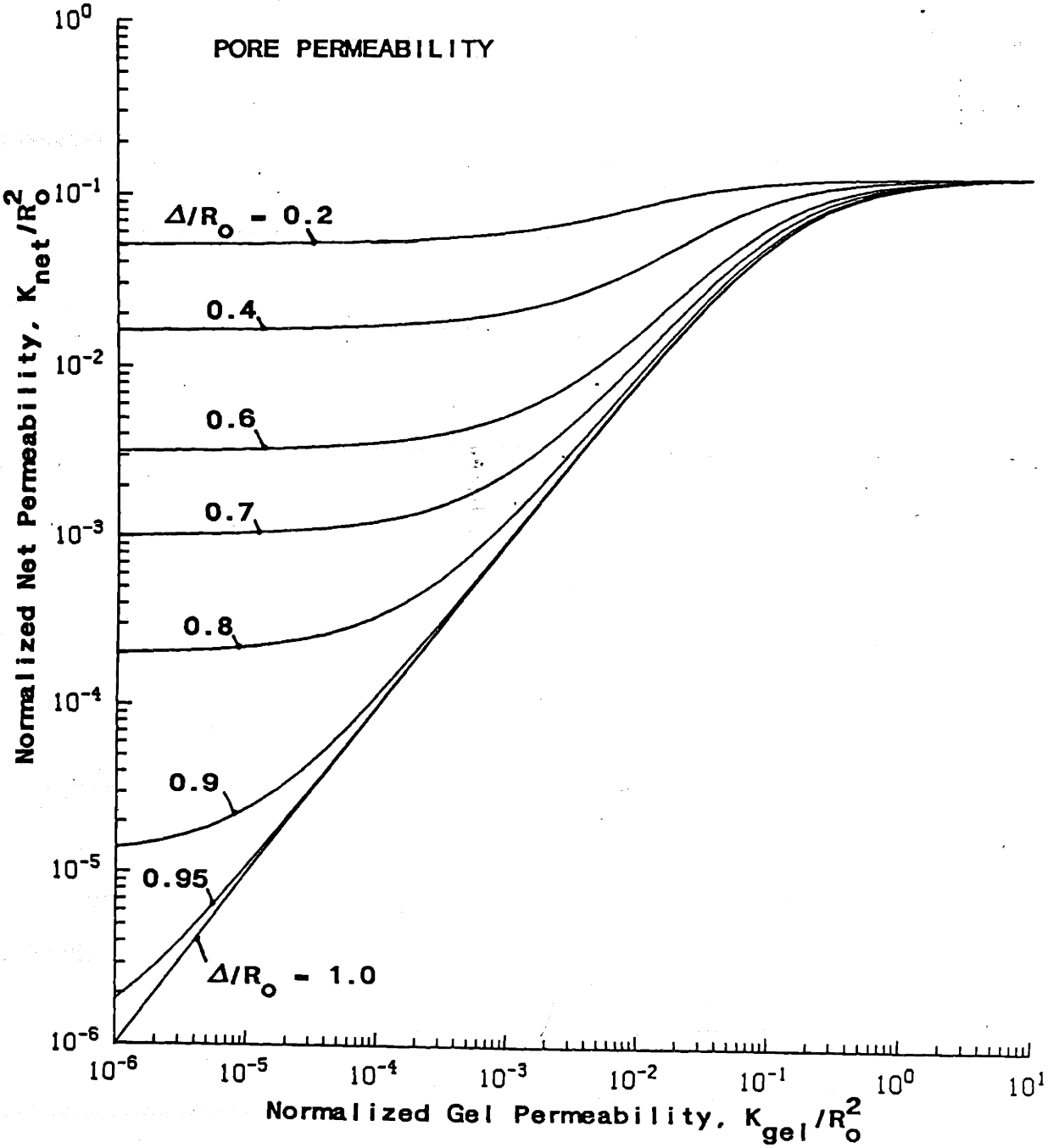

calculated. To handle the case in which Δ varies with axial position we may use Darcy's law to express the total pressure drop in terms of the local permeability K_{net}, viz.

$$\Delta p = -\int_0^L \frac{dp}{dx}\,dx = \frac{q\mu}{A}\int_0^L \frac{1}{K_{net}}\,dx \qquad (5.2.16)$$

Defining the overall pore permeability K_{pore} from

$$\frac{q}{A} = \frac{K_{pore}}{\mu}\frac{\Delta p}{L} \qquad (5.2.17)$$

we have

$$\frac{1}{K_{pore}} = \frac{1}{L}\int_0^L \frac{1}{K_{net}}\,dx \qquad (5.2.18)$$

Since variations in layer thickness will in general cause secondary flow within the pore, equation (5.2.18) will only be strictly valid when the magnitude of such flows is small, i.e. when radial velocity/axial velocity $\ll 1$. This ratio will scale approximately as

$$\frac{v_r}{v_x} \sim \frac{d\Delta}{dx} \qquad (5.2.19)$$

so that for $d\Delta/dx \ll 1$ we may use (5.2.18). Note also that for long pores with appreciable Δ gradients in several isolated locations equation (5.2.18) will also be approximately valid.

5.3 The Resistance of a Surface Layer

In addition to calculating the effect that adsorbed material within the pore has on membrane resistance, we have considered the analagous problem when material binds to the upstream filter face. Two different geometries have been considered: (i) a homogeneous cake of uniform thickness Δx which forms everywhere on the filter surface, and (ii) a series of homogeneous hemispherical "caps" which overlie each pore (Figures 5.4 and 5.7). The appropriate geometry will depend on the details of the protein deposition pattern, and hence on the upstream flow field.

The flow pattern upstream of a filter is such that fluid which is far from the filter must accelerate as it nears the filter so as to pass through the smaller cross-sectional area offered by the pores. Thus, fluid originally travelling with superficial velocity U_{sup} will enter the pore with mean velocity U_{sup}/ϵ, where ϵ is the porosity of the membrane. Since the resistance of a gel layer depends on the permeation velocity, obstructing material close to the pore mouth will have a proportionally greater resistance than material far from the filter surface. Thus, the resistance of a uniform gel layer will depend on the pore radius R_o and the mean interpore spacing, in addition to the gel layer thickness Δx and permeability K_{gel}.

Uniform Thickness Gel Layer

It is convenient to treat the problem of a uniform thickness gel layer by using the idealized geometry of Figure 5.4, in which the gel layer is subdivided into circular cylindrical elements of radius R_1 (one per pore),

Figure 5.4 The geometry of a gel layer of uniform thickness Δx overlying a filter having pore radius R_o and mean interpore spacing $2R_1$. The gel layer is subdivided into circular cylindrical elements of radius R_1. Half of one such element is outlined (heavy lines) and boundary conditions for calculating the pressure within the gel layer are shown.

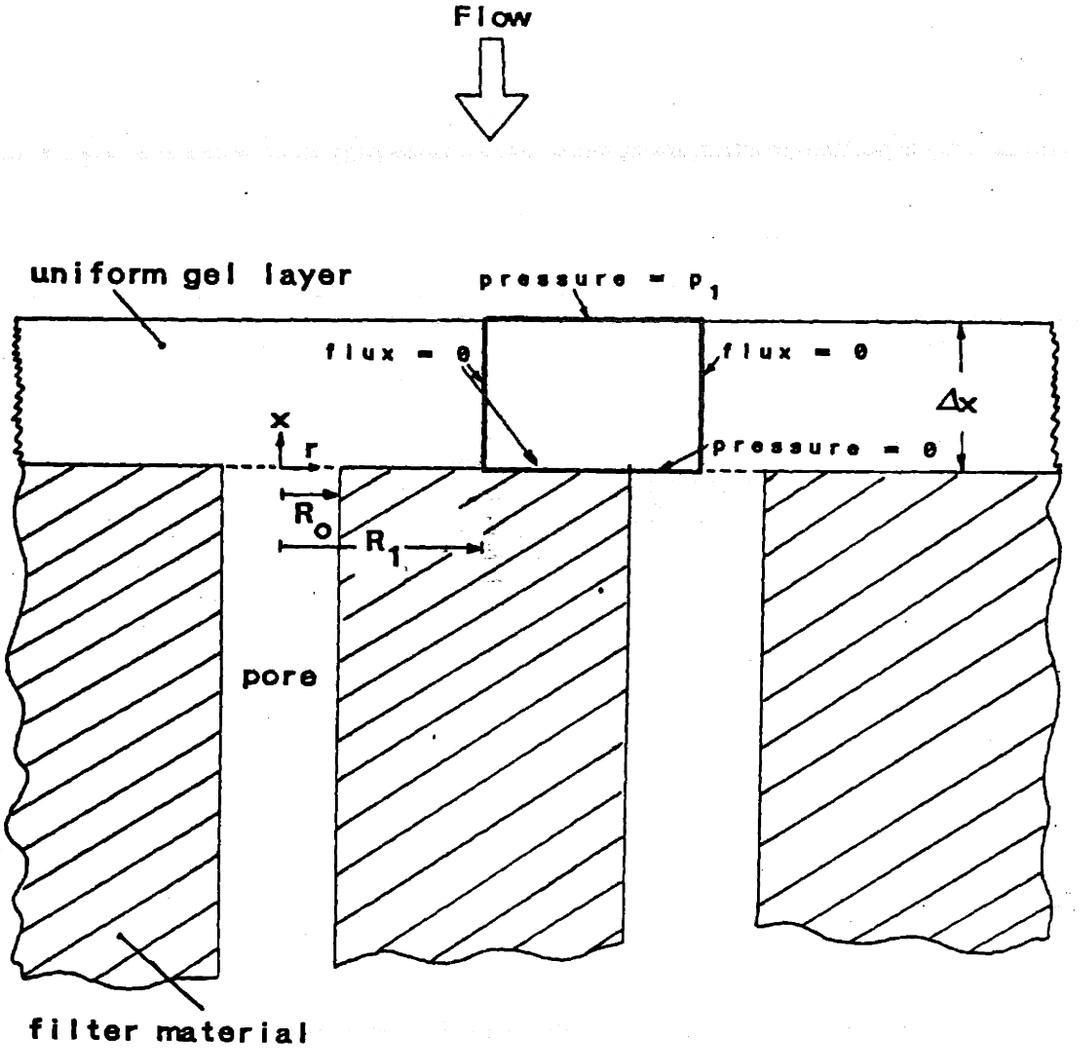

so that total membrane resistance depends on the resistance R of each element and the total number of such elements. The dimension R_1 is calculated as $\epsilon/\pi R_o^2 = (n\pi)^{-1/2}$ and equals half the mean interpore spacing. In the absence of a backing membrane each gel element will have idealized resistance R_{ideal}, given by Darcy's law as

$$R_{ideal} = \frac{\Delta p_{ideal}}{q} = \frac{\mu \, \Delta x}{K_{gel} \, \pi R_1^2} \qquad (5.3.1)$$

It is convenient to express the resistance R as

$$R = R_{ideal}/G \qquad (5.3.2)$$

where the factor G ranges between one (very thick layers) and ϵ (very thin layers). To calculate G we need to know the flowfield within the gel layer, which can be estimated by assuming that the flow obeys the generalized Darcy's law

$$\nabla p = \frac{\mu}{K_{gel}} \, \underline{u} \qquad (5.3.3)$$

which, when coupled with the usual incompressibility condition $\nabla . \underline{u} = 0$, leads to Laplace's equation for the pressure

$$\nabla^2 p = 0 \qquad (5.3.4)$$

In writing (5.3.3) we have neglected pressure losses due to conventional pore entrance effects. For long pores the

magnitude of the entrance pressure loss is small compared to filter resistance, and thus (5.3.3) will be valid for gel layer resistances comparable to filter resistance, since in this case entrance pressure losses will be negligible compared to gel layer losses.

The requirement that the normal velocity vanish on the solid portion of the filter produces the boundary condition

$$\frac{\partial p}{\partial n} = 0 \qquad \text{for } R_1 \geq r \geq R_o \text{ , } x = 0 \qquad (5.3.5)$$

where n denotes the normal to the filter surface. For the particular case of a uniform gel layer the remaining boundary conditions are (Figure 5.4)

$$\begin{aligned} p &= 0 && R_o \geq r \geq 0 \text{ , } x = 0 \\ p &= p_1 && x = \Delta x \\ \frac{\partial p}{\partial r} &= 0 && r = 0 \text{ and } r = R_1 \end{aligned} \qquad (5.3.6)$$

corresponding to uniform pressure at the pore mouth and the upstream surface, and the symmetry required by the chosen geometry.

This system of equations has been numerically solved in a different context by Lonsdale et al. (1971), and Figure 5.5 presents their results for the geometric shape factor G defined by equation (5.3.2). In Figure 5.6 these results have been replotted (for the particular case of 0.2 μ polycarbonate membranes) as the normalized resistance per pore, $RK_{gel}R_o/\mu$, as a function of layer thickness Δx. As expected, resistance increases most rapidly for thin layers

Figure 5.5 Numerically obtained results of Lonsdale et al. (1971) for the shape factor G (defined by (5.3.2)) for flux through a uniform gel layer.

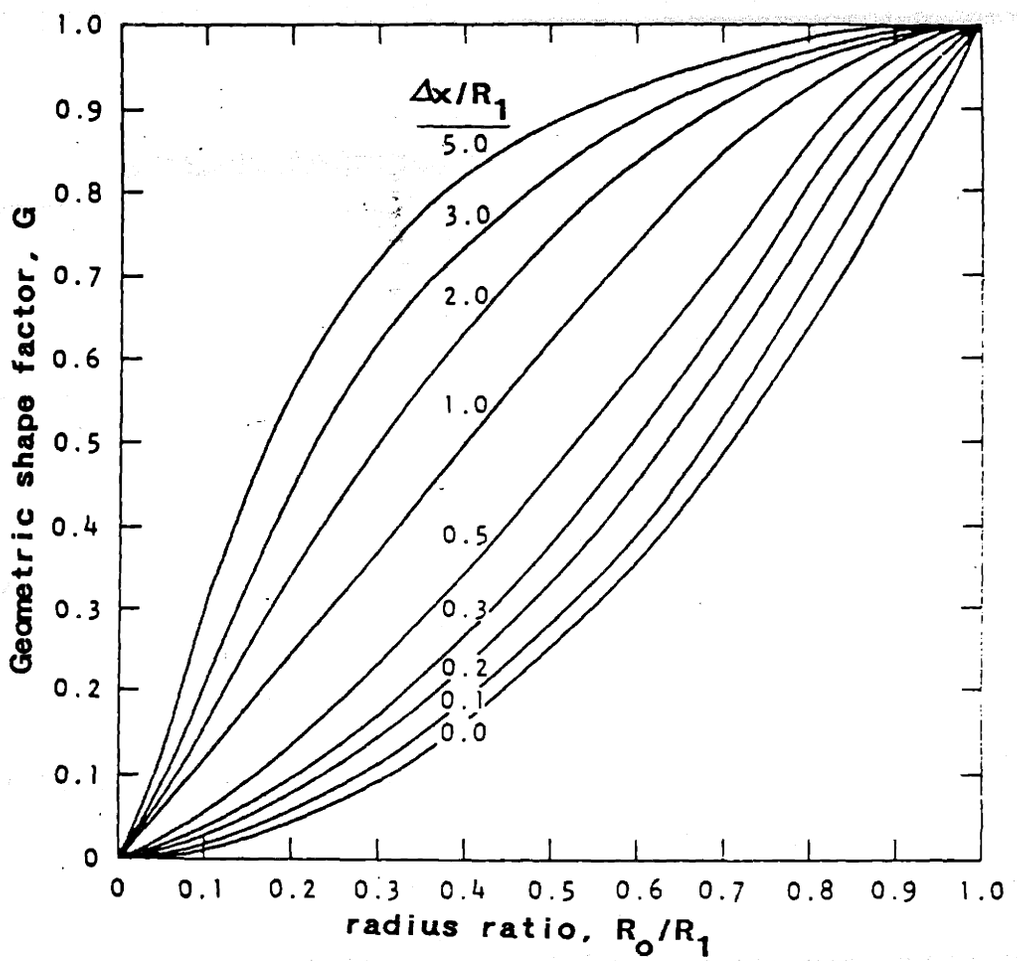

Figure 5.6 A plot of the normalized resistance per pore $R(K_{gel}R_o/\mu)$ as a function of the mean gel thickness for the uniform film geometry (solid line) and the gel cap geometry (dashed line). Graph is for the particular case of 0.2 μ nominal polycarbonate filters.

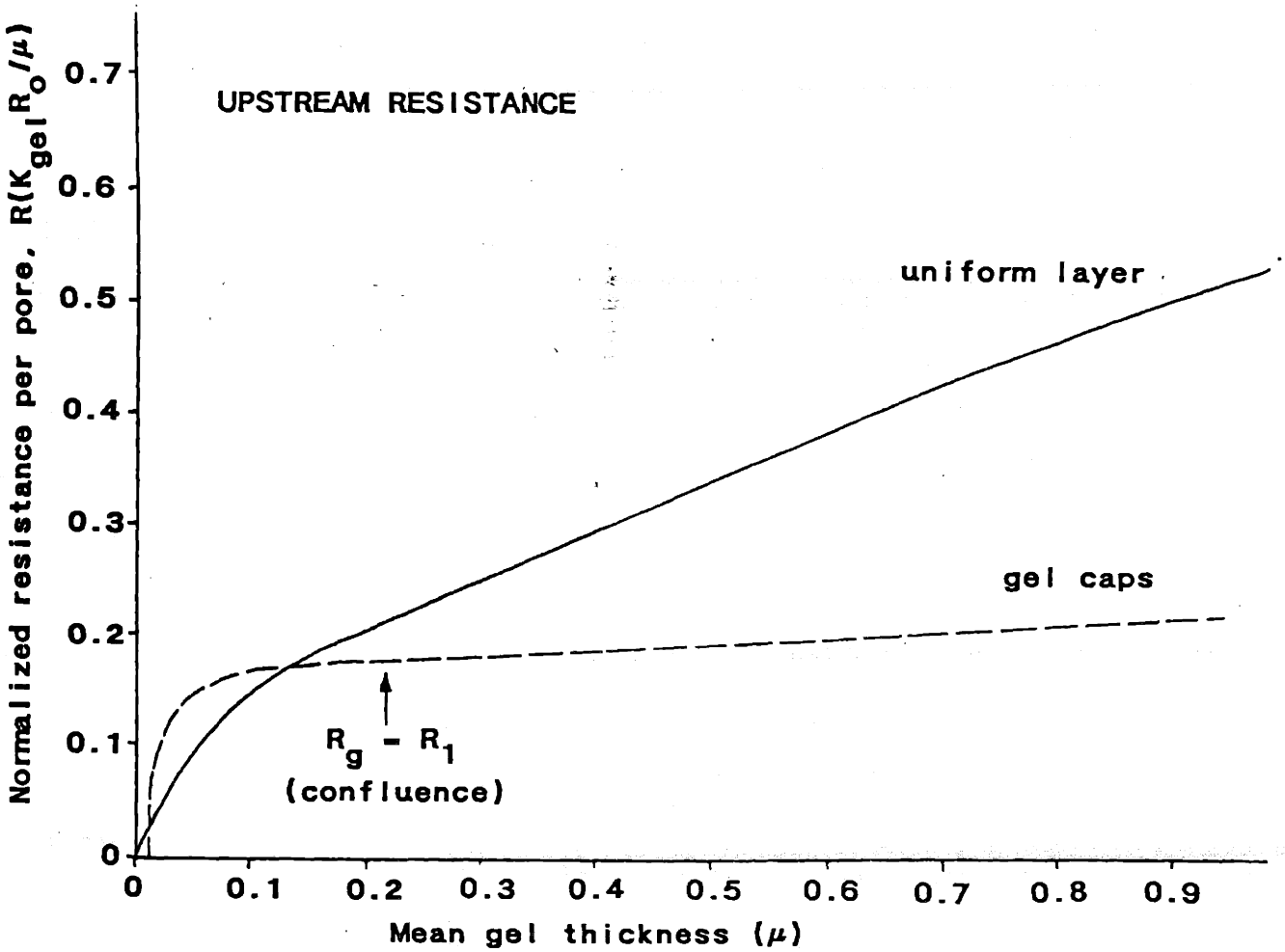

and then asymptotes to a linear rate of increase for values of $\Delta x \gg R_o$.

Hemispherical Gel Caps

Turning now to the case of isolated gel "caps" (radius = R_g) overlying pores, the governing equation and boundary conditions at the filter surface are as for the uniform thickness gel layer. The appropriate boundary condition at the outer gel surface is (Figure 5.7)

$$p = p_1 \qquad \text{at } r = R_g \tag{5.3.8}$$

Numerical solution of this problem using both finite elements and finite differences indicated that for gel radii $R_g > 2R_o$, most of the pressure drop occurs over a distance of one pore radius from the pore boundaries (Figure 5.8). This suggests that ∇p in Darcy's law will scale with $\Delta p/R_o$, so that the radial velocity u_r will have magnitude

$$u_r \sim \frac{K_{gel}}{\mu} \frac{\Delta p}{R_o} \tag{5.3.9}$$

This corresponds to a volumetric flow across a surface of area $\sim R_o^2$ of

$$q \sim \frac{K_{gel}}{\mu} \Delta p \, R_o \tag{5.3.10}$$

Figure 5.7 The geometry of isolated gel hemispheres of radius R_g overlying filter pores of radius R_o. The boundary conditions needed to calculate the flux through a given cap are indicated.

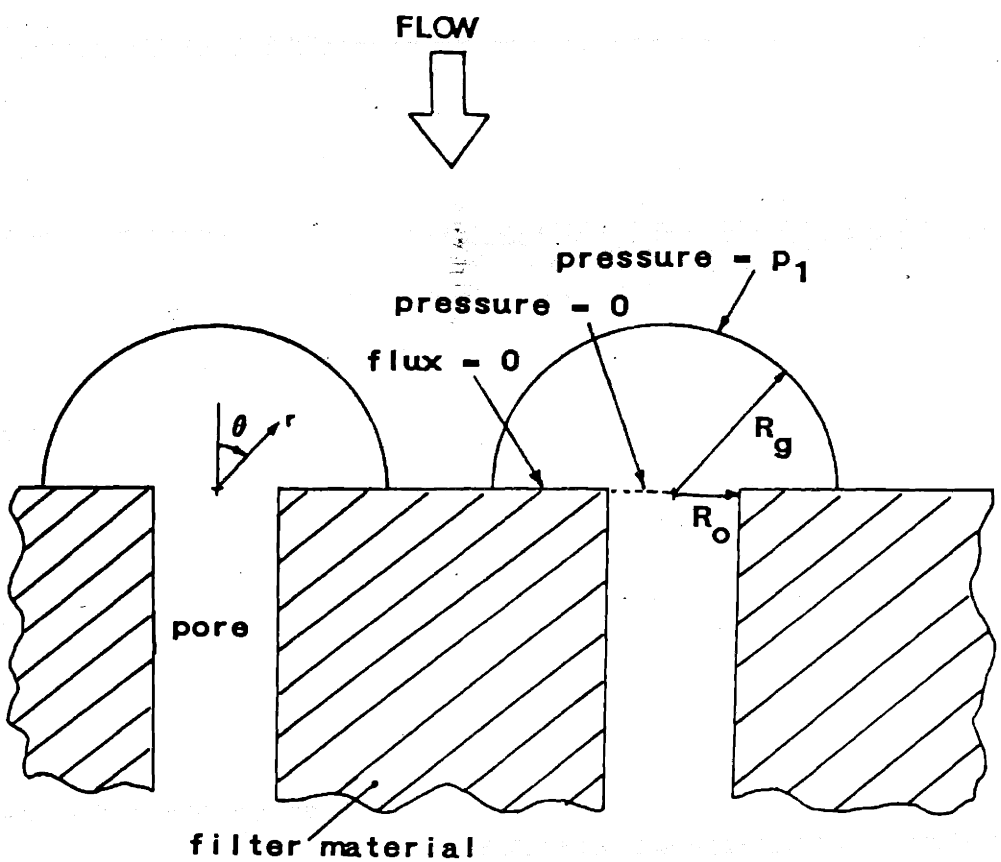

Figure 5.8 Normalized isobar profile for flow through an isolated gel hemisphere of size R_g/R_o = 4.

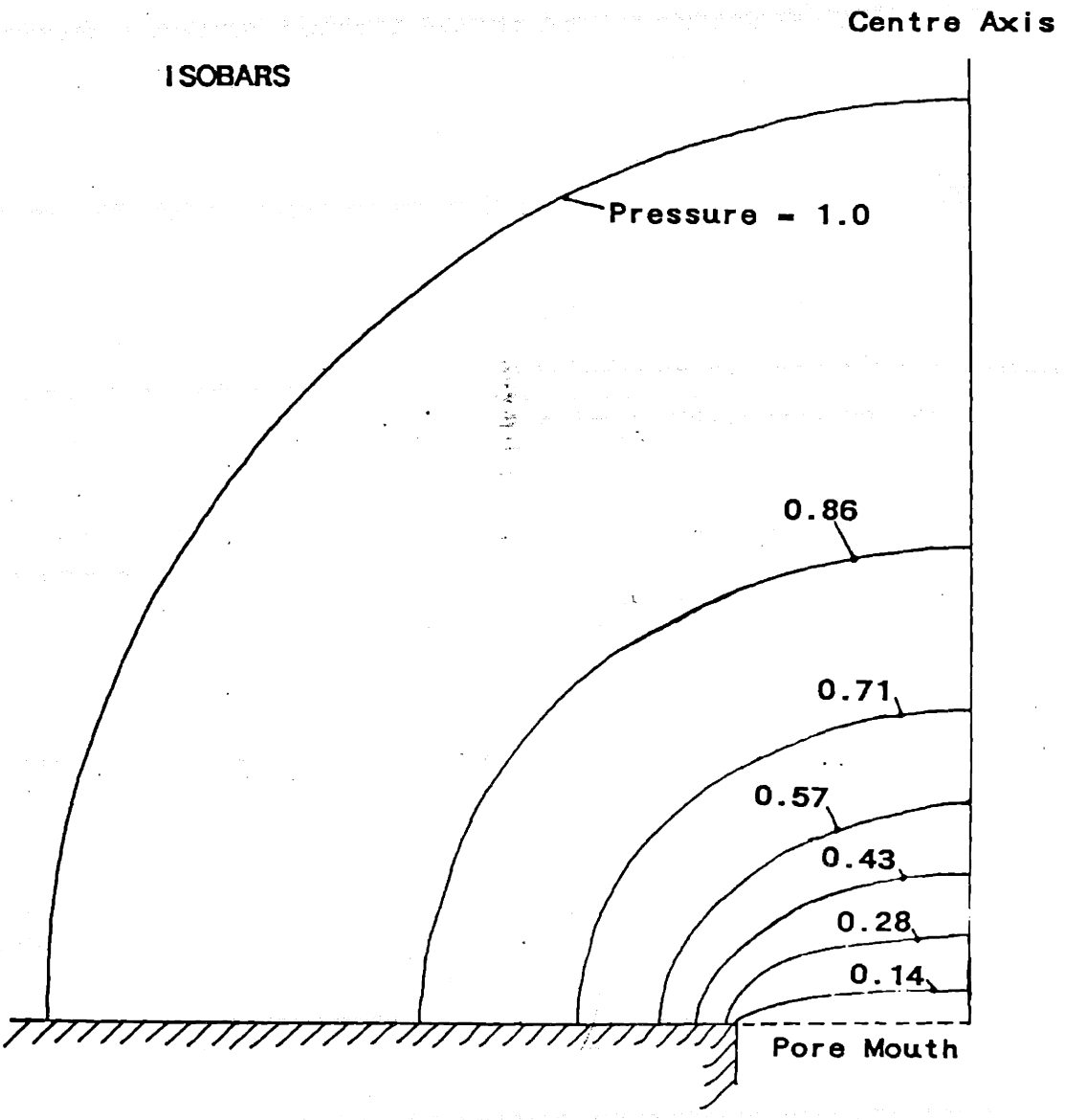

which suggests that the resistance of each gel hemisphere $\Delta p/q$ will scale with $\mu/K_{gel}R_o$, for large R_g/R_o. Figure 5.9 presents numerically obtained results for resistance normalized in this manner as a function of the dimensionless cap size R_g/R_o. Analagous to the case of a uniform layer, resistance is seen to rise most rapidly for small hemisphere dimensions.

In order to compare the results of the uniform thickness and gel hemisphere models, the gel resistance as predicted by both theories has been plotted in Figure 5.6 as a function of mean gel layer thickness for 0.2 μ polycarbonate filters (lot E). In this figure the quantity $RK_{gel}R_o/\mu$ is the normalized resistance of a single pore, while the mean gel thickness is defined as the gel volume per unit filter area (= Δx for the uniform layer and $2R_g^3/3R_1^2$ for isolated gel caps). At very low mean gel layer thicknesses it can be seen that isolated gel caps have approximately twice the resistance of a uniform layer. As isolated gel caps grow in size they will become confluent (at $R_g = R_1$), overlap, and form a continuous layer whose resistance may be approximated by that of a uniform layer. Figure 5.8 shows the point of confluence, and it is expected that for mean thicknesses greater than this value (0.22 μ) the normalized resistance can be obtained from the uniform layer theory, while for smaller mean thicknesses the resistance will depend on layer geometry. However, the influence of geometry is only moderate, since for small thicknesses the resistance differs by only a factor of two (approximately) for the two geometries considered.

Figure 5.9 Numerically obtained results for the normalized resistance $R(K_{gel}R_o/\mu)$ a a function of the normalized gel cap radius R_g/R_o for the hemispherical geometry of Figure 5.7.

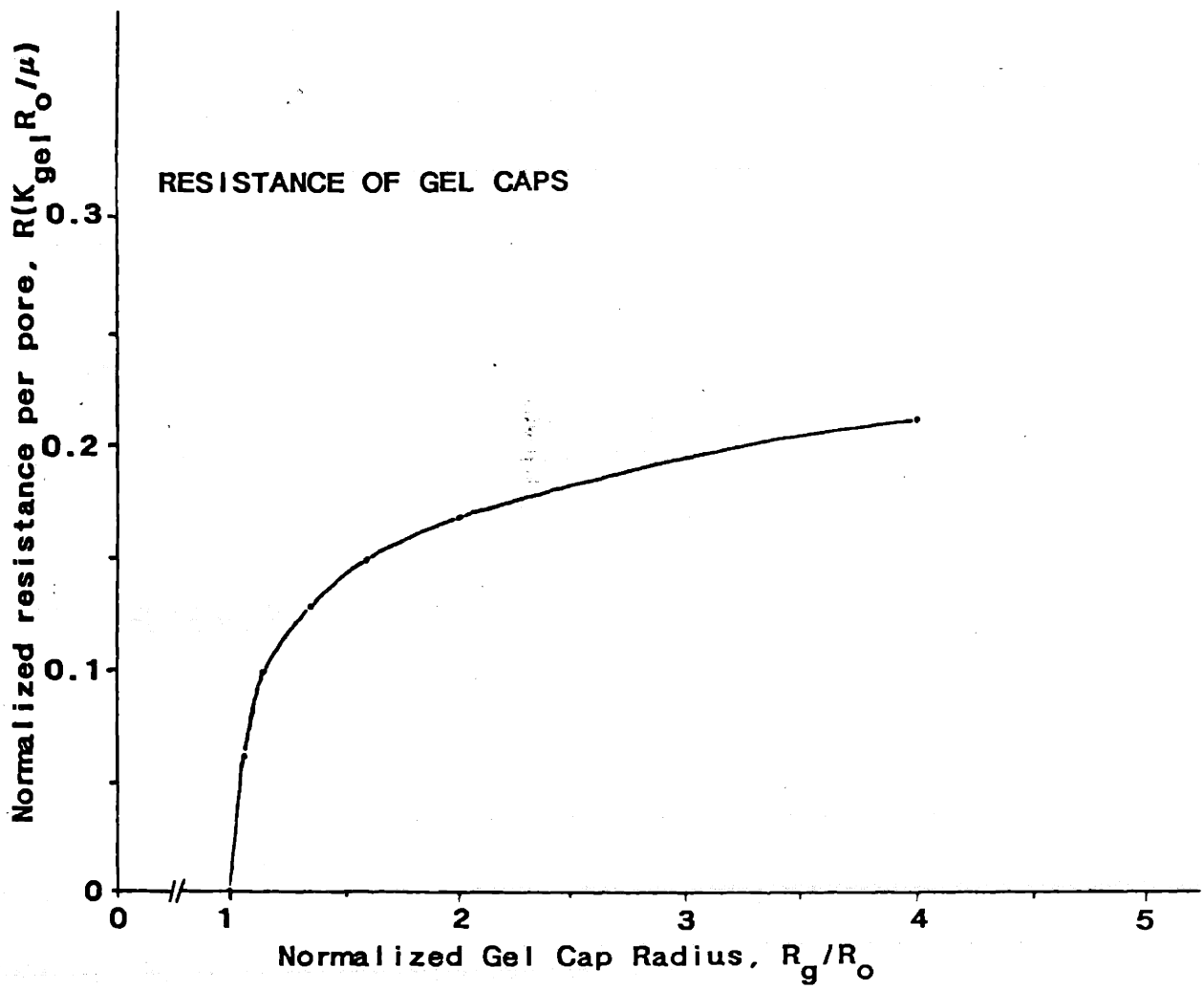

5.4 How Much Protein?

By using the results of Sections 5.2 and 5.3 we are now able to relate the two macroscopically observable quantities R (normalized filter resistance) and m (total adsorbed protein mass). In the context of filter blockage by calf aqueous such a relationship is of particular interest since a very small mass of protein (< 1 μg) substantially increases filter resistance. Hence, we consider the following problem: how much protein is required to produce a ten-fold increase in resistance for a 0.2 μ polycarbonate membrane when the protein forms: (i) an adsorbed layer within the pore, or (ii) a filter face surface cake?

In the former case a ten-fold increase in resistance corresponds to a 10-fold reduction in net permeability, which enables the required gel permeability K_{gel} to be determined from Figure 5.3 as a function of layer thickness, Δ. If the gel permeability can be related to gel concentration (equivalently, gel solid fraction ϕ) then the total protein mass on the filter is calculated as

$$m = \frac{N\pi\Delta(2R_o - \Delta)L\phi}{\bar{v}} \qquad (5.4.1)$$

where $\bar{v}$ is the protein specific volume = 7.4×10^{-7} ml/μg (Lehninger, 1975).

For the case of an adsorbed protein layer on the filter face we may use the results of Figure 5.6 to calculate the gel permeability K_{gel} needed to produce a surface layer having resistance nine times baseline (total

resistance = 10 times baseline) for various layer thicknesses Δx. As for the case of in-pore blocking, if a relationship betweeen K_{gel} and ϕ is available, the mass of adsorbed protein is then given by

$$m = \frac{\phi A \Delta x}{\bar{v}} \qquad (5.4.2)$$

where A is the filter face area (0.71 cm^2) and Δx is the mean layer thickness.

It remains to relate gel permeability K_{gel} to gel solid fraction ϕ, for which knowledge of the geometry and dimensions of the gel-forming material is required. For generality, and since these quantities are unknown for the aqueous blocking material, we consider several possible geometries and treat the characteristic dimension of the gel-forming material as a variable. Two candidates for the shape of the gel-forming material are fibres (radius-a) or spheres (radius-a). For the case of a uniform random fibrous porous material the model of Spielman and Goren (1968) has been found to closely match experimental data (Ethier, 1983; Jackson and James, 1986), and will therefore be used to relate permeability to solid fraction via

$$K_{gel} = \frac{a^2}{4\phi}\left[\frac{a^2}{3K_{gel}} + \frac{5a}{6\sqrt{K_{gel}}}\frac{K_1(a/\sqrt{K_{gel}})}{K_o(a/\sqrt{K_{gel}})}\right]^{-1} \qquad (5.4.3)$$

where K_1 and K_o are modified Bessel functions of the second kind. For the case of a highly porous material composed of spheres we use the expression of Happel and Brenner (1973)

$$K_{gel} = \frac{2}{9}\frac{a^2}{\phi}\left[\frac{3 - 9/2(\phi^{1/3} - \phi^{5/3}) - 3\phi^2}{3 + 2\phi^{5/3}}\right] \qquad (5.4.4)$$

which was derived from a cell-type model in which each sphere is surrounded by a fluid envelope having zero shear on its outer boundary.

With expressions (5.4.1) to (5.4.4) in hand the mass of protein required to cause a ten-fold increase in resistance may now be calculated as a function of the gel-forming material's characteristic dimension, a. Figure 5.10 displays the result of such a calculation for the case of a fibre-like protein gel when the protein resides in a uniform layer adsorbed to the pore wall (panel (a)) or as a uniform thickness surface layer (panel (b)). For clarity, only the results of the uniform thickness surface layer model have been presented, but from Figure 5.6 it can be estimated that results for the hemsispherical gel cap model would produce slightly lower protein masses (by at most a factor of 2). In calculating the curves in Figure 5.9 an upper limit of $\phi_{max} = 0.25$ (corresponding to $c_{max} = 0.34$ g/ml) has been imposed, which accounts for the fact that most of the the curves in panel (b) are truncated. The value 0.34 g/ml is the gelling concentration for albumin (Probstein et al., 1979), and may therefore be expected to be an appropriate estimate for the maximum packing density of aqueous-soluble proteins.

Experimental studies on perfusion of calf aqueous provide an upper bound of 1 μg protein mass per filter, while the radius of a fully denatured protein chain has been estimated as 3.5 A (Jackson and James, 1982). This latter figure must be a lower bound for fibre radius, which allows

Figure 5.10 Plot of the mass of of rod-shaped protein (per filter) needed to cause a ten-fold increase in filter resistance as a function of the fibre radius, a. Heavy curves represent boundary of possible blocking situations (see text). (a) all protein adsorbed onto pore walls with thickness Δ, (b) all protein adsorbed onto the filter face in a layer of thickness Δx.

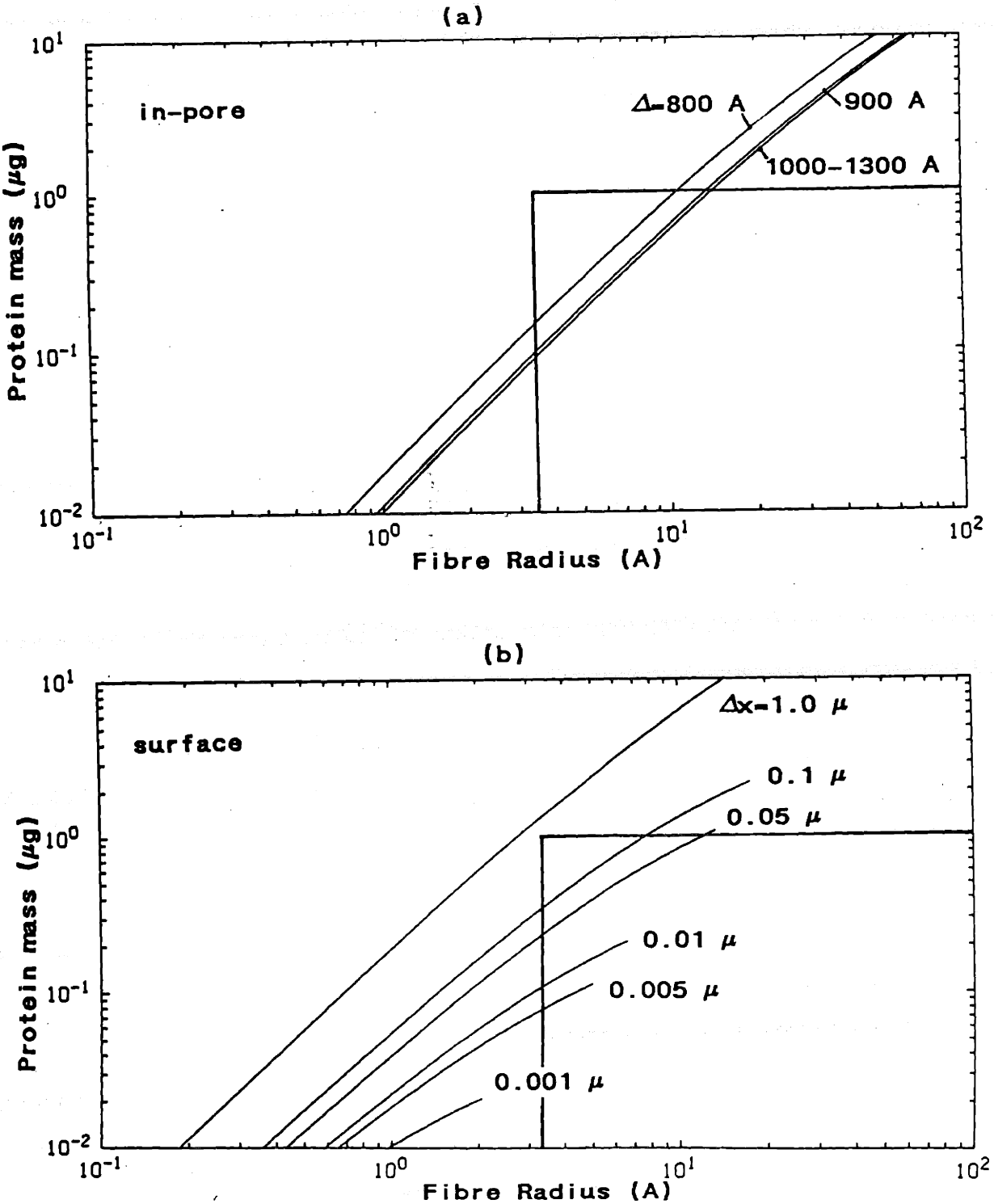

the domain of possible protein masses and fibre radii to be established (heavy line, Figure 5.10). Since several curves fall within this domain, Figure 5.10 indicates that a fibre-shaped blocking protein is a possibility, and that both in-pore and filter-face blocking are possible candidates for the obstruction process. It can be seen that thinner surface layers are more effective blockers, as expected from the results of Section 5.3. This effect is magnified for fibrous materials because they have a nonlinear dependence of permeability on solid fraction which produces a negative correlation between resistance and layer thickness, all other factors remaining constant. Figure 5.10 (b) does indicate that if blocking occurs on the filter surface the adsorbed layer must be relatively thin (in the range 0.005 to 0.5 μ), with thicknesses of 0.005 to 0.05 μ (50 to 500 A) being most likely.

The results of an analagous calculation for spherical porous materials is shown in Figure 5.11. Here an appropriate lower bound on the characteristic dimension (sphere radius) was taken as 10 A, corresponding to a globular protein of molecular weight several thousand. Electrophoretograms of the filter blocking material suggest that all adsorbed protein has a molecular weight of at least 25 kdaltons. From published values (Tanford, 1961) of dimensions and molecular weights, it is estimated that a globular protein of weight 25 kdaltons will have an effective Stokes radius of ~23 A, so that this value becomes the lower limit for the sphere radius in Figure 5.11. Such a lower limit renders nearly all blocking configurations impossible, suggesting that it is unlikely that the observed filter blockage is due to spherically-shaped molecules. This, we conclude that the observed blockage of 0.2 μ polycarbonate filters is most consistent with the adsorption of a fibre-like gel either onto the pore walls (thickness Δ

Figure 5.11 Plot of the mass of of spherically-shaped protein (per filter) needed to cause a ten-fold increase in filter resistance as a function of the sphere radius, a. Heavy curves represent boundary of possible blocking situations (see text). (a) all protein adsorbed onto pore walls with thickness Δ, (b) all protein adsorbed onto the filter face in a layer of thickness Δx.

(a)

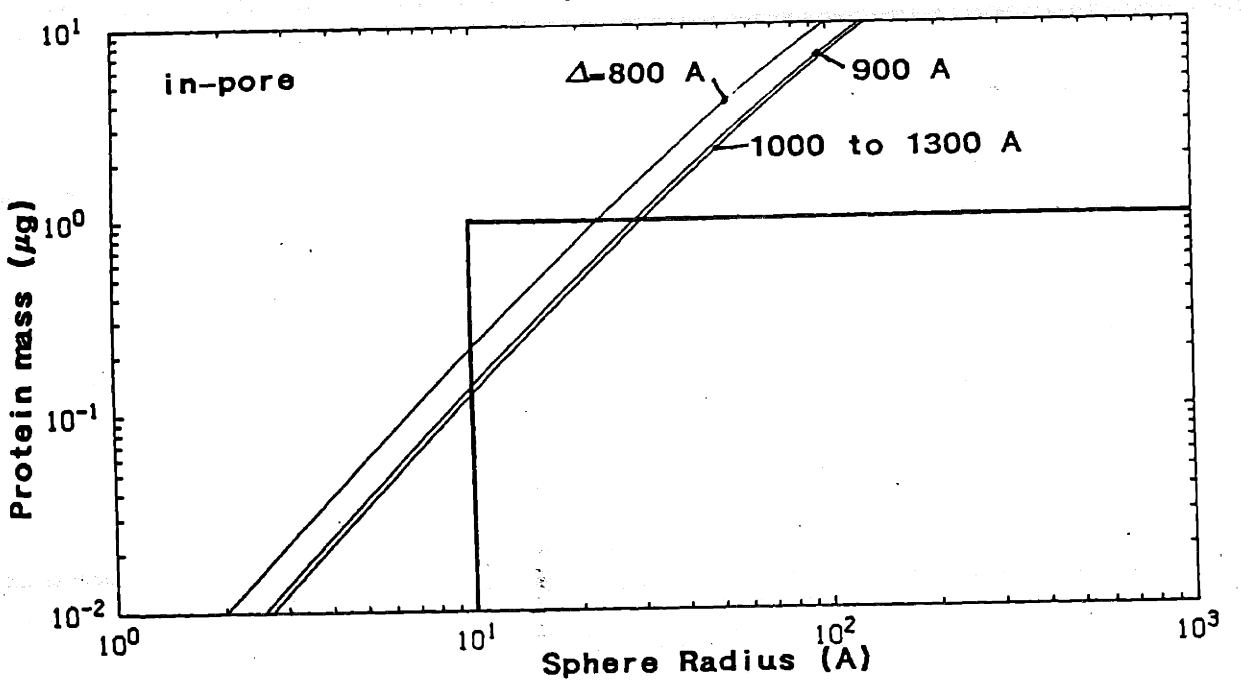

(b)

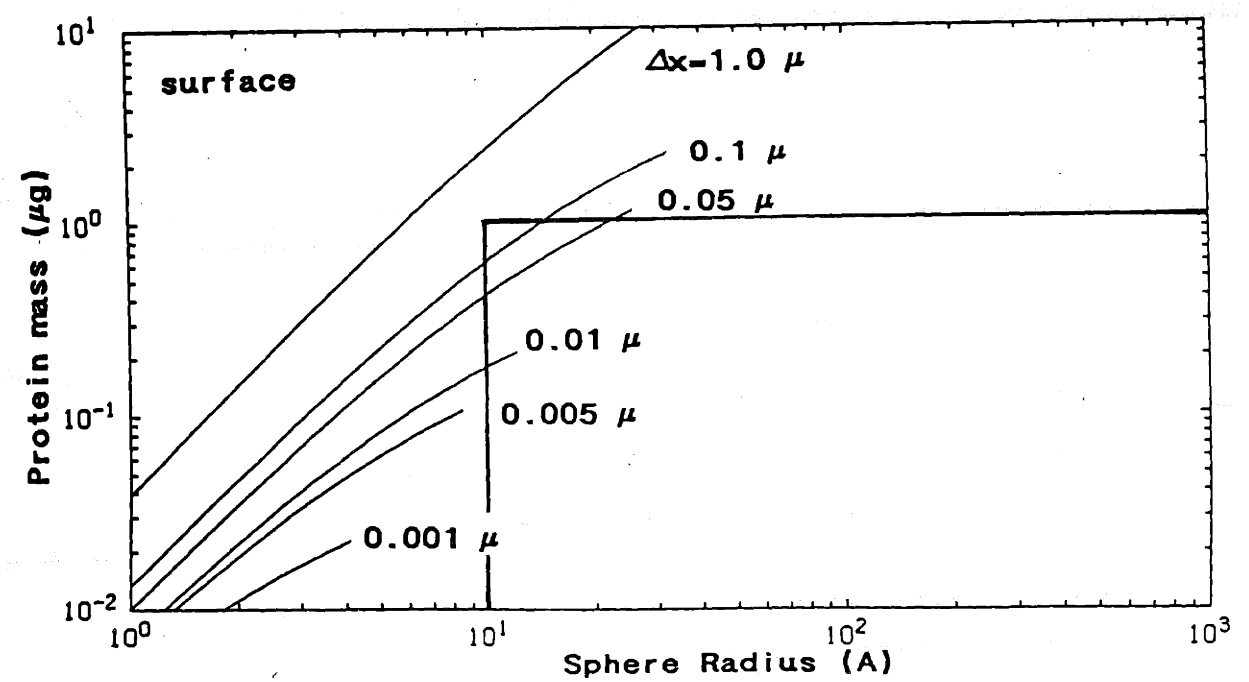

> 550 A) or onto the filter surface (mean layer thickness probably betweeen 50 and 500 A).

Dependence on Pore Diameter

We now use the results of this section to analyse the perfusion data for 0.4 and 0.6 μ polycarbonate filters. As shown in Figure 4.22 and summarized in Table 5.1, steady state normalized resistance drops off very sharply with filter pore size. Considering first in-pore protein adsorption, it is of interest to ascertain if the mean normalized filter resistances of Table 5.1 are consistent with a single value of adsorbed layer thickness and gel permeability. To test this possibility, Figure 5.3 was used to plot the gel permeability required to cause the tabulated degree of blockage for the 0.2, 0.4 and 0.6 μ filters as a function of gel layer thickness, Δ. There was no common point of intersection (or even close approach) for the three K_{gel} vs. Δ curves, leading to the conclusion that perfusion data on 0.2, 0.4 and 0.6 μ polycarbonate filters is inconsistent with the formation of a constant thickness, constant permeability adsorbed layer within the pore. If we restrict attention to 0.4 and 0.6 μ filters alone, the data of Table 5.1 are approximately consistent with the formation of an essentially impermeable layer of thickness $\Delta \simeq 375$ A or of a layer of permeability $K_{gel} \simeq 8 \times 10^{-12}$ cm^2 and $\Delta \simeq 700$ A. The measured steady-state resistance of a 0.2 μ filter is much larger than these scenarios would predict, and one might therefore postulate that secondary effects enhance the blocking of 0.2 μ filters. The most likely possibility is that incoming protein is "trapped" in a network of existing adsorbed material, which would require the adsorbed layer to fill a large fraction of the pore in a 0.2 μ membrane. For the case of an impermeable 375 A thick

layer this condition is not satisfied, while a 700 A thick layer in the 0.4 and 0.6 μ filters would also be expected to trap some protein. The permeability of the 700 A thick layer is such that the gel carries an appreciable fraction of the flow, and hence protein trapping (and concomitant decreased gel permeability) will lead to an increase in steady-state normalized resistance above the values reported in Table 5.1. Thus, such a secondary effect does not appear to explain the data.

We now attempt to reconcile the data of Figure 4.22 with the formation of an adsorbed layer on the filter surface. We first calculate the resistance (per pore) of a uniform surface layer which accounts for the observed increase in normalized resistance. This quantity, tabulated in column 4 of Table 5.1, is given by

$$R_{\text{per pore}} = (\text{normalized resist} - 1)\, R_{bl}\, N \qquad (5.4.5)$$

where R_{bl} is the appropriate filter baseline resistance and N is the total number of pores in the filter. In (5.4.5) multiplication by N converts the resistance of the entire surface layer ($-\Delta p/Q$) to the resistance of that portion of the layer corresponding to a single pore, $R_{\text{per pore}}$ ($-\Delta p/q$). From Table 5.1 it can be seen that $R_{\text{per pore}}$ varies over 3 orders of magnitude, which is far too large to be accounted for by a uniform thickness layer of constant permeability. It is also impossible to match the data to the theoretical predictions of the gel cap model for any single value of gel hemisphere radius $R_{gel} \geq 3600$ A (and constant permeability), and thus we conclude that the variation in steady-state resistance with pore size cannot be accounted for by a surface coating of constant permeability and constant mean thickness.

Nominal Pore Dia (μ)	Actual Pore Radius (A)	Steady-State Normalized Resistance	$R_{per\ pore}$ (g/cm^4s)	Hole Radius R_h (A)
0.2	1300	16.2 ± 6.8	1.29×10^{16}	130
0.4	2500	1.9 ± 0.3	5.37×10^{13}	790
0.6	3600	1.6 ± 0.4	8.28×10^{12}	1480

Table 5.1 Measured and calculated values pertaining to blockage of 0.2, 0.4 and 0.6 μ (nominal) polycarbonate membranes. Steady-state normalized resistances (column 3) are means ± standard deviations of values shown in Figure 4.22. See text for discussion of last two columns.

One possible explanation of the data in Table 5.1 is that the elements making up a surface layer are not large enough to completely span the pore mouth of the larger pore diameter membranes, so that at steady state the surface of these filters is covered by a surface layer interrupted by holes of radius R_h, each hole overlying a pore. To test this possibility, the radius R_h needed to account for the resistance $R_{per\ pore}$ of Table 5.1 was calculated from equation (2.5.4) (corresponding to an infinitely thin layer). These values, displayed in column 5 of Table 5.1, are roughly consistent with the above scenario if the blocking material is able to span the first 1900 A inward from the pore mouth boundary, i.e. for $R_o - R_h \simeq 1900$ A. In this case the surface coating on 0.2 μ filters is continuous and its resistance depends on the gel layer permeability. Note also that the time scale for blockage of 0.2 μ filters will be the same as that for complete formation of a filter cake, while for the case of 0.4 and 0.6 μ filters blocking will reach steady state once the adsorbed filter cake is essentially impermeable compared to the holes of radius R_h. This will occur when the filter cake layer is only partially formed, and thus this model is qualitatively consistent with the variation in r with membrane pore radius seen in Figure

4.21. Hence, one possible explanation of the variation in steady state resistance and τ with filter pore diameter is the above discontinuous filter cake model. However, it is not intuitively clear how a thin discontinuous layer of this type would maintain its structural integrity, and hence this model is somewhat less than satisfactory. In short, we have not been able to completely explain the perfusion data for 0.2, 0.4 and 0.6 μ filters, a point which will be further discussed in Section 6.3.

5.5 In-pore Blockage

In this section we attempt to model the dynamics of filter obstruction, which we expect will depend on the kinetics of protein adsorption onto the membrane. In the more general context the model describes the trans-filter transport of any material which is able to bind to (react with) the filter and thus impede fluid flow. We consider only a single reactive species (see below) having concentration c_o, and in this section treat only the binding of this species to the pore walls within the filter (in-pore blockage).

Although an attempt has been made to keep the presentation as general as possible, ultimately we wish to compare the predictions of the model with the blockage of filters by calf aqueous. It is therefore useful to present several properties of 0.2 μ polycarbonate membranes (lot E) of interest for modelling studies, as well as the values of mean pore velocity, Peclet and Reynolds numbers appropriate for perfusions at 40 μl/min. The flow is very clearly creeping (Re $<<$ 1), while the Peclet number based on pore length, Pe_L, is sufficiently large to ensure convection-

dominated transport. In Table 5.2 the (free solution) diffusion coefficient for the blocking protein has been taken as $D = 5 \times 10^{-7}$ cm^2/s. This value is appropriate for a globular protein of molecular weight ~ 80,000 daltons, and may be compared with values for other globular proteins such as ribonuclease (MW = 13,700, $D = 11.9 \times 10^{-7}$ cm^2/s), serum albumin (MW = 67,000, $D = 5.9 \times 10^{-7}$ cm^2/s) and urease (MW = 480,000, $D = 3.5 \times 10^{-7}$ cm^2/s) or rod-shaped proteins such as fibrinogen (MW = 330,000 $D = 2 \times 10^{-7}$ cm^2/s) (Tanford, 1961). Based on the above values it is expected that choosing $D = 5 \times 10^{-7}$ cm^2/s will be correct within a factor of three, which will be sufficient for present purposes. Unless otherwise noted, the values in Table 5.2 will be used in modelling verification.

Parameter	Value
pore radius	$R_o = 0.13\ \mu$
pore length	$L_o = 10.7\ \mu$
pore volume	$0.12\ \mu l_2$
pore wall area	18.6 cm^2
porosity	$\epsilon = 0.16$
Diffusion coefficient	$D = 5 \times 10^{-7}$ cm^2/s
mean pore velocity	$U = 5.9 \times 10^{-3}$ cm/s
Reynolds number	$Re = UR_o/\nu = 8.6 \times 10^{-6}$
radial Peclet number	$Pe_{Ro} = UR_o/D = 0.15$
axial Peclet number	$Pe_L = UL/D = 13$

Table 5.2 Parameters used in modelling transport through 0.2 μ polycarbonate membranes (lot E) at 40 μl/min. Membrane characteristics are derived from Table 4.1

Formulation of Dynamic Adsorption Model

For modelling purposes it is necessary to have a description of adsorption kinetics. In the absence of a known isotherm for the adsorbing species in aqueous and for generality we have simply assumed that binding proceeds by a Langmuir-like process, i.e. that

$$\frac{d\Gamma}{dt} = k_1 c\Gamma_\infty \left(1 - \frac{\Gamma}{\Gamma_\infty}\right) - k_2\Gamma \qquad (2.4.2)$$

Recall that Γ is the mass of protein adsorbed per unit area, while Γ_∞ is the maximal (plateau) amount adsorbed at plateau concentrations $c \gg k_2/k_1$. We wish to further restrict our attention to the dilute solution form of (2.4.2), i.e. the situation in which $c_o \ll$ the plateau concentration. As discussed in Section 2.4, a typical value for a plateau concentration is 500 μg/ml, although there is clearly substantial variability in this figure (Table 2.2). It seems likely that the concentration c_o of the blocking species in calf aqueous is less than 500 μg/ml, since the total aqueous protein content is 600 to 1000 μg/ml, and thus the dilute solution approximation is most probably valid. When this approximation applies we have $\Gamma \ll \Gamma_\infty$ and thus may rewrite (2.4.2) as

$$\frac{d\Gamma}{dt} = k_1 c\Gamma_\infty - k_2\Gamma \qquad (5.5.1)$$

which corresponds to the linear portion of the adsorption isotherm in the neighbourhood of the origin (Figure 2.3).

For the case of calf aqueous blockage of polycarbonate filters, equation (5.5.1) is clearly a simplification, for several reasons: (i) it is not clear that protein adsorption need follow Langmuir kinetics, nor is it absolutely certain that we are operating in the low concentration regime, and (ii) experimental results point to a two component binding process. Equation (5.5.1) should therefore be viewed as a model equation describing the binding of the rate-limiting species in the binding process, which has several desirable characteristics, such as simplicity, an increasing degree of binding with increasing concentration c, and saturability at a given concentration (see below). Generally speaking, in the absence of more detailed information about binding kinetics it is hoped that equation (5.5.1) will incorporate sufficient realism to provide some insight into the blocking process.

For <u>constant</u> concentration c_o (5.5.1) has solution

$$\frac{\Gamma}{\Gamma_{max}} = 1 - \exp(k_2 t) \qquad (5.5.2)$$

where the maximum (<u>not</u> plateau) binding at concentration c_o, Γ_{max}, is given by

$$\Gamma_{max} = \frac{k_1 c_o \Gamma_\infty}{k_2} \qquad (5.5.3)$$

Equations (5.5.2) and (5.5.3) clearly show the saturability of the binding process at constant concentration and the dependence of bound amount on concentration, c_o.

Turning now to the transport of the reactive species within the pore, we wish to determine whether adsorption to

the pore wall or radial diffusive transport is the rate limiting step in the binding process. From (5.5.2) the characteristic time for Γ to increase to Γ_{max} is $1/k_2$. It is convenient to obtain a characteristic reaction time scale, τ_{rxn}, defined as the time required for the bulk solution to be depleted of protein due to adsorption to the pore wall. This parameter can be obtained by multiplying the characteristic time for a protein coating of density Γ_{max} to be adsorbed to the pore wall ($1/k_2$) by the ratio of the protein mass in single pore to the protein mass adsorbed to the pore wall at density Γ_{max}, viz.

$$\tau_{rxn} \sim \frac{1}{k_2} \frac{\text{protein mass in pore}}{\text{adsorbed protein mass}}$$

$$\sim \frac{1}{k_2} \frac{c_o \pi R_o^2 L}{\Gamma_{max} 2\pi R_o L} \sim \frac{R_o}{k_1 \Gamma_\infty} \qquad (5.5.4)$$

Comparing this to the characteristic radial diffusion time $\tau_{diff} = R_o^2/D$ yields the Damkohler number

$$Da = \frac{\tau_{diff}}{\tau_{rxn}} = \frac{k_1 \Gamma_\infty R_o}{D} \qquad (5.5.5)$$

In this study we limit our attention to the regime in which $Da \ll 1$, so that diffusion is very fast compared to adsorption, and the binding process is rate-limited by adsorption kinetics. From Table 2.3 we expect values of $k_1\Gamma_\infty$ on the order of 10^{-5} cm/s, so that for the particular case of calf aqueous blockage of 0.2 μ polycarbonate filters Da is 10^{-3} to 10^{-4}, and diffusion is not rate-limiting. However, due to uncertainty in the value of $k_1\Gamma_\infty$ we briefly

consider the possibility of diffusion-limited transport, in which case we have a laminar, fully developed flow (over most of the pore length) with diffusion limited radial mass transfer to an initially bare pore wall. This is simply the mass transfer analogue of the classical Graetz problem, in which case the mean concentration decays over an axial length scale

$$\Lambda_{diff} = \frac{R_o^2 U}{D} = U \tau_{diff} \qquad (5.5.6)$$

where U is the mean fluid velocity (Jakob, 1949). For the particular case of calf aqueous perfusion at 40 μl/min through 0.2 μ polycarbonate membranes $\Lambda_{diff} = 1.99 \times 10^{-2}$ μ, so that the ratio of pore length to depletion distance $L/\Lambda_{diff} = 530$. This implies that from the pore mouth inward the concentration will be essentially constant at c_o (corresponding to a fully "coated" wall) until some axial position where the concentration will fall rapidly to zero (over the length Λ_{diff}). Stated alternately, the time scale for protein binding is much less than the residence time within the pore, so that blockage is rate limited by the rate of delivery of protein into the pore. Physically, this corresponds to the interface betweeen the "coated" (upstream) and bare (downstream) fractions of the pore moving axially down the pore at constant velocity $\sim c_o R_o U/\Gamma_{max}$, and implies that (i) blocking will proceed essentially as a linear function of time, and (ii) no blocking material will pass through the filter until blocking is nearly complete. Both implications are contradictory to the experimental observations of Chapter Four, supporting the contention that binding within the pore is not diffusion-limited in the case of calf aqueous perfusions.

We therefore idealize transport within the pore to be totally adsorption rate limited, so that the concentration profile may be considered uniform at any cross-section. In this case conservation of mass takes the simple form

$$\frac{\partial c}{\partial t} + U \frac{\partial c}{\partial x} = - \frac{2}{R_o} \frac{\partial \Gamma}{\partial t} \qquad (5.5.8)$$

where c and Γ are functions of x and t only and the mean velocity U is a constant for constant flow perfusion. Equations (5.5.8) and (5.5.1) together describe the binding of protein to the pore wall. The appropriate boundary and initial conditions are

$$\begin{aligned} &\text{b.c.:} \quad c = c_o \text{ at } x = 0 \text{ (constant pore mouth concentration)} \\ &\text{i.c.:} \quad c = c_o \text{ at } t = 0 \\ &\qquad\quad \Gamma = \Gamma_i \text{ at } t = 0 \end{aligned} \qquad (5.5.9)$$

where in the second boundary condition we have allowed the pore wall to be partially coated prior to perfusion. This corresponds to the adsorption which may occur while the filter (in the holder) is exposed to aqueous immediately prior to perfusion.

Non-dimensionalizing (5.5.1) and (5.5.8) according to

$$\begin{aligned} &\tau = k_2 t \ , \ \hat{x} = x/\Lambda \\ &\hat{c} = c/c_o, \quad \gamma = \Gamma/\Gamma_{max} \end{aligned} \qquad (5.5.10)$$

yields

$$\frac{\partial \gamma}{\partial \tau} = \hat{c} - \gamma \qquad (5.5.11)$$

$$\left[\frac{\Lambda k_2}{U}\right] \frac{\partial \hat{c}}{\partial \tau} + \frac{\partial \hat{c}}{\partial \hat{x}} = -\frac{\partial \gamma}{\partial \tau} \qquad (5.5.12)$$

We have chosen Λ to be the axial length scale over which the bulk fluid is depleted of protein, defined as

$$\Lambda = \tau_{rxn}\, U = \frac{U\, R_o c_o}{2k_2 \Gamma_{max}} \qquad (5.5.13)$$

It is of interest to estimate the magnitude of Λ for the case of calf aqueous perfusions. Just as for the case of diffusion limited transport, we conclude that Λ is not much less than L, since this would imply a linear rate of blockage and no protein passsage until complete obstruction. On the other hand, for $\Lambda \gg L$ the protein concentration within the pore is essentially indepedent of axial position, and the rate of blockage is solely a function of adsorption rate, i.e. is independent of velocity. This contradicts experimental results indicating that blockage rate scales with flow rate (Figure 4.10). Thus, if the in-pore blocking model as we have decribed it is correct, we require $\Lambda \sim L$.

Turning now to the ratio $\Lambda k_2/U$ which appears in (5.5.12), we see from (5.5.13) that

$$\frac{\Lambda k_2}{U} = \frac{R_o c_o}{2\Gamma_{max}} = \frac{\text{protein mass in a single pore}}{\text{protein mass adsorbed to pore wall}} \qquad (5.5.14)$$

(see (5.5.4)). If this quantity is $\ll 1$ we may ignore the first term in (5.5.12) and solve the quasi-steady equation

$$\frac{\partial \hat{c}}{\partial \hat{x}} = \frac{\partial \gamma}{\partial \tau} \qquad (5.5.12a)$$

In the case of calf aqueous perfusions $\Lambda k_2/U$ may be estimated by noting that Γ_{max} = adsorbed protein mass/pore wall filter area and by taking adsorbed mass to range between 0.1 and 1.0 μg (Figure 5.10). Consistent with our low concentration regime assumption we estimate $c_o \sim 25$ $\mu g/ml$ to obtain $\Lambda k_2/U \sim 0.003$ to 0.03, i.e. $<< 1$, so that the approximation (5.5.12a) is valid.

The solution of (5.5.11) and (5.5.12a) with the normalized boundary conditions

$$\begin{aligned} \hat{c} &= 1 \quad \text{at } \hat{x} = 0 \\ \gamma - \gamma_i &= \frac{\Gamma_i}{\Gamma_{max}} \quad \text{at } \tau = 0 \end{aligned} \qquad (5.5.9a)$$

is obtained by Laplace transform techniques as

$$\begin{aligned} \frac{\gamma - \gamma_i}{1 - \gamma_i} &= e^{-\hat{x}} \int_0^{\tau} e^{-\omega} I_o[2(\hat{x}\omega)^{1/2}]\, d\omega \\ \frac{\hat{c} - \gamma_i}{1 - \gamma_i} &= \frac{\gamma - \gamma_i}{1 - \gamma_i} + e^{-(\hat{x}+\tau)} I_o[2(\hat{x}\tau)^{1/2}] \end{aligned} \qquad (5.5.15)$$

where I_o is the modified Bessel function of the first kind. Note than an initial condition for $\hat{c}$ is no longer required since the $\partial \hat{c}/\partial \tau$ term in (5.5.12) has been dropped. Equations (5.5.15) describe the concentration and coverage

profiles within the pore. Recall that in deriving these expressions we have assumed that: (i) adsorption kinetics are decribed by the dilute regime Langmuir expression (5.5.1), (ii) binding is totally adsorption-rate limited (Da << 1), and (iii) the concentration distribution in the pore is quasi-steady ($\Lambda k_2/U << 1$). In using the latter assumption to ignore the first term in (5.5.12) and thus write (5.5.12a) we have assumed that $\partial\hat{c}/\partial\tau$, $\partial\hat{c}/\partial\hat{x}$ and $\partial\gamma/\partial\tau$ are all of order one, which may now be directly verified by differentiation of (5.5.15). Doing so confirms that the above derivatives are of order one, and that $\partial\hat{c}/\partial\tau$ will be bounded by $\partial\hat{c}/\partial\hat{x}$ and $\partial\gamma/\partial\tau$ except in the limit as τ becomes small while $\tau\hat{x}$ becomes large. Since in this study $\hat{x}$ is of order 1 to 10 this limit never arises, and thus the quasi-steady equation (5.5.12a) is valid.

The solution (5.5.15) has the expected limiting form as τ approaches ∞, namely γ and $\hat{\theta}$ approaching one. In addition, for small times or small axial distances ($\tau\hat{x} << 1$)

$$\frac{\gamma - \gamma_i}{1 - \gamma_i} \simeq e^{-\hat{x}}(1 + \hat{x})(1 - e^{-\tau}) \qquad (5.5.16)$$

while for large times or far from the pore mouth ($\tau\hat{x} >> 1$)

$$\frac{\gamma - \gamma_i}{1 - \gamma_i} \simeq 0.5[1 - \mathrm{erf}(\sqrt{\hat{x}} - \sqrt{\tau})] \qquad (5.5.17)$$

The latter approximation has the form of a coverage profile travelling at constant velocity whose axial breadth increases as $\sqrt{\hat{x}}$, and corresponds to the case $\Lambda << L$.

In Figure 5.12 representative profiles of the fractional pore wall coverage $(\gamma - \gamma_1)/(1 - \gamma_1)$ are plotted as a function of dimensionless axial position within the pore for various dimensionless times τ. Recall that on this plot the pore exit has dimensionless position

$$\hat{L} = \frac{L}{\Delta} = \frac{2Lk_1\Gamma_\infty}{UR_o} \qquad (5.5.18)$$

and thus the dimensionless pore length increases as the adsorption rate $k_1\Gamma_\infty$ grows. One convenient measure of the time scale for filter blockage is the dimensionless time τ_{50}, defined as the time required for the fractional pore wall coverage at the pore exit $\hat{L}$ to reach 50%. In Figure 5.13 this quantity is plotted as a function of $\hat{L}$, as are the approximate limiting relationships for large and small $\hat{L}$ derived from (5.5.16) and (5.5.17). For $\hat{L} << 1$ the blocking time is independent of pore length, while for large values of $\hat{L}$, $\tau_{50} \sim \hat{L}$, as expected.

Formulation of Filter Bocking Model

Now that we have a dynamic description of protein adsorption onto the filter pore wall we may employ the results of Section 5.2 to model dynamic filter blocking. To relate the amount of bound protein Γ to a solid fraction within the adsorbed layer (and hence a permeability) we use

$$\phi = \frac{\Gamma}{\Delta}\bar{v} \qquad (5.5.19)$$

which assumes that bound material forms a homogeneous layer of constant thickness Δ. The assumption of constant Δ

Figure 5.12 Plot of fractional wall coverage $(\gamma-\gamma_1)/(1-\gamma_1)$ as a function of dimensionless axial position $\hat{x}$ for various dimensionless times τ.

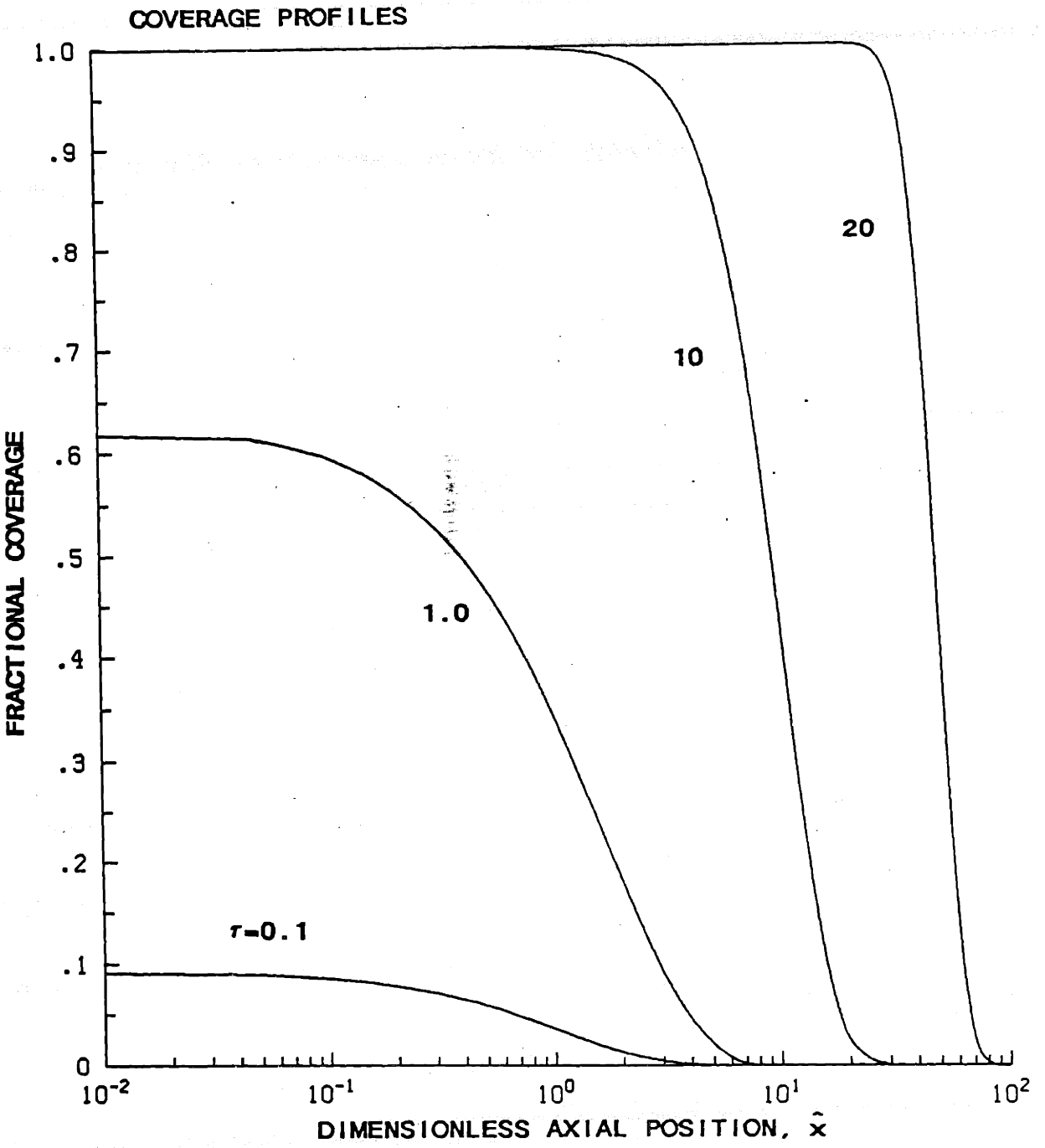

Figure 5.13 Plot of the characteristic blocking time τ_{50} as a function of the dimensionless pore length $\hat{L}$. See text for definition of τ_{50}. Circles: results of model; solid lines: approximate relations derived from asymptotic relations for $\hat{L} \ll 1$ ($\tau_{50} = 0.69$) and $\hat{L} \gg 1$ ($\tau_{50} = x$).

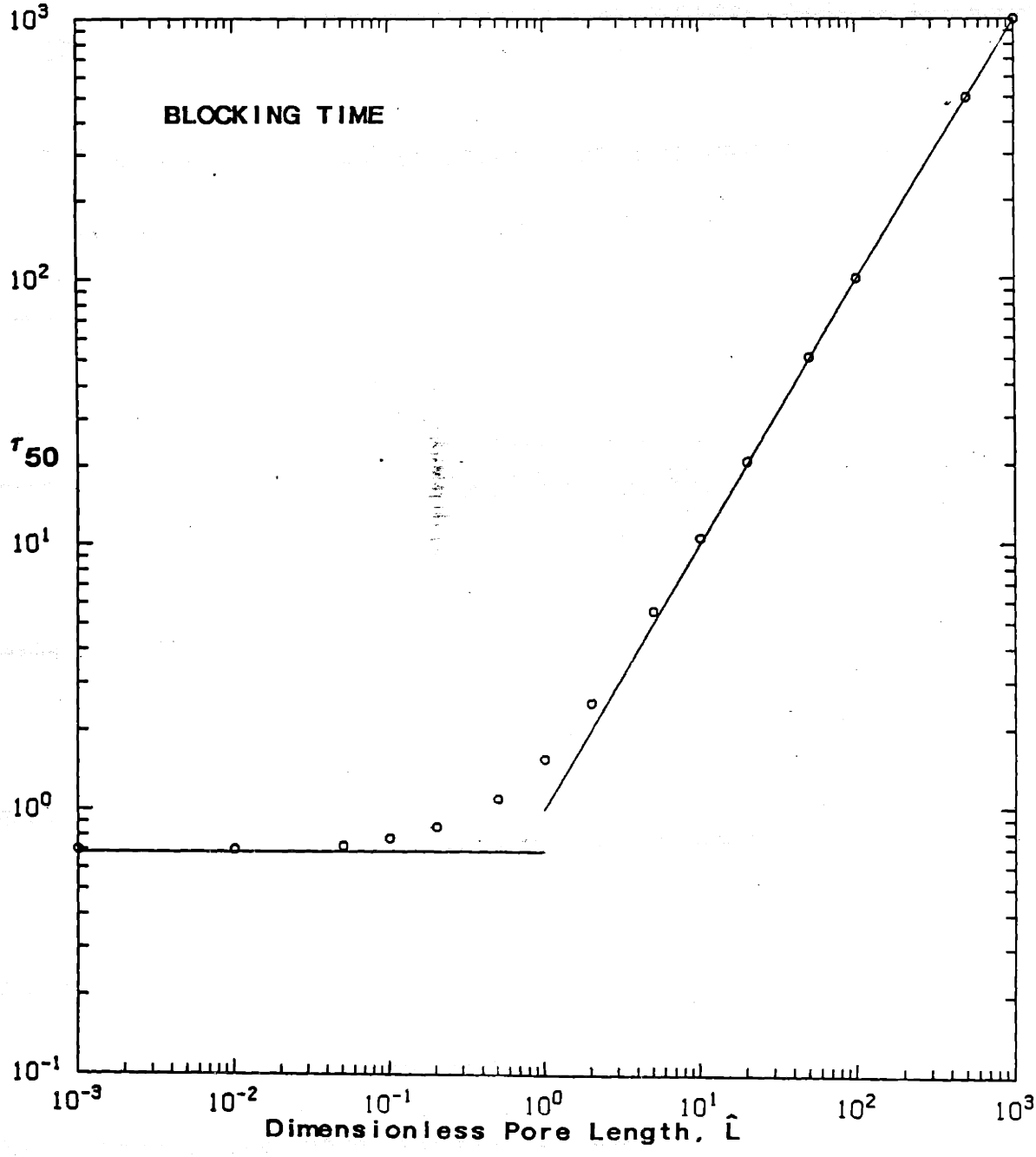

presumes that the blocking protein has dimension Δ in its adsorbed state, and the effect of more adsorption is simply to "fill in" the layer. This is in distinction to the scenario in which Δ grows with time, corresponding to multilayer adsorption. Since multilayer adorbtion is less common than monolayer coverage (Section 2.4) and it is not clear that multilayer formation will ever reach a steady state, the assumption of constant Δ seems more plausible for our particular study.

Calculation of filter resistance is accomplished by a computer model which uses the analytical expressions (5.2.14) or (5.2.15), (5.4.2), (5.5.15) and (5.5.19) to calculate the net permeability as a function of position and time, and which then numerically integrates $1/K_{net}$ along the pore length (equation (5.2.18)) to calculate overall pore resistance as a function of time. The amount of protein passing through the pore as a function of time is also calculated, and this quantity may be used as the upstream "input" for a second simulation, corresponding to a double filter perfusion. The computer model accepts as input 11 parameters, five of which are known *a priori* (pore radius, R_o, pore length, L, mean in-pore fluid velocity, U, protein specific volume, $\bar{v}$ and filter pore wall area) and six of which are adjustable (initial fractional coverage, γ_1, protein fibre radius, a, adsorbed layer thickness, Δ, desorbtion rate constant, k_2, adsorbtion rate constant, $k_1\Gamma_\infty$ and bulk concentration c_o).

Application to Calf Aqueous Data

We now wish to utilize the above model in an attempt to simulate the blocking of filters by calf aqueous. Our goal is to duplicate the results of the following five "test" experiments on 0.2 μ polycarbonate filters:

1. Perfusions at 9 and 40 μl/min (Figure 4.9),
2. Perfusions of pure and diluted calf aqueous (Figure 4.10),
3. Perfusions of aqueous preperfused in a large batch (Figure 4.27 (a)),
4. Perfusions of aqueous preperfused in small batches and then pooled (Figure 4.27 (b)),
5. Perfusion of aqueous through two in-line filters (Figure 4.28).

In all simulations adjustable parameters were constrained so as to ensure total adsorbed protein mass (at steady state) was less than 1 μg.

Ideally, a single set of adjustable model parameters would match the experimental data of these five test cases. However, in practice such a match was not possible. For example, the data of Figure 4.9, indicating that filter blockage scales linearly with flowrate, suggest that $\tau_{50} \sim 1/U \sim \hat{L}$, which from Figure 5.13 implies that $\hat{L} \geq 2$. On the other hand, in the regime $\hat{L} \geq 2$ blockage is a near linear function of time, in contrast to the data of Figure 4.10 (b). Note also that in the dilute regime of the adsorption isotherm we expect that Γ_{max} and hence filter steady state resistance will be a sensitive function of c_o, i.e. will vary with extent of dilution. Although this behavior is observed in Figure 4.10 (b), it is noticably absent from Figure 4.10 (a). Thus, we conclude that the data of Figure 4.10 (a) are fundamentally inconsistent with our model, and more generally, that the entire body of experimental data cannot be fitted by our model using a single set of parameters.

The failure of the model to fit all of the test cases with a single set of adjustable parameters can in part be

understood by noting that these experiments were performed with different batches of aqueous, i.e. each test was done on a different day. Given the variability of the aqueous batches from day to day, some degree of variation in input paramters (e.g. bulk blocking protein concentration, c_o) is to be expected. We have therefore adopted the approach of simulating experimental behavior by selecting adjustable parameters on a case by case basis so as to best fit the test data, while maintaining as small a variation in selected values as possible. In particular, in all cases γ_i was chosen between 0.01 and 0.05, protein fibre radius a was chosen as 3.5 A (corresponding to a fully denatured chain) and adsorbed layer thickness Δ was chosen as 800 A, except in the case of Figure 5.16, where it was chosen to be 850 A. The values of the other adjustable parameters and corresponding values of $\hat{L}$ and total protein mass used to generate the simulations shown in Figures 5.13 through 5.17 are shown in Table 5.3. The values of k_2 and $k_1\Gamma_\infty$ are consistent with reported values (Tables 2.3 and 2.4), the range of variability being approximately a factor of ten. The values of bulk protein concentration vary between 0.7 and 4 μg/ml, which seems quite reasonable in light of the observed inter-batch variability in total aqueous protein content.

Turning now to specific test cases, Figure 5.14 shows the predicted (panel (a)) and actual (panel (b)) results of perfusions from the same batch of aqueous at 9 and 40 μl/min, the match between theory and experiment being quite good. Figure 5.15 shows simulated (panel (a)) and experimental (panel (b)) perfusions of pure and diluted (9% and 50%) aqueous on 0.2 μ polycarbonate membranes. In this case the model correctly describes the qualitative trends in the experimental data, but it fails to exactly match the steady state resistance and time constant of the diluted

Figure 5.14 Theoretical predictions (panel (a)) and experimental data (panel (b)) for aqueous perfusion at 9 μl/min (dotted lines) and 40 μl/min (solid lines) on 0.2 μ polycarbonate membranes. Panel (b) is a replot of Figure 4.9 (a).

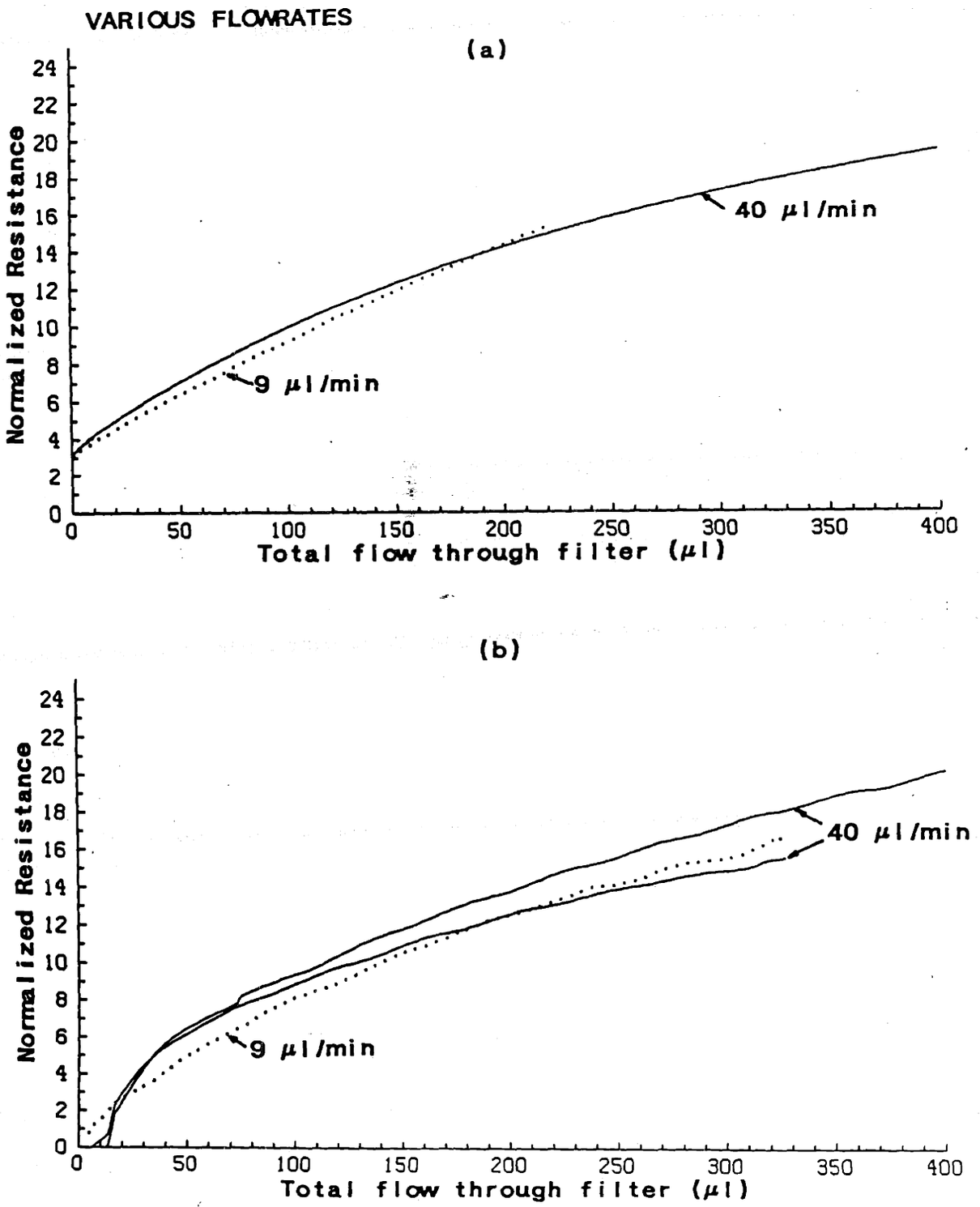

Figure 5.15 Theoretical predictions (panel (a)) and experimental data (panel (b)) for perfusion of pure and diluted aqueous at 40 μl/min on 0.2 μ polycarbonate membranes. Panel (b) is a replot of Figure 4.10 (b). Numbers on curves are fraction of aqueous in sample. Abscissa is perfused volume times aqueous fraction in sample.

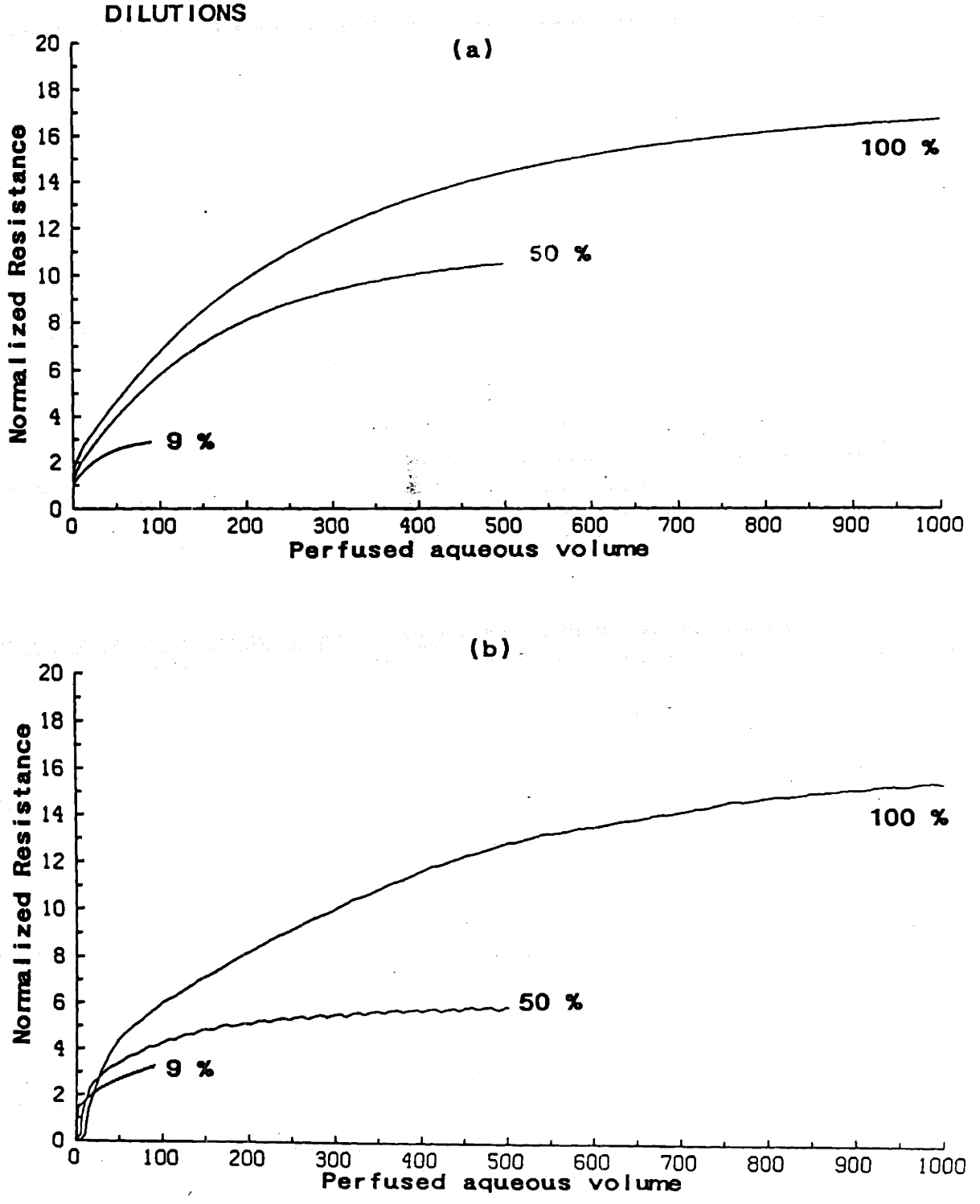

aqueous runs. The model completely fails (for any range of parameters with adsorbed mass < 1 μg) to simulate the dilution data of Figure 4.10 (a). As described above, this is due to the dependence of steady state resistance on c_o which is implicit in the dilute regime form of the adsorption isotherm.

	Figure 5.14	Figure 5.15	Figure 5.16	Figure 5.17	Figure 5.18
c_o (μg/ml)	2.0	4.0	0.7	3.0	1.2
k_2 (s^{-1})	$3x10^{-3}$	$2x10^{-3}$	$2x10^{-4}$	$7x10^{-3}$	$5x10^{-3}$
$k_1\Gamma_\infty$ (cm/s)	$8x10^{-5}$	$1.2x10^{-5}$	$1.2x10^{-5}$	$1.2x10^{-4}$	$1.6x10^{-4}$
$\hat{L}$	2.2	0.34	0.34	3.4	4.5
mass (μg)	0.99	0.45	0.78	0.96	0.71

Table 5.3 Values of the adjustable parameters c_o, k_2 and $k_1\Gamma_\infty$ used as input to the in-pore blocking model to generate Figure 5.14 through 5.18. The corresponding values of dimensionless pore length $\hat{L}$ and adsorbed protein mass are also shown.

Panel (a) of Figures 5.16 and 5.17 shows simulated results for perfusion of aqueous collected from a large (Figure 5.16) and small (Figure 5.17) volume preperfusion, while panel (b) of each figure shows the corresponding experimental data. The agreement between model and experiment for the case of large volume preperfusion (Figure 5.16) is quite good, while the agreement in Figure 5.17 is somewhat poorer (underprediction of initial perfusion resistance). However, in the latter case the model is once again qualitatively correct.

Figure 5.16 Theoretical predictions (panel (a)) and experimental data (panel (b)) for perfusion of aqueous which has been preperfused in a large batch (1.1 ml). Solid lines: preperfusion on 0.2 μ polycarbonate filter at 40 μl/min, dashed lines: second pass through 0.2 μ polycarbonate filters at 40 μl/min. Panel (b) is a replot of Figure 4.27 (a).

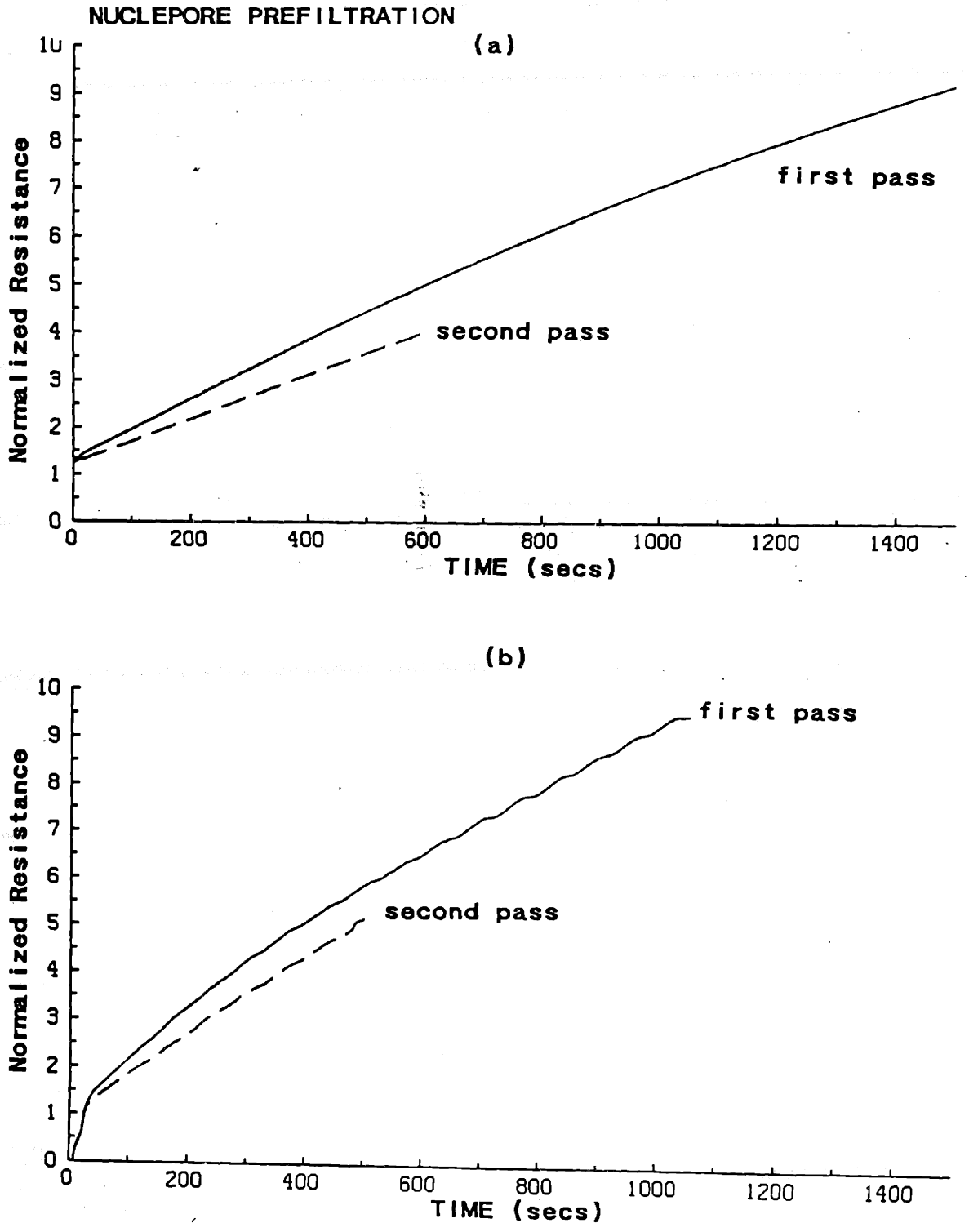

Figure 5.17 Theoretical predictions (panel (a)) and experimental data (panel (b)) for perfusion of aqueous which has been preperfused in small batches (0.2 ml) and pooled. Solid lines: preperfusion on 0.2 μ polycarbonate filter at 40 μl/min, dashed lines: second pass through 0.2 μ polycarbonate filters at 40 μl/min. Panel (b) is a replot of Figure 4.27 (b).

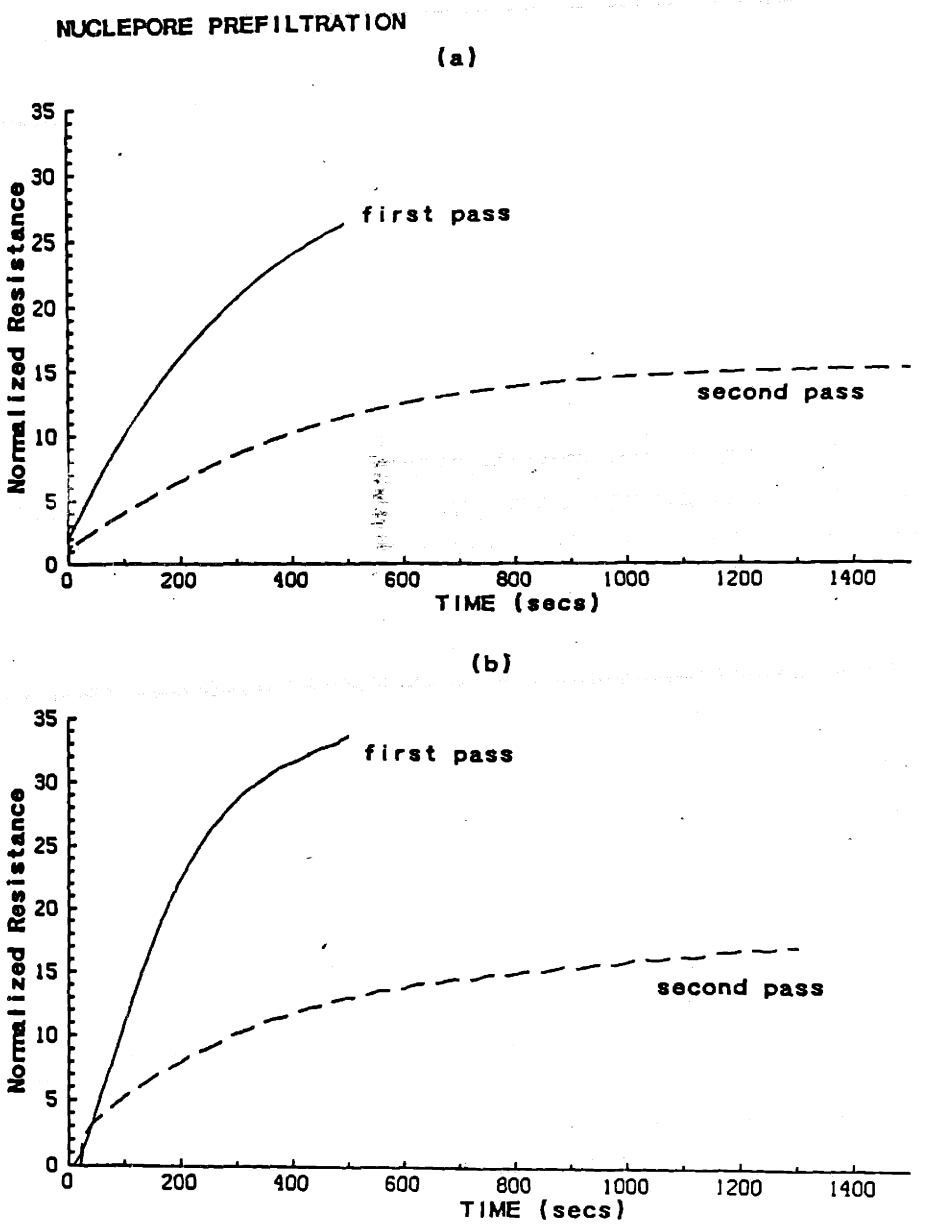

Finally, in Figure 5.18 (a) the model predictions for a double filter perfusion are shown, while Figure 5.18 (b) displays the corresponding experimental data replotted from Figure 4.28. In replotting the data of Figure 4.28 it is necessary to have some knowledge of the flowfield in the void space between the two filters, as this will determine the distribution of aqueous reaching the downstream filter face at any instant. The void space geometry is that of a cylinder (flow-wise length ~ radius) bounded by two originally identical filters. If the aqueous distribution reaching the downstream filter is such that one portion of the filter begins blocking more quickly than the remaining portions, the flow will shift away from the blocked region, producing a more uniform blockage over the entire filter area. If as a rough approximation we assume that mixing in the void space is small and that most of the aqueous leaving the upstream filter reaches the downstream filter at approximately the same time, then the effect of the void space is to simply introduce a time lag given by the void space volume divided by the flow rate (=570 seconds for our particular conditions). Thus, in Figure 5.17 (b) time zero for the downstream filter resistance trace has been taken as 570 seconds in the original data (Figure 4.28). This is clearly a very approximate treatment, but for present purposes it has been judged sufficient. Comparing the experiment and theory, qualitative agreement is seen to be quite good, although the model slightly underpredicts the resistance of the downstream filter.

In overview, the dynamic in-pore blocking model accurately predicts the qualitative trends of the experimental test cases (with the exception of the dilution data of Figure 4.10 (a)), although its quantitative performance is somewhat poorer. Given the complexity of the blocking process and the approximate nature of the model, the overall agreement can be judged as fair.

Figure 5.18 Theoretical predictions (panel (a)) and experimental data (panel (b)) for double filter perfusion on 0.2 μ polycarbonate membranes. Panel (b) is a replot of Figure 4.28 (see text).

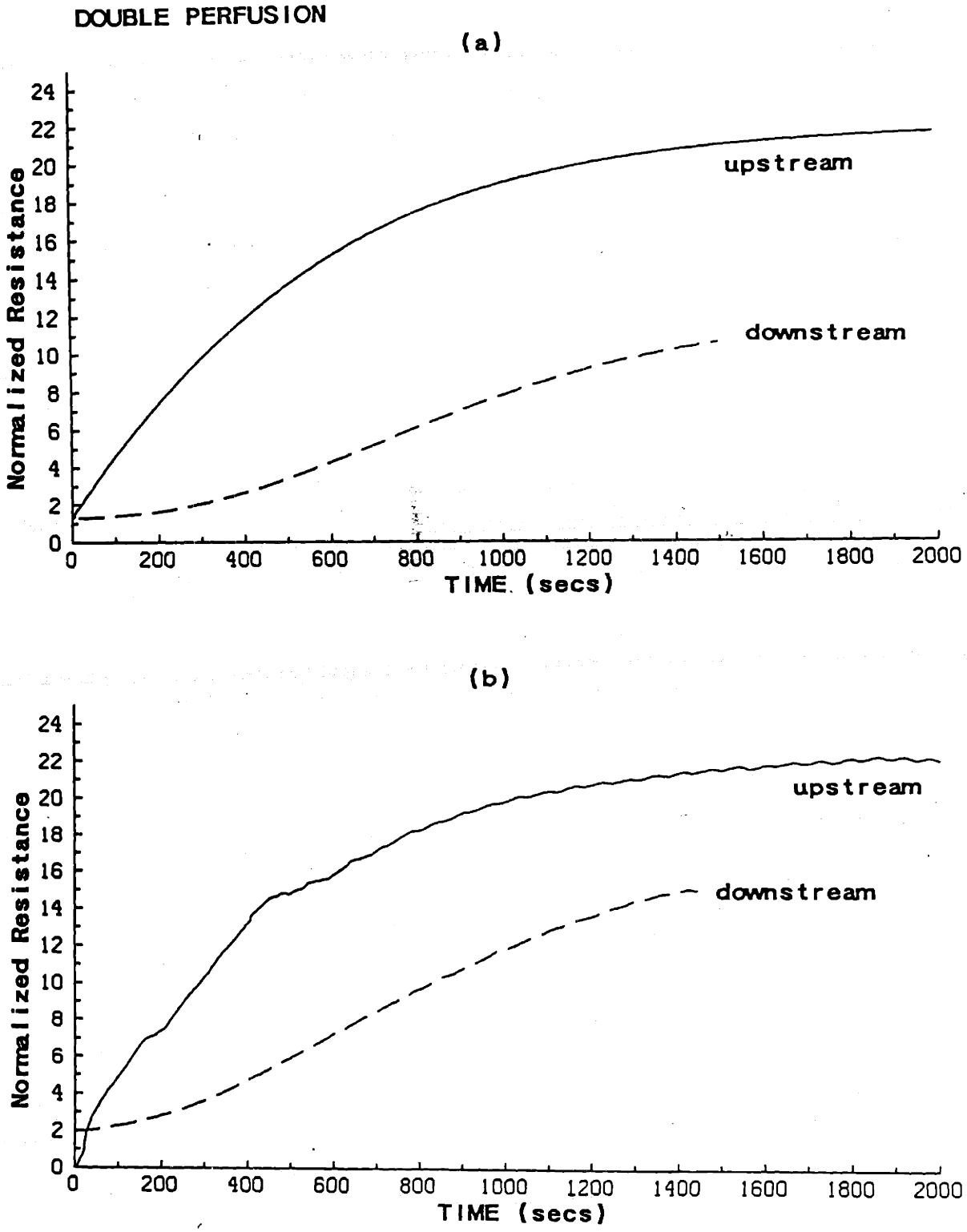

It remains to consider the implications of requiring different values of c_o, k_2, and $k_1\Gamma_\infty$ to accurately fit the data. We begin by determining the sensitivity of the model predictions to variations in these parameters. In general terms $k_1\Gamma_\infty$ controls the dimensionless pore length $\hat{L}$ (see (5.5.18)) and influences Γ_{max}, k_2 influences Γ_{max} and the characteristic blocking time, and c_o influences Γ_{max}. Empirically, it has been found that the model is sensitive to changes by a factor of five or larger in each of these parameters. This has been explored in Figure 5.19, which shows the results of three separate simulations of the large volume preperfusion experiment of Figure 5.16 in which the parameters k_2, $k_1\Gamma_\infty$ and c_o have been varied by a factor of five from the values reported in Table 5.3. As can be seen by comparing Figures 5.19 and 5.16 (a), 5-fold changes in k_2 and $k_1\Gamma_\infty$ produce appreciable alterations in the simulated resistance traces, confirming the earlier statement that the five test experiments cannot be fit by a single set of adjustable parameters.

Of the variations in $k_1\Gamma_\infty$, k_2 and c_o which are necessary to fit the experimental data, most troubling are those in k_2 and $k_1\Gamma_\infty$, since (as previously discussed) the variation in c_o does not seem unreasonable. One possible explanation for the required variability in k_2 and $k_1\Gamma_\infty$ is inter-filter differences in surface properties (e.g. PVP-coating). However, it seems unlikely that the relatively large variations of Table 5.3 can be completely explained in this manner. A second possible explanation is that protein properties vary from batch to batch. One possible mechanism whereby such variablity could arise is the existence of two (or more) populations of binding proteins, each of which has different values of k_2 and $k_1\Gamma_\infty$. The "effective" value of k_2 and $k_1\Gamma_\infty$ (as given by Table 5.3) then represents a weighted average of the appropriate individual population

Figure 5.19 Effects of varying k_2, $k_1\Gamma_\infty$ and c_o on simulated filter blockage for first and second pass aqueous. Conditions were as for the simulations of Figure 5.16 (a) except for the differences noted below. (a) Effects of a 5-fold increase in k_2 (to 1×10^{-3} s^{-1}), with attendant reduction in m to 0.16 μg. (b) Effects of a 5-fold increase in $k_1\Gamma_\infty$ (to 6×10^{-5} cm/s) and a 5-fold reduction in c_o (to 0.14 μg/ml), with attendant increase in $\hat{L}$ to 1.7.

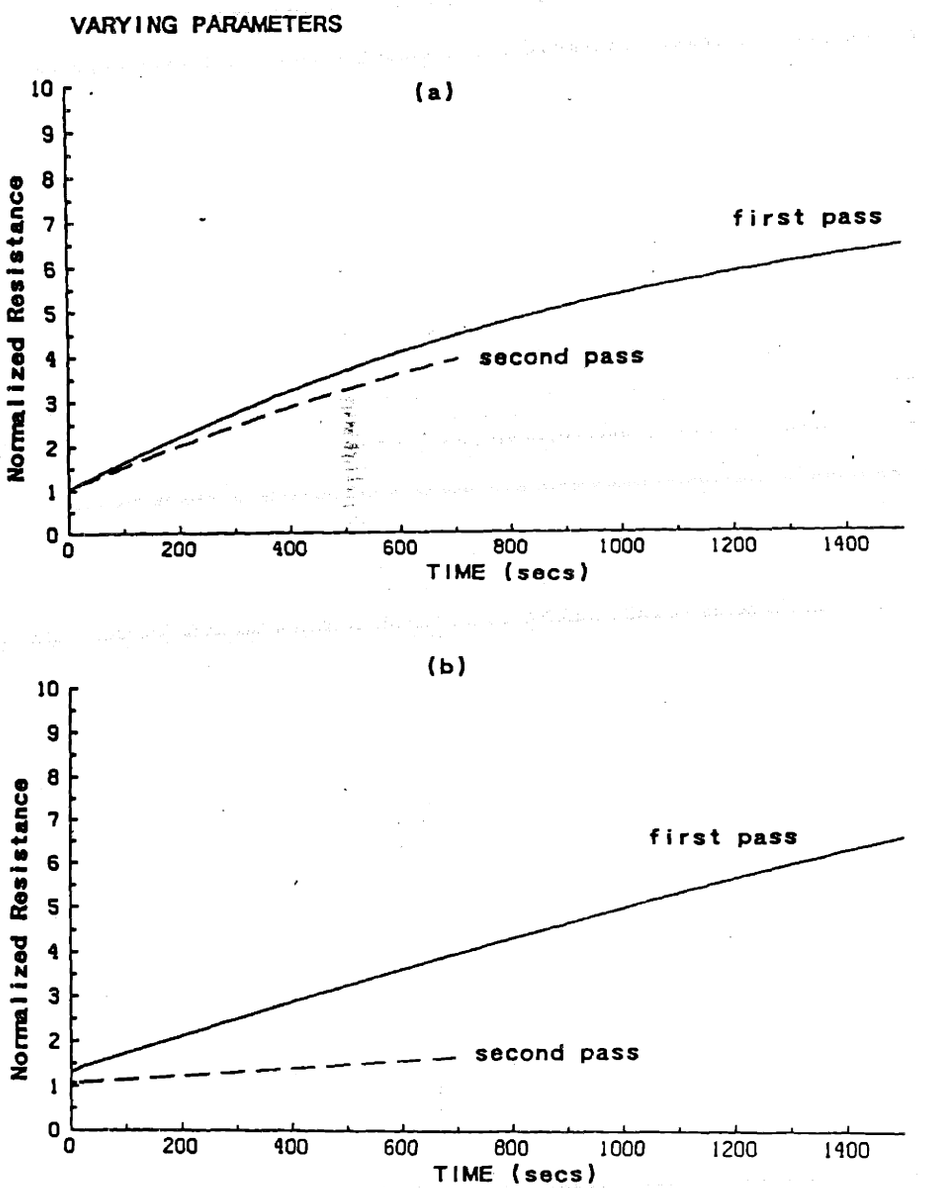

values, and variations arise due to changes in the relative fraction of each population in a given batch of aqueous. There is some experimental evidence to indicate that aqueous does in fact contain multiple populations of adsorbing species (see Section 6.2), and thus this explanation seems possible. Hoewever, such speculations are impossible to experimentally verify without a specific assay for each individual blocking component, and thus the most which can be reasonably concluded is that the dynamic in-pore blocking model is not inconsistent with the bulk of the experimental data.

5.6 Filter Face Blockage

In this section we consider the dynamics of filter blocking under the assumption that the blocking material adheres to the upstream filter surface to produce a filter cake layer. Only monolayer adsorption is considered, so that the model is appropriate for describing the formation of a very thin, uniform thickness cake, rather than, say, a gel hemisphere. Since adsorption is limited to the filter material, pore entrance occlusion will only occur when the dimensions of the adsorbing substance are larger than the pore diameter. If this is not the case a continuous surface layer interrupted by holes will be formed, as discussed in Section 5.4. Thus, relating adsorbed mass to the extent of filter blockage will generally require some knowledge of blocking material dimensions.

Because the flowfield upstream of the filter is somewhat more complex than that within the pore, a

reasonably rigorous model for filter blockage is more involved than the model of Section 5.5. Given the uncertainties about the basic nature of the blocking process, it was felt that an approximate treatment was most appropriate, and we therefore restrict this discussion to a highly simplified model of the protein deposition process.

With reference to Figure 5.20 and by analogy with Section 5.5, three basic processes can be identified: (i) convective delivery of protein to the filter face, (ii) diffusional transport upstream of the filter, and (iii) protein adsorption to the filter surface. Intuitively we expect that the streamlines in the vicinity of the pore mouth will have the form sketched in Figure 5.20, and thus a mass transfer boundary layer having characteristic thickness δx at the pore mouth will develop along the filter surface (dashed line). If the flowfield within the boundary layer is such that streamlines are nearly parallel to the filter surface, δx will scale with

$$\delta x \sim \left[\frac{D\, R_1}{U_{sup}}\right]^{1/2} \qquad (5.6.1)$$

where we have assumed that the fluid velocity within the boundary layer scales with the superficial velocity U_{sup}.

If δx as given by (5.6.1) is greater than R_1, the mean interpore spacing, we expect that the streamlines within the mass transfer boundary layer will have an appreciable component normal to the filter surface. In this case (5.6.1) is an upper bound for δx, since the incoming flow will act to compress the boundary layer. The thickness δx may be compared with the depletion layer dimension δ_D

$$\delta_D = \frac{\Gamma_{max}}{c_o} = \frac{k_1\, \Gamma_\infty}{k_2} \qquad (5.6.2)$$

Figure 5.20 Geometry of control volume used in integral mass balance derivation of upstream filter blocking model, showing sketch of streamlines and concentration boundary layer.

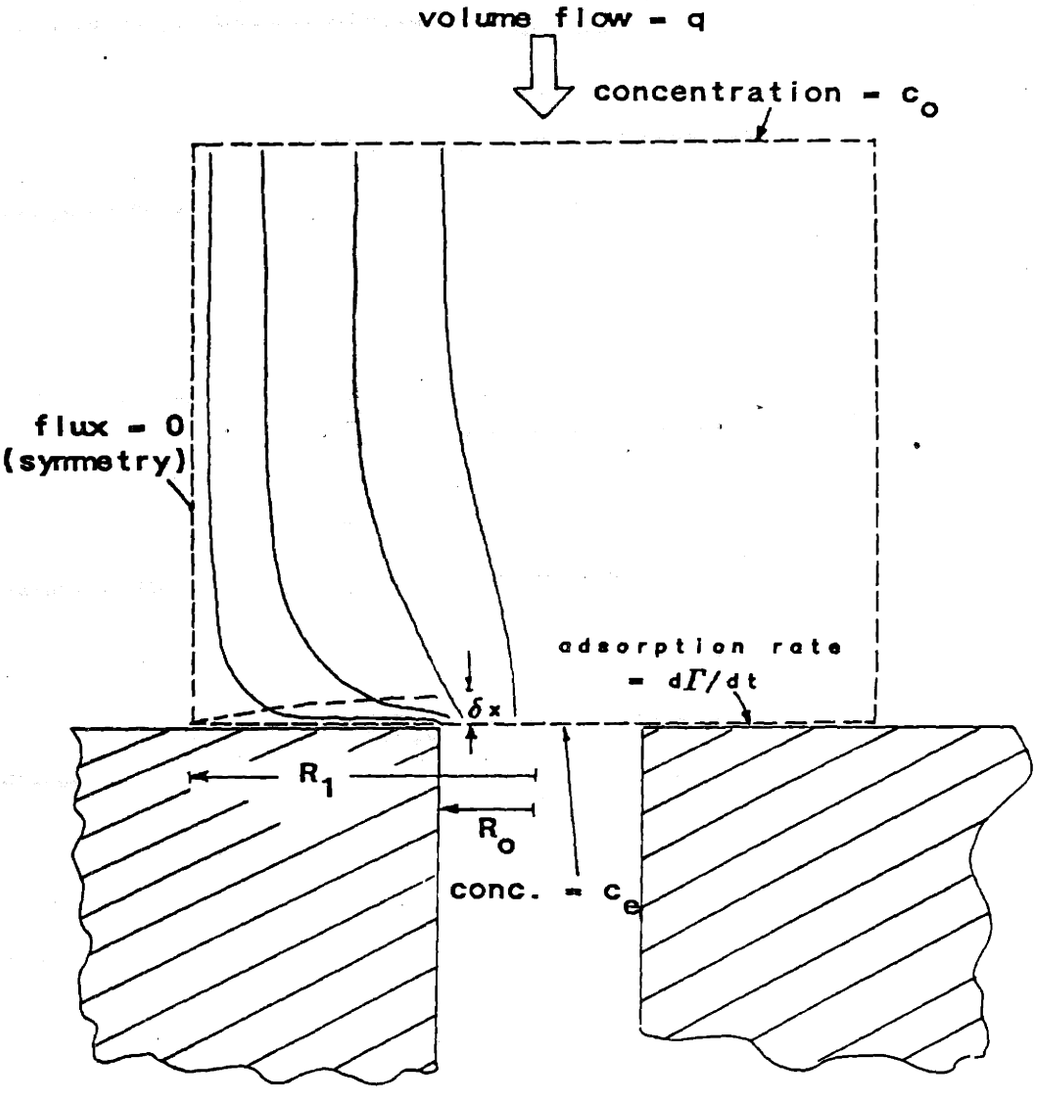

which is the thickness of a quiescent fluid layer adjacent to the filter surface which will be depleted of protein due to adsorption to the filter. If δx is much less than δ_D we expect that transport to the filter surface will be controlled by the concentration boundary layer.

For the particular case of calf aqueous perfusions on 0.2 μ polycarbonate membranes at 40 μl/min, equation (5.6.1) yields $\delta x \sim 1.3\ \mu$, which is larger than the mean interpore spacing $R_1 = 0.33\ \mu$. Thus, we expect the actual thickness δx to be less than $1.3\ \mu$. Computing the depletion layer thickness is more difficult, but to obtain a lower bound we once again set Γ_{max} = adsorbed protein mass/filter area = $0.5\ \mu g/(18.6 + 1.42)cm^2 = 2.5 \times 10^{-2}\ \mu g/cm^2$, and take $c_o \simeq 25\ \mu g/ml$ to obtain $\delta_D \sim 10\ \mu$. Thus, we have $\delta x < \delta_D$, so that the effective dimension for diffusional mass transfer to the surface is δx. By using $\delta x = 1.3\ \mu$ and assuming that $k_1\Gamma_\infty \sim 10^{-5}$ cm/s (Table 2.3) we may now compute an upper bound for the Damkohler number

$$Da = \frac{k_1\ \Gamma_\infty\ \delta x}{D} \qquad (5.6.3)$$

as 3×10^{-3}. Since $Da << 1$ we conclude that diffusional transport to the filter surface is not rate-limiting for calf aqueous perfusions, and thus we may idealize the adsorption process to be adsorption rate-limited.

In order to maintain generality, and in recognition of the fact that our above estimate for Da was based on a number of parameters for which precise numerical values are unknown and could therefore be in error, we characterize the adsorption process by an overall mass transfer coefficient h, defined by

$$h = \frac{d\Gamma/dt}{c}\bigg|_{\Gamma=0} \qquad (5.6.4)$$

where c is the bulk solution protein concentration at distance δx from the surface. In the case of reaction-limited transport where equation (5.5.1) is valid we have $h = k_1\Gamma_\infty$, while for diffusion-limited transport we have $h \sim D/\delta x$. By analogy with (5.5.1) we then assume that adsorption kinetics are given by

$$\frac{d\Gamma}{dt} = h\,c - k_2\,\Gamma \qquad (5.6.5)$$

We may now employ (5.6.5) to obtain an approximate overall protein mass balance. With reference to Figure 5.20, a quasi-steady integral balance yields

$$\pi(R_1^2 - R_0^2)\,\frac{\overline{d\Gamma}}{dt} = q(c_0 - c_e) \qquad (5.6.6)$$

where c_e is the mean concentration entering the pore mouth and the overbar denotes an average taken over the solid filter area. Defining the area-averaged mass transfer coefficient $\bar{h}$ by $\overline{hc} = \bar{h}\cdot\bar{c}$ allows us to rewrite (5.6.5) as

$$\frac{\overline{d\Gamma}}{dt} = \frac{d\bar{\Gamma}}{dt} = \bar{h}\,\bar{c} - k_2\,\bar{\Gamma} \qquad (5.6.7)$$

If we can assume that $\bar{h}$ is independent of time (for example if $h = k_1\Gamma_\infty$) we then obtain the governing equations (5.6.6) and (5.6.7) in dimensionless form as

$$\frac{d\bar{\gamma}}{d\tau} = \frac{U_{sup}}{\bar{h}(1 - \epsilon)} (1 - \hat{c}_e) \qquad (5.6.8)$$

$$\frac{d\bar{\gamma}}{d\tau} = \frac{\bar{c}}{c_o} - \bar{\gamma} \qquad (5.6.9)$$

where the dimensionless time τ and the dimensionless variables $\hat{c}_e$ and $\bar{\gamma}$ are given by

$$\tau = k_2 t$$

$$\hat{c}_e = c_e/c_o \qquad (5.6.10)$$

$$\bar{\gamma} = \bar{\Gamma}/\Gamma_{max}, \quad \Gamma_{max} = \bar{h}c_o/k_2$$

It remains to relate the area averaged concentration $\bar{c}$ to the exit concentration c_e, for which we arbitrarily choose the particularly simple relationship

$$\bar{c} = \frac{c_e + c_o}{2} \qquad (5.6.11)$$

and hence rewrite the dimensionless adsorption equation (5.6.9) as

$$\frac{d\bar{\gamma}}{d\tau} = \frac{1}{2} (1 + \hat{c}_e) - \bar{\gamma} \qquad (5.6.12)$$

With the initial condition $\bar{\gamma}(t=0) = \bar{\gamma}_i$ the system (5.6.8) and (5.6.12) has solution

$$\frac{1 - \bar{\gamma}}{1 - \bar{\gamma}_i} = e^{-\tau/\beta} \tag{5.6.13}$$

$$\frac{1 - \hat{c}}{1 - \bar{\gamma}_i} = \frac{2(\beta-1)}{\beta} e^{-\tau/\beta} \tag{5.6.14}$$

where

$$\beta = 1 + \frac{\bar{h}(1 - \epsilon)}{2U_{sup}} \tag{5.6.15}$$

The parameter β measures the relative rates of convective supply and adsorption to the surface, and for large and small values of the ratio $U_{sup}/\bar{h}$, β tends towards the limits 1 and $\bar{h}(1-\epsilon)/2U_{sup}$, respectively. The former case corresponds to mass transfer-limited adsorption (oversupply of convected protein) and in this case the value of τ_{50} (dimensionless time required for the area-averaged fractional coverage to reach 50%) is simply 0.69, independent of U. In the limit of small $U_{sup}/\bar{h}$, protein binding is limited by the convective delivery rate, and τ_{50} scales with $\bar{h}/2U_{sup}$. These two limiting cases are analogues of the situations $\hat{L} \ll 1$ and $\hat{L} \gg 1$ (respectively) of the in-pore blockage model. Examining the dependence of $\hat{c}$ on β, we note that for large $U_{sup}/\bar{h}$ (β approaching one) $\hat{c} \simeq 1$. This corresponds to the case in which a large excess of protein reaches the filter surface and only a small amount is adsorbed. In the opposite limit of small $U_{sup}/\bar{h}$ we have $\hat{c}$ increasing from $2\bar{\gamma}_i - 1$ at time zero to 1 for large τ. In summary, the general aspects of the above model are quite

similar to those of the in-pore model of Section 5.5, in that filter blockage falls into either an adsorption rate- or protein delivery rate-limited regime. In the former case blockage is essentially independent of flowrate and a large amount of protein successfully passes through the filter, while in the second case the converse is true.

Comparison with Experiments

Due to the simplicity of the above model it was felt that only a brief comparison with calf aqueous perfusion data was warranted. One particularly simple comparison is to determine whether the time scale for filter blockage is consistent with that predicted by equation (5.6.13), assuming that the adsorbed material completely occludes the pore mouth. For this purpose we have chosen as a test perfusion the 100 % curve in Figure 5.15 (b), which has a fitted exponential time scale of 580 seconds (r=0.9996). From (5.6.13) the blocking time scale is given by β/k_2, so that

$$\frac{1}{k_2}\left[1 + \frac{k_1\Gamma_\infty\,(1-\epsilon)}{2U_{sup}}\right] = 580 \text{ seconds} \qquad (5.6.16)$$

where we have set $\bar{h} = k_1\Gamma_\infty$. In this equation ϵ and U_{sup} are known, and thus we have one equation for two unknowns, one of which may be eliminated by assuming a value for $k_1\Gamma_\infty/k_2 = \Gamma_{max}/c_o = m/(A\cdot c_o)$. Choosing $m = 0.5\ \mu g$, $A=0.71\ cm^2$ and $c_o=10\ \mu g/ml$ then yields $k_2 = 1.82 \times 10^{-4}$ cm/s and $k_1\Gamma_\infty = 1.3 \times 10^{-4}$ cm/s, both of which are within the expected range (Tables 2.3 and 2.4). Hence, the surface adsorption model is not inconsistent with the experimental data.

CHAPTER SIX: DISCUSSION

6.1 Some Basic Observations on Filter Blockage

In this chapter we attempt to interpret the experimental and modelling studies previously presented, and hence draw conclusions about the nature of the filter blocking process and its relevance to the physiology of the eye. This task is made difficult by the lack of definitive identification of the blocking component(s) in aqueous humor, and thus in some instances the discussion is necessarily speculative.

In review, the experimental data regarding filter blockage by calf aqueous paint a picture of some complexity, which perhaps is to be expected given the multi-component character of aqueous and the involuted nature of protein adsorption onto artificial surfaces (Section 2.4). The picture is further complicated by the variability which has characterized our experiments, both between batches of aqueous and between tests from the same batch (see Section 6.3). This variability is especially puzzling in light of the fact that tested aqueous samples were pooled batches from many animals, so that inter-animal variability should have been reduced. The complexity of the blocking process is also substantiated by the failure of simple modelling studies to completely mimic experimentally observed behavior.

In light of the above discussion, it is perhaps useful at this point to enumerate those conclusions which are fairly well-established before proceeding to discuss some of the less clear-cut aspects of the study. We note therefore that:

(i) Calf aqueous consistently and repeatedly blocks 0.2 μ polycarbonate membranes, confirming the initial report of Johnson et al. (1986).

(ii) The blockage is strikingly specific to aqueous, especially in light of the failure of freshly collected calf plasma and serum, and "mock aqueous" to obstruct 0.2 μ filters.

(iii) The blocking process involves at least two components, one or both of which hydrophobically, and to a lesser extent ionically, bind to the filter surface. Both materials have molecular weights greater than 10 kdaltons, likely candidates being albumin and an as-yet unidentified protein of molecular weight 20-30 kdaltons and pI of 6-7.

(iv) Neither fibrinogen nor fibronectin are involved in the blocking process.

(v) Hyaluronic acid and other GAGs are involved in the blocking process in at most a secondary fashion.

(vi) Monkey and rabbit aqueous also block 0.2 μ filters, although to a lesser extent than does calf aqueous.

(vii) The blocking process is highly "efficient", in that a very small amount of protein leads to an appreciable filter blockage.

With these results in hand we proceed to discuss in more detail the nature of the filter blocking process.

6.2 The Nature of the Blocking Components in Calf Aqueous

Size

Based on the Centricon separation experiments we are assured that all blocking components have molecular weights greater than 10 kdaltons. An upper bound on the size of the blocking material may be obtained by estimating the dimensions of those macromolecules which will remain in solution after ultracentrifugation. Assuming a constant sedimentation coefficient, s, the time taken to precipitate a given material, t_{prec}, is given by

$$t_{prec} = \frac{\omega^2 s}{\ln(R_{max}/R_{min})} \qquad (6.2.1)$$

where ω is the rotor angular velocity and R_{max} (R_{min}) is the maximum (minimum) radial distance from the centre of rotation. Substituting t_{prec} = 1 hour and other appropriate values (Section 3.2) into (6.2.1) indicates that molecules having a sedimentation coefficient of $< 135 \times 10^{-13}$ sec will remain in solution, which corresponds to a spherical (globular) protein of molecular weight 7×10^6 (radius $\simeq 0.01\ \mu$). Estimating dimensions for rod-shaped proteins is more complicated, since s depends on both the rod length and diameter, but for reference it is noted that the tobacco mosaic virus molecule (MW = 50×10^6, dimensions 3000 x 150 A) has a sedimentation coefficient of 170×10^{-13} sec (Tanford, 1961). Thus, we conclude that although spherical (globular) proteins having dimensions comparable to the pore diameter of 0.2 μ filters will be removed by

ultracentrifugation, rod-shaped molecules of appreciable length will remain in solution.

It is of interest that ultracentrifugation seems to markedly reduce the blocking capacity of calf (but not monkey) aqueous, and to slightly decrease calf aqueous protein content (Figure 4.4). This raises the possibility that aqueous *in vivo* has a greater blocking capacity than suggested by our experiments. If the reduction in blocking capacity caused by ultracentrifugation is due to removal of the blocking proteins *per se* this would imply that these proteins are of quite high molecular weight. Alternately, ultracentrifugation could simply be removing particulate material which is capable of blocking the filter but which is normally absent from the aqueous humor *in situ*. A third possible explanation is that the binding of blocking material to the container walls which is thought to explain the "aging" effect (Section 4.3) could be occuring during the ultracentrifugation step as well.

No matter what size the blocking materials are in solution, once they adsorb to the filter surface they must have dimensions comparable to the pore radius to be effective in filter obstruction. There are three possibilities:

(i) blocking is due to long rod-shaped or random coiling macromolecules which remain in solution after sedimentation, consistent with the above discussion,

(ii) blocking is due to small globular molecules which denature upon adsorption to the filter, or

(iii) blocking is due to molecular aggregates which form either in solution or upon adsorption.

In Section 5.4 we concluded that the blocking material was most likely to have a fibrous shape when adsorbed to the filter. A molecular aggregate might be expected to have a more spherical shape, and thus we conclude that blocking is most probabaly due to large rod-shaped (or random coiling) molecules or small globular proteins which denature upon adsorption ((i) and (ii) above). Denaturation could be facilitated by shear stresses (Section 2.3), although previous work with albumin (Yavorsky, 1981) suggests that this occurs at wall shear stresses at least an order of magnitude greater than those used in this study.

The Two-component Process and Blocking Component Identity

Spiking studies with albumin and lens γ-crystallins have provided strong evidence that the blocking of 0.2 μ polycarbonate filters by calf aqueous involves two classes of materials, which we denote by "A" and "B". Since albumin enhances blocking and is normally present in calf aqueous at relatively high concentrations, it seems very likely that it plays a role in filter blockage. This is consistent with its appearance in fairly high levels on electrophoretograms of blocking material (but see also below). For definiteness we have assigned albumin to blocking class A. In the spiking experiments the increase in aqueous blocking capacity was less than proportional to the increase in albumin concentration, suggesting that albumin is not the limiting component in the blocking process. Hence, we postulate that substance B limits the blocking process.

Given that albumin is involved in blockage, it could play one of two possible roles: (i) it is the blocker (the material which actually inhibits flow), and thus most likely denatures upon adsorption. The role of component B is then to aid in the binding of albumin to the filter or to promote denaturation once bound (or both). Alternately, (ii) albumin is the cofactor (the material which aids in the action of the blocker) in which case component B is the blocker. We are presently unable to determine which role albumin plays.

Since the addition of lens γ-crystallins (at high concentrations) also enhanced blocking, while an albumin/crystallin mixture does not block filters, it appears that both albumin and γ-crystallin belong to class A, supporting the concept of a multi-component class of blocking materials. For example, class A could include all proteins having more than a certain number of hydrophobic binding sites.

Since low levels of lens protein, which are presumably present in normal aqueous at very low concentrations, had little effect on blocking, it seems likely that these proteins do not normally play a significant role in filter blockage. A second interesting observation concerning lens proteins is their higher effectiveness (relative to albumin) in enhancing blockage at a given spiking concentration. Since γ-crystallins are smaller than albumin this result would appear to rule out non-specific protein "trapping" by an existing macromolecule matrix as a blockage mechanism. Perhaps the greater effectiveness of the γ-crystallins is due to their hydrophobic character.

From experiments with proteases we are assured that at least one of the blocking components in calf aqueous is a protein. However, it is not necessary that both A and B be proteins, and thus it is possible that substance B is not a protein. For example, substance B could be a class of lipid or lipid-containing materials, which would accord with the hydrophobic nature of the blocking process. However, it will be seen that there currently exists a good candidate for substance B which is in fact a protein, and thus for the moment we set aside this possibility.

Although we have not definitively identified all materials which participate in the blocking process, we have eliminated four possible candidates: fibrinogen, fibronectin, ascorbate and GAGs. Fibrinogen and fibronectin (eliminated by ethanol precipitation experiments) were likely candidates because of their long rod-shaped configuration which seemed favorable for blocking, while ascorbate (eliminated because it has molecular weight < 10 kdaltons) was considered because its concentration in aqueous is strikingly high (70-fold greater than in plasma). GAGs were considered as possible blocking candidates because their extended random coil configuration is effective at impeding flow and favors these molecules lodging in pores. However, the results of the hyaluronidase experiments and experiments with GAG-containing mock aqueous suggest that GAGs do not play a role in filter blockage. The small decrease in resistivity seen upon incubation with hyaluronidase may be due to its protease activity (Knepper, 1984) or may simply be an aqueous "aging" effect.

Conclusions from Experiments with Plasma, Serum and Mock Aqueous

The lack of blocking seen with freshly collected diluted calf plasma and serum is consistent with observations that Nuclepore polycarbonate membranes have very low protein binding affinity (Hawker and Hawker, 1975; Nuclepore Tech. Bull. TB0985-1), and thus the fact that aqueous does block up such filters underlines the specificity of the blocking effect. If, as we have argued, albumin plays a role in the blocking process, the presence of large amounts of albumin in plasma and serum suggests that these fluids are missing the second component (substance B) necessary for blocking. Stated alternately, the distinguishing characteristic of aqueous is that it contains substance B, which, in the presence of albumin and other A components, confers blocking ability. This implies that contamination of a non-blocking solution (one which does not contain substance B) with blood will not produce blocking ability, while contamination of a blocking solution will increase the extent of blocking (by analogy with the albumin spiking experiments). Thus, we may conclude that the blocking capacity of aqueous is not a consequence of blood leakage into the the anterior chamber *post mortem*, although such an effect could increase the magnitude of the blocking.

In light of the above discussion, it is not surprising that "mock aqueous" was unable to block 0.2 μ filters. The materials used in preparing these solutions were blood-derived proteins (with the exception of the γ-crystallins and hyaluronic acid) and thus we conclude that these solutions lacked substance B.

One puzzling observation is that commercial serum strongly blocked 0.2 μ filters. One obvious difference between this solution and freshly collected serum is that the commercial preparation was frozen and rethawed, which is known to promote protein denaturation. Perhaps such denaturation exposed the proteins' hydrophobic cores and thus altered their affinity for the test membranes. Yet if this was the case, why then do frozen and unfrozen aqueous behave in a similar manner? This remains a puzzling and unexplained question. However, it seems most appropriate to compare the blocking capacity of calf aqueous (which is always unfrozen) with that of unfrozen serum and plasma, and thus we still conclude that the blocking phenomenon is aqueous-specific.

Interpretation of Chromatography and Electrophoresis Runs

One initially surprising result of FPLC and HPLC studies was the lack of any consistent difference between chromatographs of pre- and post-filtered aqueous. There are three possible explanations: (i) the protein removed by filtration represents such a small fraction of the total aqueous protein content that the the difference due to filtration is not resolvable, (ii) the blocking components were binding to the column material and never appear in the chromatogram, or (iii) the blocking component do not adsorb at 230 or 280 nm and thus were not visualized on the chromatogram. As discussed in Section 4.8, possibility (i) is consistent with the very small amout of protein found on the filters and is deemed to be the most plausible.

Interpretation of FPLC chromatograms of filter blocking material is difficult, in part due to the variability seen and in part due to the changes in aqueous

profile caused by ultrasound exposure. A third confounding factor in the interpretation of Figure 4.39 (b) is the possibility that the PVP surfactant was washed off the filter and altered the chromatogram. It is therefore concluded that a more sensitive and reliable method of identifying filter blocking components is 2-D gel electrophoresis.

Electrophoretograms of filter washing material indicate that certain proteins are preferentially adsorbed onto 0.2 μ PVP-free filters, as expected from the specificity of the blocking process. Of particular interest are the series of 5 spots identified in Figure 4.43, which are absent from calf serum and relatively concentrated in the blocking material. Because of these characteristics, this series of 5 spots are excellent candidates for substance B.

In interpreting electrophoretograms we have assumed that the large spot of molecular weight $\simeq$ 70 kdaltons and pI $\simeq$ 7 is albumin, which agrees well with the results of the albumin spiking experiments. However, this presumption should be checked, presumably by western blot transfer and immunoprobing. A second caveat concerning the electrophoretograms is that only proteins having pI values between approximately 4 and 8.5 are visualized. This need not represent the entire protein spectrum, and thus the possibility exists that proteins playing a role in the blocking process are not being visualized on these gels.

Resistance-Protein Correlation

Protein levels measured in this study were slightly higher than previously reported values for bovine aqueous humor (820 μg/ml *versus* 600 μg/ml). This could either be due to age differences or *post mortem* protein leakage into the aqueous. For further discussion of the latter possibility see Section 6.5.

In Section 4.3 it was noted that although aqueous protein level and resistivity are correlated, this correlation is characterized by a substantial degree of variability. This is consistent with the hypothesis that the limiting component in the blocking process is either not a protein or is present in such small quantities that it makes a negligible contribution to total protein content.

A second possible source of information on the correlation between protein levels and resistivity is the results of dilution experiments. However, as previouly noted, results from these tests are contradictory (e.g. Figure 4.10). One possible explanation of Figure 4.10 is that when blockage is independent of dilution the limiting component is present in excess (Figure 4.10 (a)), while in the case where blockage is sensitive to dilution the opposite is true (Figure 4.10 (b)). If this were the case, however, one would expect that in the former instance the extent of blockage would be greater than in the latter, which was the opposite of what was observed. This suggests that other factors, in addition to the concentration of substance B, are important for the blocking process.

6.3 The Nature of the Blocking Process

Protein/Filter Binding and Detergent Action

The data point to a direct hydrophobic association of protein with the filter surface, in agreement with previous studies indicating that proteins often bind hydrophobically to artificial surfaces (Section 2.4). The evidence leading to this conclusion is threefold: firstly, hydrophobic membranes block to a greater degree than do hydrophilic ones. Secondly, once membranes are blocked the resistive material cannot easily be washed away (e.g. by high flow postperfusion), and thirdly, surface-active agents (detergents) are effective in washing away resistance. The binding process is thought to be saturable, since binding efficiency decreases as perfused volume increases and most perfusions appear to reach steady state.

In addition to hydrophobic association, it appears that (at least on 0.2 μ polycarbonate filters) ionic effects play a role. This latter conclusion is supported by the observation that spermine preperfusion decreases (but not eliminates) aqueous blocking capability. Note however that spermine preperfusion appears to have no effect on polyester filters, suggesting that ionic effects play no role on these membranes, perhaps because membrane surface charge is less or of opposite sign. Thus, in general, it appears that ionic effects are secondary in nature, in accordance with the observation that postperfusion with 2 M salt solutions does not extensively disrupt the blocking.

The fact that binding is strongly dependent on surface hydrophobicity suggests that small variations in PVP coating on polycarbonate membranes can appreciably alter

filter blockage. However, no evidence is available on the variability of the this surfactant coating, and thus we merely speculate that this phenomenon may explain some of the observed variability. One possibility which we briefly considered is that aqueous blockage on PVP-free membranes occurs by a completely different mechanism than on regular filters. This is contradicted, however, by the fact that both aqueous and freshly collected serum exhibit the same qualitative behavior (blocking and no blocking, respectively) on regular and PVP-free filters. Thus, we conclude that the difference between the two membrane types is one of degree.

Protocol	Result
Triton-X followed by aqueous	very high filter blockage
Triton-X mixed with aqueous	no filter blockage
Aqueous followed by Triton-X	Triton washes away blockage

Table 6.1 Summary of experiments involving aqueous and 0.1 and 1.0 % Triton-X 100 on 0.2 μ polycarbonate filters.

As noted above, detergents have been found to be extremely effective in modifying the blocking behavior of aqueous. Table 6.1 summarizes the results of a series of experiments with Triton-X, which are interpreted as follows. Triton-X preperfusion acts to strip the PVP surfactant from the pore wall and thus render the pore hydrophobic and amenable to extensive blocking. This mechanism is consistent with the results of Bisio et al. (1980) who noted that Triton-X perfusion at concentrations below the critical micelle concentration (CMC) renders 0.2 μ polycarbonate filters more hydrophobic. (It is postulated that aqueous

perfusion washes preperfused Triton-X out of the pore and thus reduces the concentration below the CMC.) It is theorized that Triton-X mixed with aqueous binds to hydrophobic sites on the blocking protein and thus renders the protein less likely to bind to the filter. In a similar fashion, when Triton-X is perfused through a blocked filter it disrupts protein/filter interactions by competing for hydrophobic binding sites on both the protein and the filter. According to this theory, postperfusion with lower detergent concentrations is less effective in removing blocking (as experimentally observed) because at low detergent levels competition favors filter/protein interaction. The fact that some detergents are more effective than others may be due to the local architecture of the hydrophobic sites on the blocking proteins favoring certain detergents (e.g. non-ionic).

Regarding the structure of the adsorbed protein, in Section 5.5 it was argued that monolayer formation seems most likely, primarily because this is consistent with the approach to steady state seen experimentally. Two other possibilities for the mechanism by which blocking protein asssociates with the filter are: (i) multilayer formation in which binding affinity decreases with distance from the filter surface, and (ii) non-specific entanglement with existing adsorbed material. The latter possibility has been discussed in light of the albumin and γ-crystallin spiking experiments and deemed unlikely. The former option yields an adsorbed structure which can be operationally considered as a monolayer (assuming adsorption stops at some distance from the filter surface), and hence in all cases the adsorbed layer most probably has a finite thickness.

Surface vs. In-pore Blockage

A fundamental unresolved question is whether blockage occurs primarily within the filter pores or on the filter face. The fact that upstream stirring and scraping usually had little or no effect on filter resistance suggests that either blockage occurs within the pores or that blockage is due to a very tightly bound surface layer. If filter face blocking is occuring, the results of Section 5.4 indicate that the protein concentration in the cake is quite high (~ 0.1 g/ml), while the corresponding concentrations in the case of in-pore blockage are less, by approximately a factor of 50. This suggests (but does not prove) that in-pore blockage is the more likely mechanism.

The actual mechanism may involve a combination of both effects. In fact, since the surface chemistry of the filter face is the same as that of the pore walls, adsorption would be expected to occur onto both regions. Since the ratio of pore wall surface area to filter face area is approximately 13:1 for 0.2 μ polycarbonate membranes, we expect a greater adsorbed mass within the pores, all other factors being equal. Although it seems likely that this would translate into greater blocking, however, this need not necessarily be the case, depending on the structure of the adsorbed protein. Considering further the possibility of combined surface/in-pore blockage, it seems likely that events occuring within the pore will affect those happening on the surface, and vice versa. For example, formation of an adsorbed layer within the pore will presumably increase rejection of macromolecules and perhaps induce greater filter face adsorption. This linkage between in-pore and surface effects may explain the failure of the modelling to completely simulate dynamic blocking behavior.

Pore Geometry Effects

As previously discussed, one possible explanation for the variation in steady-state resistance and characteristic blocking time with pore diameter is the formation of a filter cake punctuated by holes which overlie pores. A second possibility is that the blocking of 0.2 μ filters is due to upstream trapping and subsequent filter face adsorption of long rod-shaped molecules which simply wash through the larger pore diameter membranes. However, this implies that little or no blocking material would successfully pass through 0.2 μ filters, and that albumin would play only a secondary role in the blockage of 0.2 μ filters (since it is not a long, rod-shaped molecule), in contradiction to observed behavior. A third possibility is that blockage of 0.2 μ filters involves secondary effects which do not occur on 0.4 and 0.6 μ membranes, although this effect was considered unlikely (Section 5.4). In short, the pore size dependence effect remains unresolved.

Considering perfusion data for 0.22 μ GVWP (hydrophilic) Millipore filters, it is interesting that these membranes do not block up even though they remove a large proportion of the blocking material in aqueous. This is most probably due to the fact that this membrane has a large number of highly interconnected pores of variable diameter, so that blockage of a smaller diameter section of pore has only a small effect on total membrane resistance. If this is the case, it suggests that the JCM (which has an architecture more akin to a Millipore than to a Nuclepore filter) would be difficult to block.

Presoaking Experiments

It is intersting that presoaking filters in calf aqueous inhibits later aqueous blockage, although this effect depends on membrane type. There are several possible explanations: (i) small molecules which can diffuse more quickly than the blocking components enter the membrane and bind to sites which would normally be occupied by the blocker, or (ii) the usual blocking proteins bind to the filter, but in the absence of shear they do not denature and thus firmly attach to the filter (age) so that they are able to sustain shearing forces. The first explanation is most consistent with the Centricon separation experiments showing that aqueous contains a blocking inhibitor of molecular weight < 10 kdaltons. Based on the above discussion, this inhibitory mechanism could be as simple as binding to and occupying sites normally used by the blocking components.

Insights from Modelling Studies

In modelling the transport of protein through filters we have clearly idealized and simplified a highly complex process. Nonetheless, the fact that the model is able to simulate many of the main trends in the experimental data indicates that it has incorporated several essential features of the blocking process. For example, the dynamic blocking model agrees well with our intuitive expectation that the transport of material through the filter will vary betweeen two limiting regimes depending on the ratio of the convective delivery rate to the adsorption rate. If this ratio is large then the filter is "oversupplied" with protein, blockage is independent of flowrate, and large amounts of protein pass through the filter, while if this

ratio is small the opposite is true. On the other hand, the model also requires a relatively large number of adjustable parameters, and thus it is perhaps most appropriate to think of it as a semi-empirical treatment which has been motivated by physical intuition.

One interesting hypothesis which was suggested by the modelling studies is that calf aqueous contains multiple populations of blocking material, i.e. that substance A is actually an entire class of components. This possibility is supported by three observations: (i) both albumin and γ-crystallins can participate in blocking, (ii) electrophoretograms of blocking material show a number of proteins, and (iii) low molecular weight material probably inhibits blockage by binding to the filter, i.e. also has the capacity to adsorb onto polycarbonate membranes. This suggests that the "profile" of the blocking materials in calf aqueous, as well as the concentration of substance B, is important in determining filter blocking behavior. Perhaps changes in this profile are the source of much of the variability seen in our experiments.

6.4 Behavior of Other Aqueous Types

When comparing the blocking behavior of calf aqueous to that of aqueous from other species it must be remembered that the calves employed in this study were neonates, while the other animals were mature. Thus, the fact that calf aqueous blocks more rapidly and to a greater extent than rabbit, human and monkey aqueous could be either an age or a species effect.

To date we have been unable to demonstrate that human aqueous blocks 0.2 μ filters. However, extrapolating from the data on monkey aqueous and taking account of the dilution which has been necessary in the human studies, it seems possible that human aqueous could block filters to the same degree as monkey aqueous. Confirmation of this possibility will require tests with undiluted fluid.

The results of filter perfusions with control and uveitic rabbit aqueous are particularly interesting, especially since uveitic aqueous, even when diluted to control aqueous protein levels, exhibits much greater blocking than does control aqueous. This suggests that uveitic aqueous contains a proportionally higher amount (relative to total protein content) of substance B, implying that additional processes are occuring in the uveitic eye above and beyond blood-aqueous protein leakage. It would therefore be particularly interesting to determine if the facility of the conventional outflow pathway in eyes having this experimentally-induced uveitis was subnormal, or alternately, if uveitic aqueous humor caused a reduction in facility (or washout) when infused into normal eyes.

6.5 Implications for Aqueous Outflow

Influence of Post Mortem Changes

Because we have tested aqueous withdrawn from enucleated eyes of calves which have been stunned and inverted before exsanguination, the possibilty exists that we have been studying a *post mortem* artifact. Arguing

against this possibility is the fact that aqueous collected from living anaesthetized rhesus monkeys exhibits the blocking effect. Recall also that the blocking capacity of calf aqueous cannot be due to blood leakage, and that if it is due to a *post mortem* change this must occur within 15 minutes of death. If leakage of non-blood derived substances into the aqueous occurs within 15 minutes of death it seems likely that a fairly direct path to the anterior and/or posterior chambers must exist, and thus that some (perhaps small) amount of leakage would normally occur. Thus, we conclude that it is unlikely that we are studying a *post mortem* artifact.

A second concern is that we are studying an artifact related to the aqueous collection procedure, e.g. aspiration of lens material. However, it is felt that the care taken with the aqueous collection procedure has avoided this possibility.

The JCM as a Protein-trapping Filter

By analogy with the results for Millipore filters, it seems likely that the JCM, with its tortuous interconnected pore geometry, will be difficult to block. On the other hand, the experiments reported in this work are acute, while the exposure of the JCM to flowing aqueous is a chronic phenomenon. Thus, a very small magnitude effect occuring on the filters, if applicable to the eye, could be significant.

It is of interest to estimate the pore wall area and total pore volume within the JCM. Assuming a flow-wise length of 15 μ and a cross-sectional area of 0.11 cm^2 (Ethier et al., 1986) yields a total JCM volume of 0.17 μl.

If the porosity at normal IOP is taken as ~ 60 % this suggests that the total pore volume is ~ 0.10 μl. Assuming a specific surface of 1.13 μ^{-1} (Section 2.2) indicates that the JCM pore wall area $\simeq$ 1.9 cm^2 (compare values in Table 5.2). Thus the JCM also presents a relatively large pore wall area per unit volume (i.e. has small diameter pores), which will be conducive to blocking if adsorption to the pore walls occurs within the JCM.

A central question is whether the blocking mechanism which occurs on 0.2 μ filters is operative within the JCM. The former process involves hydrophobic and ionic binding, and may also require denaturation of globular proteins. Such denaturation seems unphysiologic, while the body seems to favor extracellular matrix components which are hydrophilic, e.g. the glycocalyx which coats the otherwise hydrophobic cell membrane. However, in the JCM binding could occur purely by ionic effects, since there are a large number of negatively-charged components in this tissue. Alternately, hydrophobic binding could occur onto bare collagen, and thus it seems possible that some sort of binding process could occur within the JCM. It is clear that further experiments will be required to investigate this possibility. In this regard it is particularly unfortunate that the cell lysis which occured in eyes perfused with 0.2 % Triton-X prevents us from concluding that a blocking process similar to that seen on filters occurs within the JCM.

CHAPTER SEVEN: CONCLUSIONS

The blockage of 0.2 μ Nuclepore filters by calf aqueous humor has been shown to involve two components, which we have arbitrarily denoted as A and B. Strictly speaking, it is more correct to consider two classes of blocking components (rather than two individual components), since experimental and modelling studies have indicated that there are most probably multiple populations of blocking materials in calf aqueous. Although the identities of all blocking materials have not been established, albumin appears to play a role in filter blockage, and has been assigned to class A for definiteness. In addition, an as-yet unidentitified protein of molecular weight 20-30 kdaltons and iso-electric point 6-7 is an excellent candidate for substance B. This protein is concentrated in the blocking material eluted from a filter and is absent from serum.

It is not known whether albumin is the "blocker" (the material which actually impedes fluid flow) or a cofactor, since modelling studies have indicated that the blocker could be either a globular molecule which denatures upon adsorption or a long rod-shaped molecule. The role of the cofactor is postulated to involve promotion of binding (and perhaps denaturation) of the blocker.

During the course of this work several likely materials have been eliminated as blocking candidates. In particular, it has been shown that materials of molecular weight less than 10 kdaltons (including ascorbate), as well

as fibrinogen, fibronectin and GAGs do not play a role in filter blockage.

Blockage is dependent on filter surface chemistry and involves the hydrophobic, and to a lesser extent, ionic, binding of the blocking components to the membrane material, either within the pores or on the filter face. Experimental and modelling studies indicate that both binding sites are possible, and in fact the actual filter blocking process may take place at both these sites.

It has been shown that freshly collected calf plasma and serum, when diluted to aqueous protein levels, do not block 0.2 μ filters. This is explained by the fact that serum and plasma lack substance B, and in this sense calf aqueous may be considered somewhat unique. Tests with monkey aqueous (collected from live anaesthetized animals) and rabbit aqueous show that the blocking phenomenon is shared by other types of aqueous humors, although calf fluid does seem to be the most potent blocker tested to date. Tests on human aqueous have been inconclusive because of the dilutions needed to carry out the experiments. Particularly interesting are tests on normal and uveitic rabbit aqueous which show that the uveitic fluid, in addition to having a greater overall protein content, is even more enriched in substance B.

Modelling of filter blockage has been complicated by inter-batch variability and the complexity of the protein/filter binding process. However, by considering the aqueous blocking components to be a heterogeneous mixture (as they most probabaly are) with variable affinities it was possible to match the bulk of the experimental data. The basic approach used in the modelling studies was to relate the rate of filter blockage to the transport rate of protein

through the filter and the rate of protein adsorption onto the filter surface. The failure of the model to more accurately fit the data is probabaly due to the number of simplifying assumptions which were made, such as those concerning adsorption kinetics and the absence of in-pore/filter face interactions. However, the basic insights provided by modelling studies, e.g. that blocking behavior may be divided into two regimes depending on the value of the ratio of protein binding rate to trans-filter transport rate, are felt to be valid.

If a similar blockage mechanism occurs within the JCM it seems most probable that protein either ionically binds to negatively charged materials in the extracellular matrix, or hydrophobically binds to bare collagen fibrils within this tissue. Enucleated whole eye pefusions have been unable to confirm whether or not blockage occurs within the JCM.

Further Work

In the short term, it is important to establish that the protein identified in Figure 4.43 is in fact substance B. Since its molecular weight is less than 30 kdaltons (assuming that the spots in Figure 4.43 represent the entire protein and not a subunit), it should be possible to eliminate the blocking capacity of aqueous by removing materials of molecular weight < 30 kdaltons, a task for which the Centricon-30 microconcentrator is well-suited. If the identification of this protein as substance B is confirmed a number of experiments are suggested:

(i) 2-D gel electrophoresis of normal and glaucomatous human aqueous humor in order to determine if substance B is present in these fluids, and if it is enhanced in glaucomatous samples.

(ii) Extraction, homogenization and 2-D gel electrophoresis of meshwork to see if substance B is present within this tissue.

(iii) High resolution 2-D gel electrophoresis of control and uveitic rabbit aqueous.

It will also be of interest to verify that the "albumin spot" seen on electrophoretograms is actually albumin, as well as to determine whether or not undiluted human aqueous blocks 0.2 μ filters.

It is clear that considerable refinement of the model is possible. However, judging the success of such refinements would require a consistent and well-understood body of experimental data. Because aqueous humor is a complex heterogeneous mixture it is difficult to generate such a body of data from studies on aqueous, and thus model refinements will only be justified if the goal is to provide a better understanding of the transport of simple, well-characterized protein mixtures through filters.

LIST OF SYMBOLS

a: solute or protein characteristic dimension (A)

A: filter surface area (either pore wall area or filter face area) (cm^2)

c: bulk concentration ($\mu g/ml$)

D: diffusion coefficient (cm^2/s)

h: mass transfer coefficient (Section 5.6) (cm/s)

I_o, I_1: modified Bessel functions of the first kind

J_s: solute flux (equation (2.3.1))

J_v: solvent flux (equation (2.3.2))

k_1, k_2: adsorption and desorption rate constants for the Langmuir isotherm ($cm^3/\mu g/sec$ and sec^{-1})

K: permeability

K_o, K_1: modified Bessel functions of the second kind

L: pore length (μ)

L_p: filter hydraulic conductivity (equation (2.3.2))

m: adsorbed protein mass on filter (μg)

n: pore density (number of pores per unit area) (cm^{-2})

N: total number of pores on a filter

q: volume flow through a single pore ($\mu l/min$)

Q: total volume flow though a filter ($\mu l/min$)

r: radial position co-ordinate

R_m: membrane rejection coefficient, equation (2.3.1)

R_o: pore radius (μ)

R_1: half the mean interpore spacing (Figure 5.4)

R_g: radius of a gel hemisphere (Figure 5.7)

R: normalized filter resistance

R_{bl}: baseline resistance of membrane (mm Hg/μl/min)

R_{sys}: resistance of perfusion system (mm Hg/μl/min)

R_∞: normalized steady state filter resistance

R_{500}: normalized filter resistance at 500 seconds

s: sedimentation coefficient (sec) (equation (6.2.1))

t_{prec}: time taken to precipitate a given molecule (equation (6.2.1)

$\mathbf{u}$: fluid velocity field

u_1: fluid velocity in the gel-free inner core (Section 5.5)

u_2: fluid velocity in the gel filled region of a pore (Section 5.5)

U: mean fluid velocity (cm/s)

U_{sup}: superficial fluid velocity (cm/s)

x: position w.r.t. membrane face, either upstream or within the pore

Greek Letters

β: see equation (5.6.15)

Δ: thickness of the adsorbed protein layer on the pore wall (A)

Δx: uniform surface layer thickness

ϵ: membrane porosity

ϕ: gel solid fraction

Φ: equilibrium bulk/pore partitioning coefficient

γ: shear rate (s^{-1}); dimensionless adsorbed protein mass per unit area ($-\Gamma/\Gamma_{max}$)

Γ: adsorbed protein mass per unit area ($\mu g/cm^2$)

Γ_∞: plateau adsorbed protein mass per unit area ($\mu g/cm^2$)

Γ_{max}: maximal adsorbed protein mass per unit area ($\mu g/cm^2$) (equation (5.5.3))

Λ: characteristic length scale (equation 5.5.13))

μ: fluid viscosity (g/cm/s)

π: osmotic pressure

σ: membrane rejection coefficient; standard deviation

τ: dimensionless time ($-k_2 t$)

ω: solute conductivity (equation (2.3.3)); angular velocity (equation (6.2.1))

Subscripts

o: denotes upstream or reference conditions
i: refers to initial conditions

Superscripts

$\hat{}$: dimensionless quantity
$\bar{}$: area-averaged quantity

BIBLIOGRAPHY

Adamson, AW (1960). *Physical Chemistry of Surfaces.* Interscience Publishers, Inc., New York. Chapter XI.

Alexander, RR, JM Griffiths and ML Wilkinson (1986). *Basic Biochemical Methods.* John Wiley and Sons, New York.

Alvarado, J, C Murphey J Polanski and R Juster (1981). Age-related changes in trabecular meshwork cellularity. *Invest Ophthal Vis Sci*, 21, 714.

Anderson, JL (1981). Configurational effects on the rejection coefficients for rigid solutes in capillary pores. *J Theor Biol*, 90, 405.

Anderson, JL and JA Quinn (1974). Restricted transport in small pores: a model for steric exclusion and hindered particle motion. *Biophys J*, 14, 130.

Barany, EH (1953). *In vitro* studies of the resistance to flow through the angle of the anterior chamber. *Acta Soc Med Ups*, 59, 260.

Bassett-Chu, S and KA Erickson-Lamy (1986). Comparison of the facility-increasing effect of anterior chamber perfusion in eyes from different primate and subprimate species. *Invest Ophthal Vis Sci*, 27 (ARVO abstracts), 353.

Beavers, GS and DD Joseph (1967). Boundary conditions at a naturally permeable wall. *J Fluid Mech*, 30, 197.

Bill, A and B Svedbergh (1972). Scanning electron microscopic studies of the trabecular meshwork and the canal of Schlemm - an attempt to localize the main resistance to outflow of aqueous humor in man. *Acta Ophthal*, 50, 295.

Bill, A, E Lutjen-Drecoll and B Svedbergh (1980). Effects of intracameral Na_2EDTA and EGTA on aqueous outflow routes in the monkey eye. *Invest Ophthal Vis Sci*, 19, 492.

Bisio, PD, JG Cartledge, WH Keesom, and CJ Radke (1980). Molecular orientation of aqueous surfactants on a hydrophobic solid. *J Colloid Int Sci*, 78, 225.

Bradford, MM (1976). A rapid and sensitive method for the quantitation of microgram quantities of protein utilizing the principle of protein-dye binding. *Anal Biochem*, 72, 248.

Brash, JL and VJ Davidson (1976). Adsorption on glass and polyethylene from solutions of fibrinogen and albumin. *Thrombosis Res*, 9, 249.

Brash, JL and QM Samak (1978). Dynamics of interactions between human albumin and polyethylene surface. *J Colloid Int Sci*, 65, 495.

Brash, JL and P ten Hove (1984). Effect of plasma dilution on adsorption of fibrinogen to solid surfaces. *Thromb Haemostas*, 51, 326.

Brash, JL and S Uniyal (1979). Dependence of albumin-fibrinogen simple and competitive adsorption on surface properties of biomaterials. *J Polymer Sci*, 66, 377.

Brynda, E, NA Cepalova and M Stol (1984). Equalibrium adsorption of human serum albumin and human fribrinogen on hydrophobic and hydrophilic surfaces. *J Biomed Mat Res*, 18, 685.

Burghardt, TP and D Axelrod (1981). Total internal reflection/fluorescence photobleaching recovery study of serum albumin adsorption dynamincs. *Biophys J*, 33, 455.

Chan, BMC and JL Brash (1981). Adsorption of fibrinogen on glass. *J Colloid Int Sci*, 82, 217.

Cheryan, M and U Merin (1980). A study of the fouling phenomenon during ultrafiltration of cottage cheese whey *in* Ultrafiltration Membranes and Applications. AR Cooper (ed). Plenum Press, New York.

Cohn, EJ, LE Strong, WL Hughes Jr, DJ Mulford, JN Ashworth, M Melin and HL Taylor (1946). Preparation and properties of serum and plasma proteins. A system for the separation into fractions of the protein and lipoprotein components of biological tissues and fluids. *J Amer Chem Soc*, 68, 459.

Cooper, TG (1977). *The Tools of Biochemistry*. John Wiley and Sons, New York. Chapter Two.

Danfeldt, JA and HH Harrison (1984). Quality control and technical outcome of Iso-DALT 2-D electrophoresis in a clinical lab setting. *Clin Chem*, 30, 1972.

Deen, WM, MP Bohrer and NB Epstein (1981). Effects of molecular size and configuration on diffusion in microporous membranes. *J Amer Inst Chem Eng*, 27, 952.

Deen, WM and FG Smith (1982). Hindered diffusion of synthetic polyelectrolytes in charged microporous membranes. *J Memb Sci*, 12, 217.

Dernouchamps, JP (1982). The proteins of the aqueous humour. *Doc Ophthal*, 53, 193.

Epstein, DL, JM Hashimoto, WM Grant (1978a). Serum obstruction of aqueous outflow in enucleated eyes. *Amer J Ophthal*, 86, 101.

Epstein, DL, JA Jedziniak and WM Grant (1978b). Obstruction of aqueous outflow by lens particles and by heavy-molecular-weight soluble lens proteins. *Invest Ophthal Vis Sci*, 17, 272.

Erickson, KA and PL Kaufman (1981). Comparative effects of three ocular perfusates on outflow facility in the Cyromolgus monkeys. *Current Eye Res*, 1, 211.

Ethier, CR (1983). Hydrodynamics of flow through gels with applications to the eye. SM Thesis, MIT.

Ethier, CR (1986). The hydrodynamic resistance of hyaluronic acid: estimates from sedimentation studies. *Biorheology*, 23, 99.

Ethier, CR, RD Kamm, BA Palaszewski, MC Johnson and TM Richardson (1986). Calculations of flow resistance in the juxtacanalicular meshwork. To appear *Invest Ophthal Vis Sci*.

Fane, AG, CJD Fell and A Suki (1983b). The effects of pH and ionic environments on the ultrafiltration of protein solutions with retentative membranes. *J Memb Sci*, 16, 195.

Fane, AG, CJD Fell and AG Waters (1983a). Ultrafiltration of protein solutions through partially permeable membranes - the effect of adsorption and solution environment. *J Memb Sci*, 16, 211.

Gaasterland, DE, JE Pederson, HM MacLellan (1978). Perfusate effects upon resistance to aqueous humor outflow in the rhesus monkey eye. *Invest Ophthal Vis Sci*, 17, 391.

Gaasterland, DE, JE Pederson, HM MacLellan and VN Reddy (1979). Rhesus monkey aqueous humor composition and a primate ocular perfusate. *Invest Ophthal Vis Sci*, 18, 1139.

Gendreau, RM, RI Leininger, S Winters and RJ Jakobson (1982). Fourier transform infrared spectroscopy for protein-surface studies *in* Biomaterials: Interfacial Phenomenon and Applications. SL Cooper and NA Peppas (eds). Advances in Chemistry Series, 199, American Chemical Society. Washington, DC. Chapter 24.

Grabner, G, G Zehetbauer, H Bettelheim, C Honigsmann and W Dorda (1978). The blood-aqueous barrier and its permeability for proteins of different molecular weight. *Graef's Arch Clin Exp Ophthalmol*, **207**, 137.

Happel, J and H Brenner (1973). *Low Reynolds Number Hydrodynamics*. Martinus Nijhoff, Boston.

Hawker, RJ and LM Hawker (1975). Protein losses during sterilizing by filtration. *Lab Practice*, **Dec**, 805.

Hazel, SJ, MA Hull-Thrall, GA Severin, LH Lauerman Jr and JD Lavach (1985). Laboratory evaluation of aqueous humor in the healthy dog, cat, horse, and cow. *Amer J Vet Res*, **46**, 657.

Hogan, MJ, JA Alvarado and J Weddel (1971). *Histology of the Human Eye: An Atlas and Textbook*. W.B. Saunders Co., Philadelphia.

Horbett, TA (1982). Protein Adsorption on Biomaterials *in* Biomaterials: Interfacial Phenomena and Applications. SL Cooper and NA Peppas (eds), Advances in Chemistry Series, **199**, American Chemical Society, Washington, DC. Chapter 17.

Horbett, TA (1984). Mass action effects on competitive adsorption of fibrinogen from hemoglobin solutions and from plasma. *Thromb Haemostas*, **51**, 174.

Ingham, KC, TF Busby, Y Sahlestrom and F Castino (1980). Separation of macromolecules by ultrafiltration: influence of protein adsorption, protein-protein interactions and concentration polarzation *in* Ultrafiltration Membranes and Applications. AR Cooper, (ed). Plenum Press, New York, p 141.

Iwamoto, GK, LC Winterton, RS Stoker, RA Van Wagenen, JD Andrade and DF Mosher (1985). Fibronectin adsorption detected by interfacial fluorescence. *J Colloid Int Sci*, **106**, 459.

Jackson, GW and DF James (1982). The hydrodynamic resistance of hyaluronic acid and its contribution to tissue permeability. *Biorheology*, **19**, 317.

Jackson, GW and DF James (1986). The permeability of fibrous porous media. *Canadian J Chem Eng*, **64**, 364.

Johnson, M, CR Ethier, RD Kamm, WM Grant, DL Epstein and D Gaasterland (1986). The flow of aqueous humor through micro-porous filters. *Invest Ophthal Vis Sci*, **27**, 92.

Johnson, MC and RD Kamm (1983). The role of Schlemm's canal in aqueous outflow from the human eye. *Invest Ophthal Vis Sci*, 24, 320.

Jakob, M (1949). *Heat Transfer*, Volume one. John Wiley and Sons, New York.

Jonsson, U, B Ivarsson, I Lundstrom and L Berghem (1982). Adsorption behavior of fibronectin on well-characterized silica surfaces. *J Colloid Int Sci*, 90, 148.

Kedem, O and A Katchalsky (1958). Thermodynamic analysis of the permeability of biological membranes to non-electrolytes. *Biochim et Biophys Acta*, 27, 229.

Knepper, PA, M Breen, HG Weinstein and LJ Black (1978). IOP and GAG distribution in the rabbit eye: effect of age and dexamethasone. *Exp Eye Res*, 27, 567.

Knepper, PA, AI Farbman and AG Telser (1984). Exogenous hyaluronidases and degradtion of hyaluronic acid in the rabbit eye. *Invest Ophthal Vis Sci*, 25, 286.

Krause, U and V Raunio (1969). Protein content of normal human aqueous humor *in vivo*. *Acta Ophthal*, 47, 215.

Lam, KW, AM Mansour, RF Fox, PF Lee and R Smith (1983). Fibrinogen concentration in the aqueous humor of buphthalmic rabbits. *Current Eye Res*, 2, 153.

Larson, RE and JJL Higdon (1986). Microscopic flow near the surface of two-dimensional porous media. Part 1. Axial flow. *J Fluid Mech*, 166, 449.

Laurent, UBG (1981). Hyaluronate in aqueous humor. *Exp Eye Res*, 33, 147.

Lee, RG and SW Kim (1974). Adsorption of proteins onto hydrophobic polymer surfaces: adsorption isotherms and kinetics. *J Biomed Mater Res*, 8, 251.

Lehninger, AL (1975). *Biochemistry* (Second Edition). Worth Publishers Inc, New York.

Liabastre, AA and C Orr (1978). An evaluation of pore structure by mercury penetration. *J Colloid Int Sci*, 64, 1.

Lindemayer, JM, MG Kahn, E Hertzmark and DL Epstein (1983). Morphology and function of the aqueous outflow system in monkey eyes perfused with sulfhydryl reagents. *Invest Ophthal Vis Sci*, 24, 710.

Litin, BS and J Herschler (1984). Silver staining of human aqueous humor proteins resolved by gel electrophoresis. *Graef's Arch Clin Exp Ophthalmol*, **221**, 290.

Lok, BK, YL Cheng and CR Robertson (1983). Protein adsorption on cross-linked polydimethylsiloxane using total internal reflection fluorescence. *J Colloid Int Sci*, **91**, 104.

Lonsdale, HK, RL Riley, CR Lyons and DP Carosella Jr (1971). Transport in composite reverse osmosis membranes *in* Symposium on Membrane Processes in Industry and Biomedicine. M Bier (ed). Plenum Press, New York. 101.

Lutjen-Dreooll, E (1973). Structural factors influencing outflow facility and its changeability under drugs. A study in *Macaca arctoides*. *Invest Ophthal*, **12**, 280.

Lyklema, J (1984). Proteins at solid-liquid interfaces. *Colloids and Surfaces*, **10**, 33.

Marmur, A and SL Cooper (1982). A model for the deposition and detachment of proteins and platelets on biomaterials. *J Colloid Int Sci*, **89**, 458.

Marshall, T, KM Williams and G Vesterberg (1984). Two-dimensional electrophoresis of proteins in human serum: improved resolution by use of narrow pH gradients and prolonged electrophoresis. *Clin Chem*, **30**, 2008.

Matthiasson, E (1983). The role of macromolecular adsorption in fouling of ultrafiltration membranes. *J Memb Sci*, **16**, 23.

Meares, P and KR Page (1972). Rapid force-flux transitions in highly porous membranes. *Proc Royal Soc*, **A272**, 1.

Michaels, AS, L Nelson and MC Porter (1971). Ultrafiltration *in* Symposium on Membrane Processes in Industry and Biomedicine. M Bier (ed). Plenum Press, New York, p 197.

Mitchell BD and WM Deen (1984). Theoretical effects of macromolecular concentration and charge on membrane rejection coeffients. *J Memb Sci*, **19**, 75.

Motomura, K and R Matuura (1969). Conformation of adsorbed polymeric chain: II. *J Chemical Phys*, **50**, 1281.

Moses, RA (1979). Circumferential flow in Schlemm's canal. *Amer J Ophthal*, **88**, 585.

Munch, WD, LP Zestar, JL Anderson (1979). Rejection of polyelectrolytes from microporous membranes. *J Memb Sci*, **5**, 77.

Neupert, JR and C Lawrence (1970). Protein release during aqueous withdrawal in rabbits. *Invest Ophthal*, **9**, 865.

O'Farrell, PH (1975). High resolution two-dimensional electrophoresis of proteins. *J Biol Chem*, **250**, 4407.

Paynter, RW, BD Ratner, TA Horbett and HR Thomas (1984). XPS studies on the organization of adsorbed protein films on fluoropolymers. *J Colloid Int Sci*, **101**, 233.

Price, PB and RM Walker (1962). Observation of charged-particle tracks in solids. *J Appl Phys*, **33**, 3400. Chemical etching of charged-patricle tracks in solids. *ibid*, 3407.

Probstein, RF, WF Leung and Y Alliance (1979). Determination of diffusivity and gel concentration in macromolecular solutions by ultrafiltration. *J Phys Chem*, **83**, 1228.

Raviola, G and E Raviola (1981). Paracellular route of aqueous outflow in the trabecular meshwork and canal of Schlemm. *Invest Ophthal Vis Sci*, **21**, 52.

Reid, T, MC Kenney and GO Waring (1982). Isolation and characterization of fibronectin from bovine aqueous humour. *Invest Ophthal Vis Sci*, **22**, 57.

Reihanian, H, CR Robertson and AS Michaels (1983). Mechanisms of polarization and fouling of ultrafiltration membranes by proteins. *J Memb Sci*, **16**, 237.

Rosenquist, RC, DL Epstein, MC Johnson, WM Grant and S Melamed (1986). Resistance variation with perfusion pressure after trabeculotomy. *Invest Ophthal Vis Sci*, **26** (ARVO abstracts), 159.

Ruben, JB, RA Moses,and WJ Grodzki Jr (1985). Perfusion outflow facility in the rabbit eye. *Invest Ophthal Vis Sci*, **26**, 153.

Rudee, ML, TM Price (1985). The initial stages of adsorption of plasma derived proteins on artificial surfaces in a controlled flow environment. *J Biomed Mat Res*, **19**, 57.

Saari, KM, E Aine and MT Parviainen (1983). Determination of protein content in aqueous humour by high-performance gel filtration chromatography. *Acta Ophthal*, **61**, 611.

Sandberg, HO and O Closs (1979). The alpha and gamma crystallin content in aqueous humor of eyes with clear lenses and with cataracts. *Exp Eye Res*, **28**, 601.

Schultz, JS, R Valentine and CY Choi (1979). Rejection coefficients of homopore membranes: effect of molecular size and configuration. *J Gen Physiol*, **73**, 49.

Spiegler, KS and O Kedem (1966). Thermodynamics of hyperfiltration (reverse osmosis): criteria for efficient membranes. *Desalination*, **1**, 311.

Spielman, L and SL Goren (1968). Model for predicting pressure drop and filtration efficiency in fibrous media. *Environmental Sci Tech*, **2**, 279.

Sonderquist, ME and AG Walton (1980). Structural changes in proteins adsorbed on polymer surfaces. *J Colloid Int Sci*, **75**, 386.

Spurny, K and JP Lodge Jr (1968). Analytical methods for determination of aerosols by means of membrane ultrafiltration. *Collection Czechoslov Chem Commun*, **33**, 3679.

Svedbergh, B (1974). Effects of artificial IOP elevation on the outflow facility and the ultrastructure of the chamber angle in the Vervet monkey. *Acta Ophthal*, **52**, 829.

Tanford, C (1961). *Physical Chemistry of Macromolecules*. John Wiley and Sons, New York.

Trettin, DR and MR Doshi (1980). Ultrafiltration in an unstirred batch cell. *Ind Eng Chem Fundam*, **19**, 189.

Trope, GE and AG Rumley (1985). Catecholamines in human aqueous humor. *Invest Ophthal Vis Sci*, **26**, 399.

Ujiie, K and A Bill (1984). The drainage routes for aqueous humor as revealed by scanning electron microscopy of corrosion casts. *Scanning Electron Microscopy*, **2**, 829.

Van Buskirk, EM and WM Grant (1974). Influence of temperature and the question of involvement of cellular metabolism in aqueous outflow. *Amer J Ophthal*, **77**, 565.

Van Dulm, P and W Norde (1983). The adsorption of human plasma albumin on solid surfaces, with special attention to the kinetic aspects. *J Colloid Int Sci*, **91**, 248.

Van Wagenen, RA, S Rockhold and JD Andrade (1982). Probing protein adsorption: total internal reflection intrinsic

flourescence *in* Biomaterials: Interfacial Phenomena and Applications. SL Cooper and NA Peppas (eds), Advances in Chemistry Series, 199, American Chemical Society, Washington, DC. Chapter 23.

Varoqui, R and P Desjardin (1977). Hydrodynamic thickness of adsorbed polymers. *J Chem Phys*, 66, 4395.

Vilker, VL, CA Colton and KA Smith (1981). Concentraion polarization in protein ultrafiltration, I and II. *AIChE J*, 27, 632.

Walton, AG and B Koltisko (1982). Protein structure and the kinetics of interaction with surfaces *in* Biomaterials: Interfacial Phenomena and Applications. SL Cooper and NA Peppas (eds), Advances in Chemistry Series, 199, American Chemical Society, Washington, DC. Chapter 18.

Wiegel, FW (1980). *Fluid flow through porous macromolecular systems*. Lecture Notes in Physics, Volume 121. Springer-Verlag, Berlin.

Yavorsky, DP (1981). Static and hydrodynamic studies of the conformation of adsorbed macromolecules at the solid/liquid interface. PhD thesis, University of Pennsylvania.

Zirm, M and O Schmut (1976). Immunologische untersuchungen des kammerwassers und deren ergebnisse. *Wien Klin Wochenschr*, 88, 343.